toxics

Chemical and Biological Threats, Hazard Potential and Countermeasures

Edited by

Jan Korabecny and Ondrej Soukup

Printed Edition of the Special Issue Published in *Toxics*

www.mdpi.com/journal/toxics

MDPI

Chemical and Biological Threats, Hazard Potential and Countermeasures

Chemical and Biological Threats, Hazard Potential and Countermeasures

Editors

Jan Korabecny
Ondrej Soukup

MDPI • Basel • Beijing • Wuhan • Barcelona • Belgrade • Manchester • Tokyo • Cluj • Tianjin

Editors
Jan Korabecny
University Hospital Hradec Kralove
Czech Republic

Ondrej Soukup
University Hospital Hradec Kralove
Czech Republic

Editorial Office
MDPI
St. Alban-Anlage 66
4052 Basel, Switzerland

This is a reprint of articles from the Special Issue published online in the open access journal *Toxics* (ISSN 2305-6304) (available at: https://www.mdpi.com/journal/toxics/special_issues/chemical_and_biological_threats).

For citation purposes, cite each article independently as indicated on the article page online and as indicated below:

LastName, A.A.; LastName, B.B.; LastName, C.C. Article Title. *Journal Name* **Year**, *Volume Number*, Page Range.

ISBN 978-3-0365-5037-4 (Hbk)
ISBN 978-3-0365-5038-1 (PDF)

Contents

About the Editors

Jan Korabecny

Jan Korabecny graduated from the Faculty of Pharmacy (Charles University, Prague, Czech Republic) in 2008. He finished his Ph.D. studies at the Department of Pharmaceutical Chemistry and Drug Control at the same university in 2012. In 2020, he received Associate Professor degree from Pharmaceutical Chemistry at the Faculty of Pharmacy in Hradec Kralove (Charles University). He is currently the head of the Laboratory of Chemistry at the Department of Toxicology and Military Pharmacy, senior researcher and deputy head at the Biomedical Research Centre (University Hospital, Hradec Kralove, Czech Republic) and the head of the Synthesis of Novel Drugs laboratory at National Institute of Mental Health. His area of research is pharmaceutical/medicinal chemistry, biochemistry, and toxicology. His interests are neuroscience, especially the development of novel treatments of Alzheimer's disease based on choliesterase inhibitors, antidotes against organophosphorus poisoning, anticancer agents, and receptor modulators (e.g. NMDA, D2, 5-HT3 etc.). Currently, he is author or co-author of more than 130 scientific publication, with more than 2,300 citation (excluding self-citation) and H-index 30.

Ondrej Soukup

Ondrej Soukup Tgraduated from the Faculty of Pharmacy (Charles University, Prague, Czech Republic) in 2007. He finished his Ph.D. studies at the University of Defence, Faculty of Military Health Sciences (Hradec Kralove, Czech Republic) in 2011. Currently the head of Biomedical Research Center (University Hospital Hradec Kralove, Czech Republic) and Assoc. Prof. at Department of Toxicology and Military Pharmacy Faculty of Military Health Sciences (University of Defence, Hradec Kralove, Czech Republic). His area of research is pharmaceutical/medicinal chemistry, biochemistry, and toxicology, where he received Associate Professor degree in 2018. His research interests are neuroscience, especially the development of novel treatments for Alzheimer's disease based on choliesterase inhibitors, antidotes against organophosphorus poisoning, disinfectants and receptor modulators (e.g. cholinergic, NMDA, D2, 5-HT3 etc.). Currently, he is author or co-author of more than 150 scientific publication, with more than 2,200 citation (excluding self-citation) and H-index 30.

Preface to "Chemical and Biological Threats, Hazard Potential and Countermeasures"

The scope of this special issue is to pay attention to various aspects of toxicology specifically focused on the chemical and biological threats, which may accidentally or on purpose endanger human health. Besides the characterization of such threats and their biological consequences we focus on the available and novel experimental countermeasures capable to protect from and/or treat such exposures. In particular, we have focused, in this special issue, on the neuroprotective approaches against organophosphorus poisoning, decontamination approaches against organophosphates and sulphur mustard. From a civilian sphere, we bring original reports describing occupational exposure risk to phthalates and diacetyl, commonly occurring plastic components and flavouring additive respectively and its health consequences. Finally, we present a review focused on micro and nanoplastics, their relation to human health and their exposure routes through the environment.

Jan Korabecny and Ondrej Soukup
Editors

toxics

MDPI

Editorial

Chemical and Biological Threats, Hazard Potential and Countermeasures

Ondrej Soukup [1,2,*] and Jan Korabecny [1,2,*]

[1] Biomedical Research Center, University Hospital Hradec Kralove, Sokolska 581, 50005 Hradec Kralove, Czech Republic
[2] Faculty of Military Health Sciences, University of Defence, Trebesska 1575, 50005 Hradec Kralove, Czech Republic
* Correspondence: ondrej.soukup@fnhk.cz (O.S.); jan.korabecny@fnhk.cz (J.K.)

The scope of this Special Issue is to pay attention to various aspects of toxicology specifically focused on the chemical and biological threats, which may accidentally, or on purpose, endanger human health. Besides the characterization of such threats and their biological consequences, we will focus on the available and novel experimental countermeasures able to provide protection from and/or threaten such exposures. In particular, we have focused, in this Special Issue, on the neuroprotective approaches against organophosphorus poisoning, decontamination approaches against organophosphates and sulphur mustard. From a civilian sphere, we bring original reports that describe the occupational exposure risk to phthalates and diacetyl, commonly occurring plastic components and flavoring additives, respectively, and their health consequences. Finally, we present a review focused on micro and nanoplastics, their relation to human health and their exposure routes through the environment.

In detail, the team of M. Braga, in a paper on the antiseizure and neuroprotective efficacy of midazolam in comparison with tezampanel (LY293558) against soman-induced status epilepticus, present the neuroprotective efficacy of novel glutamatergic inhibitor tezampanel in comparison to commonly used midazolam (MDZ). The neuroprotective efficacy of the two drugs was studied in the basolateral amygdala, 30 days post-exposure. To highlight the findings, significant neuronal and interneuronal loss, reduced ratio of interneurons to the total number of neurons, and reduction in spontaneous inhibitory postsynaptic currents, accompanied by increased anxiety, were found in the MDZ-treated group. Rats treated with tezampanel did not differ from the control rats (not exposed to soman) in any of these measurements. Thus, tezampanel has significantly greater efficacy than midazolam in protecting against prolonged seizures and brain damage caused by acute nerve agent exposure [1]. Another work, 'Molecular Evidence on the Inhibitory Potential of Metformin against Chlorpyrifos-Induced Neurotoxicity' by Daniali et al, presents an in vivo study on the neuroprotective effect of metformin upon chlorpyrifos (CPF) poisoning. Indeed, following the 28 days of CPF and metformin administration, the levels of inflammatory biomarkers, such as tumor necrosis factor alpha (TNFα) and interleukin 1β (IL-1β), as well as the expression of 5HT1 and 5HT2 genes, were analyzed. Moreover, the levels of malondialdehyde (MDA), reactive oxygen species (ROS), and the ADP/ATP ratio, in addition to the activity of acetylcholinesterase (AChE) and superoxide dismutase (SOD), were tested through in vitro experiments. This study demonstrated the potential role of metformin in alleviating the mentioned biomarkers, which can be altered negatively as a result of CPF toxicity. Moreover, metformin showed protective potential in modulating inflammation, as well as oxidative stress, the expression of genes, and histological analysis, in a concentration-dependent manner [2]. Finally, Kassa et al. in their paper 'Influence of Experimental End Point on the Therapeutic Efficacy of Essential and Additional Antidotes in Organophosphorus Nerve Agent-Intoxicated Mice' report the effect of antinicotinic

Citation: Soukup, O.; Korabecny, J. Chemical and Biological Threats, Hazard Potential and Countermeasures. *Toxics* **2022**, *10*, 444. https://doi.org/10.3390/toxics10080444

Received: 27 July 2022
Accepted: 1 August 2022
Published: 2 August 2022

compound MB327 on the survival of mice upon nerve agents (sarin, soman, tabun and cyclosarin) exposure. To sum up, MB327 increased the therapeutic efficacy of atropine alone for sarin, soman and tabun intoxication, and that of the standard antidotal treatment (atropine and oxime) for sarin and tabun intoxication; however, the therapeutic efficacy of MB327 was lower than the oxime-based antidotal treatment. To compare the 6 and 24 h end points, the influence of the experimental end point was not observed, with the exception of the higher dose of MB327. Despite the fact that only a negligible beneficial impact of the compound MB327 was observed, antinicotinics may offer an additional avenue for countering poisoning by nerve agents that are difficult to treat. Of note, LD_{50} values of sarin, soman, tabun and cyclosarin, both treated and untreated, in mice for experimental end points of 6 and 24 h are reported in this study [3].

The second area covered by this Special Issue deals with the decontamination of chemical warfare agents. Markova et al. in their study '**Synthesis and Decontamination Effect on Chemical and Biological Agents of Benzoxonium-Like Salts**' describe antimicrobial, as well as decontamination, potential of novel series based on benzoxonium scaffolds. In particular, biocidal activity against a panel of bacterial strains, including *Staphylococcus aureus* in biofilm form and *Francisella tularensis* as a representative of potential biological warfare agents, was screened. From a point of view of decontamination potential, the efficiency of BOC-like compounds to degrade the organophosphate simulant fenitrothion was examined. In summary, despite the fact that no single compound with universal effectiveness was identified, a mixture of only two compounds from this group would be able to satisfactorily cover the proposed decontamination spectrum. Furthermore, the dual effect on chemical and biological agents of benzoxonium-like salts offer attractive potential as active components of decontamination mixtures in the case of a terrorist threat or chemical or biological accidents [4]. In another work entitled '**Reactive Organic Suspensions Comprising ZnO, TiO2, and Zeolite Nanosized Adsorbents: Evaluation of Decontamination Efficiency on Soman and Sulfur Mustard**' by Ginghina and Bratu, the decontamination efficiency of three types of reactive organic suspensions (based on nanosized adsorbents) on two real chemical warfare agents, soman (GD) and sulfur mustard (HD), is described. Three types of nanoparticles (ZnO, TiO2, and zeolite) were employed in the decontamination formulations for enhancing the degradation of the toxic agents. The conversion of the two chemical warfare agents into their decontamination products was also monitored up to 24 h. Four main degradation products, resulting from the decontamination of sulfur mustard, and five main degradation products, resulting from the decontamination of GD, were identified and quantified by the GC-MS technique as well. In terms of efficacy, the organic suspensions that comprised ZnO, TiO2, and zeolite nanoparticles proved their decontamination efficiency on soman and sulfur mustard, whereas the conversion study into the harmless degradation products offers a comprehensive image on the decontamination process [5].

Finally, the third part that refers to the occupational exposures is introduced by a review entitled 'Scientific Evidence about the Risks of Micro and Nanoplastics (MNPLs) to Human Health and Their Exposure Routes through the Environment' by Rodrigues et al., focusing mainly on ingestion and inhalation routes and their medical consequences [6]. Inhalation route of exposure is the subject of an original work entitled 'Diacetyl Vapor Inhalation Induces Mixed, Granulocytic Lung Inflammation with Increased $CD4^+CD25^+$ T Cells in the Rat' by McGraw's group. Diacetyl (DA) is a highly reactive alpha diketone associated with flavoring-related lung disease. The study characterizes different T cell populations within the lung following repetitive DA vapor exposures. In particular, while no significant change was observed in percent lung $CD3^+$, $CD4^+$, or $CD8^+$ T cells, a significant increase in lung $CD4^+CD25^+$ T cells developed after 1 week that persisted at 2 weeks post-exposure. In addition, BALF IL-17a increased significantly after 2 weeks in DA-exposed rats compared to the air controls. Lung $CD4^+CD25^+$ T cells and BALF IL17a correlated directly with BALF total protein and inversely with rat oxygen saturations. In summary, repetitive DA vapor exposure at occupationally relevant concentrations induced mixed,

granulocytic lung inflammation with increased $CD4^+CD25^+$ T cells in rats [7]. Finally, the original paper 'Risk of Abdominal Obesity Associated with Phthalate Exposure of Nurses' by Kolena et al assesses potential phthalate exposure among nurses by high-performance liquid chromatography and tandem mass spectrometry and anthropometric measurements, along with questionnaires. As a result, associations between mono-benzyl phthalate (MBzP) and body mass index (BMI), hip circumference (HC), waist circumference (WC), waist to height ratio (WHtR), and fat mass index (FMI), visceral fat content, BMI risk and hip index risk (HIrisk) were observed, suggesting that occupational exposure to phthalates may induce abdominal obesity and result in obesity-related metabolic disorders [8].

To conclude, this Special Issue describes important findings related to chemical and biological threats, their hazard potential on human health and potential countermeasures. All these findings broaden the knowledge in this field and will stimulate further research, which hopefully will result in an impact on practical applications in the near future.

Funding: This work was supported by a grant of the Ministry of Defence "Long Term Development Plan" Medical Aspects of Weapons of Mass Destruction of the Faculty of Military Health Sciences, University of Defence; and by MH CZ - DRO (University Hospital Hradec Kralove, No. 00179906).

Conflicts of Interest: The authors declare no conflict of interest.

References

1. Figueiredo, T.H.; Aroniadou-Anderjaska, V.; Pidoplichko, V.I.; Apland, J.P.; Braga, M.F. Antiseizure and Neuroprotective Efficacy of Midazolam in Comparison with Tezampanel (LY293558) against Soman-Induced Status Epilepticus. *Toxics* **2022**, *10*, 409. [CrossRef] [PubMed]
2. Daniali, M.; Baeeri, M.; Farhadi, R.; Gholami, M.; Hassani, S.; Navaei-Nigjeh, M.; Rahimifard, M.; Abdollahi, M. Molecular Evidence on the Inhibitory Potential of Metformin against Chlorpyrifos-Induced Neurotoxicity. *Toxics* **2022**, *10*, 197. [CrossRef] [PubMed]
3. Kassa, J.; Timperley, C.M.; Bird, M.; Green, A.C.; Tattersall, J.E. Influence of Experimental End Point on the Therapeutic Efficacy of Essential and Additional Antidotes in Organophosphorus Nerve Agent-Intoxicated Mice. *Toxics* **2022**, *10*, 192. [CrossRef] [PubMed]
4. Markova, A.; Hympanova, M.; Matula, M.; Prchal, L.; Sleha, R.; Benkova, M.; Pulkrabkova, L.; Soukup, O.; Krocova, Z.; Jun, D. Synthesis and decontamination effect on chemical and biological agents of benzoxonium-like salts. *Toxics* **2021**, *9*, 222. [CrossRef] [PubMed]
5. Ginghina, R.E.; Bratu, A.E.; Toader, G.; Moldovan, A.E.; Tiganescu, T.V.; Oncioiu, R.E.; Deliu, P.; Petre, R.; Epure, G.; Purica, M. Reactive Organic Suspensions Comprising ZnO, TiO_2, and Zeolite Nanosized Adsorbents: Evaluation of Decontamination Efficiency on Soman and Sulfur Mustard. *Toxics* **2021**, *9*, 334. [CrossRef] [PubMed]
6. Rodrigues, A.C.B.; de Jesus, G.P.; Waked, D.; Gomes, G.L.; Silva, T.M.; Yariwake, V.Y.; da Silva, M.P.; Magaldi, A.J.; Veras, M.M. Scientific Evidence about the Risks of Micro and Nanoplastics (MNPLs) to Human Health and Their Exposure Routes through the Environment. *Toxics* **2022**, *10*, 308. [CrossRef]
7. House, E.L.; Kim, S.-Y.; Johnston, C.J.; Groves, A.M.; Hernady, E.; Misra, R.S.; McGraw, M.D. Diacetyl Vapor Inhalation Induces Mixed, Granulocytic Lung Inflammation with Increased CD4+ CD25+ T Cells in the Rat. *Toxics* **2021**, *9*, 359. [CrossRef] [PubMed]
8. Kolena, B.; Hlisníková, H.; Kečkéšová, Ľ.; Šidlovská, M.; Trnovec, T.; Petrovičová, I. Risk of Abdominal Obesity Associated with Phthalate Exposure of Nurses. *Toxics* **2022**, *10*, 143. [CrossRef] [PubMed]

toxics

MDPI

Article

Antiseizure and Neuroprotective Efficacy of Midazolam in Comparison with Tezampanel (LY293558) against Soman-Induced Status Epilepticus

Taiza H. Figueiredo [1,†], Vassiliki Aroniadou-Anderjaska [1,2,†], Volodymyr I. Pidoplichko [1], James P. Apland [3] and Maria F. M. Braga [1,2,*]

[1] Department of Anatomy, Physiology, and Genetics, F. Edward Hébert School of Medicine, Uniformed Services University of the Health Sciences, Bethesda, MD 20814, USA; taiza.figueiredo.ctr@usuhs.edu (T.H.F.); vanderjaska@usuhs.edu (V.A.-A.); volodymyr.pidoplichko.ctr@usuhs.edu (V.I.P.)
[2] Department of Psychiatry, F. Edward Hébert School of Medicine, Uniformed Services University of the Health Sciences, Bethesda, MD 20814, USA
[3] Neuroscience Branch, U.S. Army Medical Research Institute of Chemical Defense, Aberdeen Proving Ground, Aberdeen, MD 21010, USA; James.p.apland.civ@mail.mil
* Correspondence: maria.braga@usuhs.edu; Tel.: +1-(301)-295-3524; Fax: +1-(301)-295-3566
† These authors contributed equally to this work.

Abstract: Acute exposure to nerve agents induces status epilepticus (SE), which can cause death or long-term brain damage. Diazepam is approved by the FDA for the treatment of nerve agent-induced SE, and midazolam (MDZ) is currently under consideration to replace diazepam. However, animal studies have raised questions about the neuroprotective efficacy of benzodiazepines. Here, we compared the antiseizure and neuroprotective efficacy of MDZ (5 mg/kg) with that of tezampanel (LY293558; 10 mg/kg), an AMPA/GluK1 receptor antagonist, administered 1 h after injection of the nerve agent, soman (1.2 × LD_{50}), in adult male rats. Both of the anticonvulsants promptly stopped SE, with MDZ having a more rapid effect. However, SE reoccurred to a greater extent in the MDZ-treated group, resulting in a significantly longer total duration of SE within 24 h post-exposure compared with the LY293558-treated group. The neuroprotective efficacy of the two drugs was studied in the basolateral amygdala, 30 days post-exposure. Significant neuronal and inter-neuronal loss, reduced ratio of interneurons to the total number of neurons, and reduction in spontaneous inhibitory postsynaptic currents accompanied by increased anxiety were found in the MDZ-treated group. The rats treated with LY293558 did not differ from the control rats (not exposed to soman) in any of these measurements. Thus, LY293558 has significantly greater efficacy than midazolam in protecting against prolonged seizures and brain damage caused by acute nerve agent exposure.

Keywords: soman; seizures; neuroprotection; amygdala; midazolam; tezampanel

Citation: Figueiredo, T.H.; Aroniadou-Anderjaska, V.; Pidoplichko, V.I.; Apland, J.P.; Braga, M.F.M. Antiseizure and Neuroprotective Efficacy of Midazolam in Comparison with Tezampanel (LY293558) against Soman-Induced Status Epilepticus. *Toxics* **2022**, *10*, 409. https://doi.org/10.3390/toxics10080409

Academic Editors: Ondrej Soukup and Jan Korabecny

Received: 28 June 2022
Accepted: 20 July 2022
Published: 22 July 2022

1. Introduction

Acute nerve agent exposure affects both the peripheral and the central nervous system, and can result in an agonizing death if not treated in a timely manner. The primary action of these organophosphorus agents is the inhibition of acetylcholinesterase; the resulting elevation of acetylcholine and the hyperstimulation of cholinergic receptors are the main causes of both the peripheral and central effects [1]. Rapid death can ensue, due to respiratory failure caused by bronchospasms and thick secretions in the airways, weakness and eventual paralysis of the respiratory muscles, and suppression of the respiratory center [2]. These effects can be prevented or adequately controlled by the prompt administration (or auto-injection) of available and efficacious drugs, such as atropine, which counteracts the excessive activation of muscarinic cholinergic receptors, primarily in the peripheral nervous system. In the brain, acute nerve agent exposure induces unrelenting status epilepticus (SE), which can also lead to death. If death is prevented but SE is not adequately

controlled, the brain will be damaged by the intense seizures, which will result in long-term neurological and behavioral deficits [3]. Therefore, control of the seizures after acute nerve agent exposure is necessary to prevent death or brain damage.

The seizures induced by nerve agent exposure are initiated primarily due to hyperstimulation of muscarinic receptors by the elevated acetylcholine [4–8]. The hyperstimulation of the muscarinic receptors triggers excessive activity in the glutamatergic synapses [9–11], which reinforces and sustains seizures [12], and is the main cause of excitotoxic neuronal damage and death [13,14]. Excessive glutamatergic excitation can be suppressed by enhancing the $GABA_A$ receptor-mediated inhibitory activity. Benzodiazepines—mainly diazepam (DZP) and midazolam (MDZ) which are positive modulators of $GABA_A$ receptors [15–17]—are most often used for the suppression of seizures and are administered as the first-line treatment for SE, regardless of the etiology [18–20]. However, seizures often reoccur after a transient suppression by the administration of DZP or MDZ [21–23]. Furthermore, benzodiazepines may be ineffective if administered at delayed time points after the onset of SE, and for this reason, they are recommended for early treatment [18,20,24]. There are also cases where the seizures are completely refractory to benzodiazepines [18,20,25].

Some of these drawbacks have also been observed when benzodiazepines are administered to terminate SE induced by nerve agents, in animal models of nerve agent exposure. Thus, the anticonvulsant efficacy of DZP decreases as the latency from the onset of SE induced by the nerve agent soman increases [26–28]. In addition, the seizures induced by exposure to soman or other organophosphorus agents return after a temporary cessation by administration of DZP [29,30]. More importantly, cessation of nerve agent-induced SE by DZP does not prevent brain damage, or the appearance of behavioral and neurological deficits [29,31–33].

Despite this knowledge, DZP is the current FDA-approved anticonvulsant for treating the victims of acute nerve agent exposure. MDZ has a more rapid absorption and onset of action than DZP, as well as greater water solubility and a longer shelf life [34]; for these reasons, the FDA is currently considering the approval of MDZ for the treatment of nerve agent-induced SE. However, it is unclear if, in the same way as DZP, MDZ is not a good neuroprotectant, particularly if administered with some delay after the exposure. The present study was undertaken to enhance knowledge of the antiseizure and neuroprotective efficacy of MDZ when used to control nerve agent-induced SE. The efficacy of MDZ was compared with that of a compound that directly counteracts glutamatergic hyperexcitation, the AMPA/GluK1 receptor antagonist (3*S*, 4*aR*, 6*R*, 8*aR*)-6-[2-(1(2)*H*-tetrazole-5-yl)ethyl]decahydroisoquinoline-3-carboxylic acid (LY293558 [35]; also known as Tezampanel), which we previously tested against soman under various experimental conditions and obtained promising results [36–40].

2. Materials and Methods

2.1. Animals

Sprague-Dawley male rats, purchased from Charles River Laboratories (Wilmington, MA, USA), were individually housed in an environmentally controlled room (20–23 °C, 12-h light/12-h dark cycle, lights on 06:00 a.m.), with food and water available ad libitum. The rats weighed 150–250 g at the start of the experiments. The experiments performed followed the Guide for the Care and Use of Laboratory Animals (Institute of Laboratory Animal Resources, National Research Council), and were approved by the Institutional Animal Care and Use Committees of the Uniformed Services University of the Health Sciences and the U.S. Army Medical Research Institute of Chemical Defense (Approval number APG-18-677). The animal care and use programs of both of the institutions are accredited by the Association for Assessment and Accreditation of Laboratory Animal Care International.

2.2. Soman Administration and Drug Treatment

Soman (pinacolyl methylphosphonofluoridate) was obtained from Edgewood Chemical Biological Center (Aberdeen Proving Ground, MD, USA); it was diluted in cold saline and administered via a single subcutaneous injection (132 μg/kg, 1.2 × LD_{50}). To alleviate the peripheral effects of soman we injected the rats with 2 mg/kg atropine sulfate (IM; Sigma-Aldrich, St. Louis, MO, USA), a muscarinic receptor antagonist, and 125 mg/kg HI-6 (IP; Starks Associates, Buffalo, NY, USA), a bispyridinium oxime that reactivates inhibited AChE, primarily in the periphery [41], within 1 min after injection of soman. One hour after the soman exposure, the rats were injected (IM) with either MDZ (5 mg/kg; Hospira Inc., Lake Forest, IL, USA) or LY293558 (10 mg/kg; kindly provided by Raptor Pharmaceutical Corp., Novato, CA, USA). In deciding the appropriate anticonvulsant dose to use, we aimed for the lowest dose that will completely stop seizure activity in less than 30 min (Figure S1), as high anticonvulsant doses may contribute to cardiorespiratory depression, particularly in an animal undergoing SE. In the present study, we did not use a group of rats that was exposed to soman but did not receive any anticonvulsant treatment because (1) we have obtained such data in previous studies [29,36–38,42–45] and, therefore, considered it unnecessary to have more animals experiencing prolonged, unalleviated SE; and (2) the focus of the present study was to compare the outcomes when soman-exposed rats are treated with LY293558 versus MDZ.

The rats, implanted with electrodes for electroencephalographic (EEG) recordings, were exposed to soman two weeks after the electrode implantation. After the exposure, all of the rats (electrode implanted and non-implanted) were injected with 5 mL Lactate Ringer's solution every 8 h for 24 h, which continued for another 24 h in the animals that had not completely recovered and appeared to need more hydration. The rats implanted with EEG electrodes were euthanized after the completion of 24 h of recording. For the evaluation of neuropathology and anxiety-like behavior, only the rats that were not implanted with electrodes were used, so as to avoid potential confounded variables (for example, additional stress in the electrode-implanted rats, arising from the presence of the headpiece and the electrodes, particularly during SE).

2.3. Electrode Implantation and EEG Recordings

The rats were anesthetized with isoflurane using a gas anesthesia system (Kent Scientific, Torrington, CT, USA), and five stainless steel, cortical screw electrodes were stereotaxically implanted, as previously described (Figure 1B) [29]. The video-EEG recordings were obtained in the freely-moving rats at a sampling rate of 200 Hz, using an EEG system (Stellate, Montreal, QC, Canada). The recordings were visually analyzed offline with the filters set to 0.3 Hz for the low frequency filter, 60 Hz for the notch filter, and 70 Hz for the high frequency filter, using the Harmonie Viewer 6.1e from Stellate (Montreal). The EEG recordings were obtained starting 1 to 2 h before the soman exposure and continuing for another 24 h after the soman injection. The disappearance of large amplitude, repetitive discharges (>1 Hz with at least double the amplitude of the background activity) was considered to be evidence of cessation of SE.

2.4. Preparation of Brain Sections

The neuropathological analysis was performed in the basolateral amygdala (BLA), 30 days after the exposure. The rats were deeply anesthetized with pentobarbital (75–100 mg/kg, i.p.) and transcardially perfused with PBS (100 mL), followed by 4% paraformaldehyde (200 mL). The brains were removed and placed in 4% paraformaldehyde, overnight at 4 °C, for post-fixation. The next day, the brains were transferred to a solution of 30% sucrose in PBS for 72 h, and frozen with dry ice before storage at −20 °C, until sectioning. A one-in-five series of sections (for every five sections cut in series, one was kept), starting from the rostral extent of the amygdala, were cut at 40 μm on a sliding microtome and mounted on Superfrost Plus slides (Daigger, Vernon Hills, IL, USA). Two adjacent sections from every

five were used, one for Nissl staining with Cresyl Violet and one for immunohistochemical labeling for GAD-67. The neuropathological evaluation was completed in a blind fashion.

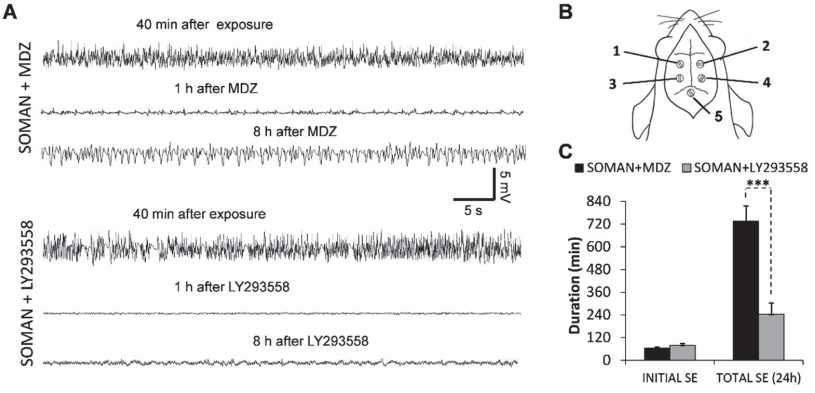

Figure 1. Intramuscular administration of midazolam (MDZ) or LY293558 stopped soman-induced SE within less than 30 min of administration, but seizures reoccurred significantly more in the MDZ-treated group. MDZ (5 mg/kg) or LY293558 (10 mg/kg) were administered at 1 h after injection of soman (1.2 × LD_{50}). Representative EEG traces at 40 min after soman exposure, as well as at 1 h and 8 h after administration of MDZ or LY293558 are shown in (**A**). Notice the persistence of low-amplitude epileptiform activity and the return of seizures in the MDZ-treated rats, but not in the LY293558-treated rats. Electrode placement for the recordings is shown diagrammatically in (**B**) (one, two, three, and four, parietal electrodes; five, cerebellar reference electrode). The group data in (**C**) show the duration of the initial SE in each of the two groups and the total duration of SE throughout the 24 h period after soman exposure (*** $p < 0.001$, Independent Samples *t*-test). Sample sizes are n = eight for each of the two groups.

2.5. GAD-67 Immunohistochemistry

Our GAD-67 immuno-labeling procedure was previously described [36,44]. The sections were collected from the cryoprotectant solution, washed three times for 5 min each in 0.1 M PBS, and then kept for 1 h in a solution containing 10% normal goat serum (Chemicon, CA, USA) and 0.5% Triton X-100 in PBS, at room temperature. The sections were then incubated with mouse anti-GAD-67 serum (1:1000, MAB5406; Chemicon), 5% NGS, 0.3% Triton X-100, and 1% bovine serum albumin, overnight at 4 °C. After rinsing three times for 10 min each in 0.1% Triton X-100 in PBS, the sections were incubated with Cy3-conjugated goat anti-mouse antibody (1:1000; Jackson ImmunoResearch, West Grove, PA, USA) and 0.0001% DAPI (Sigma, St. Louis, MO, USA) in PBS, for 1 h at room temperature. Subsequently, the sections were rinsed in PBS for 10 min, mounted on slides, air dried for 30 min, and cover-slipped with ProLong Gold antifade reagent (Invitrogen, Waltham, MA, USA).

2.6. Estimation of Neuronal and Interneuronal Loss

Design-based stereology was used to quantify the total number of neurons in the Nissl-stained sections, and the interneurons in the GAD-67 immuno-stained sections, in the BLA, as previously described [36,44]. The sections were viewed with a Zeiss Axioplan 2ie fluorescent microscope (Oberkochen, Germany), equipped with a motorized stage, and interfaced with a computer running StereoInvestigator 8.0 (MicroBrightField, Williston, VT, USA). The BLA was identified under a 2.5× objective on slide-mounted sections, using as the reference the atlas of Paxinos and Watson, 2005 [46]. All of the counting was completed under a 63× oil immersion objective. The total number of Nissl-stained and GAD-67-immunostained neurons was estimated, using the optical fractionator probe, and, along with the coefficient of error (CE), were calculated using the Stereo Investigator 8.0

(MicroBrightField, Williston, VT, USA). The CE was calculated by the software, according to the Gundersen (m = 1; [47]) and Schmitz–Hof (second estimation; [48]) equations.

To determine the number of Nissl-stained neurons in the BLA, one section in a series of five sections was analyzed (seven sections were used on average from each rat). The counting frame was 35 × 35 µm, the counting grid was 190 × 190 µm, and the dissector height was 12 µm. The nuclei were counted when the cell body came into focus within the dissector, which was placed 2 µm below the section surface. The section thickness was measured at every counting site, and the average mounted section thickness was 20 µm. An average of 345 neurons per rat was counted, and the average CE was 0.05 for both the Gundersen and Schmitz–Hof equations.

To determine the number of neurons immuno-labeled for GAD-67, one section in a series of 10 sections was analyzed (on average, five sections from each rat). The counting frame was 60 × 60 µm, the counting grid was 100 × 100 µm, and the dissector height was 20 µm. The nuclei were counted when the top of the nucleus came into focus within the dissector, which was placed 2 µm below the section surface. The section thickness was measured at every fifth counting site, and the average mounted section thickness was 27 µm. An average of 235 neurons per rat was counted, and the average CE was 0.08 for both the Gundersen and Schmitz–Hof equations.

2.7. Electrophysiological Experiments

The procedures followed to obtain the whole-cell recordings from the BLA have been previously described [49]. The rats were anesthetized with isoflurane before decapitation. The coronal brain slices (400 µm-thick) containing the amygdala were cut in ice-cold solution (consisting in mM: 115 sucrose; 70 NMDG; 1 KCl; 2 $CaCl_2$; 4 $MgCl_2$; 1.25 NaH_2PO_4; 30 $NaHCO_3$; 25 d-glucose) with the use of a vibratome (Leica VT 1200 S; Leica Microsystems, Buffalo Grove, IL, USA). The slices were transferred to a holding chamber at room temperature, in a bath solution containing (in mM): 125 NaCl; 2.5 KCl; 1.25 NaH_2PO_4; 21 $NaHCO_3$; 2 $CaCl_2$; 1 $MgCl_2$; and 11 D-glucose. The recording solution (artificial cerebrospinal fluid; ACSF) was the same as the holding bath solution. All of the solutions were saturated with 95% O_2/5% CO_2 to achieve a pH near 7.4. The recording chamber (0.7 mL capacity) had continuously flowing ACSF (~8 mL/min) at 30 to 31 °C. The osmolarity of the ACSF was adjusted to 325 mOsm with D-glucose.

To visualize the neurons in the BLA, we used a 40× water immersion objective equipped with a CCD-100 camera (Dage-MTI, Michigan City, IN, USA), under infrared light, using Nomarski optics of an upright microscope (Zeiss Axioskop 2, Thornwood, NY, USA). The recording electrodes had resistances of 3.5~4.5 MΩ when filled with the internal solution (in mM): 60 $CsCH_3SO_3$; 60 KCH_3SO_3; 5 KCl; 10 EGTA; 10 HEPES; 5 Mg-ATP; 0.3 Na_3GTP (pH 7.2; osmolarity was adjusted to 290 mOsm with potassium gluconate). Tight-seal (over 1 GΩ) whole-cell recordings were obtained from the cell body of the principal neurons, distinguished from the interneurons by their larger size, pyramidal shape, and electrophysiological characteristics [49–52]. Access resistance (5~24 MΩ) was regularly monitored during the recordings, and the cells were rejected if the resistance changed by more than 15% during the experiment.

The currents were amplified and filtered (1 kHz) using the Axopatch 200B amplifier (Axon Instruments, Foster City, CA, USA) with a four-pole, low-pass Bessel filter, digitally sampled (up to 2 kHz) using the pClamp 10.5 software (Molecular Devices, Sunnyvale, CA, USA), and subsequently analyzed using the Mini Analysis program (Synaptosoft Inc., Fort Lee, NJ, USA) and Origin (OriginLab Corporation, Northampton, MA, USA).

2.8. Behavioral Experiments

Anxiety-like behavior in the open field and the responses to acoustic startle were examined 30 days after soman exposure. The behavioral tests used were previously described [44,51]. The open field apparatus consisted of a clear Plexiglas arena (40 × 40 × 30 cm). One day prior to testing (on day 29 after soman exposure), the animals were acclimated to the apparatus

for 20 min. On the test day, the rats were placed in the center of the open field, and activity was measured and recorded for 20 min, using an Accuscan Electronics infrared photocell system (Accuscan Instruments Inc., Columbus, OH, USA). The automatic collection of the data was completed with a computer equipped with Fusion software (Accuscan). Locomotion (distance traveled in cm), total movement time, and time spent in the center of the open field were analyzed. Anxiety-like behavior was measured as the ratio of the time spent in the center over the total movement time, expressed as a percentage of the total movement time.

The responses to acoustic startle were assessed, using the Med Associates Acoustic Response Test System (Med Associates, Georgia, VT, USA). This system consists of weight-sensitive platforms inside individual sound-attenuating chambers, and includes a ventilating fan to provide background noise. Each rat was individually placed in a ventilated holding cage. The holding cages were small enough to restrict extensive locomotion, but large enough to allow the subject to turn around and make other small movements. Each cage was placed on a weight-sensitive platform. Movements in response to acoustic stimuli were measured as a voltage change by a strain gauge inside each platform. The rats were placed in the apparatus for two sessions, on post-soman days 28 and 29, for acclimation. The startle stimuli consisted of 110- or 120 dB noise bursts (burst duration 20 ms). Each stimulus had a 2 ms rise and decay time, such that the onset and offset were abrupt, which is a primary requirement for startle. Each trial type (110 dB or 120 dB stimulus) was presented eight times. The trial types were presented in random order to avoid effects and habituation, and the inter-trial intervals ranged randomly from 15 to 25 s. An interfaced Pentium computer, with the Med Associates software, recorded startle amplitude as the difference between the maximal voltage change during the startle period and the maximal voltage change during the no-stimulus periods, and assigned a value based on an arbitrary scale used by the software of the test system.

2.9. Statistical Analysis

A Fisher exact test was used to compare the survival rate between the two soman-exposed groups treated with MDZ or LY293558. The other variables of the study were tested for normal distribution, using the Kolgomorov–Smirnov normality test, and all of the results showed a normal distribution ($p > 0.05$). Thus, the Independent Samples *t*-test was used to determine whether there were significant differences between the two groups (treated with MDZ or LY293558) in the time it took for cessation of seizures after anticonvulsant administration, the duration of the initial SE, and the total duration of SE within 24 h after soman exposure. Before comparing the differences between the three groups (soman-exposed group treated with MDZ, soman-exposed group treated with LY293558, and control group not exposed to soman) using analysis of variance (ANOVA), we tested for homogeneity of the variances between the groups, using Levene's test. The only variable that showed unequal variances ($p = 0.0002$) was the "Total Charge transferred by sIPSCs" (in the electrophysiological experiments); therefore, we used Welch's ANOVA followed by Games–Howell post hoc test for comparisons of these results. The ANOVA followed by the Bonferroni post hoc test was used to compare stereological estimations of the total number of neurons and interneurons, and ANOVA followed by Holm–Šídák was used to compare the results from the behavioral tests. The statistical values are presented as mean and standard error of the mean. For all of the tests, differences were considered significant when $p < 0.05$. The sample sizes (n) refer to the number of animals, except for the in vitro experiments, where n refers to the number of recorded neurons.

3. Results

3.1. Seizure Termination by MDZ or LY293558 and Survival Rates

The male rats implanted with electrodes for monitoring electrographic seizure activity were exposed to soman; the rats were treated with atropine and HI-6 within 1 min after the soman injection, and were administered 5 mg/kg MDZ ($n = 10$, SOMAN + MDZ group) or

10 mg/kg LY293558 (n = 11, SOMAN + LY293558 group), 1 h later. The status epilepticus (SE) developed within an average of 9 min after the injection of soman (8.75 ± 0.79 and 9.25 ± 0.75 min for the SOMAN + MDZ and the SOMAN + LY293558 group, respectively). The seizures were completely suppressed within 19.75 ± 1.8 min after administration of the MDZ, and within 29.5 ± 1.75 min after administration of the LY293558 (significantly longer in the LY293558 group, p = 0.0017). Thus, the duration of the initial SE (the SE triggered by soman injection and ceased by anticonvulsant administration) was 65 ± 5 min in the SOMAN + MDZ group and 80 ± 9 min in the SOMAN + LY293558 group (p = 0.0729, n = eight in each group; two rats in the MDZ group and three rats in the LY293558 group died during SE). Monitoring the seizure activity for 24 h after the soman exposure revealed that SE returned after administration of either MDZ or LY293558, but to a significantly greater extent in the MDZ-treated group (representative samples of EEG activity at different time points after soman exposure are shown in Figure 1A). Thus, the total duration of SE within the 24 h post-exposure period was 735 ± 80 min in the SOMAN + MDZ group and 244 ± 59 min in the SOMAN + LY293558 group (p = 0.0002; Figure 1C).

Among the animals implanted with electrodes, the 24 h survival rate was 80% (8/10) in the SOMAN + MDZ group and 72.7% (8/11) in the SOMAN + LY293558 group (Fisher exact probability test p = 0.77). However, the survival rate among the animals not implanted with electrodes was 100% in both the SOMAN + MDZ and the SOMAN + LY293558 group. The results are summarized in Table 1.

Table 1. Effects of MDZ (5 mg/kg, i.m) or LY293558 (10 mg/kg, i.m) on soman-induced status epilepticus (SE) and survival rate, when the anticonvulsants are administered 1 h after soman exposure.

Experimental Groups	SOMAN + MDZ	SOMAN + LY293558
Time to cessation of the initial SE (min)	19.75 ± 1.8	29.5 ± 1.75 **
Duration of the initial SE (min)	65 ± 5	80 ± 5.9
Total duration of SE in 24 h (min)	735 ± 80	244 ± 59 ***
Survival rate: electrode-implanted rats	80% (8/10)	72.7% (8/11)
Survival rate: non-implanted rats	100% (11/11)	100% (11/11)

** $p < 0.01$, significantly longer compared with the MDZ group; *** $p < 0.001$, significantly shorter compared with the MDZ group (Independent Samples t-test).

3.2. LY293558 but Not MDZ Provides Full Protection against Neuronal and Interneuronal Loss in the BLA

Only the rats that were not implanted with EEG electrodes were used for neuropathology and behavioral testing. Thirty days after soman exposure, the total number of neurons in the BLA was estimated, using an unbiased stereological method in the Nissl-stained sections. The BLA was selected to study both the pathology and pathophysiology because this amygdala nucleus plays a central role in seizure initiation and propagation after nerve agent exposure [53–55], and the amygdala is one of the brain regions where nerve agents cause the most severe neuropathology [42].

The number of neurons in the BLA of the SOMAN + MDZ group (71,771 ± 3980; n = 8) was significantly lower than the number of neurons in the BLA of the SOMAN + LY293558 group (97,305 ± 5872; n = 8; p = 0.003) and a control group that was not exposed to soman (98,587 ± 4287; n = 8; p = 0.002; Figure 2). The number of neurons in the SOMAN + LY293558 group did not differ from the control (p = 0.9).

The estimation of the total number of GABAergic interneurons in the BLA, using an unbiased stereological method on the GAD-67 immuno-stained sections, showed that thirty days after soman exposure the number of interneurons in the BLA of the SOMAN + MDZ group (9125 ± 597, n = 8) was significantly lower than that in the SOMAN + LY293558 group (14,466 ± 1070, n = 8; $p < 0.01$) and a control group that was not exposed to soman (14,657 ± 1.281, n = 8; $p < 0.01$; Figure 3). The ratio of the GABAergic interneurons to the total number of neurons was also significantly lower in the SOMAN + MDZ group

(12.7% ± 0.3), compared to either the SOMAN + LY293558 group (14.86% ± 0.47, $p < 0.01$), or the control group (14.86% ± 0.45, $p < 0.01$; Figure 3). The number of interneurons and the ratio of interneurons to the total number of neurons in the BLA of the SOMAN + LY293558 group did not differ from the control ($p = 0.9$).

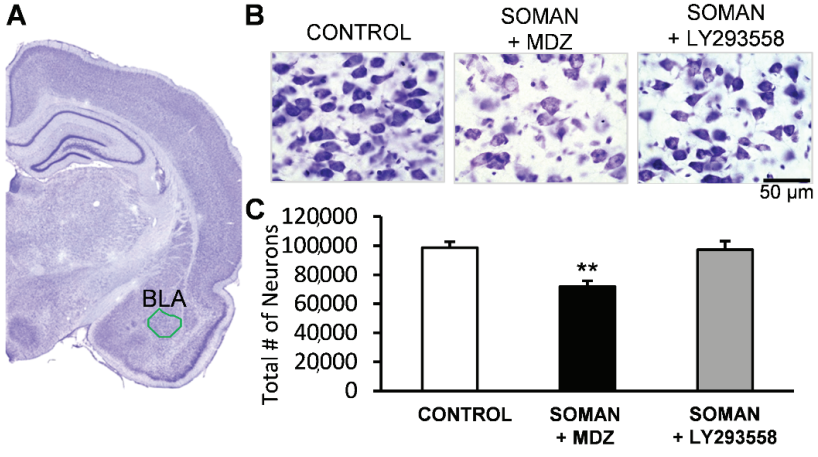

Figure 2. Thirty days after soman exposure, there was significant neuronal loss in the BLA of the MDZ-treated group but not the LY293558-treated group. (**A**) Panoramic view of a Nissl-stained section showing the area where neuronal loss was assessed; (**B**) Representative photomicrographs from a control (not exposed) rat and an MDZ- or LY293558-treated soman-exposed rat (total magnification 630×; scale bar, 50 µm); (**C**) Group data; sample sizes: $n = 8$ for each group; ** $p < 0.01$ compared with either the control or the SOMAN + LY293558 group (ANOVA, Bonferroni post hoc test).

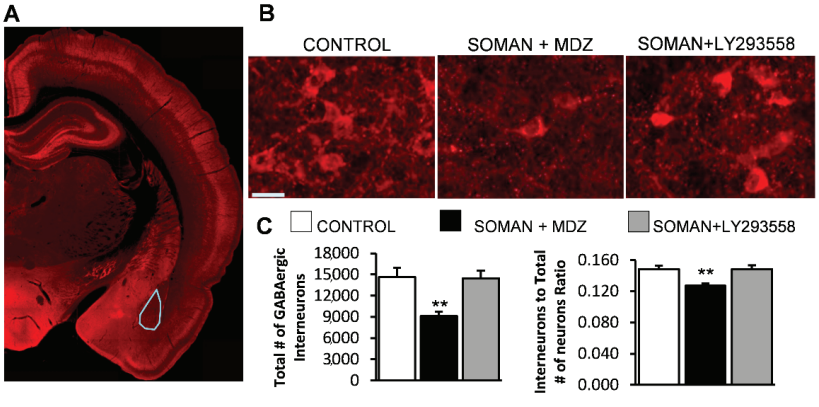

Figure 3. Thirty days after soman exposure, there was significant loss of GABAergic interneurons in the BLA of the MDZ-treated group but not the LY293558-treated group. (**A**) Panoramic view of a GAD-67 immuno-stained section showing the area where interneuronal loss was assessed; (**B**) Representative photomicrographs of GAD-67 immuno-stained interneurons in the BLA from a control (not exposed) rat and an MDZ- or LY293558-treated soman-exposed rat (total magnification 630×; scale bar, 50 µm); (**C**) Group data of the total number of GABAergic interneurons (left panel) and the ratio of the number of GABAergic interneurons to the total number of neurons (right) for the two experimental groups and a control group. Sample sizes: $n = 8$ for each group; ** $p < 0.01$ compared with either the control or the SOMAN + LY293558 group (ANOVA, Bonferroni post hoc test).

3.3. LY293558 but Not MDZ Prevents a Reduction of Background Inhibition in the BLA

We have previously shown that, along with the loss of interneurons in the BLA after soman-induced SE that is not treated with an anticonvulsant [36,44], there is a reduction in the background inhibitory activity [45]. Therefore, we investigated whether the treatment of soman-exposed rats with MDZ or LY293558 prevented a reduction in the spontaneous IPSCs in the BLA.

In the BLA of the control rats (not exposed to soman), the principal/pyramidal neurons generated synchronous "bursts" of $GABA_A$ receptor-mediated IPSCs (in 12 out of 14 neurons; Figure 4A), which is consistent with previous reports [49,56–58]. In the rats exposed to soman and treated with MDZ, this rhythmic synchronous inhibitory activity was absent at 30 days after exposure, in all of the recorded neurons (n = 14; Figure 4B). In contrast, the soman-exposed rats treated with LY293558, displayed bursts of sIPSCs (Figure 4C) in six out of eight neurons. To quantify the differences between the groups we calculated the total charge transferred (the area delimited by the inhibitory current and the baseline) in picocoulombs (pC), for a time window of 10 s; we included all of the recorded neurons in these comparisons, whether they generated rhythmic sIPSC bursts or displayed only conventional spontaneous inhibitory activity. The total charge transferred by the sIPSCs in the SOMAN + MDZ group (135.61 ± 22.18 pC; n = 14) was significantly different from that in the SOMAN + LY293558 group (883.45 ± 210.29; n = 8; $p < 0.001$) and a control group that was not exposed to soman (897.27 ± 139.36 pC; n = 14; Figure 4D). The total charge transferred by the sIPSCs in the SOMAN + LY293558 group did not differ from the control (p = 0.12).

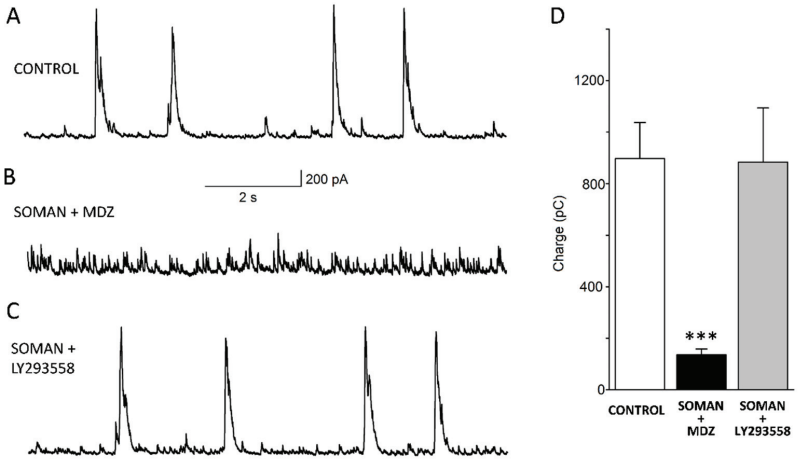

Figure 4. Thirty days after soman exposure, spontaneous inhibitory activity was reduced in the BLA of the MDZ-treated group but not the LY293558-treated group. Representative $GABA_A$ receptor-mediated sIPSC current traces recorded from BLA principal neurons from a control rat (**A**) and from soman-exposed rats treated with MDZ (**B**) or LY293558 (**C**). Recordings were obtained at +30 mV holding potential; (**D**) Group data of charge transferred by sIPSCs, during a 10 s time window. *** $p < 0.001$ when inhibitory activity of neurons from the MDZ-treated group (n = 14) is compared with the inhibitory activity in either the control (n = 14) or the LY293558-treated group (n = 8; Welch's ANOVA followed by Games–Howell post hoc test).

3.4. LY293558 but Not MDZ Prevents an Increase in Anxiety-like Behavior

To investigate whether the neuropathology observed in the BLA of the MDZ-treated rats and the reduction in spontaneous inhibitory activity had translated into behavioral deficits, we examined anxiety-like behavior with the use of two tests, the open field [59] and the acoustic startle response (ASR; [60]). Thirty days after the soman exposure,

the SOMAN + MDZ group spent significantly less time in the center of the open field (6.3 ± 0.9% of the total movement time, n = 8), when compared with either the SOMAN + LY293558 group (12.1 ± 1.2 % of the total movement time, n = 8) or a control group which was not exposed to soman (13.8 ± 0.95 % of the total movement time, n = 8; $p < 0.001$ for both comparisons; Figure 5A). The time spent in the center for the SOMAN + LY293558 group did not differ from the control (p = 0.5). The distance traveled in the open field did not differ between the control rats (2530 ± 330 cm) and the SOMAN + MDZ (2580 ± 290 cm) or the SOMAN + LY293558 (2189 ± 300 cm) treated groups (p = 0.6; Figure 5B).

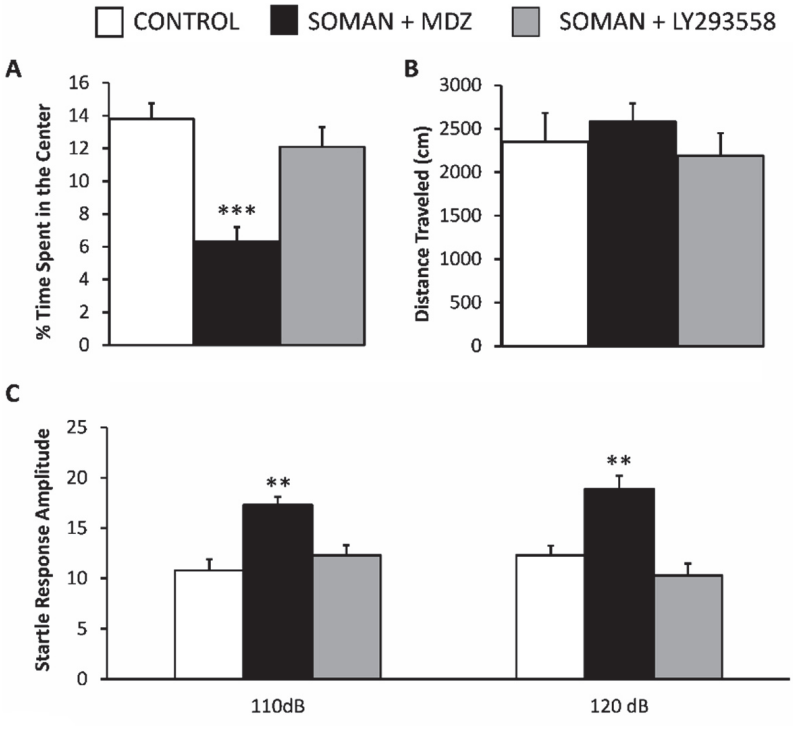

Figure 5. Thirty days after soman exposure, anxiety-like behavior was increased in the MDZ-treated group but not the LY293558-treated group. (**A**) Percentage of time spent in the center of the open field; (**B**) Distance traveled in the open field; (**C**) Amplitude of startle responses to 110- and 120-db acoustic stimuli. Sample sizes: n = 8 for each group. Control group is rats not exposed to soman. ** $p < 0.01$, *** $p < 0.01$ (One-Way ANOVA with Holm-Šídák post hoc test).

In the acoustic startle response test, the startle amplitude in response to the 110 dB acoustic stimulus was significantly greater in the SOMAN + MDZ group (17.3 ± 0.8, n = 8) compared with either the SOMAN + LY293558 group (12.3 ± 1, n = 8) or the control group that was not exposed to soman (10.8 ± 1.1, n = 8; $p < 0.01$ for both comparisons; Figure 5C, left set of bars). Similarly, the startle amplitude in response to the 120 dB acoustic stimulus was significantly greater in the SOMAN + MDZ group (18.9 ± 1.3, n = 8) than in the SOMAN + LY293558 group (10.3 ± 1.2, n = 8) or the control group that was not exposed to soman (12.3 ± 0.95, n = 8; $p < 0.01$ for both comparisons; Figure 5C, right set of bars). The startle amplitude in the SOMAN + LY293558 group in response to either 110 or 120 dB did not differ from the control (p = 0.53 and p = 0.45 for the 110 and 120 dB, respectively).

4. Discussion

In this study, we compared the efficacy of MDZ—a benzodiazepine commonly used in the treatment of SE and currently considered by the FDA for approval as a better alternative to DZP for the control of nerve agent-induced SE—with the efficacy of an AMPA/GluK1 receptor antagonist, LY293558 [35], in suppressing seizures and protecting the brain in adult male rats exposed to soman. We found that both MDZ and LY293558 promptly stopped the initial SE, with MDZ suppressing seizures significantly faster than LY293558. In addition, both of the anticonvulsant treatments produced a 100% survival rate. However, the seizures reoccurred significantly more in the MDZ-treated rats; as a result, the total duration of SE in the 24 h period after soman exposure was significantly longer in the MDZ-treated group compared with the LY293558-treated group. Furthermore, when the brain damage was examined 30 days later, it was found that in the BLA of the MDZ-treated group there was a significant loss of interneurons and a reduced total number of neurons. The neuronal and interneuronal loss in the BLA of the MDZ-treated rats was accompanied by reduced GABAergic inhibition and loss of rhythmic GABAergic activity, as well as increased anxiety-like behavior. Such alterations had not occurred in the group treated with LY293558, in which the number of neurons and interneurons in the BLA, GABAergic inhibition, and anxiety-like behavior did not differ from the control rats that were not exposed to soman.

A significant reoccurrence of the seizures after cessation of SE by administration of a benzodiazepine was previously observed in both animals [6,29,30,61] and humans [23,62]. In the present study, the average total duration of SE in the MDZ-treated group within 24 h after soman exposure was 735 min, which is nearly identical to the average duration of SE in same-age male rats exposed to the same dose of soman as in the present study, but without receiving anticonvulsant treatment (609 min total duration of SE; [43]). A plausible explanation for the return of SE after a prompt but transient cessation by MDZ or DZP may be based on the weakening of the GABAergic inhibition. Intense seizure activity induces the internalization of postsynaptic $GABA_A$ receptors [63–66]; this may be caused by the excess GABA being released during synaptic hyperactivity [65,67], and/or mechanisms related to intense NMDA receptor activation [68,69]. When a benzodiazepine is administered, the activity of the $GABA_A$ receptors may be enhanced sufficiently to halt seizures. However, the availability of the $GABA_A$ receptors is progressively reduced, making these drugs ineffective in sustaining enhanced synaptic inhibition, even more so as they are cleared from the blood. Therefore, glutamatergic hyperexcitability overrides and seizures reoccur.

A reduction in the total number of neurons and a loss of interneurons in the BLA was found in the MDZ-treated group; this is consistent with a previous study in which the extent of the neuropathology in soman-exposed rats who received DZP treatment 1 h after exposure was virtually the same as in the soman-exposed group that did not receive anticonvulsant treatment [29]. The limited or absent neuroprotective efficacy of MDZ has been previously reported, and the timing of MDZ administration appears to be important in this regard. Thus, MDZ protects against nerve agent- or other organophosphate-induced neuropathology in adult or young-adult rats, if it is administered at the time of exposure [70], or at the onset of seizures [71], or after 5 min of seizure activity [72], but not if it is given at 1 h [70,73], 30 min, or 2 h after SE onset [73]. Therefore, it is commonly presumed that the brain damage that is seen when the anticonvulsant administration is delayed is caused primarily by the SE that occurred before the anticonvulsant administration [70,73]; this seems to be a reasonable assumption, particularly if the SE was severe. However, our results suggest that SE lasting up to 1 h does not necessarily produce long-term brain damage, and that the outcome may significantly depend on whether or not the type of the anticonvulsant used can limit the total duration of SE. Thus, in the present study, both MDZ and LY293558 were administered after about 50 min of ongoing SE, both of the anticonvulsants completely suppressed seizures in less than 30 min, but only LY293558 protected from brain damage (at least at the 30-day time point that we examined). In previous studies in immature rats exposed to soman, in which DZP, LY293558, or LY293558 + caramiphen were

administered 1 h after soman exposure, all three treatments promptly stopped the initial SE, but only LY293558 and LY293558 + caramiphen protected against brain damage [31]. Similarly, when DZP or UBP302 was administered 1 h after the exposure of adult rats to soman, UBP302 took significantly longer than DZP to stop the initial SE, and yet only UBP302 provided significant neuroprotection [29]. The main observation that is common among these studies is that the seizures reoccurred to a dramatically increased extent after the benzodiazepine treatment. Taken together, these findings suggest that the most important factor determining the extent of the brain damage is the total duration of the SE. The extent of neuroprotection may also depend on the mechanisms of action of the administered anticonvulsant, which may halt the pathological processes triggered by the initial SE, or allow them to progress unopposed.

The reduction in the GABAergic interneurons and total number of neurons in the BLA of the MDZ-treated rats, and the decreased ratio of the number of interneurons to the total number of neurons, were accompanied by a reduction in the spontaneous inhibitory activity. Remarkably, there was a loss of the spontaneous "bursts" of $GABA_A$ receptor-mediated IPSCs that are typically generated by the principal neurons in the BLA, in an oscillatory fashion, at an average frequency of 0.5 Hz [49,56–58]. This synchronous, rhythmic inhibitory activity, which was found to be triggered by the rhythmic burst firing of the interneurons dependent on the GluN2A-NMDA receptors [49] and ASIC1a channels [58], may play an important role in the oscillatory activity patterns generated by the BLA network; these have been associated with cognitive and emotional functions, such as the perception of safety [74,75], and the expression of fear [76]. Therefore, the loss of this inhibitory bursting in the BLA of the MDZ-treated rats may have implications for cognitive and/or emotional behavior. Accordingly, in the present study, the MDZ-treated group displayed increased anxiety-like behavior. The level of increase in anxiety in the MDZ-treated rats, as determined with the use of the open field and the acoustic startle response tests (6.3% of total movement time was spent in the center of the open field, while the average startle amplitude was about 18), is almost identical to that obtained from same-age male rats exposed to the same dose of soman as in the present study, but without receiving anticonvulsant treatment (6.7% of total movement time was spent in the center of the open field and the average startle amplitude was about 18; [37]), indicating the minimal neuroprotective effects of this drug.

5. Conclusions

In the event of a mass exposure to nerve agents, there will likely be a delay before the victims are under medical care and monitoring. The administration of MDZ with some delay after the onset of SE can be expected to save lives by controlling the initial SE, but it will not protect against brain damage and long-term morbidity. Perhaps a higher dose of MDZ, or repeated injections of MDZ to suppress the reoccurrence of seizures —thus limiting the total duration of SE—could have a better outcome on neuroprotection, but clinical experience clearly points to the need for anticonvulsants other than MDZ or DZP for the long-term management of SE. Furthermore, if the victims of nerve agent exposure are very young, when the GABAergic system in the brain is still immature and $GABA_A$ receptor activation may produce depolarization [77–79], MDZ administration could be detrimental [80]. The glutamate receptor antagonists, such as LY293558, do not only stop the initial SE and decrease mortality rate, but also provide significant protection against brain damage. Assessment of brain damage at longer post-exposure time points (beyond 30 days after soman exposure) will confirm whether the neuroprotection by LY293558 after acute nerve agent exposure can be considered lifelong.

Supplementary Materials: The following supporting information can be downloaded at: https://www.mdpi.com/article/10.3390/toxics10080409/s1, Figure S1: Dose-response graphs showing the time to cessation of SE after administration of different doses of midazolam (MDZ) or LY293558.

Author Contributions: Conceptualization, M.F.M.B. and V.A.-A.; Methodology, M.F.M.B. and V.A.-A.; Investigation, T.H.F., V.I.P. and J.P.A.; Formal Analysis, T.H.F. and V.I.P.; Validation, M.F.M.B. and V.A.-A.; Resources, M.F.M.B. and J.P.A.; Data Curation, T.H.F., V.I.P., V.A.-A. and M.F.M.B.; Project administration, M.F.M.B., J.P.A. and V.A.-A.; Supervision, M.F.M.B. and V.A.-A.; Writing—Original Draft Preparation, V.A.-A.; Writing—Review and Editing, V.A.-A., M.F.M.B., T.H.F. and J.P.A.; Funding Acquisition, M.F.M.B. and V.A.-A. All authors have read and agreed to the published version of the manuscript.

Funding: This research was supported by the CounterACT Program, National Institutes of Health, Office of the Director and the National Institute of Neurologic Disorders and Stroke (Grant Number 5R21NS094131-02 and 1U01NS102135-01A1).

Institutional Review Board Statement: The experiments performed followed the Guide for the Care and Use of Laboratory Animals (Institute of Laboratory Animal Resources, National Research Council), and were approved by the Institutional Animal Care and Use Committees of the Uniformed Services University of the Health Sciences and the U.S. Army Medical Research Institute of Chemical Defense. The animal care and use programs of both institutions are accredited by the Association for Assessment and Accreditation of Laboratory Animal Care International. The views expressed are those of the authors and do not reflect the official policy or position of the Uniformed Services University of the Health Sciences, the Department of Defense, or the United States government.

Data Availability Statement: The data that support the findings of this study are available from the corresponding author upon reasonable request.

Conflicts of Interest: The authors declare no conflict of interest.

Abbreviations

BLA, basolateral amygdala; DZP, diazepam; LY293558, (3S,4aR,6R,8aR)-6-[2-(1(2)H-tetrazole-5-yl)ethyl]decahydroisoquinoline-3-carboxylic acid; HI-6, (1-(2-hydroxyiminomethylpyridinium)-3-(4-carbamoylpyridinium)-2-oxapropane dichloride; MDZ, midazolam; SE, status epilepticus.

References

1. Aroniadou-Anderjaska, V.; Apland, J.P.; Figueiredo, T.H.; de Araujo Furtado, M.; Braga, M.F. Acetylcholinesterase inhibitors (nerve agents) as weapons of mass destruction: History, mechanisms of action, and medical countermeasures. *Neuropharmacology* **2020**, *181*, 108298. [CrossRef]
2. Hulse, E.J.; Davies, J.O.; Simpson, A.J.; Sciuto, A.M.; Eddleston, M. Respiratory complications of organophosphorus nerve agent and insecticide poisoning. Implications for respiratory and critical care. *Am. J. Respir. Crit. Care Med.* **2014**, *190*, 1342–1354. [CrossRef]
3. Aroniadou-Anderjaska, V.; Figueiredo, T.H.; Apland, J.P.; Prager, E.M.; Pidoplichko, V.I.; Miller, S.L.; Braga, M.F. Long-term neuropathological and behavioral impairments after exposure to nerve agents. *Ann. N. Y. Acad. Sci.* **2016**, *1374*, 17–28. [CrossRef]
4. Lallement, G.; Dorandeu, F.; Filliat, P.; Carpentier, P.; Baille, V.; Blanchet, G. Medical management of organophosphate-induced seizures. *J. Physiol.* **1998**, *92*, 369–373. [CrossRef]
5. McDonough, J.H.; Shih, T.M. Pharmacological modulation of soman-induced seizures. *Neurosci. Biobehav. Rev.* **1993**, *17*, 203–215. [CrossRef]
6. Shih, T.M.; McDonough, J.H. Organophosphorus nerve agents-induced seizures and efficacy of atropine sulfate as anticonvulsant treatment. *Pharmacol. Biochem. Behav.* **1999**, *64*, 147–153. [CrossRef]
7. Shih, T.M.; McDonough, J.H.; Koplovitz, I. Anticonvulsants for soman-induced seizure activity. *J. Biomed. Sci.* **1999**, *6*, 86–96. [CrossRef] [PubMed]
8. Skovira, J.W.; McDonough, J.H.; Shih, T.M. Protection against sarin-induced seizures in rats by direct brain microinjection of scopolamine, midazolam or MK-801. *J. Mol. Neurosci.* **2010**, *40*, 56–62. [CrossRef] [PubMed]
9. Lallement, G.; Carpentier, P.; Collet, A.; Pernot-Marino, I.; Baubichon, D.; Sentenac-Roumanou, H.; Blanchet, G. Involvement of glutamatergic system of amygdala in generalized seizures induced by soman: Comparison with the hippocampus. *C. R. Acad. Sci. III.* **1991**, *313*, 421–426.
10. Miller, S.L.; Aroniadou-Anderjaska, V.; Pidoplichko, V.I.; Figueiredo, T.H.; Apland, J.P.; Krishnan, J.K.S.; Braga, M.F. The M1 muscarinic receptor antagonist VU0255035 delays the development of status epilepticus after organophosphate exposure and prevents hyperexcitability in the basolateral amygdala. *J. Pharmacol. Exp. Ther.* **2017**, *360*, 23–32. [CrossRef]
11. Williamson, J.; Singh, T.; Kapur, J. Neurobiology of organophosphate-induced seizures. *Epilepsy Behav.* **2019**, *101*, 106426. [CrossRef] [PubMed]

12. McDonough, J.H.; Shih, T.M. Neuropharmacological mechanisms of nerve agent-induced seizure and neuropathology. *Neurosci. Biobehav. Rev.* **1997**, *21*, 559–579. [CrossRef]
13. Deshpande, L.S.; Carter, D.S.; Phillips, K.F.; Blair, R.E.; DeLorenzo, R.J. Development of status epilepticus, sustained calcium elevations and neuronal injury in a rat survival model of lethal paraoxon intoxication. *Neurotoxicology* **2014**, *44*, 17–26. [CrossRef]
14. Shih, T.M.; Duniho, S.M.; McDonough, J.H. Control of nerve agent-induced seizures is critical for neuroprotection and survival. *Toxicol. Appl. Pharmacol.* **2003**, *188*, 69–80. [CrossRef]
15. Campo-Soria, C.; Chang, Y.; Weiss, D.S. Mechanism of action of benzodiazepines on $GABA_A$ receptors. *Br. J. Pharmacol.* **2006**, *148*, 984–990. [CrossRef]
16. Gielen, M.C.; Lumb, M.J.; Smart, T.G. Benzodiazepines modulate $GABA_A$ receptors by regulating the preactivation step after GABA binding. *J. Neurosci.* **2012**, *32*, 5707–5715. [CrossRef]
17. Olkkola, K.T.; Ahonen, J. Midazolam and other benzodiazepines. In *Modern Anesthetics*; Handbook of Experimental, Pharmacology; Schüttler, J., Schwilden, H., Eds.; Springer: Berlin/Heidelberg, Germany, 2008; pp. 335–360.
18. Cherian, A.; Thomas, S.V. Status epilepticus. *Ann. Indian Acad. Neurol.* **2009**, *12*, 140–153.
19. Rogalski, R.; Rogalski, A. Benzodiazepine selection in the management of status epilepticus: A review. *Adv. Emerg. Nurs. J.* **2015**, *37*, 83–94. [CrossRef]
20. Trinka, E.; Kälviäinen, R. 25 years of advances in the definition, classification and treatment of status epilepticus. *Seizure* **2017**, *44*, 65–73. [CrossRef]
21. Chamberlain, J.M.; Okada, P.; Holsti, M.; Mahajan, P.; Brown, K.M.; Vance, C.; Gonzalez, V.; Lichenstein, R.; Stanley, R.; Brousseau, D.C.; et al. Lorazepam vs diazepam for pediatric status epilepticus: A randomized clinical trial. *Pediatric Emerg. Care Appl. Res. Netw. (PECARN) JAMA* **2014**, *311*, 1652–1660. [CrossRef]
22. Cock, H.R.; Schapira, A.H. A comparison of lorazepam and diazepam as initial therapy in convulsive status epilepticus. *QJM* **2002**, *95*, 225–231. [CrossRef] [PubMed]
23. Singhi, S.; Murthy, A.; Singhi, P.; Jayashree, M. Continuous midazolam versus diazepam infusion for refractory convulsive status epilepticus. *J. Child Neurol.* **2002**, *17*, 106–110. [CrossRef] [PubMed]
24. Crawshaw, A.A.; Cock, H.R. Medical management of status epilepticus: Emergency room to intensive care unit. *Seizure* **2020**, *75*, 145–152. [CrossRef] [PubMed]
25. Dubey, D.; Kalita, J.; Misra, U.K. Status epilepticus: Refractory and super-refractory. *Neurol. India* **2017**, *65*, S12–S17.
26. McDonough, J.H.; McMonagle, J.D.; Shih, T.M. Time-dependent reduction in the anticonvulsant effectiveness of diazepam against soman-induced seizures in guinea pigs. *Drug Chem. Toxicol.* **2010**, *33*, 279–283. [CrossRef]
27. Niquet, J.; Baldwin, R.; Suchomelova, L.; Lumley, L.; Naylor, D.; Eavey, R.; Wasterlain, C.G. Benzodiazepine-refractory status epilepticus: Pathophysiology and principles of treatment. *Ann. N. Y. Acad. Sci.* **2016**, *1378*, 166–173. [CrossRef]
28. Todorovic, M.S.; Cowan, M.L.; Balint, C.A.; Sun, C.; Kapur, J. Characterization of status epilepticus induced by two organophosphates in rats. *Epilepsy Res.* **2012**, *101*, 268–276. [CrossRef]
29. Apland, J.P.; Aroniadou-Anderjaska, V.; Figueiredo, T.H.; Rossetti, F.; Miller, S.L.; Braga, M.F. The limitations of diazepam as a treatment for nerve agent-induced seizures and neuropathology in rats: Comparison with UBP302. *J. Pharmacol. Exp. Ther.* **2014**, *351*, 359–372. [CrossRef]
30. Rojas, A.; Ganesh, T.; Wang, W.; Wang, J.; Dingledine, R. A rat model of organophosphate-induced status epilepticus and the beneficial effects of EP2 receptor inhibition. *Neurobiol Dis.* **2019**, *25*, 104399. [CrossRef]
31. Apland, J.P.; Aroniadou-Anderjaska, V.; Figueiredo, T.H.; Pidoplichko, V.I.; Rossetti, K.; Braga, M.F.M. Comparing the antiseizure and neuroprotective efficacy of LY293558, diazepam, caramiphen, and LY293558-caramiphen combination against soman in a rat model relevant to the pediatric population. *J. Pharmacol. Exp. Ther.* **2018**, *365*, 314–326. [CrossRef]
32. Langston, J.L.; Wright, L.K.; Connis, N.; Lumley, L.A. Characterizing the behavioral effects of nerve agent-induced seizure activity in rats: Increased startle reactivity and perseverative behavior. *Pharmacol. Biochem. Behav.* **2012**, *100*, 382–391. [CrossRef] [PubMed]
33. de Araujo Furtado, M.; Lumley, L.A.; Robison, C.; Tong, L.C.; Lichtenstein, S.; Yourick, D.L. Spontaneous recurrent seizures after status epilepticus induced by soman in Sprague-Dawley rats. *Epilepsia* **2010**, *51*, 1503–1510. [CrossRef] [PubMed]
34. Reddy, S.D.; Reddy, D.S. Midazolam as an anticonvulsant antidote for organophosphate intoxication–A pharmacotherapeutic appraisal. *Epilepsia* **2015**, *56*, 813–821. [CrossRef] [PubMed]
35. Bleakman, R.; Schoepp, D.D.; Ballyk, B.; Bufton, H.; Sharpe, E.F.; Thomas, K.; Ornstein, P.L.; Kamboj, R.K. Pharmacological discrimination of GluR5 and GluR6 kainate receptor subtypes by (3S,4aR,6R,8aR)-6-[2-(1(2)H-tetrazole-5-yl)ethyl]decahyd roisdoquinoline-3 carboxylic-acid. *Mol. Pharmacol.* **1996**, *49*, 581–585. [PubMed]
36. Figueiredo, T.H.; Qashu, F.; Apland, J.P.; Aroniadou-Anderjaska, V.; Souza, A.P.; Braga, M.F. The GluK1 (GluR5) Kainate/{alpha}-amino-3-hydroxy-5-methyl-4-isoxazolepropionic acid receptor antagonist LY293558 reduces soman-induced seizures and neuropathology. *J. Pharmacol. Exp. Ther.* **2011**, *336*, 303–312. [CrossRef]
37. Prager, E.M.; Figueiredo, T.H.; Long, R.P., 2nd; Aroniadou-Anderjaska, V.; Apland, J.P.; Braga, M.F. LY293558 prevents soman-induced pathophysiological alterations in the basolateral amygdala and the development of anxiety. *Neuropharmacology* **2015**, *89*, 11–18. [CrossRef]

38. Apland, J.P.; Aroniadou-Anderjaska, V.; Figueiredo, T.H.; Green, C.E.; Swezey, R.; Yang, C.; Qashu, F.; Braga, M.F.M. Efficacy of the GluK1/AMPA receptor antagonist LY293558 against seizures and neuropathology in a soman-exposure model without pretreatment and its pharmacokinetics after intramuscular administration. *J. Pharmacol. Exp. Ther.* **2013**, *344*, 133–140. [CrossRef]
39. Apland, J.P.; Aroniadou-Anderjaska, V.; Figueiredo, T.H.; Prager, E.M.; Olsen, C.H.; Braga, M.F.M. Susceptibility to soman toxicity and efficacy of LY293558 against soman-induced seizures and neuropathology in 10-month-old male rats. *Neurotox. Res.* **2017**, *32*, 694–706. [CrossRef]
40. Aroniadou-Anderjaska, V.; Figueiredo, T.H.; Apland, J.P.; Braga, M.F. Targeting the glutamatergic system to counteract organophosphate poisoning: A novel therapeutic strategy. *Neurobiol. Dis.* **2020**, *133*, 104406. [CrossRef]
41. Mercey, G.; Verdelet, T.; Renou, J.; Kliachyna, M.; Baati, R.; Nachon, F.; Jean, L.; Renard, P.Y. Reactivators of acetylcholinesterase inhibited by organophosphorus nerve agents. *Acc. Chem. Res.* **2012**, *45*, 756–766. [CrossRef]
42. Apland, J.P.; Figueiredo, T.H.; Qashu, F.; Aroniadou-Anderjaska, V.; Souza, A.P.; Braga, M.F. Higher susceptibility of the ventral versus the dorsal hippocampus and the posteroventral versus anterodorsal amygdala to soman-induced neuropathology. *Neurotoxicology* **2010**, *31*, 485–492. [CrossRef] [PubMed]
43. Apland, J.P.; Aroniadou-Anderjaska, V.; Figueiredo, T.H.; de Araujo Furtado, M.; Braga, M.F.M. Full protection against soman-induced seizures and brain damage by LY293558 and caramiphen combination treatment in adult rats. *Neurotox. Res.* **2018**, *34*, 511–524. [CrossRef] [PubMed]
44. Prager, E.M.; Aroniadou-Anderjaska, V.; Almeida-Suhett, C.P.; Figueiredo, T.H.; Apland, J.P.; Rossetti, F.; Olsen, C.H.; Braga, M.F. The recovery of acetylcholinesterase activity and the progression of neuropathological and pathophysiological alterations in the rat basolateral amygdala after soman-induced status epilepticus: Relation to anxiety-like behavior. *Neuropharmacology* **2014**, *81*, 64–74. [CrossRef]
45. Prager, E.M.; Pidoplichko, V.I.; Aroniadou-Anderjaska, V.; Apland, J.P.; Braga, M.F. Pathophysiological mechanisms underlying increased anxiety after soman exposure: Reduced GABAergic inhibition in the basolateral amygdala. *Neurotoxicology* **2014**, *44*, 335–343. [CrossRef] [PubMed]
46. Paxinos, G.; Watson, C. *The Rat Brain in Stereotaxic Coordinates*, 4th ed.; Elsevier: New York, NY, USA, 2005.
47. Gundersen, H.J.; Jensen, E.B.; Kieu, K.; Nielsen, J. The efficiency of systematic sampling in stereology–reconsidered. *J. Microsc.* **1999**, *193*, 199–211. [CrossRef] [PubMed]
48. Schmitz, C.; Hof, P.R. Recommendations for straightforward and rigorous methods of counting neurons based on a computer simulation approach. *J. Chem. Neuroanat.* **2000**, *20*, 93–114. [CrossRef]
49. Aroniadou-Anderjaska, V.; Pidoplichko, V.I.; Figueiredo, T.H.; Braga, M.F.M. Oscillatory synchronous inhibition in the basolateral amygdala and its primary dependence on NR2A-containing NMDA receptors. *Neuroscience* **2018**, *373*, 145–158. [CrossRef]
50. Sah, P.; Faber, E.S.; Lopez De Armentia, M.; Power, J. The amygdaloid complex: Anatomy and physiology. *Physiol. Rev.* **2003**, *83*, 803–834. [CrossRef]
51. Aroniadou-Anderjaska, V.; Pidoplichko, V.I.; Figueiredo, T.H.; Almeida-Suhett, C.P.; Prager, E.M.; Braga, M.F. Presynaptic facilitation of glutamate release in the basolateral amygdala: A mechanism for the anxiogenic and seizurogenic function of GluK1 receptors. *Neuroscience* **2012**, *221*, 157–169. [CrossRef]
52. Pidoplichko, V.I.; Aroniadou-Anderjaska, V.; Prager, E.M.; Figueiredo, T.H.; Almeida-Suhett, C.P.; Miller, S.L.; Braga, M.F. ASIC1a activation enhances inhibition in the basolateral amygdala and reduces anxiety. *J. Neurosci.* **2014**, *34*, 3130–3141. [CrossRef]
53. McDonough, J.H.; McLeod, C.G.; Nipwoda, M.T. Direct microinjection of soman or VX into the amygdala produces repetitive limbic convulsions and neuropathology. *Brain Res.* **1987**, *435*, 123–137. [CrossRef]
54. Prager, E.M.; Aroniadou-Anderjaska, V.; Almeida-Suhett, C.P.; Figueiredo, T.H.; Apland, J.P.; Braga, M.F. Acetylcholinesterase inhibition in the basolateral amygdala plays a key role in the induction of status epilepticus after soman exposure. *Neurotoxicology* **2013**, *38*, 84–90. [CrossRef] [PubMed]
55. Aroniadou-Anderjaska, V.; Fritsch, B.; Qashu, F.; Braga, M.F. Pathology and pathophysiology of the amygdala in epileptogenesis and epilepsy. *Epilepsy Res.* **2008**, *78*, 102–116. [CrossRef] [PubMed]
56. Rainnie, D.G. Serotonergic modulation of neurotransmission in the rat basolateral amygdala. *J. Neurophysiol.* **1999**, *82*, 69–85. [CrossRef] [PubMed]
57. Popescu, A.T.; Paré, D. Synaptic interactions underlying synchronized inhibition in the basal amygdala: Evidence for existence of two types of projection cells. *J. Neurophysiol.* **2011**, *105*, 687–696. [CrossRef]
58. Pidoplichko, V.I.; Aroniadou-Anderjaska, V.; Figueiredo, T.H.; Wilbraham, C.; Braga, M.F.M. Increased inhibitory activity in the basolateral amygdala and decreased anxiety during estrus: A potential role for ASIC1a channels. *Brain Res.* **2021**, *1770*, 147628. [CrossRef]
59. Prut, L.; Belzung, C. The open field as a paradigm to measure the effects of drugs on anxiety-like behaviors: A review. *Eur. J. Pharmacol.* **2003**, *463*, 3–33. [CrossRef]
60. Li, L.; Du, Y.; Li, N.; Wu, X.; Wu, Y. Top-down modulation of prepulse inhibition of the startle reflex in humans and rats. *Neurosci. Biobehav. Rev.* **2009**, *33*, 1157–1167. [CrossRef]
61. de Araujo Furtado, M.; Aroniadou-Anderjaska, V.; Figueiredo, T.H.; Apland, J.P.; Braga, M.F.M. Electroencephalographic analysis in soman-exposed 21-day-old rats and the effects of midazolam or LY293558 with caramiphen. *Ann. N. Y. Acad. Sci.* **2020**, *1479*, 122–133. [CrossRef]

62. Fernandez, A.; Lantigua, H.; Lesch, C.; Shao, B.; Foreman, B.; Schmidt, J.M.; Hirsch, L.J.; Mayer, S.A.; Claassen, J. High-dose midazolam infusion for refractory status epilepticus. *Neurology* **2014**, *82*, 359–365. [CrossRef]
63. Goodkin, H.P.; Yeh, J.L.; Kapur, J. Status epilepticus increases the intracellular accumulation of GABAA receptors. *J. Neurosci.* **2005**, *25*, 5511–5520. [CrossRef] [PubMed]
64. Goodkin, H.P.; Joshi, S.; Mtchedlishvili, Z.; Brar, J.; Kapur, J. Subunit-specific trafficking of GABA(A) receptors during status epilepticus. *J. Neurosci.* **2008**, *28*, 2527–2538. [CrossRef] [PubMed]
65. Naylor, D.E.; Liu, H.; Wasterlain, C.G. Trafficking of GABA(A) receptors, loss of inhibition, and a mechanism for pharmacoresistance in status epilepticus. *J. Neurosci.* **2005**, *25*, 7724–7733. [CrossRef] [PubMed]
66. Deeb, T.Z.; Maguire, J.; Moss, S.J. Possible alterations in GABA(A) receptor signaling that underlie benzodiazepine-resistant seizures. *Epilepsia* **2012**, *53*, 79–88. [CrossRef] [PubMed]
67. Overstreet, L.S.; Westbrook, G.L. Paradoxical reduction of synaptic inhibition by vigabatrin. *J. Neurophysiol.* **2001**, *86*, 596–603. [CrossRef]
68. Stelzer, A.; Slater, N.T.; ten Bruggencate, G. Activation of NMDA receptors blocks GABAergic inhibition in an in vitro model of epilepsy. *Nature* **1987**, *326*, 698–701. [CrossRef]
69. Lu, Y.M.; Mansuy, I.M.; Kandel, E.R.; Roder, J. Calcineurin-mediated LTD of GABAergic inhibition underlies the increased excitability of CA1 neurons associated with LTP. *Neuron* **2000**, *26*, 197–205. [CrossRef]
70. Chapman, S.; Yaakov, G.; Egoz, I.; Rabinovitz, I.; Raveh, L.; Kadar, T.; Gilat, E.; Grauer, E. Sarin-induced brain damage in rats is attenuated by delayed administration of midazolam. *Neurotoxicology* **2015**, *49*, 132–138. [CrossRef]
71. RamaRao, G.; Afley, P.; Acharya, J.; Bhattacharya, B.K. Efficacy of antidotes (midazolam, atropine and HI-6) on nerve agent induced molecular and neuropathological changes. *BMC Neurosci.* **2014**, *15*, 47. [CrossRef]
72. Gilat, E.; Kadar, T.; Levy, A.; Rabinovitz, I.; Cohen, G.; Kapon, Y.; Sahar, R.; Brandeis, R. Anticonvulsant treatment of sarin-induced seizures with nasal midazolam: An electrographic, behavioral, and histological study in freely moving rats. *Toxicol. Appl. Pharmacol.* **2005**, *209*, 74–85. [CrossRef]
73. Spampanato, J.; Pouliot, W.; Bealer, S.L.; Roach, B.; Dudek, F.E. Antiseizure and neuroprotective effects of delayed treatment with midazolam in a rodent model of organophosphate exposure. *Epilepsia* **2019**, *60*, 1387–1398. [CrossRef] [PubMed]
74. Likhtik, E.; Stujenske, J.M.; Topiwala, M.A.; Harris, A.Z.; Gordon, J.A. Prefrontal entrainment of amygdala activity signals safety in learned fear and innate anxiety. *Nat. Neurosci.* **2014**, *17*, 106–113. [CrossRef] [PubMed]
75. Stujenske, J.M.; Likhtik, E.; Topiwala, M.A.; Gordon, J.A. Fear and safety engage competing patterns of theta-gamma coupling in the basolateral amygdala. *Neuron* **2014**, *83*, 919–933. [CrossRef] [PubMed]
76. Karalis, N.; Dejean, C.; Chaudun, F.; Khoder, S.; Rozeske, R.R.; Wurtz, H.; Bagur, S.; Benchenane, K.; Sirota, A.; Courtin, J.; et al. 4-Hz oscillations synchronize prefrontal-amygdala circuits during fear behavior. *Nat. Neurosci.* **2016**, *19*, 605–612. [CrossRef] [PubMed]
77. Ben-Ari, Y.; Woodin, M.A.; Sernagor, E.; Cancedda, L.; Vinay, L.; Rivera, C.; Legendre, P.; Luhmann, H.J.; Bordey, A.; Wenner, P.; et al. Refuting the challenges of the developmental shift of polarity of GABA actions: GABA more exciting than ever! *Front. Cell Neurosci.* **2012**, *6*, 35. [CrossRef]
78. Ben-Ari, Y.; Khalilov, I.; Kahle, K.T.; Cherubini, E. The GABA excitatory/inhibitory shift in brain maturation and neurological disorders. *Neuroscientist* **2012**, *18*, 467–486. [CrossRef]
79. Khazipov, R.; Valeeva, G.; Khalilov, I. Depolarizing GABA and developmental epilepsies. *CNS Neurosci. Ther.* **2015**, *21*, 83–91. [CrossRef]
80. Torolira, D.; Suchomelova, L.; Wasterlain, C.G.; Niquet, J. Phenobarbital and midazolam increase neonatal seizure-associated neuronal injury. *Ann. Neurol.* **2017**, *82*, 115–120. [CrossRef]

toxics

MDPI

Article

Molecular Evidence on the Inhibitory Potential of Metformin against Chlorpyrifos-Induced Neurotoxicity

Marzieh Daniali [1,2], Maryam Baeeri [1,2,*], Ramtin Farhadi [1,2], Mahdi Gholami [1,2], Shokoufeh Hassani [1,2], Mona Navaei-Nigjeh [2,3], Mahban Rahimifard [1,2] and Mohammad Abdollahi [1,2,*]

[1] Department of Toxicology and Pharmacology, Faculty of Pharmacy, Tehran University of Medical Sciences, Tehran 11369, Iran; marziehdaniali75@gmail.com (M.D.); ramtinfarhadi@gmail.com (R.F.); m_gholami2068@yahoo.com (M.G.); shokoufehasani@gmail.com (S.H.); mahban.rahimifard@gmail.com (M.R.)

[2] Toxicology and Diseases Specialty Group, Pharmaceutical Sciences Research Center (PSRC), The Institute of Pharmaceutical Sciences (TIPS), Tehran University of Medical Sciences, Tehran 11369, Iran; mnavaei@sina.tums.ac.ir

[3] Department of Pharmaceutical Biomaterials, Medical Biomaterials Research Center, Faculty of Pharmacy, Tehran University of Medical Sciences (TUMS), Tehran 11369, Iran

* Correspondence: baeeri.maryam@gmail.com (M.B.); mohammad@tums.ac.ir (M.A.)

Abstract: Chlorpyrifos (CPF) is an organophosphorus (OP) pesticide, resulting in various health complications as the result of ingestion, inhalation, or skin absorption, and leads to DNA damage and increased oxidative stress. Metformin, derived from *Galega officinalis*, is reported to have anti-inflammatory and anti-apoptotic properties; thus, this study aimed to investigate the beneficial role of metformin in neurotoxicity induced by sub-acute exposure to CPF in Wistar rats. In this study, animals were divided into nine groups and were treated with different combinations of metformin and CPF. Following the 28 days of CPF and metformin administration, brain tissues were separated. The levels of inflammatory biomarkers such as tumor necrosis factor alpha (TNFα) and interleukin 1β (IL-1β), as well as the expression of 5HT1 and 5HT2 genes, were analyzed. Moreover, the levels of malondialdehyde (MDA), reactive oxygen species (ROS), and the ADP/ATP ratio, in addition to the activity of acetylcholinesterase (AChE) and superoxide dismutase (SOD), were tested through in vitro experiments. This study demonstrated the potential role of metformin in alleviating the mentioned biomarkers, which can be altered negatively as a result of CPF toxicity. Moreover, metformin showed protective potential in modulating inflammation, as well as oxidative stress, the expression of genes, and histological analysis, in a concentration-dependent manner.

Keywords: brain; chlorpyrifos; *Galega officinalis*; metformin; neurotoxicity

Citation: Daniali, M.; Baeeri, M.; Farhadi, R.; Gholami, M.; Hassani, S.; Navaei-Nigjeh, M.; Rahimifard, M.; Abdollahi, M. Molecular Evidence on the Inhibitory Potential of Metformin against Chlorpyrifos-Induced Neurotoxicity. *Toxics* **2022**, *10*, 197. https://doi.org/10.3390/toxics10040197

Academic Editors: Ondrej Soukup and Jan Korabecny

Received: 17 March 2022
Accepted: 17 April 2022
Published: 18 April 2022

1. Introduction

Chlorpyrifos (CPF) is an organophosphorus (OP) pesticide that has been heavily used and demonstrated various health complications in humans. CPF was introduced in 1965 as the most widely used pesticide in agriculture and non-agriculture environments [1]. According to the United States Environmental Protection Agency (EPA), elderly Americans consume CPF at 0.009 μg/kg daily through food and water consumption. However, ingestion, inhalation, and skin absorption are among the possible exposure routes of this pesticide [1,2]. The toxicity of CPF depends widely on the dose and duration of exposure; however, due to the half-life of CPF in water and food residue (as the main route of exposure for humans), many studies have focused on its subchronic exposures [1,2]. Different studies demonstrated the molecular mechanism of toxicity of CPF as DNA damage. Moreover, some studies reported CPF as a pesticide affecting the functionality and activity of cellular enzymes [3–5]. This pesticide is also reported to affect the regulation of serotonin receptors (5HT1 and 5HT2), which mediate hyperpolarization and the reduction of the firing rate of postsynaptic neurons [6,7].

Metformin is a biguanide drug originally developed from *Galega officinalis*, commonly known as goat's rue or French lilac [8]. Since G. officinalis was found to contain guanidine and was associated with glucose-lowering potential, Jean Sterne initiated his studies of metformin as a glucose-lowering medication in the 1950s, and metformin was introduced as an antidiabetic medication in France and the United States in 1957 and 1995, respectively [9,10]. Nowadays, metformin is used as the first-line therapy in diabetes type 2 (T2D). Although the exact mechanism of metformin is not fully understood, suggested underlying mechanisms can be divided into two groups of adenosine 3′,5′-monophosphate (AMP)-dependent, and AMP-independent pathways [11]. Metformin is reported to have anti-inflammatory, anti-apoptotic, and anti-oxidative roles in different tissues [12–16]. Various studies also reported the beneficial impacts of metformin on diseases associated with the central nervous system (CNS), including reducing the risk of ischemic stroke and improvements in short-term neurological functions in traumatic brain injury [17,18]. Several in vivo studies noticed that chronic treatment with metformin (500 mg/kg for 30 days) reduced acetylcholinesterase (AChE) activity and levels of oxidative stress biomarkers [19,20]. Moreover, the amount of butyrylcholinesterase, which is involved in the prevalence of Alzheimer's disease, was alleviated through the administration of metformin [21]. Thus, the focus of some recent studies was to investigate the role of metformin in Alzheimer's disease, amnestic mild cognitive implications, Huntington's, and Parkinson's diseases [22–25].

Due to the lack of investigation on the role of metformin in CPF's induced neurotoxicity, in the present study, the authors aimed to determine the beneficial role of metformin in attenuating the neurotoxicity symptoms of CPF. Biological, molecular, and analytical assays were performed after the administration of metformin in Wistar rats that were exposed to CPF for 28 days (sub-acute exposure).

2. Materials and Methods

2.1. Chemicals

The chemicals used in this study, including metformin and CPF, were purchased from Sigma-Aldrich® (Munich, Germany). In addition, experimental kits for RNA extraction, cDNA synthesis, rat IL-1β and TNFα enzyme-linked immunosorbent assay (ELISA), and SOD activity were obtained from Sacace® (Como, Italy), Thermo Scientific® (Waltham, MA, USA), Diaclone® (Besançon, France), and Teb Pazhouhan Razi® (Tehran, Iran), respectively.

2.2. Animals

Healthy, adult, male Wistar rats weighing approximately 160 g were selected and kept in the animal house of the School of Pharmacy, Tehran University of Medical Sciences (TUMS). Wistar rats were adapted to the laboratory conditions two weeks before initiating the in vivo step. Animals were kept in an environment with a temperature of 25 ± 1 °C, humidity of 50–55%, and a 12 h light and dark cycle.

Moreover, all steps of this study were performed according to the regulations regarding animal experiments and it received ethical approval from the National Institute for Medical Research Development (NIMAD), on 18 November 2020, with the approval code of IR.NIMAD.REC.1399.257.

2.3. Study Design

In this study, animals were divided into nine groups of 6 Wistar rats. Proper concentrations of dissolved metformin in normal saline (NS) and CPF in corn oil were administered to the animals through intraperitoneal (IP) injection and oral gavage, respectively [1–4]. Administration of toxin and drug was performed in a sub-acute period (for 28 days), according to the following plan:

- Group 1 (Control corn oil): receiving oral gavage of corn oil;
- Group 2 (Control NS): receiving IP injection of NS;
- Group 3 (CPF): receiving oral gavage of 7.5 mg/kg (1/20 LD50) CPF;
- Group 4 (Met-30): receiving IP injection of 30 mg/kg/day metformin;

- Group 5 (Met-60): receiving IP injection of 60 mg/kg/day metformin;
- Group 6 (Met-120): receiving IP injection of 120 mg/kg/day metformin;
- Group 7 (CPF + Met-30): receiving oral gavage of 7.5 mg/kg CPF and IP injection of 30 mg/kg/day metformin;
- Group 8 (CPF + Met-60): receiving oral gavage of 7.5 mg/kg CPF and IP injection of 60 mg/kg/day metformin;
- Group 9 (CPF + Met-120): receiving oral gavage of 7.5 mg/kg CPF and IP injection of 120 mg/kg/day metformin.

After 28 days of CPF and metformin administration to the rats, ketamine and xylazine were injected into the rats at 100 mg/kg and 10 mg/kg, respectively. Four of the separated brain tissues of each group were frozen at −80 °C for further biochemical experiments, and 2 of the brain tissues were kept in 10 mL of 10% formalin, following washing with phosphate buffer two times (pH = 7.4).

2.4. Oxidative Stress Markers

First, 0.1 g samples of the cortex of the brain tissue were homogenized with 1 mL of phosphate buffer (PBS) and centrifuged for 5 min at 3000× *g*. The supernatant of the samples was collected for measuring oxidative stress biomarkers.

2.4.1. Determination of ROS Level

ROS is produced through electron transport in mitochondria and is indicative of the free radicals associated with oxygen, leading to damages in cellular function [26]. First, 25 µL of the supernatant of the homogenized brain tissues was added to 81 µL of assay buffer and 5 µL of dichlorodifluorcein diacetate (DCFH-DA). Following 15 min of incubation at 37 °C, the fluorometric absorbance was measured for 60 min at the wavelength of 485 nm.

Moreover, to normalize the ROS level, protein level measurement was performed according to the Bradford Protein Assay (BPA). Here, 100 µL Bradford reagent was added to 10 µL of sample and was kept for 30 min in a dark place. The amount of protein was investigated by a spectrophotometer at the wavelength of 595 nm [27].

2.4.2. Determination of MDA Level

The MDA level in brain tissue indicates the peroxidation of lipids and oxidative stress. First, 150 mL thiobarbituric acid of 1% w/v for was added to 600 mL supernatant. After placing the samples in boiling water for 15 min, 400 mL of n-butanol was added, and the level of MDA was investigated at the wavelength of 532 nm [28].

2.5. Determination of SOD Activity

First, 0.1 g samples of the cortex of the brain tissue were homogenized with 1 mL of KCl (150 mM) and centrifuged for 5 min at 3000× *g*. The supernatant of the samples was collected for the SOD activity assay. According to the kit manufacturer's protocol, the activity of SOD was measured using a rat-specific enzyme-linked immunoassay (ELISA) kit.

2.6. Determination of Inflammatory Cytokine Levels (TNFα and IL-1β)

First, 0.1 g samples of the cortex of the brain tissue were homogenized with 1 mL of phosphate buffer and centrifuged for 15 min at 3000× *g*. The supernatant of the samples was collected for measuring inflammatory cytokines. Measurement of inflammatory biomarkers, including TNFα and IL-1β, was performed using rat-specific ELISA kits, according to the kit manufacturer's protocol [29].

2.7. Determination of AChE Inhibition

First, 0.1 g samples of the cortex of the brain tissue were homogenized with 1 mL of phosphate buffer and centrifuged for 15 min at 3000× *g*. To determine the level of AChE inhibition, 10 µL of the homogenized samples were added to 3 mL of 5, 5′-dithiobis-(2-

nitrobenzoic acid) (DTNB) solution (25 mM DTNB in 75 mM phosphate buffer). Following the addition of 10 µL of 3 mM acetylcholine iodide, a two-fold spectrophotometer was used to measure the absorbance change at the wavelength of 412 nm [30].

2.8. Gene Expression

The expression of specific genes, including 5HT1 and 5HT2, which are associated with the expression of serotonin receptors, was investigated by the real-time polymerase chain reaction (PCR) technique. In the first step, total RNA was extracted according to the Sacace® RNA extraction kit protocol and then its concentration was measured by nanodrop. Complementary DNA (cDNA) was formed using a reverse transcription Thermo Scientific® cDNA synthesis kit. In this study, the β-actin gene has been used as the housekeeping gene to study the expression of 5HT1 and 5HT2 genes. Finally, the double delta analysis was used to assess the expression of the mentioned genes. The sequences of the primers used in the real-time PCR step are listed in Table 1.

Table 1. Sequences of the genes used in real-time PCR analysis.

Name	Symbol	Primer Sequence
Rattus norvegicus actin, beta (Actb)	β-actin	F: AGGGAAATCGTGCGTGACAT R: CCGATAGTGATGACCTGACC
Rattus norvegicus 5-hydroxytryptamine receptor 1A (Htr1a)	5HT1	F: GTCCACTTGTTGAGCACCTG R: ACGTGACCTTCAGCTACCAA
Rattus norvegicus 5-hydroxytryptamine receptor 2A (Htr2a)	5HT2	F: TAGTTTGGCTCGAGTGCTGA R: TCCATGCCAATCCCAGTCTT

2.9. Determination of ADP/ATP Ratio

First, 0.1 g samples of the cortex of the brain tissue were homogenized in 1 mL of 6% cold trichloroacetic acid (TCA) solution. Following the centrifuging of the samples at 16,000× *g* for 10 min, the pH of the supernatants was neutralized using 0.5 M KOH solution. The neutral solutions were injected into a high-performance liquid chromatography (HPLC) instrument, and the ADP/ATP ratio was calculated and normalized according to the standard curves of ADP and ATP [31,32].

2.10. Histopathological Studies

The samples kept in formalin were embedded in paraffin, and 5 µm sections were prepared for staining with hematoxylin and eosin (H&E). Using an Olympus BX51 light microscope, histological slides from the cortexes of the brains were evaluated, and the changes in tissue sections, such as inflammatory responses, necrosis, hemorrhage, etc., were reported [33].

2.11. Statistical Analysis

Results of this study were presented as mean ± standard error of means (SEM). One-way analysis of variance (ANOVA) and Tukey's multi-comparison tests were performed in GraphPad Prism, version 9.3.0. The significance of the changes was reported and set at $p < 0.05$.

3. Results

3.1. Oxidative Stress Biomarkers

3.1.1. ROS

Results of the ROS test, summarized in Figure 1A, demonstrated that the administration of CPF to the animals led to a significant increase in the ROS level (p-value < 0.001). However, metformin in all three concentrations did not change the brain tissue's ROS level,

which indicates the safety of this medication. Despite the safety of metformin, the Met-30, Met-60, and Met-120 groups showed lower ROS markers in brain tissue in a concentration-dependent manner, and the Met-120 group resulted in the formation of the lowest level of ROS. Moreover, the groups receiving CPF and metformin simultaneously showed a concentration-dependent decrease in the ROS level of the brain tissue. However, the level of ROS in the CPF + Met-30 and CPF + Met-60 groups was significantly higher than in the control groups (p-value < 0.001 for both), the CPF + Met-120 group resulted in the most significant decline in ROS level in comparison with the CPF group (p-value < 0.001), and the lack of significant difference in ROS levels in comparison with the control groups demonstrated the beneficial role of metformin in the modulation of ROS markers in CPF-induced neurotoxicity.

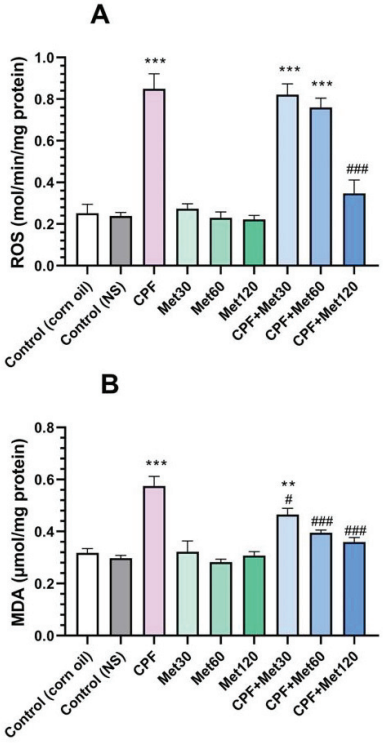

Figure 1. Results of oxidative stress biomarker tests on the brain tissue of 6 Wistar rats in each group. Data were obtained from 4 repeated measurements and are reported as the mean ± SEM. (**A**) Reactive oxygen species (ROS) assay. (**B**) Malondialdehyde (MDA) assay.** p-value < 0.005, *** p-value < 0.001; compared with the control groups. # p-value < 0.05 and ### p-value < 0.001; compared with chlorpyrifos (CPF) group.

3.1.2. MDA

In the MDA test, which is provided in Figure 1B, the CPF group showed a significant increase in this marker in the brain tissue (p-value < 0.001). However, the lack of significant changes in the MDA marker in the groups receiving different concentrations of metformin indicated the safety of metformin in the formation of the MDA marker in brain tissue. Simultaneous administration of CPF and metformin to the animals resulted in fewer MDA biomarkers. In other words, the CPF + Met-30, CPF + Met-60, and CPF + Met-120 groups showed significantly decreased levels of MDA when compared to the CPF group, in a concentration-dependent manner (p-value < 0.05, p-value < 0.001, and p-value < 0.001,

respectively). Results of the MDA test also demonstrated that the simultaneous administration of higher concentrations of metformin (60 mg/kg and 120 mg/kg) with CPF did not yield significant differences from the control groups, indicating its beneficial potential in the modulation of the MDA marker in CPF-induced neurotoxicity.

3.2. Inflammatory Cytokines

3.2.1. TNFα

According to the results of the TNFα test, the CPF group showed significantly increased levels of the TNFα inflammatory cytokine compared to the control groups (p-value < 0.001). In contrast, the administration of metformin in 30 mg/kg, 60 mg/kg, and 120 mg/kg concentrations did not cause any changes in the level of the TNFα inflammatory cytokine. Results also demonstrated that the concentration-dependent administration of metformin with CPF could decrease the level of the TNFα cytokine compared to the CPF group. Although the level of the TNFα marker in the CPF + Met-30 and CPF + Met-60 groups did not show a significant difference in comparison with the CPF group but showed a significant difference from the control groups (p-value < 0.001 and p-value < 0.005, respectively), the CPF + Met-120 group showed a significant decrease in TNFα inflammatory cytokine levels in comparison with the CPF group (p-value < 0.05). Figure 2A summarizes the results of the TNFα cytokine test.

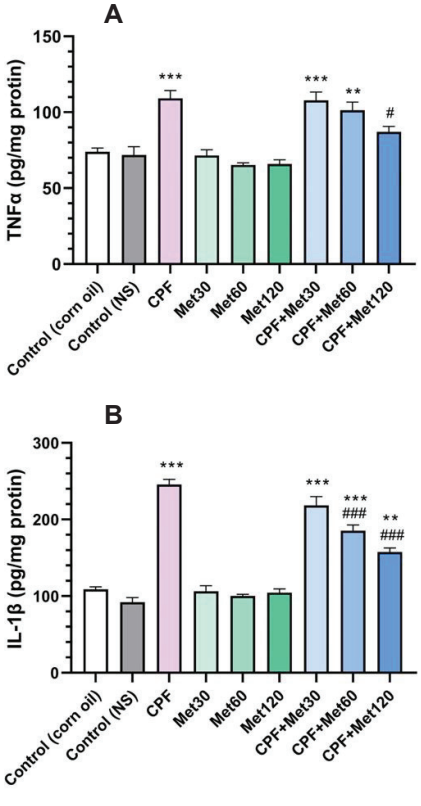

Figure 2. Results of inflammatory cytokine tests on the brain tissue of 6 Wistar rats in each group. Data were obtained from 4 repeated measurements and are reported as mean ± SEM. (**A**) Tumor necrosis factor alpha (TNFα) assay. (**B**) Interleukin 1 beta (IL-1β) assay. ** p-value < 0.005, *** p-value < 0.001; compared with the control groups. # p-value < 0.05 and ### p-value < 0.001; compared with chlorpyrifos (CPF) group.

3.2.2. IL-1β

Results of the IL-1β test confirmed the beneficial role of metformin in the modulation of inflammatory cytokines in CPF-induced neurotoxicity, which is demonstrated in Figure 2B. According to the results, the administration of CPF to the animals resulted in a significant increase in IL-1β inflammation cytokine levels. Moreover, metformin did not change the level of the IL-1β biomarker in the brain tissue at any of the three concentrations. However, the administration of metformin in the groups receiving CPF could alleviate the toxicity and IL-1β formation associated with CPF's administration in a concentration-dependent manner. The co-administration of CPF and metformin in the CPF + Met-30, CPF + Met-60, and CPF + Met-120 groups demonstrated a decrease in the IL-1 marker level compared to the CPF group; however, the reductions in the IL-1β cytokine in the CPF + Met-60 and CPF + Met-120 groups were significant, with a p-value of <0.001 for both groups. Despite the modulatory impact of metformin in CPF-induced neurotoxicity, the CPF + Met-30, CPF + Met-60, and CPF + Met-120 groups showed significant differences when compared to the control groups (p-value < 0.001, p-value < 0.001, and p-value < 0.005, respectively).

3.3. AChE Inhibition

The results of AChE inhibition are explored in Figure 3. Results demonstrated that the administration of CPF in the animals significantly increased AChE inhibition in the brain tissue compared to the control groups (p-value < 0.001), which demonstrates the accumulation of ACh in the synaptic cleft, which can over-stimulate the relevant receptors, resulting in neurotoxicity. However, in the groups receiving 30 mg/kg, 60 mg/kg, and 120 mg/kg of metformin, the inhibition of AChE did not show any changes compared to the control groups, which confirms metformin's safety profile in AChE inhibition. Results also demonstrated that metformin has modulatory potential to prevent the inhibition of AChE. These results also showed significant reductions in AChE inhibition in the CPF + Met-30, CPF + Met-60, and CPF + Met-120 groups (p-value < 0.005, p-value < 0.001, and p-value < 0.001, respectively). Moreover, the CPF + Met-60 and CPF + Met-120 groups did not show significant differences compared to the control groups, indicating the concentration-dependent modulatory impacts of metformin.

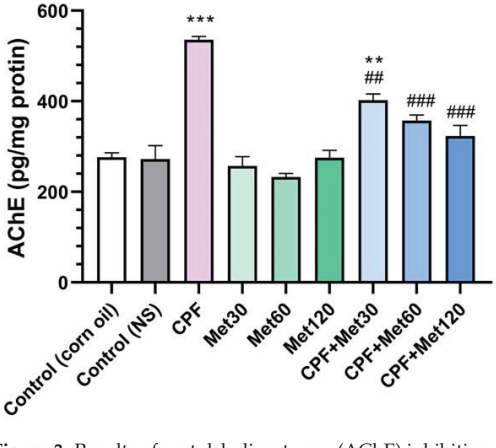

Figure 3. Results of acetylcholinesterase (AChE) inhibition test on the brain tissue of 6 Wistar rats in each group. Data were obtained from 4 repeated measurements and are reported as mean ± SEM. ** p-value < 0.005, *** p-value < 0.001; compared with the control groups. ## p-value < 0.005, ### p-value < 0.001; compared with chlorpyrifos (CPF) group.

3.4. SOD Activity

According to the results obtained from the SOD activity test, the treatment of Wistar rats with CPF significantly reduced SOD activity compared to the control groups (p-value < 0.001). Although metformin showed neutral impacts on SOD activity and the groups receiving metformin at 30 mg/kg, 60 mg/kg, and 120 mg/kg concentrations did not show changes in the level of SOD activity, metformin could improve SOD activity when administrated with CPF. The concentration-dependent modulatory effect of metformin has been demonstrated in Figure 4. Elevated activity of SOD in the CPF + Met-30, CPF + Met-60, and CPF + Met-120 groups showed that although the SOD activity of CPF + Met-30 had a significant difference from that of the control groups (0.005), the lack of significant differences in the SOD activity of the CPF + Met-60 and CPF + Met-120 groups confirmed the beneficial role of metformin in the neurotoxicity induced by CPF.

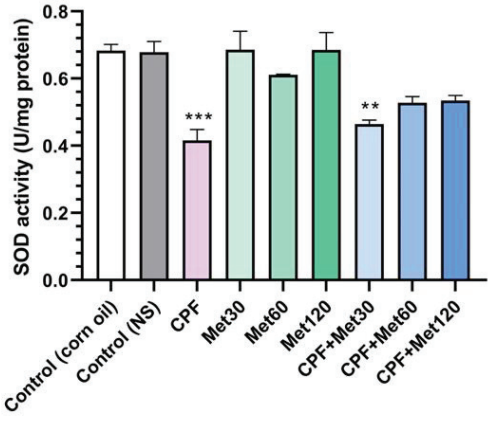

Figure 4. Superoxide dismutase (SOD) activity assay on the brain tissue of 6 Wistar rats in each group. Data were obtained from 4 repeated measurements and are reported as mean ± SEM. ** p-value < 0.005, *** p-value < 0.001; compared with the control groups.

3.5. Serotonin Receptor Gene Expression

3.5.1. *5HT1*

According to the real-time PCR results, the expression of 5HT1 in the brain tissue of Wistar rats treated with CPF was significantly elevated compared to the control groups (p-value < 0.001). Moreover, the expression of the 5HT1 gene was not altered in the groups receiving metformin at 30 mg/kg, 60 mg/kg, and 120 mg/kg concentrations. Additionally, metformin showed a concentration-dependent, beneficial impact in alleviating the expression of this gene when administered simultaneously with CPF. Nonetheless, the CPF + Met-30, CPF + Met-60, and CPF + Met-120 groups showed significant reductions in 5HT1 expression when compared to the CPF group (p-value < 0.001), as well as significant increases in 5HT1 expression when compared to the control groups (p-value < 0.001). Figure 5A indicates the results of 5HT1 expression in the brain tissue through a real-time PCR test.

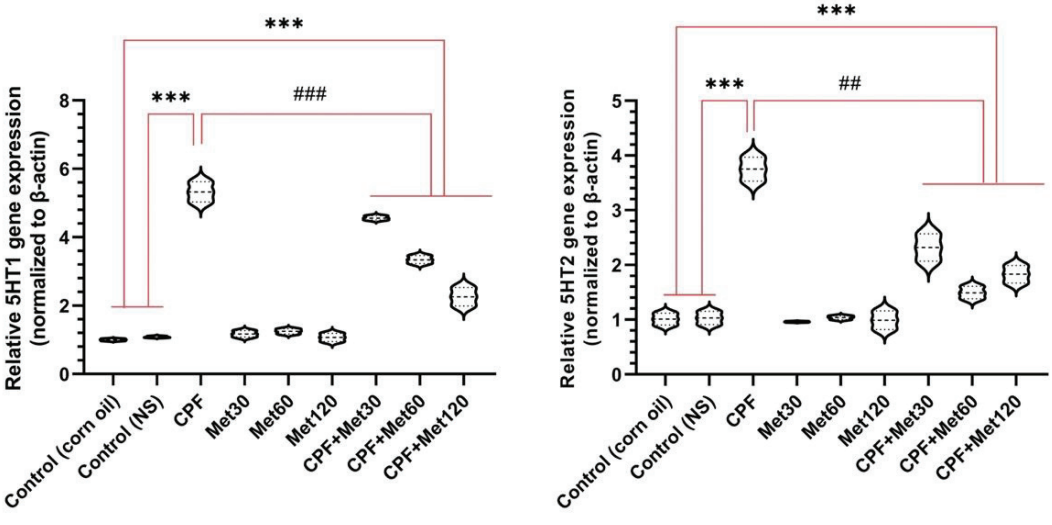

Figure 5. Expression of the genes associated with serotonin receptors (5HT1 and 5HT2, in (**A**,**B**), respectively) in the brain tissue of 6 Wistar rats in each group. Data were obtained from 4 repeated measurements and are reported as mean ± SEM. *** p-value < 0.001; compared with the control groups. ## p-value < 0.005 and ### p-value < 0.001; compared with chlorpyrifos (CPF) group.

3.5.2. *5HT2*

According to the real-time PCR results, the expression of 5HT2 in the brain tissue of Wistar rats treated with CPF was significantly elevated in comparison with the control groups (p-value < 0.001). Moreover, the expression of the 5HT2 gene was not altered in the groups receiving metformin at 30 mg/kg, 60 mg/kg, and 120 mg/kg concentrations. Additionally, metformin showed a concentration-dependent, beneficial impact in alleviating the expression of this gene when administered simultaneously with CPF. Nonetheless, the CPF + Met-30, CPF + Met-60, and CPF + Met-120 groups showed significant reductions in 5HT2 expression when compared to the CPF group (p-value < 0.005), as well as significant increases in 5HT2 expression when compared to the control groups (p-value < 0.001). Figure 5B indicates the results of 5HT2 expression in the brain tissue through a real-time PCR test.

3.6. ADP/ATP Ratio

The ADP/ATP ratio test results showed a significant increase in the ADP/ATP ratio in the group treated with CPF compared to the control group (p-value < 0.001). Moreover, the administration of lower metformin concentrations increased the ADP/ATP ratio in the brain tissue. In other words, although a significant difference was not observed in the Met-120 and control groups, the Met-30 and Met-60 groups showed an increased ADP/ATP ratio, with p-values of <0.005 and <0.05, respectively, which is associated with the AMP-dependent mechanism of metformin. Moreover, this concentration-dependent impact of metformin was observed in the groups exposed to CPF and metformin. These groups, including CPF + Met-30, CPF + Met-60, and CPF + Met-120, showed a significant increase in the ADP/ATP ratio compared to the control groups (p-value < 0.001 for all of the groups). However, in the CPF + Met-60 and CPF + Met-120 groups, the ADP/ATP ratio was significantly lower than in the CPF group (p-value < 0.001 for both groups). Nonetheless, the ADP/ATP ratio test results in the CPF + Met-120 group showed the lowest ratio among

other groups receiving metformin and CPF simultaneously. Figure 6 demonstrates the results obtained from the ADP/ATP ratio test.

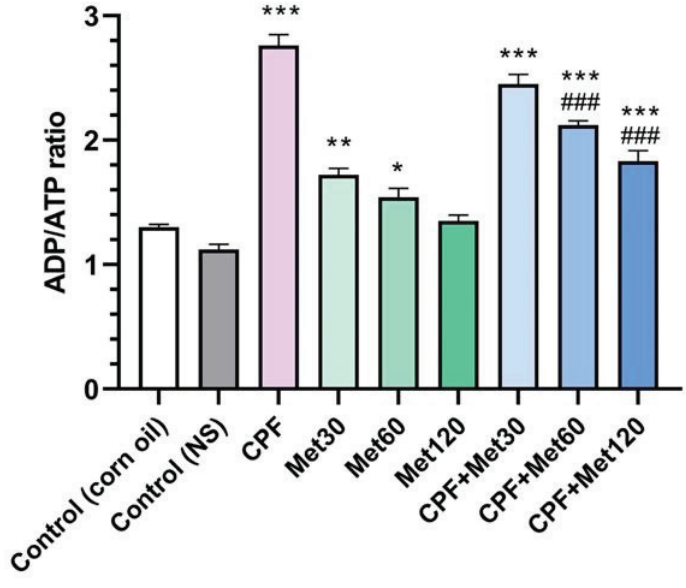

Figure 6. Results of ADP/ATP ratio assay on brain tissue of 6 Wistar rats in each group. Data were obtained from 4 repeated measurement and are reported as mean ± SEM. * p-value < 0.05, ** p-value < 0.005, *** p-value < 0.001; compared with the control groups. ### p-value < 0.001; compared with chlorpyrifos (CPF) group.

3.7. Histological Evaluation

Results of the histological analysis of the brain tissue are presented in Figure 7. In the control (corn oil) group (A), healthy tissue with glial cells (green arrows), perikaryon (red arrows), and axonal projections (brown arrows) was seen; likewise, no histological change was seen in the control (NS) group (B). Moreover, no histological alterations were seen in the Met-treated groups at the concentrations of 30 mg/kg, 60mg/kg, or 120 mg/kg (G, H, and I, respectively). The histological evaluations also showed that in the CPF group (C), tissue damage was observed, with vacuolated space and slight pyknosis (marked with yellow and gray arrows, respectively). However, some degree of vacuolization was observed in the CPF + Met-30 mg/kg group (D), as indicated with yellow arrows. Nevertheless, the CPF + Met-60 and CPF + Met-120 groups (E and F, respectively) were not reported to be histologically damaged, confirming the modulatory and beneficial role of metformin.

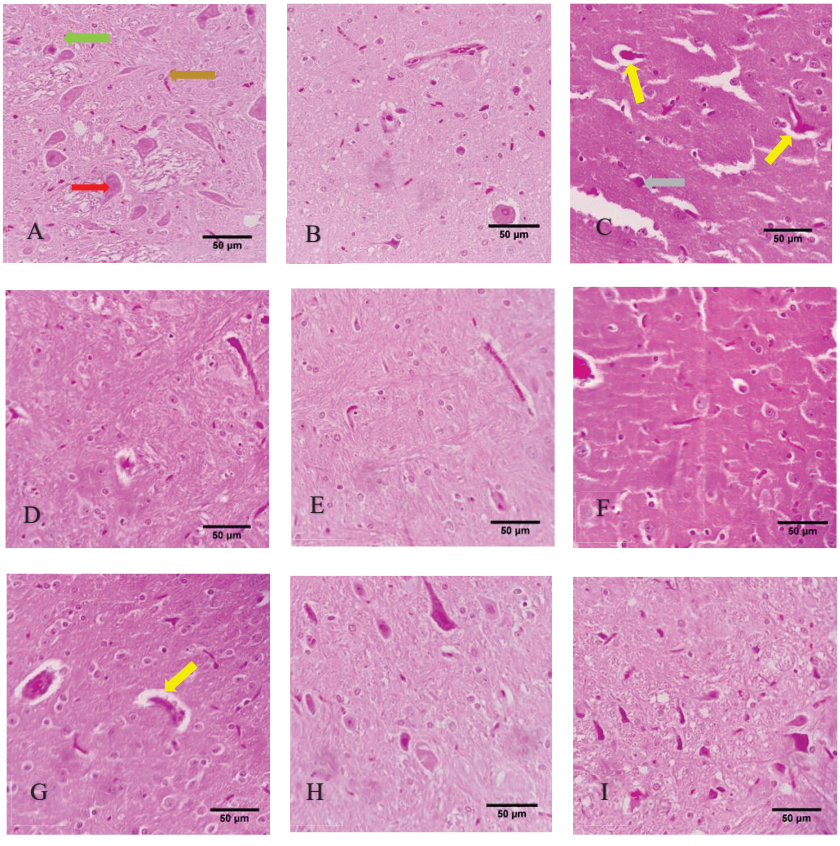

Figure 7. Histological sections of the cortex of the brain tissue of 6 Wistar rats in each group. Yellow, gray, green, red, and brown arrows indicate vacuolization, pyknosis, glial cells, perikaryon, and projections. (**A**) Control (corn oil), (**B**) Control (NS), (**C**) CPF, (**D**) Met-30, (**E**) Met-60, (**F**) Met-120, (**G**) CPF + Met-30, (**H**) CPF + Met-60, (**I**) CPF + Met-120.

4. Discussion

Among OPs, CPF is linked to various neurological problems, and it is frequently used as an insecticide worldwide [34]. Several studies established different cellular pathways to explain the neurotoxicity of CPF [35–38]. CPF is associated with irreversible consequences in the brain tissue due to chronic exposure [5]. Despite the significant impairments of oxidative stress biomarkers, inflammatory cytokines, the activity of enzymes, and the expression of genes as the result of CPF exposure, metformin modulates the altered characteristics of the brain tissue [39]. Metformin, as a compound with natural botanic sources, is beneficial and preventive in various brain disorders [40]. Mechanisms impacting the formation of oxidative stress markers and the inflammatory cytokines are considered essential underlying mechanisms for the beneficial role of metformin [41].

In this study, metformin has been used to investigate its possible beneficial role in CPF-induced neurotoxicity. Oxidative stress biomarkers such as ROS and MDA, and inflammatory cytokines such as TNFα and IL-1β, were measured in this study. Results demonstrated that exposure to metformin alleviates and reduces the increased levels of the mentioned biomarkers associated with CPF. Moreover, the inhibition of AChE and the activity of SOD, which were increased and decreased, respectively, as a consequence of CPF treatment, were positively and significantly changed through metformin administration.

Metformin can also impact the expression of the 5HT1 and 5HT2 genes and lower the expression levels to normal ones. Moreover, despite the histological injuries, including vacuolization and pyknosis, induced by CPF exposure, co-administration with the highest (120 mg/kg) concentrations of metformin did not demonstrate such damages in the brain's histological sections. All of the tests performed in this study confirmed the role of metformin in modulating the neurotoxicity associated with CPF exposure and demonstrated the concentration-dependent impact of metformin.

Various studies investigated the influence of exposure to CPF, particularly neurotoxicity induced by CPF, which confirm the results obtained from our research. A study on Atlantic salmon demonstrated that CPF could affect protein degradation and lipid metabolism in the brain and liver, and also showed CPF's impact on the disruption of encoding proteins involved in neuron function. This study found that CPF significantly altered the transcription of the genes involved in the neurological function of Atlantic salmon fish [35]. Moreover, another study on the neurotoxicity of CPF in mice reached the same results for AChE and SOD biomarkers. This study investigated the toxicity in the brain tissue and studied the abnormalities in AChE, SOD, catalase activity (CAT), glutathione peroxidase (GPX), and an increase in oxidative stress biomarkers. According to this study, CPF activates the formation of oxidative stress biomarkers and consequently alters significantly the activity of the mentioned enzymes [36].

AChE has been the focus of attention in various studies due to CPF-induced neurotoxicity. Although the exact mechanism of AChE alteration is not fully known, following the intracerebroventricular (ICV) injection of cytochrome P450 2B enzyme (CYP2B) inhibitors, the effect of the subcutaneous (SC) administration of CPF was assessed. Results of AChE neurochemical analysis showed that the CYP2B inhibitor attenuates the reduction in brain AChE. Thus, CYP2B is suggested as a factor involved in the neurotoxicity of CPF [37]. The expression of the genes involved in encoding AChE and monoamine oxidase A (MAO-A) has been examined. Results showed that the expression of the mentioned genes was reduced significantly when the animals were treated with CPF. This pesticide also significantly reduces the levels of neurotransmitters such as dopamine and serotonin and the activity of MAO-A, AChE, and sodium-potassium adenosine triphosphatase. The oxidative stress increase associated with exposure to CPF has been suggested to be relevant to a significant increase in MDA and nitric oxide (NO) markers [38]. Serotonin receptor assays have studied the impact of CPF on serotonin neurotransmitters. A study on an avian model showed that CPF directly increases the receptor binding of cerebrocortical 5HT2, demonstrating its upregulatory impacts on the expression of this serotonin receptor, and it also reduces the activity of presynaptic AChE in a concentration-dependent manner [42].

Furthermore, the role of CPF in 5HT signaling in noncholinergic neurotoxicity has been established. CPF is reported to alter the expected levels of the 5HT1A and 5HT2 receptors, in addition to 5HT transporters [7]. CPF is also suggested to modify the concentrations of pro-inflammatory and inflammatory biomarkers in the brain, plasma, and other tissues. Chronic exposure to CPF led to higher concentrations of TNFα, interleukin 6 (IL-6), and IL-1β in Wistar rats [43]. According to the literature, CPF impacts various cellular pathways in the brain tissue, and some of the most important mechanisms were discussed earlier. Due to the same cellular pathway of CPF and metformin, we benefited from metformin as the protective agent in our study.

The positive potential of metformin in neurotoxicity has been confirmed in several studies. Impaired mitochondrial oxidative metabolism as a result of insulin resistance is associated with cognitive decline. It is suggested to elevate ROS formation and consequently reduce mitochondrial ATP production. However, a recent study investigated metformin's effect on mitochondrial proteins and mitochondrial fission, preventing ROS formation and inflammation [44]. Moreover, metformin showed beneficial roles in the cerebral ischemia of the brain by impacting mitochondrial dysregulation, oxidative stress, blood–brain barrier (BBB) breakdown, and inflammation. Various underlying mechanisms

are suggested for the mentioned influences, including decreasing IL-6, TNFα, IL-1β, and intercellular adhesion molecule-1 (ICAM1) and consequent apoptosis prevention [45].

The neuroprotective role of metformin has also been studied in patients with acute stroke. The disrupted function of the brain as the result of impaired glucose control can be managed with the administration of metformin. This study suggested metformin's role in controlling the blood glucose level, as well as altering the activated protein kinase (AMPK)/mammalian target of rapamycin (mTOR) signaling pathway and decreasing and increasing MDA and SOD biomarkers, respectively [46]. An animal study on streptozotocin (STZ)-induced diabetic rats showed that although brain injuries associated with diabetes are reported to reduce the activity of SOD to 65% and increase the MDA level to 59%, metformin has significant protective impacts against these injuries (p-value < 0.01) [47]. Another study on sepsis-induced brain injury showed that metformin ameliorates neuronal apoptosis by increasing the phosphorylation of protein kinase B (PKB) and activating phosphoinositide 3-kinase (PI3K)/Akt signaling [48].

5. Conclusions

The main conclusion to be drawn is that CPF-induced neurotoxicity is associated with increased levels of oxidative stress biomarkers as well as inflammatory cytokines. Moreover, CPF can impair the activity of SOD while increasing the expression of the genes relevant to serotonin receptors. CPF alters the ratio of ADP to ATP, and this pesticide can result in histological injuries in the brain tissue. Administration of metformin is reported to modulate the changes associated with the neurotoxicity of CPF, and metformin demonstrated its beneficial impacts in a concentration-dependent manner. Thus, this study suggests metformin as a protective agent against the neurotoxicity of CPF. Moreover, in future studies, other biomarkers and pathways can be studied with sub-acute and chronic exposure to CPF.

Author Contributions: Conceptualization, M.A., M.B., and M.D.; methodology, M.D., R.F., M.B., M.N.-N., M.G., and S.H.; validation, M.A. and M.B. formal analysis, M.B., M.G., S.H., and M.D.; writing—original draft preparation, M.D.; writing—review and editing, M.A., M.B., and M.R.; supervision, M.A.; project administration, M.B.; funding acquisition, M.A. All authors have read and agreed to the published version of the manuscript.

Funding: This research was funded by the NIMAD, Islamic Republic of Iran, grant number 995321.

Institutional Review Board Statement: The study was conducted according to the guidelines of the Declaration of Helsinki and approved by the Ethics Committee of NIMAD (IR.NIMAD.REC.1399.257; 18 November 2020).

Informed Consent Statement: Not applicable.

Conflicts of Interest: The authors declare no conflict of interest.

References

1. United States Environmental Protection Agency. *EPA Proposes New Safety Measures for Chlorpyrifos*; United States Environmental Protection Agency: Washington D.C., VA, USA, 2020. Available online: https://www.epa.gov/pesticides/epa-proposes-new-safety-measures-chlorpyrifos (accessed on 3 March 2022).
2. Dutra Calda, E. CHLORPYRIFOS-METHYL (090). 2020. Available online: https://pubchem.ncbi.nlm.nih.gov/compound/Chlorpyrifos-methyl (accessed on 3 March 2022).
3. Sharma, S.; Singh, P.; Chadha, P.; Saini, H.S. Toxicity Assessment of Chlorpyrifos on Different Organs of Rat: Exploitation of Microbial-Based Enzymatic System for Neutralization. *Environ. Sci. Pollut. Res.* **2019**, *26*, 29649–29659. [CrossRef] [PubMed]
4. Qiao, D.; Seidler, F.J.; Padilla, S.; Slotkin, T.A. Developmental Neurotoxicity of Chlorpyrifos: What Is the Vulnerable Period? *Environ. Health Perspect.* **2002**, *110*, 1097–1103. [CrossRef] [PubMed]
5. Burke, R.D.; Todd, S.W.; Lumsden, E.; Mullins, R.J.; Mamczarz, J.; Fawcett, W.P.; Gullapalli, R.P.; Randall, W.R.; Pereira, E.F.R.; Albuquerque, E.X. Developmental Neurotoxicity of the Organophosphorus Insecticide Chlorpyrifos: From Clinical Findings to Preclinical Models and Potential Mechanisms. *J. Neurochem.* **2017**, *142* (Suppl. 2), 162–177. [CrossRef]
6. Karmakar, S.; Lal, G. Role of Serotonin Receptor Signaling in Cancer Cells and Anti-Tumor Immunity. *Theranostics* **2021**, *11*, 5296–5312. [CrossRef] [PubMed]

7. Aldridge, J.E.; Seidler, F.J.; Slotkin, T.A. Developmental Exposure to Chlorpyrifos Elicits Sex-Selective Alterations of Serotonergic Synaptic Function in Adulthood: Critical Periods and Regional Selectivity for Effects on the Serotonin Transporter, Receptor Subtypes, and Cell Signaling. *Environ. Health Perspect.* **2004**, *112*, 148–155. [CrossRef]
8. Thomas, M. Weekly Dose: Metformin, the Diabetes Drug Developed from French Lilac. *Conversation*. 2016. Available online: https://theconversation.com/weekly-dose-metformin-the-diabetes-drug-developed-from-french-lilac-64430 (accessed on 3 March 2022).
9. Bailey, C.; Day, C. Metformin: Its Botanical Background. *Pract. Diab. Int.* **2004**, *21*, 115–117. [CrossRef]
10. Bailey, C.J. Metformin: Historical Overview. *Diabetologia* **2017**, *60*, 1566–1576. [CrossRef]
11. Rena, G.; Hardie, D.G.; Pearson, E.R. The Mechanisms of Action of Metformin. *Diabetologia* **2017**, *60*, 1577–1585. [CrossRef]
12. Ismail Hassan, F.; Didari, T.; Khan, F.; Niaz, K.; Mojtahedzadeh, M.; Abdollahi, M. A Review on The Protective Effects of Metformin in Sepsis-Induced Organ Failure. *Cell J.* **2019**, *21*, 363–370. [CrossRef]
13. Ismail Hassan, F.; Didari, T.; Baeeri, M.; Gholami, M.; Haghi-Aminjan, H.; Khalid, M.; Navaei-Nigjeh, M.; Rahimifard, M.; Solgi, S.; Abdollahi, M.; et al. Metformin Attenuates Brain Injury by Inhibiting Inflammation and Regulating Tight Junction Proteins in Septic Rats. *Cell J.* **2020**, *22*, 29–37. [CrossRef]
14. Didari, T.; Hassani, S.; Baeeri, M.; Navaei-Nigjeh, M.; Rahimifard, M.; Haghi-Aminjan, H.; Gholami, M.; Nejad, S.M.; Hassan, F.I.; Mojtahedzadeh, M.; et al. Short-Term Effects of Metformin on Cardiac and Peripheral Blood Cells Following Cecal Ligation and Puncture-Induced Sepsis. *Drug Res.* **2021**, *71*, 257–264. [CrossRef] [PubMed]
15. Bharath, L.P.; Nikolajczyk, B.S. The Intersection of Metformin and Inflammation. *Am. J. Physiol.-Cell Physiol.* **2021**, *320*, C873–C879. [CrossRef] [PubMed]
16. Bai, B.; Chen, H. Metformin: A Novel Weapon Against Inflammation. *Front. Pharmacol.* **2021**, *12*, 622262. [CrossRef]
17. Tao, L.; Li, D.; Liu, H.; Jiang, F.; Xu, Y.; Cao, Y.; Gao, R.; Chen, G. Neuroprotective Effects of Metformin on Traumatic Brain Injury in Rats Associated with NF-KB and MAPK Signaling Pathway. *Brain Res. Bull.* **2018**, *140*, 154–161. [CrossRef]
18. Selvin, E.; Hirsch, A.T. Contemporary Risk Factor Control and Walking Dysfunction in Individuals with Peripheral Arterial Disease: NHANES 1999–2004. *Atherosclerosis* **2008**, *201*, 425–433. [CrossRef] [PubMed]
19. Bhutada, P.; Mundhada, Y.; Bansod, K.; Tawari, S.; Patil, S.; Dixit, P.; Umathe, S.; Mundhada, D. Protection of Cholinergic and Antioxidant System Contributes to the Effect of Berberine Ameliorating Memory Dysfunction in Rat Model of Streptozotocin-Induced Diabetes. *Behav. Brain Res.* **2011**, *220*, 30–41. [CrossRef] [PubMed]
20. Saliu, J.A.; Oboh, G.; Omojokun, O.S.; Rocha, J.B.T.; Schetinger, M.R.; Guterries, J.; Stefanello, N.; Carvalho, F.; Schmatz, R.; Morsch, V.M.; et al. Effect of Dietary Supplementation of Padauk (Pterocarpus Soyauxii) Leaf on High Fat Diet/Streptozotocin Induced Diabetes in Rats' Brain and Platelets. *Biomed. Pharmacother.* **2016**, *84*, 1194–1201. [CrossRef]
21. Greig, N.H.; Utsuki, T.; Ingram, D.K.; Wang, Y.; Pepeu, G.; Scali, C.; Yu, Q.-S.; Mamczarz, J.; Holloway, H.W.; Giordano, T.; et al. Selective Butyrylcholinesterase Inhibition Elevates Brain Acetylcholine, Augments Learning and Lowers Alzheimer -Amyloid Peptide in Rodent. *Proc. Natl. Acad. Sci. USA* **2005**, *102*, 17213–17218. [CrossRef]
22. Asadbegi, M.; Yaghmaei, P.; Salehi, I.; Ebrahim-Habibi, A.; Komaki, A. Neuroprotective Effects of Metformin against Aβ-Mediated Inhibition of Long-Term Potentiation in Rats Fed a High-Fat Diet. *Brain Res. Bull.* **2016**, *121*, 178–185. [CrossRef]
23. Luchsinger, J.A.; Perez, T.; Chang, H.; Mehta, P.; Steffener, J.; Pradabhan, G.; Ichise, M.; Manly, J.; Devanand, D.P.; Bagiella, E. Metformin in Amnestic Mild Cognitive Impairment: Results of a Pilot Randomized Placebo Controlled Clinical Trial. *J. Alzheimers Dis.* **2016**, *51*, 501–514. [CrossRef]
24. Mor, D.E.; Sohrabi, S.; Kaletsky, R.; Keyes, W.; Tartici, A.; Kalia, V.; Miller, G.W.; Murphy, C.T. Metformin Rescues Parkinson's Disease Phenotypes Caused by Hyperactive Mitochondria. *Proc. Natl. Acad. Sci. USA* **2020**, *117*, 26438–26447. [CrossRef] [PubMed]
25. Tang, B.L. Could Metformin Be Therapeutically Useful in Huntington's Disease? *Rev. Neurosci.* **2020**, *31*, 297–317. [CrossRef] [PubMed]
26. An Introduction to Reactive Oxygen Species-Measurement of ROS in Cells. *Agilent*. Available online: https://www.biotek.com/resources/white-papers/an-introduction-to-reactive-oxygen-species-measurement-of-ros-in-cells/#:~{}:text=Reactive%20Oxygen%20Species%20(ROS)%20is,bane%20to%20all%20aerobic%20species (accessed on 7 April 2021).
27. Baeeri, M.; Shariatpanahi, M.; Baghaei, A.; Ghasemi-Niri, S.F.; Mohammadi, H.; Mohammadirad, A.; Hassani, S.; Bayrami, Z.; Hosseini, A.; Rezayat, S.M.; et al. On the Benefit of Magnetic Magnesium Nanocarrier in Cardiovascular Toxicity of Aluminum Phosphide. *Toxicol. Ind. Health* **2013**, *29*, 126–135. [CrossRef] [PubMed]
28. Lapenna, D.; Cuccurullo, F. TBA Test and "Free" MDA Assay in Evaluation of Lipid Peroxidation and Oxidative Stress in Tissue Systems. *Am. J. Physiol.-Heart Circ. Physiol.* **1993**, *265*, H1030–H1032. [CrossRef]
29. Abdollahi, M.; Esmaily, H.; Baeeri, M.; Asadi-Shahmirzadi, A.; Mozaffari, S.; Rahimi, R.; Sanei, Y.; Salehi-Surmaghi, M.-H. Effects of Hypericum Perforatum Extract on Rat Irritable Bowel Syndrome. *Phcog. Mag.* **2011**, *7*, 213. [CrossRef]
30. Bocquené, G.; Galgani, F.; Truquet, P. Characterization and Assay Conditions for Use of ACHe Activity from Several Marine Species in Pollution Monitoring. *Mar. Environ. Res.* **1990**, *30*, 75–89. [CrossRef]
31. Ghafour-boroujerdi, E.; Rahmani, S.; Sanadgol, N.; Baeeri, M.; Hassani, S. Investigation of Alpha-Lipoic Acid Effect on Memory Impairment Considering Strain-Dependent Differences in Mice. *Life Sci.* **2021**, *281*, 119766. [CrossRef]

32. Abdolghaffari, A.H.; Baghaei, A.; Solgi, R.; Gooshe, M.; Baeeri, M.; Navaei-Nigjeh, M.; Hassani, S.; Jafari, A.; Rezayat, S.M.; Dehpour, A.R.; et al. Molecular and Biochemical Evidences on the Protective Effects of Triiodothyronine against Phosphine-Induced Cardiac and Mitochondrial Toxicity. *Life Sci.* **2015**, *139*, 30–39. [CrossRef]
33. Hassani, S.; Maqbool, F.; Salek-Maghsoudi, A.; Rahmani, S.; Shadboorestan, A.; Nili-Ahmadabadi, A.; Amini, M.; Norouzi, P.; Abdollahi, M. Alteration of Hepatocellular Antioxidant Gene Expression Pattern and Biomarkers of Oxidative Damage in Diazinon-Induced Acute Toxicity in Wistar Rat: A Time-Course Mechanistic Study. *EXCLI J.* **2018**, *17*, 57–71. [CrossRef]
34. Kaur, S.; Singla, N.; Dhawan, D.K. Neuro-Protective Potential of Quercetin during Chlorpyrifos Induced Neurotoxicity in Rats. *Drug Chem. Toxicol.* **2019**, *42*, 220–230. [CrossRef]
35. Olsvik, P.A.; Berntssen, M.H.G.; Søfteland, L.; Sanden, M. Transcriptional Effects of Dietary Chlorpyrifos-methyl Exposure in Atlantic Salmon (Salmo Salar) Brain and Liver. *Comp. Biochem. Physiol. Part D Genom. Proteom.* **2019**, *29*, 43–54. [CrossRef] [PubMed]
36. Gu, J.; Xu, S.; Liu, Y.; Chen, X. Chlorpyrifos-Induced Toxicity Has No Gender Selectivity in the Early Fetal Brain. *J. Environ. Sci. Health Part B* **2020**, *55*, 803–812. [CrossRef] [PubMed]
37. Khokhar, J.Y.; Tyndale, R.F. Rat Brain CYP2B-Enzymatic Activation of Chlorpyrifos to the Oxon Mediates Cholinergic Neurotoxicity. *Toxicol. Sci.* **2012**, *126*, 325–335. [CrossRef] [PubMed]
38. Abd El-Moneim Ibrahim, K.; Mohamed Abdelrahman, S.; Elhakim, H.K.A.; Ali Ragab, E. Single or Combined Exposure to Chlorpyrifos and Cypermethrin Provoke Oxidative Stress and Downregulation in Monoamine Oxidase and Acetylcholinesterase Gene Expression of the Rat's Brain. *Environ. Sci. Pollut. Res.* **2020**, *27*, 12692–12703. [CrossRef]
39. Garg, G.; Singh, S.; Singh, A.K.; Rizvi, S.I. Antiaging Effect of Metformin on Brain in Naturally Aged and Accelerated Senescence Model of Rat. *Rejuvenat. Res.* **2017**, *20*, 173–182. [CrossRef]
40. Rotermund, C.; Machetanz, G.; Fitzgerald, J.C. The Therapeutic Potential of Metformin in Neurodegenerative Diseases. *Front. Endocrinol.* **2018**, *9*, 400. [CrossRef]
41. Dehkordi, A.H.; Abbaszadeh, A.; Mir, S.; Hasanvand, A. Metformin and Its Anti-Inflammatory and Anti-Oxidative Effects; New Concepts. *J. Ren. Inj. Prev.* **2018**, *8*, 54–61. [CrossRef]
42. Slotkin, T.A.; Seidler, F.J.; Ryde, I.T.; Yanai, J. Developmental neurotoxic effects of chlorpyrifos on acetylcholine and serotonin pathways in an avian model. *Neurotoxicol. Teratol.* **2008**, *30*, 433–439. [CrossRef]
43. Li, J.-W.; Fang, B.; Pang, G.-F.; Zhang, M.; Ren, F.-Z. Age- and Diet-Specific Effects of Chronic Exposure to Chlorpyrifos on Hormones, Inflammation and Gut Microbiota in Rats. *Pestic. Biochem. Physiol.* **2019**, *159*, 68–79. [CrossRef]
44. Ruegsegger, G.N.; Vanderboom, P.M.; Dasari, S.; Klaus, K.A.; Kabiraj, P.; McCarthy, C.B.; Lucchinetti, C.F.; Nair, K.S. Exercise and Metformin Counteract Altered Mitochondrial Function in the Insulin-Resistant Brain. *JCI Insight* **2019**, *4*, e130681. [CrossRef]
45. Leech, T.; Chattipakorn, N.; Chattipakorn, S.C. The Beneficial Roles of Metformin on the Brain with Cerebral Ischaemia/Reperfusion Injury. *Pharmacol. Res.* **2019**, *146*, 104261. [CrossRef] [PubMed]
46. Zhao, M.; Li, X.W.; Chen, D.Z.; Hao, F.; Tao, S.X.; Yu, H.Y.; Cheng, R.; Liu, H. Neuro-Protective Role of Metformin in Patients with Acute Stroke and Type 2 Diabetes Mellitus via AMPK/Mammalian Target of Rapamycin (MTOR) Signaling Pathway and Oxidative Stress. *Med. Sci. Monit.* **2019**, *25*, 2186–2194. [CrossRef] [PubMed]
47. Clark, G.J.; Pandya, K.; Lau-Cam, C.A. The Effect of Metformin and Taurine, Alone and in Combination, on the Oxidative Stress Caused by Diabetes in the Rat Brain. In *Taurine 10*; Lee, D.-H., Schaffer, S.W., Park, E., Kim, H.W., Eds.; Advances in Experimental Medicine and Biology; Springer: Dordrecht, The Netherlands, 2017; Volume 975, pp. 353–369. ISBN 978-94-024-1077-8.
48. Tang, G.; Yang, H.; Chen, J.; Shi, M.; Ge, L.; Ge, X.; Zhu, G. Metformin Ameliorates Sepsis-Induced Brain Injury by Inhibiting Apoptosis, Oxidative Stress and Neuroinflammation via the PI3K/Akt Signaling Pathway. *Oncotarget* **2017**, *8*, 97977–97989. [CrossRef] [PubMed]

toxics

MDPI

Article

Influence of Experimental End Point on the Therapeutic Efficacy of Essential and Additional Antidotes in Organophosphorus Nerve Agent-Intoxicated Mice

Jiri Kassa [1,*], Christopher M. Timperley [2], Mike Bird [2], A. Christopher Green [2] and John E. H. Tattersall [2]

[1] Department of Toxicology and Military Pharmacy, Faculty of Military Health Sciences, University of Defence, 60200 Brno, Czech Republic
[2] Chemical, Biological and Radiological Division, Defence Science and Technology Laboratory (DSTL), Salisbury SP4 0JQ, UK; cmtimperley@mail.dstl.gov.uk (C.M.T.); mbird@dstl.gov.uk (M.B.); acgreen@dstl.gov.uk (A.C.G.); jtattersall@dstl.gov.uk (J.E.H.T.)
* Correspondence: kassa@pmfhk.cz; Tel.: +420-973255164

Abstract: The therapeutic efficacy of treatments for acute intoxication with highly toxic organophosphorus compounds, called nerve agents, usually involves determination of LD_{50} values 24 h after nerve agent challenge without and with a single administration of the treatment. Herein, the LD_{50} values of four nerve agents (sarin, soman, tabun and cyclosarin) for non-treated and treated intoxication were investigated in mice for experimental end points of 6 and 24 h. The LD_{50} values of the nerve agents were evaluated by probit-logarithmical analysis of deaths within 6 and 24 h of i.m. challenge of the nerve agent at five different doses, using six mice per dose. The efficiency of atropine alone or atropine in combination with an oxime was practically the same at 6 and 24 h. The therapeutic efficacy of the higher dose of the antinicotinic compound MB327 was slightly higher at the 6 h end point compared to the 24 h end point for soman and tabun intoxication. A higher dose of MB327 increased the therapeutic efficacy of atropine alone for sarin, soman and tabun intoxication, and that of the standard antidotal treatment (atropine and oxime) for sarin and tabun intoxication. The therapeutic efficacy of MB327 was lower than the oxime-based antidotal treatment. To compare the 6 and 24 h end points, the influence of the experimental end point was not observed, with the exception of the higher dose of MB327. In addition, only a negligible beneficial impact of the compound MB327 was observed. Nevertheless, antinicotinics may offer an additional avenue for countering poisoning by nerve agents that are difficult to treat, and synthetic and biological studies towards the development of such novel drugs based on the core bispyridinium structure or other molecular scaffolds should continue.

Keywords: atropine; MB327; nerve agents; oximes; mice

Citation: Kassa, J.; Timperley, C.M.; Bird, M.; Green, A.C.; Tattersall, J.E.H. Influence of Experimental End Point on the Therapeutic Efficacy of Essential and Additional Antidotes in Organophosphorus Nerve Agent-Intoxicated Mice. *Toxics* **2022**, *10*, 192. https://doi.org/10.3390/toxics10040192

Academic Editors: Ondrej Soukup and Jan Korabecny

Received: 18 March 2022
Accepted: 13 April 2022
Published: 15 April 2022

1. Introduction

Organophosphorus nerve agents are highly toxic chemical warfare agents. Their signs and symptoms can appear rapidly [1]. They inhibit acetylcholinesterase (AChE, EC 3.1.1.7) irreversibly [2]. Acetylcholine (ACh) then accumulates in the nervous system. The ACh overstimulates muscarinic (mAChRs) and nicotinic acetylcholine receptors (nAChRs) causing muscarinic and nicotinic effects: muscle twitching, lachrymation, miosis, salivation, seizures and coma [3]. Death arises from the inability to breathe, bronchial spasm and hypersecretion, and paralysis of the diaphragm and the brain respiratory centers [4,5].

The acute poisoning is usually treated by injecting a reactivator of the inhibited AChE (such as pralidoxime, HI-6, obidoxime or trimedoxime), an antimuscarinic (usually atropine to counter the muscarinic effects) and an anticonvulsant (e.g., diazepam to counter the centrally-mediated seizures) [1–5]. The treatment does not include drugs able to directly reduce the nicotinic effects. Its effectiveness is generally insufficiently broad because of the limitation of a single oxime to reactivate AChE inhibited by all nerve agents equally [6–8].

The search for more efficient therapies continues [9–11]. One option is to use an nAChR antagonist to counter the nicotinic effects [12]. Nicotinic antagonists administered with the aforementioned standard drug combination can help [13] as atropine cannot reverse the nerve agent-induced overstimulation of nAChRs [14]. Some bispyridinium compounds can do this, by blocking the nAChR open ion channel and/or orthosteric sites, or by positive allosteric modulation of nAChRs [15–20].

The bispyridinium non-oxime [1,1′-(propane-1,3-diyl) bis(4-tert-butyl pyridinium) diiodide] (MB327) was prepared at Dstl Porton Down, Salisbury, United Kingdom, and was found to be effective for treating the actions of nerve agents in guinea pigs [21,22]. MB327 has been shown to have a positive therapeutic effect due to a non-competitive action at muscle type nAChRs and positive allosteric activity at neuronal nAChRs [20].

MB327 is more effective over shorter timescales due its rapid elimination from the circulation (in guinea pigs) [23]. The therapeutic efficacy of antidotes is most often investigated 24 h after the nerve agent challenge. However, given that clearance of the treatment drugs, including MB327 and atropine, may impact their efficacy, the use of an earlier end point may provide a more realistic or useful assessment of their benefit as immediate or first aid treatments.

The present study measured the 6 h LD_{50} of sarin, soman, tabun or cyclosarin in mice either alone, or in the presence of atropine with or without an effective oxime (HI-6, obidoxime or trimedoxime) and/or MB327 (Figure 1). The results were compared to the 24 h LD_{50} measurements.

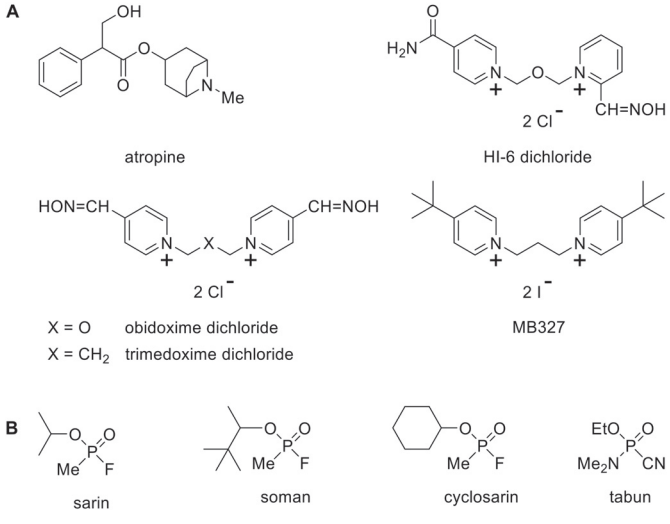

Figure 1. Components (**A**) of the therapies tested—the antimuscarinic atropine, the oximes HI-6, obidoxime and trimedoxime, and the antinicotinic MB327—against the panel of nerve agents shown (**B**).

2. Materials and Methods

2.1. Animals

Male NMRI mice aged 7 weeks, weighing 30–35 g from VELAZ (Prague, Czech Republic) were housed in polypropylene solid bottom cages in climate- and access-controlled rooms (22 ± 2 °C and 50 ± 10% relative humidity) with light from 07:00 to 19:00 h and access to standard food and tap water ad libitum. The mice were acclimatized in the laboratory vivarium for 14 days before the experiments commenced. They were divided into groups of 6 animals and handled under the supervision of the Ethics Committee of the Faculty of Military Health Sciences in Hradec Kralove (Czech Republic).

2.2. Chemicals

The nerve agents were obtained in 85–90% purity (by acidimetric titration) from the Military Technical Institute in Brno (Czech Republic). Stock solutions of these (1 mg/mL) were prepared in propylene glycol 3 days before starting the experiments. The solutions were diluted with saline immediately before administration. HI-6, obidoxime and trimedoxime dichlorides were synthesized in the Department of Toxicology and Military Pharmacy of the Faculty of Military Health Sciences in Hradec Kralove. Their purity was assessed by high performance liquid chromatography (HPLC) with ultraviolet detection (310 nm) and exceeded 95% [24]. MB327 of 99% purity was synthesized at Dstl Porton Down [22]. Other chemicals of a similar analytical grade were purchased commercially and used as received. All substances were administered by intramuscular (i.m.) injection at a volume of 10 mL/kg body weight (b.w.). The volume of administered substances was higher than recommended for i.m. administration in mice but there were no adverse effects observed.

2.3. In Vivo Experiments

The LD_{50} values of the nerve agents and 95% confidence limits in mice were evaluated by probit-logarithmical analysis of deaths within 6 and 24 h of i.m. administration of the nerve agent at 5 different doses, using 6 mice per dose [25]. The intoxicated mice were treated i.m. with atropine or with an oxime and/or MB327. An effective oxime was used for each nerve agent: obidoxime for sarin, trimedoxime for tabun, and HI-6 for soman and cyclosarin [4,7,26,27].

The oximes were delivered at equitoxic doses (obidoxime 5.8 mg/kg; trimedoxime 5.3 mg/kg; and HI-6 at 25 mg/kg) corresponding to 5% of their respective LD_{50}. MB327 was administered at doses (16.7 and 33.4 mg/kg) corresponding to 10 and 20% of its respective LD_{50} [22]. Equitoxic doses were used to ensure that sufficiently safe doses with respect to their different toxicities were given. Consistent with previous work, atropine (10 mg/kg) was injected at a dose approximating 2% of its LD_{50} [28]. All antidotes were applied as an admix 1 min after i.m. administration of the nerve agent.

The LD_{50} values of the nerve agents and 95% confidence limits in mice treated with the antidotes were evaluated by the method used to determine the toxicity of the nerve agents without antidotal treatment [25]. The therapeutic efficacy of the antidotal combinations was expressed as a protective ratio A (LD_{50} value of the nerve agent in protected mice/LD_{50} value of the nerve agent in unprotected mice) for the 6 or 24 h end points. The influence of end point on the therapeutic efficacy of the antidotes was expressed as a protective ratio B (LD_{50} value of the nerve agent in mice for the 6 h end point/LD_{50} value of the nerve agent in mice for the 24 h end point). Statistical significance was determined by a one-way ANOVA test with Tukey's post hoc test and differences were considered significant when $p < 0.05$ [25].

3. Results

Clinical signs in mice intoxicated with sarin, soman, tabun and cyclosarin included salivation, lachrymation, nasal secretion and tonic-clonic convulsions. Signs were observed within a few minutes of administration of the nerve agents. In the case of treatment for nerve agent poisoning, nerve agent-induced signs and symptoms did not disappear but their intensity was decreased regardless of the type of nerve agent used. The decrease in the intensity of toxic signs and symptoms was especially observed when atropine in combination with an oxime was used as a treatment of nerve agent poisoning. Observations and potencies of the antidotes studied are now discussed in turn.

3.1. The Efficacy of Antidotes (Atropine, Obidoxime, MB327) for Prevention of Sarin Lethality

The dependence of the therapeutic efficacy of the various combinations of treatments on the selected experimental end point is summarized in Table 1. The times to death were similar for all treatment groups. Most mice died within the first hour. The average time

to death within the first 6 h was 7.4 min for non-treated animals and 8.1 min for treated animals. Only in the atropine alone group did some deaths occur after 6 h. All deaths occurred within 6 h of intoxication for the other groups: atropine with obidoxime or MB327, and atropine with obidoxime and MB327. Atropine increased the LD_{50} of sarin 1.25-fold at 6 h and 1.10-fold at 24 h. The combination of atropine and obidoxime increased it 1.45-fold. With the lower dose of MB327, it increased it 1.21-fold, and with the higher dose of MB327 it increased it 1.23-fold. Atropine and obidoxime and the higher dose of MB327 increased it 1.80-fold, regardless of the end point. The efficacy of atropine and obidoxime was higher than that of atropine and MB327 regardless of the dose of the latter. With atropine and MB327, a slight increase in protection ratio versus atropine alone was seen at 24 h but the difference was not significant. A significant benefit of MB327 on the efficacy of atropine and obidoxime was not observed.

Table 1. The effect of experimental endpoint on the protection provided against lethal effects of sarin in mice.

Treatment	LD_{50} (μg/kg) ± 95% Confidence Limit—6 h	Protective Ratio A	LD_{50} (μg/kg) ± 95% Confidence Limit—24 h	Protective Ratio A	Protective Ratio B
——	328.2 (270.1–360.2)	—-	328.2 (270.1–360.2)	—-	—-
Atropine	411.9 (329.9–514.2)	1.25	361.2 (324.9–430.7)	1.10	1.14
Atropine + obidoxime	**476.9 (375.8–539.1) ***	**1.45**	**476.9 (375.8–539.1) ***	**1.45**	**1.00**
Atropine + MB327 (lower dose)	397.8 (354.1–446.8)	1.21	397.8 (354.1–446.8)	1.21	1.00
Atropine + MB327 (higher dose)	402.7 (269.1–496.3)	1.23	402.7 (269.1–496.3)	1.23	1.00
Atropine + obidoxime + MB327	**591.6 (456.9–766.1) ***	**1.80**	**591.6 (456.9–766.1) ***	**1.80**	**1.00**

* $p < 0.05$ (comparison with the untreated values). Bold values are significantly different from untreated values at the level of $p < 0.05$.

3.2. The Efficacy of Antidotes (Atropine, HI-6, MB327) for Prevention of Soman Lethality

The data for soman appear in Table 2. The times to death differed slightly between the treatment groups; nevertheless, most mice died within the first hour. The average time to death within the first 6 h was 6.7 min for non-treated animals and 22.4 min for treated animals. Only for atropine with the higher dose of MB327 did deaths occur after 6 h. Thus, with the higher dose of MB327 the LD_{50} of soman was increased 1.48-fold at 6 h, but only 1.31-fold at 24 h. In the other groups—atropine alone, or with HI-6 or the lower dose of MB327, or with HI-6 and the higher dose of MB327—all deaths occurred within 6 h. Atropine increased the LD_{50} 1.36-fold, atropine and HI-6 increased it 1.81-fold, atropine and the lower dose of MB327 increased it 1.32-fold, and atropine and HI-6 with a higher dose of MB327 increased it 1.80-fold, at both end points. The efficacy of HI-6 with atropine exceeded that of atropine and MB327 regardless of the MB327 dose and end point. With atropine and the higher dose of MB327, a small increase in protection ratio compared to atropine alone was apparent at 6 h but the difference was not significant. A significant benefit of MB327 on the efficacy of atropine and HI-6 was not observed.

Table 2. The effect of experimental endpoint on the protection provided against the lethal effects of soman in mice.

Treatment	LD_{50} (μg/kg) ± 95% Confidence Limit—6 h	Protective Ratio A	LD_{50} (μg/kg) ± 95% Confidence Limit—24 h	Protective Ratio A	Protective Ratio B
——	110.5 (79.4–137.1)	—-	110.5 (79.4–137.1)	—-	—-
Atropine	150.1 (92.8–190.1)	1.36	150.1 (92.8–190.1)	1.36	1.00
Atropine + HI-6	**199.9 (140.6–282.3) ***	**1.81**	**199.9 (140.6–282.3) ***	**1.81**	**1.00**
Atropine + MB327 (lower dose)	145.7 (124.7–186.0)	1.32	145.7 (124.7–186.0)	1.32	1.00
Atropine + MB327 (higher dose)	**163.1 (137.6–225.5) ***	**1.48**	144.4 (117.9–196.8)	1.31	1.13
Atropine + HI-6 + MB327	**198.8 (158.4–248.3) ***	**1.80**	**198.8 (158.4–248.3) ***	**1.80**	**1.00**

* $p < 0.05$ (comparison with the untreated values). Bold values are significantly different from untreated values at the level of $p < 0.05$.

3.3. The Efficaccy of Antidotes (Atropine, Trimedoxime, MB327) for Prevention of Tabun Lethality

The tabun results feature in Table 3. Times to death differed slightly between treatment groups. All deaths occurred within 6 h in mice given atropine and trimedoxime, atropine and the lower dose of MB327, and atropine with trimedoxime and MB327. Most mice died within the first hour. The average time to death within the first 6 h was 14.3 min for non-treated animals and 17.6 min for treated animals. With atropine alone, and with atropine in combination with the higher dose of MB327, some deaths occurred after 6 h. Thus, atropine increased the LD_{50} of tabun 1.20-fold at 6 h but only 1.09-fold at 24 h. Atropine and the higher dose of MB327 increased it 1.52-fold at 6 h and only 1.32-fold at 24 h. Atropine and the lower dose of MB327 increased it only 1.20-fold, atropine and trimedoxime increased it 1.95-fold, and atropine and trimedoxime and the higher dose of MB327 increased it 2.06-fold. With atropine and the higher dose of MB327, the protection ratio increased compared to atropine alone, at both experimental end points but the differences were not significant. The efficacy of atropine and trimedoxime was higher than that of atropine and MB327 regardless of the dose of the latter and end point. A significant benefit of MB327 on the efficacy of atropine and trimedoxime was not observed.

Table 3. The effect of experimental endpoint on the protection provided against the lethal effects of tabun in mice.

Treatment	LD_{50} (μg/kg) ± 95% Confidence Limit—6 h	Protective Ratio A	LD_{50} (μg/kg) ± 95% Confidence Limit—24 h	Protective Ratio A	Protective Ratio B
——	420.5 (370.8–470.2)	—-	420.5 (370.8–470.2)	—-	—-
Atropine	504.2 (447.4–533.3)	1.20	458.3 (405.2–494.0)	1.09	1.10
Atropine + trimedoxime	**818.9 (774.2–866.2) *,x**	**1.95**	**818.9 (774.2–866.2) *,x**	**1.95**	**1.00**
Atropine + MB327 (lower dose)	503.7 (466.5–543.9)	1.20	503.7 (466.5–543.9)	1.20	1.00
Atropine + MB327 (higher dose)	**639.4 (492.2–822.3) ***	**1.52**	**554.2 (472.7–602.9) ***	**1.32**	**1.15**
Atropine + trimedoxime + MB327	**866.0 (738.9–1017.5) *,x**	**2.06**	**866.0 (738.9–1017.5) *,x**	**2.06**	**1.00**

* $p < 0.05$ (comparison with the untreated values). ^{x} $p < 0.05$ (comparison with the values treated with atropine alone). Bold values are significantly different from untreated values and values treated with atropine alone at the level of $p < 0.05$.

3.4. The Efficacy of Antidotes (Atropine, HI-6, MB327) for Prevention of Cyclosarin Lethality

The efficacies of the antidotes to cyclosarin appear in Table 4. A difference in distribution of times to death among treatment groups was not observed; all deaths occurred within the first 6 h. Most mice died within the first hour. The average time to death within the first 6 h was 9.3 min for non-treated animals and 12.5 min for treated animals. With atropine alone the LD_{50} of cyclosarin increased 1.31-fold. In combination with HI-6 it increased by 3.15-fold, with the lower or higher dose of MB327 it increased it 1.24- or 1.34-fold, respectively, and with HI-6 and the higher dose of MB327 it increased it 3.12-fold. Atropine and the higher dose of MB327 produced a slightly increased therapeutic efficacy compared to atropine with the lower dose of MB327 but the difference was not significant. The efficacy of atropine and HI-6 was superior to that of atropine and MB327. A benefit of MB327 on the efficacy of atropine and HI-6 was not observed.

Table 4. The effect of experimental endpoint on the protection provided against the lethal effects of cyclosarin in mice.

Treatment	LD_{50} (μg/kg) ± 95% Confidence Limit—6 h	Protective Ratio A	LD_{50} (μg/kg) ± 95% Confidence Limit—24 h	Protective Ratio A	Protective Ratio B
——	248.4 (192.8–287.9)	—-	248.4 (192.8–287.9)	—-	—-
Atropine	326.8 (254.9–417.7)	1.31	326.8 (254.9–417.7)	1.31	1.00
Atropine + HI-6	**782.9 (680.6–856.4) *,x**	**3.15**	**782.9 (680.6–856.4) *,x**	**3.15**	**1.00**
Atropine + MB327 (lower dose)	309.1 (268.0–394.4)	1.24	309.1 (268.0–394.4)	1.24	1.00
Atropine + MB327 (higher dose)	333.4 (247.1–400.9)	1.34	333.4 (247.1–400.9)	1.34	1.00
Atropine + HI-6 + MB327	**775.9 (635.3–878.8) *,x**	**3.12**	**775.9 (635.3–878.8) *,x**	**3.12**	**1.00**

* $p < 0.05$ (comparison with the untreated values). ^{x} $p < 0.05$ (comparison with the values treated with atropine alone). Bold values are significantly different from untreated values and values treated with atropine alone at the level of $p < 0.05$.

4. Discussion

Oximes are key components of nerve agent antidotes due to their capability to reactivate nerve agent-inhibited AChE. However, their therapeutic efficacy is restricted, as reactivation of inhibited AChE is not universally effective because all nerve agents and current oximes are generally ineffective in the central compartment due to their difficulty crossing the blood–brain barrier [4]. Generally, the reactivating efficacy of each oxime depends on the chemical structure of the nerve agent and it is not the same for all nerve agents studied. Therefore, one of the most effective oximes was chosen for each nerve agent (obidoxime for sarin, trimedoxime for tabun, and HI-6 for soman and cyclosarin [4,7,26,27]). Although obidoxime, used for the treatment of sarin poisoning, has a lower efficacy against sarin than the oxime HI-6 [26], it was used for sarin poisoning in this study due to the need to compare our results with previously published data where obidoxime was used for the treatment of sarin poisoning.

Additionally, anticholinergic drugs such as atropine cannot counter the overstimulation of nAChRs. Therefore, novel potential antidotes, based on bispyridinium non-oxime structures, were developed to mitigate the overstimulation of nAChRs and to reduce the therapeutic reliance on oxime-based reactivation of AChE in the treatment of nerve agent poisoning [12,29].

Several bispyridinium compounds have been shown to counter the acute toxicity of nerve agents [12,21–23,30]. Their efficacy hinges on modulating nAChRs at the ion channel, orthosteric ACh binding sites, or both [31,32]. One of the most promising is MB327. It has been shown to have a positive therapeutic effect due to a non-competitive antagonistic action at muscle type nAChRs and has been found to have a positive allosteric activity at muscle and neuronal AChRs [20,33,34]. MB227 has been characterized as a re-sensitizer of

the desensitized nAChR. MB327 is thereby capable of restoring its functional activity and restoring nerve agent-induced irreversibly disrupted neurotransmission at the neuromuscular junctions. The re-sensitizing effect of MB327 is probably based on its positive allosteric activity, as was repeatedly demonstrated [32,35]. Two putative binding sites were found for MB327. Both sites are located inside the channel: one in the extracellular domain between the γ and α subunits, and the other between β and δ subunits in the transmembrane region [17,33,34]. By comparison, MB327 does not interact with the orthosteric ACh binding sites [16]. It is known that conventional nAChR antagonists have a low therapeutic index between sufficient antagonism and muscle paralysis and, therefore, they have a negative impact on respiration However, MB327, which acts as a re-sensitizer of the desensitized nAChR, has a low impact on respiration when administered at recommended doses [13]. In addition, MB327, like other bispyridinium non-oxime compounds, is a charged polar species. It has a high aqueous solubility and comparatively low hydrophobicity. It is therefore expected to exert its biological action mainly in the periphery rather than in the brain, and to have a low capacity to cross the blood–brain barrier.

In the present study, the significant benefit of MB327 for the therapeutic efficacy of standard antidotal treatment of nerve agent poisoning was not shown.

To determine the optimal potential of antidotes, a pharmacologically relevant time following intoxication should be selected based on the pharmacokinetics and mechanisms of action of the drugs tested. An effective concentration of MB327 in the blood and at key nicotinic synapses in tissues is required for nicotinic antagonism and consequent protection. Due to the predicted rapid elimination of MB327 from the body [23], a decrease in the efficacy of MB327 from 6 to 24 h was anticipated. However, a slight reduction in the efficacy of MB327 from 6 to 24 h was only observed for the higher dose of MB327 for soman and tabun intoxication.

To compare the influence of the end point on the therapeutic efficacy of MB327 with other MB antinicotinics, the analogue MB408 showed a higher decrease in its efficacy from 6 to 24 h in the case of intoxication with nerve agents, especially sarin and soman [36]. Generally, the changes in protection ratio seen with atropine with MB327 at 6 h compared to 24 h were small, were only observed for the higher MB327 dose, and were not statistically significant. In contrast, the effects of MB327 in guinea pigs showed a very marked increase in protection at a 6 h compared to a 24 h end point [37]. This disparity may reflect MB327 pharmacokinetic differences between the mouse and guinea pig: in size, absorption, distribution, metabolism and elimination.

The present and previous studies in mice [36] and in guinea pigs [37] demonstrate that earlier experimental end points can show that certain treatments can provide increased protection against acute intoxication by nerve agents. This is also supported theoretically by the reversible, pharmacological mechanism of action of certain antidotes, and therefore a reliance on their pharmacokinetics, ensuring that therapeutically effective drug concentrations are maintained. Importantly, then, the shorter experimental end point may reduce the risk of falsely rejecting effective treatments, particularly if these are intended for immediate, first-aid treatment of nerve agent casualties. Our study has limitations because only one animal species and one end point (besides the standard 24 h) were used. Due to species differences, especially in the pharmacokinetics of MB327 (and analogues), the end point chosen should be matched to the animal species studied, as different species or end points may provide different results.

5. Conclusions

Although MB327 may provide limited benefit for the treatment of nerve agent poisoning in the absence of an oxime, the data from the evaluation of the therapeutic efficacy of MB327 in this particular study do not support the presumption that this non-competitive antinicotinic may significantly benefit the standard antidotal treatment (atropine + oxime) of nerve agent intoxication, at least in mice. Its effectiveness did not approach any of the oximes studied in this animal species. Therefore, atropine and an oxime should continue to

be the core elements of treatment. As only a negligible beneficial impact of the compound MB327 was observed, novel compounds with similar action to MB327 but which exhibit better nicotinic selectivity and increased antinicotinic efficacy should be developed.

Author Contributions: J.K.: conceptualization; formal analysis; writing—original draft preparation; C.M.T.: conceptualization; writing—review and editing; M.B.: synthesis of MB327; formal analysis; A.C.G.: investigation, writing—review and editing; J.E.H.T.: investigation; supervision. All authors have read and agreed to the published version of the manuscript.

Funding: This research was funded by the Ministry of Defence of the Czech Republic under the grant entitled the "Long-term organization development plan—Medical Aspects of Weapons of Mass Destruction" of the Faculty of Military Health Sciences Hradec Kralove, University of Defence, Czech Republic.

Institutional Review Board Statement: The study was conducted according to the guidelines of the Declaration of Helsinki and approved by the Ethics Committee of the Faculty of Military Health Sciences in Hradec Kralove, Czech Republic (protocol code MO 80162/2021-1457 and date of approval 18 March 2021).

Informed Consent Statement: Not applicable.

Data Availability Statement: The data from this study are available on request from the corresponding author. They are not publicly available due to ethical restrictions.

Acknowledgments: The authors thank Eng. Jana Hatlapatkova and Bc. Iveta Kaderabkova for valued technical assistance and Rebecca L. Williams for checking that MB327 was pure by NMR spectroscopy.

Conflicts of Interest: The authors declare no conflict of interest.

References

1. Hrvat, N.M.; Kovarik, Z. Counteracting poisoning with chemical warfare agents. *Arh. Hig. Rada Toksikol.* **2020**, *71*, 266–284. [CrossRef] [PubMed]
2. Tattersall, J.E.H. Anticholinesterase toxicity. *Curr. Opin. Physiol.* **2018**, *4*, 49–56. [CrossRef]
3. Leibson, T.; Lifshitz, M. Organophosphate and carbamate poisoning: Review of the current literature and summary of clinical and laboratory experience in southern Israel. *Isr. Med. Assoc. J.* **2008**, *10*, 767–770. [PubMed]
4. Bajgar, J. Organophosphates/nerve agent poisoning: Mechanism of action, diagnosis, prophylaxis, and treatment. *Adv. Clin. Chem.* **2004**, *38*, 151–216.
5. Colović, M.B.; Krstić, D.Z.; Lazarević-Pašti, T.D.; Bondžić, A.M.; Vasić, V.M. Acetylcholinesterase inhibitors: Pharmacology and toxicology. *Curr. Neuropharmacol.* **2013**, *11*, 315–335. [CrossRef]
6. Marrs, T.C.; Rice, P.; Vale, J.A. The role of oximes in the treatment of nerve agent poisoning in civilian casualties. *Toxicol. Rev.* **2006**, *25*, 297–323. [CrossRef]
7. Jokanović, M. Structure-activity relationship and efficacy of pyridinium oximes in the treatment of poisoning with organophosphorus compounds: A review of recent data. *Curr. Top. Med. Chem.* **2012**, *12*, 1775–1789. [CrossRef]
8. Timperley, C.M.; Tattersall, J.E.H. Toxicology and medical treatment of organophosphorus compounds. In *Best Synthetic Methods—Organophosphorus (V) Chemistry*; Timperley, C.M., Ed.; Elsevier: Oxford, UK, 2015; pp. 33–89.
9. Sharma, R.; Gupta, B.; Singh, N.; Acharya, J.R.; Musilek, K.; Kuca, K.; Ghosh, K.K. Development and structural modifications of cholinesterase reactivators against chemical warfare agents in last decade: A review. *Mini Rev. Med. Chem.* **2015**, *15*, 58–72. [CrossRef]
10. Timperley, C.M.; Forman, J.E.; Abdollahi, M.; Al-Amri, A.S.; Baulig, A.; Benachour, D.; Borrett, V.; Cariño, F.A.; Geist, M.; Gonzalez, D.; et al. Advice on assistance and protection provided by the Scientific Advisory Board of the Organisation for the Prohibition of Chemical Weapons: Part 1. On medical care and treatment of injuries from nerve agents. *Toxicology* **2019**, *415*, 56–69. [CrossRef]
11. Timperley, C.M.; Abdollahi, M.; Al-Amri, A.S.; Baulig, A.; Benachour, D.; Borrett, V.; Cariño, F.A.; Geist, M.; Gonzalez, D.; Kane, W.; et al. Advice on assistance and protection provided by the Scientific Advisory Board of the Organisation for the Prohibition of Chemical Weapons: Part 2. On preventing and treating health effects from acute, prolonged, and repeated nerve agent exposure, and the identification of medical countermeasures able to reduce or eliminate the longer term health effects of nerve agents. *Toxicology* **2019**, *413*, 13–23.
12. Turner, S.R.; Chad, J.E.; Price, M.E.; Timperley, C.M.; Bird, M.; Green, A.C.; Tattersall, J.E.H. Protection against nerve agent poisoning by a noncompetitive nicotinic antagonist. *Toxicol. Lett.* **2011**, *206*, 105–111. [CrossRef] [PubMed]
13. Sheridan, R.D.; Smith, A.P.; Turner, S.R.; Tattersall, J.E.H. Nicotinic antagonists in the treatment of nerve agent intoxication. *J. R. Soc. Med.* **2006**, *98*, 114–115. [CrossRef]

14. McDonough, J.H.; Shih, T.M. Atropine and other anticholinergic drugs. In *Chemical Warfare Agents: Toxicology and Treatment*, 2nd ed.; Marrs, T.C., Maynard, R.I., Sidell, F.R., Eds.; John Wiley & Sons Ltd.: Chichester, UK, 2007; pp. 287–303.
15. Tattersall, J.E.H. Ion channel blockade by oximes and recovery of diaphragm muscle from soman poisoning in vitro. *Br. J. Pharmacol.* **1993**, *108*, 1006–1015. [CrossRef] [PubMed]
16. Niessen, K.V.; Tattersall, J.E.H.; Timperley, C.M.; Bird, M.; Green, A.C.; Seeger, T.; Thiermann, H.; Worek, F. Interaction of bispyridinium compounds with the orthosteric binding site of human α7 and Torpedo californica nicotinic acetylcholine receptors (nAChRs). *Toxicol. Lett.* **2011**, *206*, 100–104. [CrossRef] [PubMed]
17. Wein, T.; Höfner, G.; Rappenglück, S.; Sichler, S.; Niessen, K.V.; Seeger, T.; Worek, F.; Thiermann, H.; Wanner, K.T. Searching for putative binding sites of the bispyridinium compound MB327 in the nicotinic acetylcholine receptor. *Toxicol. Lett.* **2018**, *293*, 184–189. [CrossRef] [PubMed]
18. Sichler, S.; Höfner, G.; Rappenglück, S.; Wein, T.; Niessen, K.V.; Seeger, T.; Worek, F.; Thiermann, H.; Paintner, F.F.; Wanner, K.T. Development of MS binding assays targeting the binding site of MB327 at the nicotinic acetylcholine receptor. *Toxicol. Lett.* **2018**, *293*, 172–183. [CrossRef] [PubMed]
19. Epstein, M.; Bali, K.; Piggot, T.J.; Green, A.C.; Timperley, C.M.; Bird, M.; Tattersall, J.E.H.; Bermudez, I.; Biggin, P.C. Molecular determinants of binding of non-oxime bispyridinium nerve agent antidote compounds to the adult muscle nAChR. *Toxicol. Lett.* **2021**, *340*, 114–122. [CrossRef]
20. Scheffel, C.; Niessen, K.V.; Rappenglück, S.; Wanner, K.T.; Thiermann, H.; Worek, F.; Seeger, T. Counmeracting desensitization of human α7-nicotinic acetylcholine receptors with bispyridinium compounds as an approach against organophosphorus poisoning. *Toxicol. Lett.* **2018**, *293*, 149–156. [CrossRef]
21. Timperley, C.M.; Bird, M.; Green, A.C.; Price, M.E.; Chad, J.E.; Turner, S.R.; Tattersall, J.E.H. 1,1′-(Propane-1,3-diyl)bis(4-tert-butylpyridinium) di(methane sulfonate) protects guinea pigs from soman poisoning when used as part of a combined therapy. *Med. Chem. Commun.* **2012**, *3*, 352–356. [CrossRef]
22. Kassa, J.; Pohanka, M.; Timperley, C.M.; Bird, M.; Green, A.C.; Tattersall, J.E.H. Evaluation of the benefit of the bispyridinium compound MB327 for the antidotal treatment of nerve-agent poisoned mice. *Toxicol. Mech. Methods.* **2016**, *26*, 334–339. [CrossRef]
23. Price, M.E.; Docx, C.J.; Rice, H.; Fairhall, S.J.; Poole, S.J.C.; Bird, M.; Whiley, L.; Flint, D.P.; Green, A.C.; Timperley, C.M.; et al. Pharmacokinetic profile and quantitation of protection against soman poisoning by the antinicotinic compound MB327 in the guinea-pig. *Toxicol. Lett.* **2016**, *244*, 154–160. [CrossRef] [PubMed]
24. Jun, D.; Kuca, K.; Stodulka, P.; Koleckar, V.; Dolezal, B.; Simon, P.; Veverka, M. HPLC analysis of HI-6 dichloride and dimethanesulfonate—antidotes against nerve agents and organophosphorus pesticides. *Anal. Lett.* **2007**, *40*, 2783–2787. [CrossRef]
25. Tallarida, R.; Murray, R. *Manual of Pharmacological Calculation with Computer Programs*; Springer: New York, NY, USA, 1987.
26. Kassa, J. Review of oximes in the antidotal treatment of poisoning by organophosphorus nerve agents. *J. Toxicol. Clin. Toxicol.* **2002**, *40*, 803–816. [CrossRef] [PubMed]
27. Antonijevic, B.; Stojiljkovic, P. Unequal efficacy of pyridinium oximes in acute organophosphate poisoning. *Clin. Med. Res.* **2007**, *5*, 71–82. [CrossRef]
28. Sevelova, L.; Kuca, K.; Krejcova-Kunesova, G. Antidotal treatment of GF-agent intoxication in mice with bispyridinium oximes. *Toxicology* **2005**, *207*, 1–6. [CrossRef]
29. Ring, A.; Strom, B.O.; Turner, S.R.; Timperley, C.M.; Bird, M.; Green, A.C.; Chad, J.; Worek, F.; Tattersall, J.E.H. Bispyridinium compounds inhibit both muscle and neuronal nicotinic acetylcholine receptors in human cell lines. *PLoS ONE* **2015**, *10*, e0135811. [CrossRef]
30. Kassa, J.; Timperley, C.M.; Bird, M.; Williams, R.L.; Green, A.C.; Tattersall, J.E.H. Some benefit from non-oximes MB408, MB442 and MB444 in combination with the oximes HI-6 or obidoxime and atropine in antidoting sarin or cyclosarin poisoned mice. *Toxicology* **2018**, *408*, 95–100. [CrossRef]
31. Niessen, K.V.; Seeger, T.; Tattersall, J.E.H.; Timperley, C.M.; Bird, M.; Green, A.C.; Thiermann, H.; Worek, F. Affinities of bispyridinium non-oxime compounds to [3H]epibatidine binding sites of Torpedo californica nicotinic acetylcholine receptors depend on linker length. *Chem. Biol. Interact.* **2013**, *206*, 545–554. [CrossRef]
32. Seeger, T.; Eichhorn, M.; Lindner, M.; Niessen, K.V.; Tattersall, J.E.H.; Timperley, C.M.; Bird, M.; Green, A.C.; Thiermann, H.; Worek, F. Restoration of soman-blocked neuromuscular transmission in human and rat muscle by the bispyridinium non-oxime MB327 in vitro. *Toxicology* **2012**, *294*, 80–84. [CrossRef]
33. Rappenglück, S.; Sichler, S.; Höfner, G.; Wein, T.; Niessen, K.V.; Seeger, T.; Paintner, F.F.; Worek, F.; Thiermann, H.; Wanner, K.T. Synthesis of a series of structurally diverse MB327 derivatives and their affinity characterization at the nicotinic acetylcholine receptor. *ChemMedChem* **2018**, *13*, 1806–1816. [CrossRef]
34. Rappenglück, S.; Sichler, S.; Höfner, G.; Wein, T.; Niessen, K.V.; Seeger, T.; Paintner, F.F.; Worek, F.; Thiermann, H.; Wanner, K.T. Synthesis of a series of non-symmetric bispyridinium and related compounds and their affinity characterization at the nicotinic acetylcholine receptor. *ChemMedChem* **2018**, *13*, 2653–2663. [CrossRef] [PubMed]
35. Niessen, K.V.; Muschik, S.; Langguth, F.; Rappenglück, S.; Seeger, T.; Thiermann, H.; Worek, F. Functional analysis of Torpedo Californica nicotinic acetylcholine receptors in multiple activation states by CCM-based electrophysiology. *Toxicol. Lett.* **2016**, *247*, 1–10. [CrossRef] [PubMed]

36. Kassa, J.; Timperley, C.M.; Bird, M.; Green, A.C.; Tattersall, J.E.H. Influence of experimental end point on the therapeutic efficacy of the antinicotinic compounds MB408, MB422 and MB444 in treating nerve agent poisoned mice—A comparison with oxime-based treatment. *Toxicol. Mech. Methods* **2020**, *30*, 703–710. [CrossRef] [PubMed]
37. Price, M.E.; Whitmore, C.L.; Tattersall, J.E.H.; Green, A.C.; Rice, H. Efficacy of the antinicotinic compound MB327 against soman poisoning—Importance of experimental end point. *Toxicol. Lett.* **2018**, *293*, 167–171. [CrossRef] [PubMed]

toxics

MDPI

Article

Synthesis and Decontamination Effect on Chemical and Biological Agents of Benzoxonium-Like Salts

Aneta Markova [1,2], Michaela Hympanova [1,3], Marek Matula [2], Lukas Prchal [1], Radek Sleha [3], Marketa Benkova [1], Lenka Pulkrabkova [1,2], Ondrej Soukup [1,2], Zuzana Krocova [4], Daniel Jun [2] and Jan Marek [1,3,*]

[1] Biomedical Research Centre, University Hospital Hradec Kralove, Sokolska 581, 500 05 Hradec Kralove, Czech Republic; aneta.markova@fnhk.cz (A.M.); michaela.hympanova@fnhk.cz (M.H.); lukas.prchal@fnhk.cz (L.P.); Marketa.Benkova@fnhk.cz (M.B.); lenka.pulkrabkova@fnhk.cz (L.P.); ondrej.soukup@fnhk.cz (O.S.)
[2] Department of Toxicology and Military Pharmacy, Faculty of Military Health Sciences, University of Defence in Brno, Trebesska 1575, 500 05 Hradec Kralove, Czech Republic; marek.matula@unob.cz (M.M.); daniel.jun@unob.cz (D.J.)
[3] Department of Epidemiology, Faculty of Military Health Sciences, University of Defence in Brno, Trebesska 1575, 500 05 Hradec Kralove, Czech Republic; radek.sleha@unob.cz
[4] Department of Molecular Pathology and Biology, Faculty of Military Health Sciences, University of Defence in Brno, Trebesska 1575, 500 05 Hradec Kralove, Czech Republic; zuzana.krocova@unob.cz
* Correspondence: marekjjja@gmail.com; Tel.: +420-495-833-447

Abstract: Benzoxonium chloride belongs to the group of quaternary ammonium salts, which have been widely used for decades as disinfectants because of their high efficacy, low toxicity, and thermal stability. In this study, we have prepared the C_{10}-C_{18} set of benzoxonium-like salts to evaluate the effect of their chemical and biological decontamination capabilities. In particular, biocidal activity against a panel of bacterial strains including *Staphylococcus aureus* in biofilm form was screened. In addition, the most promising compounds were successfully tested against *Francisella tularensis* as a representative of potential biological warfare agents. From a point of view of chemical warfare protection, the efficiency of BOC-like compounds to degrade the organophosphate simulant fenitrothion was examined. Notwithstanding that no single compound with universal effectiveness was identified, a mixture of only two compounds from this group would be able to satisfactorily cover the proposed decontamination spectrum. In addition, the compounds were evaluated for their cytotoxicity as a basic safety parameter for potential use in practice. In summary, the dual effect on chemical and biological agents of benzoxonium-like salts offer attractive potential as active components of decontamination mixtures in the case of a terrorist threat or chemical or biological accidents.

Keywords: quaternary ammonium salts; benzoxonium; decontamination; organophosphates; disinfection; micellar catalysis

Citation: Markova, A.; Hympanova, M.; Matula, M.; Prchal, L.; Sleha, R.; Benkova, M.; Pulkrabkova, L.; Soukup, O.; Krocova, Z.; Jun, D.; et al. Synthesis and Decontamination Effect on Chemical and Biological Agents of Benzoxonium-Like Salts. *Toxics* **2021**, *9*, 222. https://doi.org/10.3390/toxics9090222

Academic Editor: Eduardo Rocha

Received: 28 July 2021
Accepted: 4 September 2021
Published: 15 September 2021

1. Introduction

Benzoxonium chloride (N-benzyl-N,N-bis(2-hydroxyethyl)dodecan-1-aminium chloride, BOC), known for over 30 years [1], manifests strong antimicrobial activity against certain bacterial strains, especially non-spore forming, yeasts and protozoa. In practice, BOC is widely used against buccopharyngeal pathogens as a mucous membrane disinfectant. It is commercially available in the form of gargle solutions, lozenges, and oral sprays, often in combination with lidocaine [2,3]. Likewise in dentistry it is used against dental plaque and dental caries [4,5]. Further applications include disinfection of medical instruments in hospitals, and of skin burns, seborrheic dermatitis, and cutaneous leishmaniosis [4,6,7], as a veterinary fungicide and bactericide in the treatment of animal skin, in the food and beverage industry, and in the textile industry as a bactericide in textile fibers [1,8,9]. Of note, BOC is one of the few quaternary ammonium salts (together with

cetrimide and benzalkonium chloride (BAC)) highly efficient in preservation of topical eye medications [10,11].

BOC belongs in the wide group of quaternary ammonium salts (QACs)—substances with surface-active properties. They are still considered an important component of hygienic and anti-epidemic measures against the spread of nosocomial diseases, due to their high efficacy, low price, and only modest toxicity to eukaryotic cells [12,13].

QACs are predominantly supposed to have relatively unspecific mechanisms of antimicrobial action. Owing to the positively charged nitrogen moiety, QACs are able to interact with the negatively charged outermost surface of cell walls and membranes and penetrate into the phospholipid bilayer with their long alkyl chain, thus causing leakages, ruptures, and disintegration of the cell [14]. QACs exhibit higher activity against Gram-positive (G+) bacteria as these possess a single phospholipid cellular membrane and a thicker cell wall composed of peptidoglycan, whereas Gram-negative (G-) bacteria are enveloped by two cellular membranes and a thinner layer of peptidoglycan. The outer membrane causes decreased antimicrobial activity in the case of Gram-negative bacteria [15].

However, recent studies show that some QACs can be also used as micellar catalysts because of their ability to accelerate the decomposition of neurotoxic organophosphate esters [16–20]. Such esters (e.g., fenitrothion, chlorpyrifos, paraoxon) are widely used as pesticides in agriculture. Similarly, highly toxic organophosphates, so-called nerve agents (tabun, soman and sarin and VX), have been reported be also susceptible to decomposition of their organophosphorus ester moieties by quaternary ammonium salt-type cationic surfactants.

The above-mentioned properties of QACs render benzoxonium salts as suitable active ingredients of a decontamination mixture against chemical and biological agents. Despite the fact that BOC is a well-known compound, there is a lack of comprehensive information describing its potential decontamination properties, and the preparation and evaluation of the whole series [21].

Therefore, within this study, we have designed and synthesized a novel series of BOC-like compounds differing in the long alkyl chain (C_{10}-C_{18}) with an expected dual effect on biological and chemical agents including agents with warfare potential. The decontamination properties screening assessed the antimicrobial effect against eight floating-form strains and a representative biofilm-forming strain of *S. aureus* [22]. The cells in biofilms possess different characteristics than single cells and due to their specific structure present decreased susceptibility [23,24]. We further focused on potentially misused warfare agents. Antimicrobial activity was determined against the Gram-negative *Francisella tularensis*, with potential to be misused as a biological weapon; also determined was the efficiency of BOC-like compounds to decompose fenitrothion as an organophosphate simulant. Finally, the cytotoxicity on a mammalian cell line was evaluated as one of the key safety parameters for new substances. Despite the above-mentioned properties, the substances can have practical use in the military (the main active ingredient of a universal decontamination mixture for chemical and biological warfare agents in form of solution or foam). Further, in the civil sector use as disinfectant in healthcare (viruses, bacteria, fungi) or as active ingredients for decontamination of organophosphorus pesticides (from water, soil, etc.).

2. Materials and Methods

2.1. Synthesis and Analysis

Analytical grade reagents were purchased from Sigma-Aldrich, Fluka, and Merck (Darmstadt, Germany). The solvents were purchased from Penta Chemicals (Prague, Czech Republic). Reactions were monitored by thin-layer chromatography (TLC) using pre-coated silica gel 60 F254 TLC alumina sheet. Column chromatography was performed with silica gel 0.063e0.200 mm. Melting points (m. p.) were determined on a micro heating stage PHMK 05 (VEB Kombinat Nagema, Radebeul, Germany) and are uncorrected. All compounds were fully characterized by NMR spectra and HRMS. NMR spectra were recorded

on a Varian VNMR S500 (operating at 500 MHz for ^{1}H and 125 MHz for ^{13}C; Varian Co., Palo Alto, CA, USA). The chemical shifts (d) are given in ppm, relative to tetramethylsilane (TMS) as internal standard. Coupling constants (*J*) are reported in Hz. Splitting patterns are designated as s, singlet; d, doublet; t, triplet; and m, multiplet. Mass spectra were recorded using a combination of liquid chromatography and mass spectrometry: high-resolution mass spectra (HRMS) and sample purities were obtained by high-performance liquid chromatography (HPLC) with UV and mass spectrometric (MS) detection gradient method. The system used in this study was a Dionex Ultimate 3000 UHPLC: RS Pump, RS Column Compartment, RS Autosampler, Diode Array Detector, controlled by Chromeleon (version 7.2.9 build 11323) software (Thermo Fisher Scientific, Germering, Germany) with Q Exactive Plus Orbitrap mass spectrometer with Thermo Xcalibur (version 3.1.66.10.) software (Thermo Fisher Scientific, Bremen, Germany). Detection was performed by mass spectrometer in positive mode. Settings of the heated electrospray source were: Spray voltage 3.5 kV, Capillary temperature: 262 °C, Sheath gas: 55 arbitrary units, Auxiliary gas: 15 arbitrary units, Spare gas: 3 arbitrary units, Probe heater temperature: 250 °C, Max spray current: 100 mA, S-lens RF Level: 50. C18 column (Kinetex EVO C18, 3 × 150 mm, 2.6 μm, Phenomenex, Torrance, CA, USA) was used in this study. Mobile phase A was ultrapure water of ASTM I type (resistivity 18.2 MΩ.cm at 25 °C) prepared by Barnstead Smart2Pure 3 UV/UF apparatus (Thermo Fisher Scientific, Bremen, Germany) with 0.1% (*v*/*v*) formic acid (HPLC-MS grade, Sigma Aldrich, Steinheim, Germany); mobile phase B was acetonitrile (MS grade, Honeywell-Sigma Aldrich) with 0.1% (*v*/*v*) of formic acid. The flow was constant at 0.4 mL/min. The method started with 1 min of isocratic flow of 5% B, and then the gradient of B rose to 100% B in 3 min and remained constant at 100% B for 1 min. The composition then went back to 5% B and equilibrated for 5 min. Total runtime of the method was 10 min. The column was heated to 27 °C. Samples were dissolved in methanol (LC-MS grade, Fluka-Sigma Aldrich) at a concentration 1 mg/mL and sample injection was 1 μL. Purity was determined from UV spectra measured at wavelength 254 nm. HRMS was determined by total ion current spectra from the mass spectrometer collected at resolution of 140,000 in a range 105–1000 *m*/*z*. Clog *P* was calculated with the MarvinSketch (version 14.9.8.0) software.

2.1.1. General Procedure for Synthesis of N,N-bis(2-hydroxyethyl)-N-alkylamines (**3a-e**)

Diethanolamine (**1**) (22.5 mmol), anhydrous potassium carbonate (30 mmol), and potassium iodide (3 mmol) were dispersed in 40 mL of acetonitrile. Subsequently, the appropriate 1-bromoalkane **2a-e** (15 mmol) was added. The reaction mixture was refluxed under nitrogen atmosphere for 12 h. After filtration the acetonitrile was evaporated under reduced pressure. The residue was dissolved in water (30 mL) and extracted twice with dichloromethane. The organic layer was dried over anhydrous sodium sulfate, filtered, and evaporated to obtain a yellow oily product in 65–96% yields. The intermediates **3a-e** were of satisfactory purity for the next reaction step (>95%).

2.1.2. General Procedures for Synthesis of N-benzyl-N,N-bis(2-hydroxyethyl)alkane-1-aminium Chloride (**5a-e**)

A mixture of the appropriate intermediate *N*,*N*-bis(2-hydroxyethyl)-*N*-alkylamine **3a-e** (14 mmol) and benzyl chloride (**4**, 28 mmol) was heated in a 100 mL flask at 100 °C for 2 h as a solvent-free reaction. Subsequently, the reaction was allowed to stand for 5 days at room temperature. Crude products were purified by crystallization in a medley of 1:10 methanol/ethyl acetate and subsequently in 1:10 methanol/diethyl ether to obtain white solid in 42–79% yields.

2.1.3. NMR and HRMS Analysis

N,N-Bis(2-hydroxyethyl)-N-decylamine (**3a**). Yellow oil, (2.40 g, 65%); ^{1}H-NMR (chloroform-*d*) δ 3.63 (t, *J* = 5.4 Hz, 4H), 2.68 (t, *J* = 5.4 Hz, 4H), 2.57–2.50 (m, 2H), 1.51–1.44 (m, 2H), 1.35–1.21 (m, 14H), 0.89 (t, *J* = 6.8 Hz, 3H); ^{13}C-NMR (chloroform-*d*) δ 59.67, 56.05, 54.79,

31.88, 29.61, 29.55, 29.30, 27.36, 27.17, 22.67, 14.10; HRMS: *m/z* 246.2424 $[M + H]^+$ (calculated *m/z* 246.2428 for $[C_{14}H_{32}NO_2]$).

N,N-Bis(2-hydroxyethyl)-N-dodecylamine (**3b**). Yellow oil, (3.75 g, 91%); ^{1}H-NMR (chloroform-*d*) δ 3.63 (t, *J* = 5.4 Hz, 4H), 2.68 (t, *J* = 5.4 Hz, 4H), 2.58–2.51 (m, 2H), 1.52–1.44 (m, 2H), 1.32–1.22 (m, 18H), 0.89 (t, *J* = 7.1, 1.7 Hz, 3H); ^{13}C-NMR (chloroform-*d*) δ 59.46, 56.08, 54.80, 31.87, 29.62, 29.59, 29.52, 29.30, 27.33, 26.80, 22.64, 14.07; HRMS: *m/z* 274.2736 $[M + H]^+$ (calculated *m/z* 274.2741 for $[C_{16}H_{36}NO_2]$).

N,N-Bis(2-hydroxyethyl)-N-tetradecylamine (**3c**). Yellow oil, (3.07 g, 67%); ^{1}H-NMR (chloroform-*d*) δ 3.62 (t, *J* = 5.4 Hz, 4H), 2.66 (t, *J* = 5.4 Hz, 4H), 2.55–2.49 (m, 2H), 1.49–1.43 (m, 2H), 1.32–1.22 (m, 22H), 0.88 (t, *J* = 6.9 Hz, 3H); ^{13}C-NMR (chloroform-*d*) δ 59.65, 56.05, 54.79, 31.90, 29.67, 29.65, 29.63, 29.62, 29.57, 29.56, 29.34, 27.37, 27.08, 22.67, 14.09; HRMS: *m/z* 302.3054 $[M + H]^+$ (calculated *m/z* 302.3054 for $[C_{18}H_{40}NO_2]$).

N,N-Bis(2-hydroxyethyl)-N-hexadecylamine (**3d**). Yellow oil, (3.82 g, 77%); ^{1}H-NMR (chloroform-*d*) δ 3.62 (t, *J* = 5.4 Hz, 4H), 2.66 (t, *J* = 5.4 Hz, 4H), 2.56–2.49 (m, 2H), 1.51–1.43 (m, 2H), 1.29–1.25 (m, 26H), 0.89 (t, *J* = 6.9 Hz, 3H); ^{13}C-NMR (chloroform-*d*) δ 59.65, 56.05, 54.79, 31.91, 29.68, 29.66, 29.64, 29.62, 29.56, 29.34, 27.37, 27.09, 22.67, 14.09; HRMS: *m/z* 330.3361 $[M + H]^+$ (calculated *m/z* 330.3367 for $[C_{20}H_{44}NO_2]$).

N,N-Bis(2-hydroxyethyl)-N-octadecylamine (**3e**). Yellow solid, m. p. 48.1–49.7 °C (5.17 g, 96%); ^{1}H-NMR (chloroform-*d*) δ 3.62 (t, *J* = 5.4 Hz, 4H), 2.66 (t, *J* = 5.4 Hz, 4H), 2.55–2.49 (m, 2H), 1.49–1.43 (m, 2H), 1.29–1.24 (m, 30H), 0.88 (t, *J* = 6.9 Hz, 3H); ^{13}C-NMR (chloroform-*d*) δ 61.10, 59.62, 56.04, 54.78, 50.94, 31.90, 29.67, 29.64, 29.61, 29.56, 29.33, 27.37, 27.00, 22.66, 14.09; HRMS: *m/z* 358.3675 $[M + H]^+$ (calculated *m/z* 358.3680 for $[C_{22}H_{48}NO_2]$).

N-benzyl-N,N-bis(2-hydroxyethyl)decan-1-aminium chloride (**5a**). White solid, m. p. 114.0–114.6 °C (4.09 g, 78%); ^{1}H-NMR (chloroform-*d*) δ 7.63–7.57 (m, 2H), 7.47–7.39 (m, 3H), 5.73 (t, *J* = 5.4 Hz, 2H), 4.86 (s, 2H), 4.29–4.10 (m, 4H), 3.71–3.52 (m, 4H), 3.39–3.32 (m, 2H), 1.89–1.80 (m, 2H), 1.38–1.14 (m, 14H), 0.87 (t, *J* = 6.9 Hz, 3H); ^{13}C-NMR (chloroform-*d*) δ 133.18, 130.61, 129.25, 127.27, 64.39, 60.20, 59.60, 55.83, 31.78, 29.37, 29.36, 29.18, 29.13, 26.22, 22.69, 22.59, 14.05; HRMS: *m/z* 336.2888 $[M]^+$ (calculated *m/z* 336.2897 for $[C_{21}H_{38}NO_2]^+$).

N-benzyl-N,N-bis(2-hydroxyethyl)dodecan-1-aminium chloride (**5b**). White solid, m. p. 118.7–119.0 °C (4.68 g, 41%); ^{1}H-NMR (chloroform-*d*) δ 7.62–7.57 (m, 2H), 7.47–7.39 (m, 3H), 5.30 (t, *J* = 5.4 Hz, 2H), 4.86 (s, 2H), 4.27–4.14 (m, 4H), 3.71–3.53 (m, 4H), 3.38–3.31 (m, 2H), 1.89–1.80 (m, 2H), 1.36–1.19 (m, 18H), 0.88 (t, *J* = 6.9 Hz, 3H); ^{13}C-NMR (chloroform-*d*) δ 133.17, 130.61, 129.26, 127.27, 64.39, 60.21, 59.61, 55.83, 31.84, 29.55, 29.42, 29.39, 29.27, 29.15, 26.23, 22.69, 22.62, 14.06; HRMS: *m/z* 364.3207 $[M]^+$ (calculated *m/z* 364.3210 for $[C_{23}H_{42}NO_2]^+$).

N-benzyl-N,N-bis(2-hydroxyethyl)tetradecan-1-aminium chloride (**5c**). White solid, m. p. 120.6–120.9 °C (3.92 g, 65%); ^{1}H-NMR (methanol-d_4) δ 7.68–7.62 (m, 2H), 7.60–7.49 (m, 3H), 4.79 (s, 2H), 4.09 (t, *J* = 5.1 Hz, 4H), 3.51 (t, *J* = 7.4, 5.0 Hz, 4H), 3.38–3.31 (m, 2H), 1.98–1.88 (m, 2H), 1.45–1.28 (m, 22H), 0.90 (t, *J* = 6.9 Hz, 3H); ^{13}C-NMR (methanol-d_4) δ 134.34, 131.79, 130.36, 129.11, 65.40, 61.34, 61.08, 56.71, 33.06, 30.79, 30.77, 30.75, 30.71, 30.61, 30.53, 30.46, 30.18, 27.34, 23.72, 23.49, 14.44; HRMS: *m/z* 392.3515 $[M]^+$ (calculated *m/z* 392.3523 for $[C_{25}H_{46}NO_2]^+$).

N-benzyl-N,N-bis(2-hydroxyethyl)hexadecan-1-aminium chloride (**5d**). White solid, m. p. 121.6–121.9 °C (4.39 g, 68%); ^{1}H-NMR (chloroform-*d*) δ 7.63–7.57 (m, 2H), 7.48–7.40 (m, 3H), 5.73 (t, *J* = 5.4 Hz, 2H), 4.86 (s, 2H), 4.28–4.14 (m, 4H), 3.69–3.55 (m, 4H), 3.39–3.32 (m, 2H), 1.90–1.80 (m, 2H), 1.32–1.23 (m, 26H), 0.87 (t, *J* = 6.9 Hz, 3H); ^{13}C-NMR (chloroform-*d*) δ 133.22, 130.67, 129.31, 127.31, 64.43, 60.25, 59.65, 55.89, 31.92, 29.70, 29.66, 29.61, 29.48, 29.45, 29.36, 29.21, 26.28, 22.75, 22.68, 14.11; HRMS: *m/z* 420.3828 $[M]^+$ (calculated *m/z* 420.3836 for $[C_{27}H_{50}NO_2]^+$).

N-benzyl-N,N-bis(2-hydroxyethyl)octadecan-1-aminium chloride (**5e**). White solid, m. p. 124.2–124.7 °C (3.59 g, 52%); ^{1}H-NMR (chloroform-*d*) δ 7.62–7.57 (m, 2H), 7.49–7.39 (m, 3H), 5.72 (t, *J* = 5.4 Hz, 2H), 4.87 (s, 2H), 4.22 (t, *J* = 10.8, 6.3, 5.6 Hz, 4H), 3.62 (t, *J* = 39.6, 14.4, 6.5, 3.3 Hz, 4H), 3.38–3.31 (m, 2H), 1.90–1.81 (m, 2H), 1.38–1.15 (m, 30H), 0.88 (t, *J* = 6.8 Hz, 3H); ^{13}C-NMR (chloroform-*d*) δ 133.19, 130.63, 129.28, 127.28, 64.40, 60.22, 59.61, 55.87, 31.88,

29.68, 29.64, 29.62, 29.59, 29.46, 29.42, 29.32, 29.18, 26.24, 22.71, 22.65, 14.08; HRMS: *m/z* 448.4153 $[M]^+$ (calculated *m/z* 448.4149 for $[C_{29}H_{54}NO_2]^+$).

All spectra are available in the Supplementary Materials (Figures S1–S15).

2.2. Conductivity

The conductivity of surfactant solutions was measured in triplicate on a Tristar Orion conductivity meter in a conductivity cell 013005MD (Thermo Scientific, Waltham, MA, USA). The apparatus was controlled with the software Navigator 21 (Thermo Scientific) using continuous data collection. The solutions were temperature-controlled to 49 ± 0.1 °C. The surfactant stock solutions had a range of concentrations of 15-200 mM and these stock solutions were diluted further to determine the CMC. A linear pump Lineomat (VEB MLW Labortechnik Ilmenau, Germany) was used with a flow rate of 0.43 mL/min. An AREX stirrer (VELP Scientifica Srl, Usmate, Italy) was used for continuous agitation, and the conductivity was recorded every 3 s. The resulting data were captured into an MS Excel datasheet for subsequent analysis. The transformation of the time axis to a concentration axis was performed according to the parameters defining the measurements (starting volume of a liquid in the titration vessel, the concentration of the surfactant solution in the syringe, and the solution feed rate):

$$C_t = \frac{C_0}{1 + \frac{V_{start}}{v_{inj} * t}}$$

where C_t = concentration at time t, C_0 = starting concentration of the surfactant, V_{start} = volume of distilled water at start, v_{inj} = surfactant solution dosing rate and t = time recorded by Navigator21

2.3. Micellar Catalysis

A solution of fenitrothion (O,O-dimethyl O-(3-methyl-4-nitrophenyl) phosphorothioate) was diluted with methanol to obtain a concentration of 10^{-2} M (10 mM). The surfactant stock solutions were diluted in distilled water with a concentration of 500 mM, 100 mM, or 10 mM (pursuant to the value of their CMC). Furthermore, these solutions were diluted in the range of concentrations of 10^{-1}–10^{-5} M. Carbonate buffer 0.1 M was adjusted to pH 10 or 11. Carbonate buffer 250 µL, surfactant stock solution 250 µL, and the solution of fenitrothion 10 µL were homogenized in a 1 cm thick cuvette. The absorption changes were measured by Helios α spectrophotometer (Thermo Fisher Scientific) with a set wavelength of 394 nm. The measurement was temperature-controlled to 37 ± 0.1 °C and stopped at the time when the difference between adjacent absorptions was minimal. The resulting data were processed in Thermo Scientific Vision software (Thermo Fisher Scientific) and then converted into MS Excel. The rate constant was calculated by the procedure described by Guggenheim [25], with modification introduced by Zajicek and Radl [26]. The procedure used is based on the acceptance of the following equation:

$$A_{t+\Delta t} = A_t \times \exp(k_{obs} \times \Delta t) + A_n \times (1-\exp(-k_{obs} \times \Delta t)),$$

where $A_{t+\Delta t}$ = absorption at time t+Δt, A_t = absorption at time t, exp = base of natural logarithm, k_{obs} = observed rate constant, Δt = time between two successive measurements and A_n = absorption at infinite time

This relationship is a linear equation with slope $\exp(k_{obs} \times \Delta t)$ and intersection $A_n \times (1-\exp(-k_{obs} \times \Delta t))$. Data from ten minutes' measurement were put in two columns of MS Excel so that the second column was shifted one row up. This shift presents one value Δt. Data prepared in such a way were displayed in an XY scatter chart. A trends line with a print-out of the coefficient regression equation was interlaid through the displayed points. The slope thus obtained was used for the calculation of the rate constant k_{obs} from the term $\exp(k_{obs} \times \Delta t)$. Rate constants were recalculated to the reaction halftimes [27].

2.4. Bacterial Strains

In vitro antibacterial activity of the prepared compounds was tested on a panel of four Gram-positive and four Gram-negative bacterial strains: *Staphylococcus aureus* (C1947), methicillin-resistant *Staphylococcus aureus* (C1926), *Staphylococcus epidermidis* (C1936), vancomycin-resistant *Enterococcus* (S2484), *Escherichia coli* (A1235), extended-spectrum β-lactamase (ESBL) non-producing *Klebsiella pneumoniae* (C1950), ESBL-producing *Klebsiella pneumoniae* (C1934), and multi-resistant *Pseudomonas aeruginosa* (A1245). All named bacteria used in the study were obtained as clinical isolates from patients (University Hospital, Hradec Kralove, Czech Republic) and stored at −70 °C in the cryobank according to the manufacturer's instructions. When needed, each bacterial strain was inoculated and cultivated on Mueller-Hinton agar (HiMedia, Cadersky-Envitek, Prague, Czech Republic). *Francisella tularensis* LVS, live vaccine strain, was obtained from the collection of Faculty of Military Health Sciences, University of Defense (Hradec Kralove, Czech Republic) and cultured on McLeod plates.

2.5. Biofilm Cultivation

The second-subculture colonies of *S. aureus* were suspended in Mueller-Hinton broth (MHB) to reach 1.0 McFarland Standard. This suspension was diluted with MHB medium 1:30 and subsequently used as the inoculum. The initial bacterial number of the inoculum was verified by viable cell counting and equaled approximately 10^7 CFU/mL. Each well from the MBEC microtiter plate (Innovotech, Edmonton, AB, Canada) was inoculated with 150 µL of inoculum. The inoculated device was incubated for 24 h at 35 °C ± 1 °C while being shaken at 110 rpm. For every MBEC assay, the formed biofilm was verified by viable cell counting of disrupted biofilms after removing four pegs from the lid, rinsing and sonication (Bandelin Sonorex, Bandeline Electronics, Berlin, Germany) in MHB for 15 min. The established bacterial number in formed biofilms equals approximately 10^7 CFU/mL.

2.6. Antimicrobial Activity Evaluation

2.6.1. Broth Microdilution Method

The antibacterial susceptibility against bacteria was determined by the broth microdilution method according to standard M07-A10 [28]; the optimized protocol has been published previously [29,30]. Mueller-Hinton broth (Merck, Prague, Czech Republic) adjusted to pH 7.4 (±0.2) was used as the test medium. Dimethyl sulfoxide (DMSO) served as a diluent for all compounds and its final concentration did not exceed 1% in the test medium. The wells of the microdilution tray contained 200 µL of the MH broth with two-fold serial dilutions of the compounds (500–0.49 µmol/L) and were inoculated with 10 µL of the bacterial suspension. The bacterial suspensions were controlled densitometrically to reach 1.5×10^8 viable colony forming units (CFU) per 1 mL. The MIC values, defined as 95% inhibition of bacterial growth, were determined after 24 h and 48 h incubation at 36 °C ± 1 °C. The MBC values were determined as the concentration of compound causing a decrease in the number of bacterial colonies by ≥99.9%, after subculturing of a 10 µL aliquot of each well without visible growth.

2.6.2. Flow Cytometry Assay

F. tularensis LVS bacterial suspension in PBS was prepared from fresh overnight subculture to reach O.D. 1.0 (optic density at 600 nm) which in the case of *F. tularensis* means 4×10^9 CFU (colony forming units)/mL. 1 mL aliquots were centrifuged for 7 min, 7000× *g* at 4 °C and the supernatant was replaced by 500 µL of the tested compound. After 5 min exposure the treated bacterial suspension was again centrifuged for 7 min, 7000× *g* at 4 °C and the solution of the tested compound was removed. Cells were re-suspended in 1 mL PBS and stored on ice until flow cytometry measurement. A negative control was prepared from dead bacterial suspension resuspended in PBS (OD 1), where the bacteria had been exposed overnight to 36% formaldehyde. Fresh bacteria cultured overnight on McLeod agar plates were resuspended in PBS (OD 1) and used as a positive control. All

samples were diluted 100× in 1 mL of PBS, stained with 1 µL of propidium iodide and 1.5 µL of Syto 9, and incubated in the dark for 15 min. 10 µL of vortexed microspheres were added and samples were properly mixed before measurement. All samples we analyzed with a CyAn ADP Flow Cytometer (Beckman Coulter, Indianapolis, IN, USA). Listmode data were analyzed by Summit v4.3 software (Beckman Coulter). At least three independent experiments were performed.

2.6.3. MBEC Assay

The determination of minimal biofilm eradication concentration (MBEC) against *S. aureus* was determined using MBEC assay plates (Innovotech) according to the manufacturer's instructions using a modified Calgary method [22]. The biofilm formed on the lid of the MBEC assay microtiter plate was rinsed with saline and inserted on the challenge plate. Each microtiter challenge plate contained tested compounds serially diluted two-fold in MHB, with sterility and growth controls. After incubation for 24 h at 35 °C ± 1 °C, the lid with treated biofilm was removed, rinsed with saline, and the biofilm was disrupted by sonication. Disrupted biofilm was released into a new microtiter plate with MHB supplemented by 0.5% Tween 80 as an antimicrobial neutralizer. The MBEC was determined after 24 h of incubation at 35 °C ± 1° by reading OD_{600}. The challenge plate was covered with a new, sterile lid and after 24 h of incubation at 35 °C ± 1 °C was used for MIC determination by reading OD_{600}.

2.7. Antiviral Activity Evaluation

2.7.1. Viruses and Cell Cultures

Murine cytomegalovirus (MCMV) and SARS-CoV-2 virus were used in the experiments. The viral stocks were prepared by infecting susceptible cells. For MCMV, NIH 3T3 cells (murine embryonic fibroblasts) were used, and for SARS-CoV-2 (clinical isolate kindly provided by Assoc. prof. Daniel Ruzek, University of South Bohemia, Ceske Budejovice, Czech Republic), Vero cells CCL81 (African green monkey kidney) were used.

The viral stocks were prepared after virus inoculation of the appropriate cells in a suitable cell culture medium (DMEM with high glucose, containing 10% fetal calf serum, 2 mM glutamine, 100 U/mL penicillin and 100 µg/mL streptomycin). The cells were incubated at 37 °C under 5% CO_2 until 80–90% of cells exhibited cytopathic effect (5–7 days). Following 5 min of centrifugation at 500× *g* the supernatant was collected and frozen in aliquots at −80 °C.

2.7.2. Virucidal Activity Testing

The virucidal activity of the synthesized agents was evaluated by a quantitative suspension test. Briefly, one part of the virus suspension was mixed with one part of bovine serum albumin (final concentration 0.03%; 'clean conditions' as specified in EN 14476) and eight parts of the novel tested compounds. The mixtures were kept at room temperature for 5 min (exposure time). After the exposure period, the mixtures were serially diluted tenfold with ice-cold DMEM and 100 µL of each dilution were seeded into a 96-well microtiter plate with the appropriate cell and incubated at 37 °C in a 5% CO_2 atmosphere until a cytopathic effect was detected, approximately 5–7 days. Six wells per sample dilution were inoculated. Virus-untreated controls with identical protein concentrations were also tested.

Virus titer was determined using the method of Spearman and Karber and expressed as $\log_{10}$ $TCID_{50}$/mL [31,32]. According to the European Standard EN 14476 for the virucidal activity of disinfection, a product should demonstrate at least a $\log_{10}$ reduction of 4 in virus titer, corresponding to 99.99% inactivation [33]. To differentiate between virus-induced cytopathogenic changes and the toxic effect caused by the tested compounds, the cell monolayer was monitored until the end of the virucidal activity testing period for morphological changes after exposure to the disinfectant solution.

2.8. In Vitro Cytotoxicity and Selectivity Index

The standard 3-(4,5-dimethylthiazol-2-yl)-2,5-diphenyltetrazolium bromide (MTT, Merck) cell viability assay was applied according to the manufacturer's protocol on the Chinese hamster ovary cell line CHO-K1 (ECACC, Salisbury, UK) [34]. The cells were cultured according to ECACC recommended conditions and seeded at a density of 8×10^3 per well in the 96-well plate. The tested compounds were dissolved in DMSO (Merck,) and subsequently in the Nutrient Mixture F-12 Ham growth medium (Merck) supplemented with 10% Fetal Bovine Serum and 1% Penicillin-Streptomycin (both Merck) so that the final concentration of DMSO did not exceed 1% (*v*/*v*) per well. Cells were exposed to the tested compounds for 24 h. The medium was replaced by a medium containing 0.5 mg/mL of MTT and the cells were allowed to produce formazan for approximately 3 h under surveillance. Thereafter, the medium with MTT was removed and the crystals of formazan were dissolved in DMSO (100 µL/well; Ing. Petr Švec–PENTA s.r.o., Prague, Czech Republic). Cell viability was assessed spectrophotometrically by the amount of formazan produced. Absorbance was measured at 570 nm with 650 nm as a reference wavelength on Synergy HT (BioTek, Winooski, VT, USA). The IC_{50} value was then calculated from the control-subtracted triplicates using non-linear regression (four parameters) by GraphPad Prism 5.03 or 7.03 software (GraphPad Software, Inc., San Diego, CA, USA). Final IC_{50} values including SEM (standard error of the mean) were obtained as the mean of three independent measurements. The selectivity indices of compounds have been calculated as the ration of the cytotoxicity (IC_{50}) and minimum inhibitory concentrations after 24 h (MIC) for all bacterial strains.

3. Results and Discussion

3.1. Synthesis

The series of alkyl-bis(2-hydroxyethyl)benzylammonium chlorides **5a-e** was prepared by the two-step reaction according to Limanov et al. [35]. The reaction process is shown in Scheme 1.

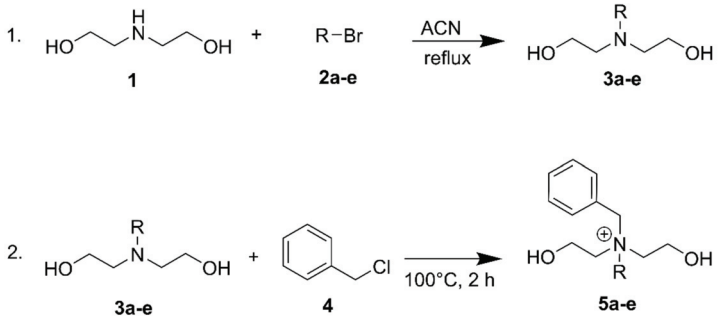

Scheme 1. Two-step preparation of benzoxonium-like salts.

Yields, melting points, purity, and Clog *P* are listed in Table 1. Compound **5b** was prepared with a superior yield compared to Chernyavskaya et al. [36], but with inferior yield according to Limanov et al. [35] prepared in the same way. Homologues **5a** and **5d** were obtained in a yield comparable to that of Stefanovic et al. [37]. The decreased yields are the result of repeated crystallizations to reach satisfactory purity of the final products. Compounds **5c** and **5e** were reported for the first time.

Table 1. Synthesis of BOC-like salts.

Compound	R	Yield (%)	m.p. (°C)	Purity (%)	Clog *P*
5a	$C_{10}H_{21}$	79	114.0–114.6	97	−1.907
5b	$C_{12}H_{25}$	42	118.7–119.0	95	−1.018
5c	$C_{14}H_{29}$	67	120.6–120.9	95	−0.129
5d	$C_{16}H_{33}$	69	121.6–121.9	98	0.76
5e	$C_{18}H_{37}$	7	120.6–122.3	95	1.649

3.2. Conductometry

The critical micelle concentrations (CMC) of the new series of compounds were assessed by a conductometric study performed in aqueous solutions at 49 °C, which takes advantage of the dependency between conductivity change and rising concentration of surfactant. The dependence curve is linear until the unimers of the surfactants can balance the interactions between solution and micelle aggregation. This change is manifested as a breaking of the curve as shown in Figure 1.

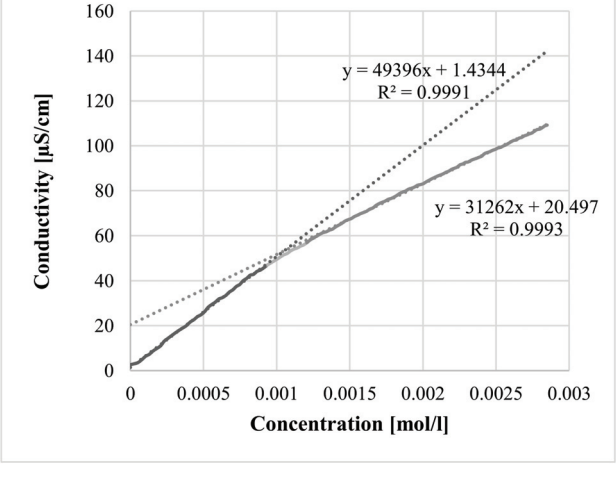

Figure 1. Dependency of conductivity on concentration. The curve was divided into three parts: lower and upper linear parts, and a transition section. The equation of the line and the coefficient of determination were calculated for both linear parts. The CMC value was determined at the intersection of both axes [38].

According to Taube's rule [39], obtained data confirm the dependency of CMC on the elongation of the alkyl chain (Figure 2). The CMC values (Table 2) are the basic characteristics of surfactants needed for further chemical decontamination measurement.

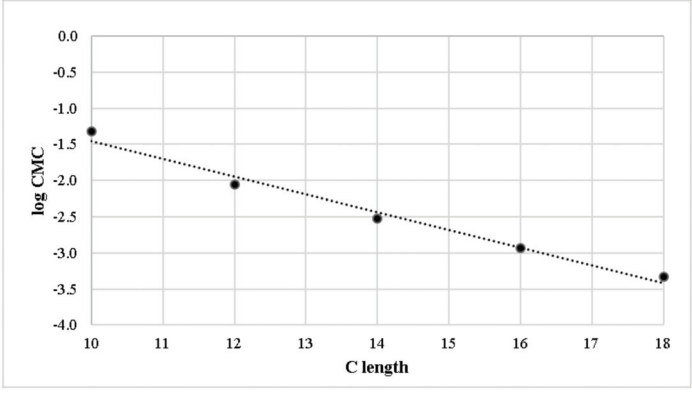

Figure 2. Dependency of log CMC on length of alkyl chain.

Table 2. CMC value of compounds **5a-5e**.

C Length (Compound)	CMC [mol/L]	log CMC
10 (**5a**)	4.836×10^{-2}	−1.316
12 (**5b**)	8.710×10^{-3}	−2.060
14 (**5c**)	3.003×10^{-3}	−2.522
16 (**5d**)	1.159×10^{-3}	−2.936
18 (**5e**)	4.707×10^{-4}	−3.332E

3.3. Micellar Catalysis

Next, the hydrolytic activity against fenitrothion was measured. Because the pesticide fenitrothion contains a 4-nitrophenol group detectable by UV/VIS spectrophotometry, it is a suitable candidate for micellar catalysis investigation as a representative of highly toxic organophosphorus compounds with chemical warfare potential [40]. Reaction of fenitrothion with a micellar catalyst provides 3-methyl-4-nitrophenol, which in alkaline medium creates the yellow-colored nitrophenoxide anion with absorption maximum at 400 nm [27]. This decomposition reaction is monitored by the spectrophotometer. Hydrolytic activity was evaluated in this way using the Guggenheim method for the whole series of synthesized compounds **5a-e** as an assessment of chemical decontamination potential (Table 3). This method is applicable in the case of first order or pseudo-first order reactions and enables processing of the data using linear regression [25]. Compound **5d** is the most efficient micellar catalyst with half-life 2.3 min at 0.01M concentration, and half-life 2.4 min at 0.005M (pH 11 and 37 °C). In comparison with the spontaneous hydrolysis of fenitrothion ($k = 14.00 \times 10^{-6}$, $T_{1/2}$ = 808.4 min) under the same conditions, the novel compounds were 60–160 times more effective at pH 11. It is evident that increasing the pH by one unit causes a significant acceleration of the organophosphate degradation. Spontaneous hydrolysis of fenitrothion at pH 10 was so slow that it could not be determined by the given methodology.

Table 3. Summary data of fenitrothion degradation.

Compound	c (mM)	pH 11, t 37 °C		pH 10, t 37 °C	
		10^4 k (s^{-1})	$T_{1/2}$ (min)	10^4 k (s^{-1})	$T_{1/2}$ (min)
5a	500	6.20	18.6	2.30	50.3
	100	12.82	9.0	3.97	29.2
	50	12.68	9.1	3.77	30.7
	10	0.50	230.8	0.18	606.3
	5	0.35	323.2	-	-
5b	100	8.17	14.1	1.67	69.1
	50	9.35	12.4	2.35	49.3
	10	8.23	14.0	2.65	43.5
	5	5.93	19.5	1.15	100.8
	1	1.80	64.5	-	-
5c	10	**24.62**	**4.7**	6.77	17.1
	5	**23.62**	**4.9**	5.82	19.9
	1	11.28	10.2	2.02	57.5
	0.5	3.80	30.5	1.12	103
	0.1	1.17	98.8	0.50	230.8
5d	10	**50.73**	**2.3**	11.56	10.0
	5	**49.06**	**2.4**	11.14	10.4
	1	12.32	9.4	3.97	29.2
	0.5	6.47	17.9	2.30	50.3
	0.1	1.77	65.3	1.10	105.2
5e	5	23.30	5.0	6.98	16.5
	1	13.95	8.3	4.37	26.4
	0.5	7.82	14.8	2.97	38.9
	0.1	1.87	62.0	0.82	142.5
	0.05	0.83	138.4	0.28	404.1
SH		0.14	808.4	-	-

(–) values were outside the instrumental range. Concentration (c), half-life ($T_{1/2}$), and rate constant (k). Left column includes measurement at pH 11 and 37 °C and right column includes measurement at pH 10 and 37 °C. The compounds are sorted in descending effect as follows **5d** > **5c** > **5e** > **5a** > **5b**. Spontaneous hydrolysis (SH) of fenitrothion at pH 11–$T_{1/2}$ = 808.4 min; at pH 10 it could not be determined by given methodology.

The rate constants determined in the concentrations below the CMC values were affected by spontaneous hydrolysis at a given temperature, by pH, and the presence of hydroxyl groups hydrolyzing the fenitrothion ester bond. Once the concentration exceeds the CMC, the rate constant noticeably rises. Hydroxyl groups and formed micelles together create a counterion cationic surfactant, and fenitrothion is attracted to the Stern layer where it adopts a favorable orientation for nucleophile access and is finally decomposed [41].

The structure-activity relationship evaluation showed a clear effect of the presence of the hydroxyethyl groups on the rate constant of OP decomposition. Indeed, Figure 3 shows asymptotic dependence between rate constant and concentration for the commercially used compounds with identical length of alkyl chain C_{12} at pH 11. Whereas DTMA (*N*-dodecyl-*N*,*N*,*N*-trimethylammonium chloride) and BAC (*N*-benzyl-*N*,*N*-dimethyl-*N*-dodecylammonium chloride), commercially used QAS without hydroxyethyl groups, show poor decontamination effect, DHEMA (*N*,*N*-bis(hydroxyethyl)-*N*-dodecyl-*N*-methylammonium chloride) containing hydroxyethyl groups shows a significant increase in decontamination effect. Notably, 5**b** was found to be much superior to all the reference compounds. Finally, we proved the necessity for the hydroxyl groups potentiated by the benzyl moiety for justification of the choice of BOC-like compounds.

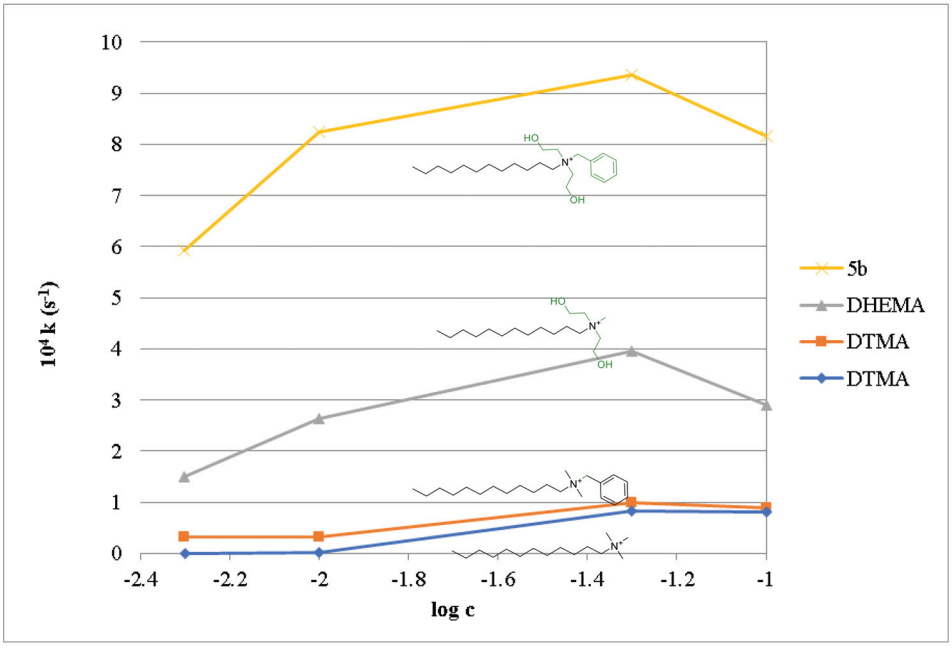

Figure 3. Commercially used compounds at pH 11. The influence of QAS structure on the decontamination effect (rate constant) at pH 11; DTMA (*N*-dodecyl-*N*,*N*,*N*-trimethylammonium chloride), BAC (*N*-benzyl-*N*,*N*-dimethyl-*N*-dodecylammonium chloride), DHEMA (*N*,*N*-bis(hydroxyethyl)-*N*-dodecyl-*N*-methylammonium chloride) and **5b** (*N*-benzyl-*N*,*N*-bis(2-hydroxyethyl)dodecan-1-aminium chloride; green color highlights the positive moiety to increase the decontamination effect. The decrease in activity at high concentrations is due to an excess of surfactant. This so-called empty micelle effect has been previously described [42].

3.4. Antimicrobial Activity

To evaluate the biological decontamination potential, in vitro antimicrobial activity of compounds **5a-e** was evaluated by the broth microdilution method for four Gram-positive and four Gram-negative bacterial strains. Obtained results are presented as minimum inhibitory concentrations (MICs) after 24 h and 48 h, and the minimum bactericidal concentrations (MBCs) after 24 h (Figure 4). High antibacterial activity was found against the G+ bacteria *S. aureus* (STAU), methicillin-resistant *S. aureus* (MRSA), *S. epidermidis* (STEP), and vancomycin-resistant *Enterococcus* (VRE). The observed higher susceptibility to the tested compounds of G+ bacteria compared to G- bacteria, as discussed previously, is in agreement with the literature [43,44]. The lowest MIC and MBC values, i.e., the highest effectiveness, was observed for *S. aureus*. The relationship of alkyl chain length to antimicrobial activity showed that the compounds with C_{14} (**5c**) and C_{16} (**5d**) chains were the most efficient against G+ bacteria. In contrast, the G- bacteria *E. coli* (ESCO), *K. pneumoniae* (KLPN-), extended-spectrum *β*-lactamase-producing *K. pneumoniae* (KLPN+), and multidrug-resistant *P. aeruginosa* (PSAE MR) were most susceptible to compounds with shorter alkyl chains, C_{12} (**5b**) and C_{14} (**5c**), respectively. Unsurprisingly, the least efficient against all tested bacterial strains was the compound with the shortest alkyl chain C_{10} (**5a**) [14,29,31]. Compared with the commercially used BAC series, the **5a-e** series was comparable at a corresponding alkyl chain length. Individually, **5c** and **5b** have shown the best activity against *S. aureus* and *E. coli*, respectively.

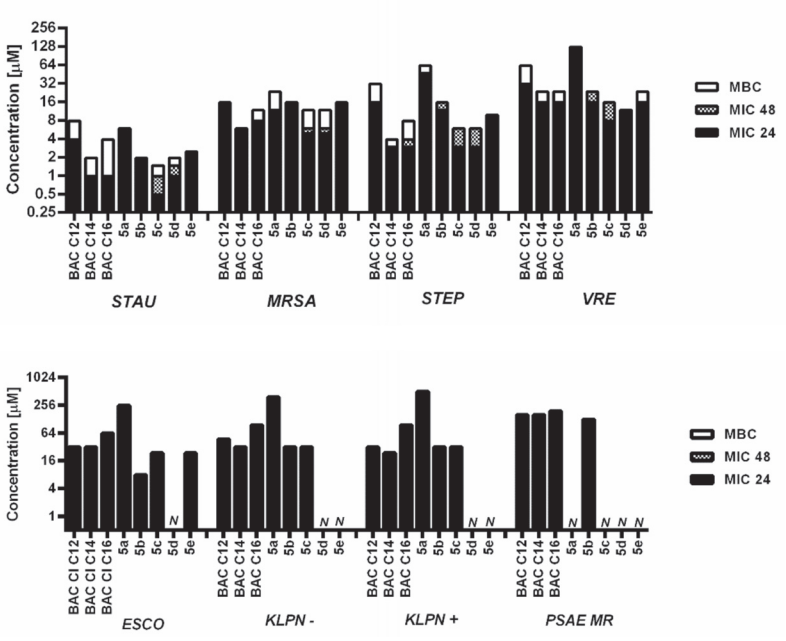

Figure 4. MIC and MBC values of tested compounds for G+ and G- bacterial strains. MIC values were determined after 24 and 48 h of incubation, MBC was determined after 24 h of incubation. The results for BACs had been published elsewhere [31,38]. *N* means that MIC or MBC was higher than the highest soluble concentration of the compound. Abbreviations: STAU = *S. aureus*, MRSA = methicillin-resistant *S. aureus*, STEP = *S. epidermidis*, VRE = vancomycin-resistant *Enterococcus*, ESCO = *E. coli*, KLPN- = *K. pneumoniae*, KLPN+ = extended-spectrum β-lactamase-producing *K. pneumoniae*, PSAE MR = multidrug-resistant *P. aeruginosa*.

According to the MICs and MBCs obtained for the traditional strains, the most efficient derivatives (**5b**, **5c**, and **5d**) underwent susceptibility testing against *Francisella tularensis* Live Vaccine Strain (LVS) by flow cytometry assay (Figure 5). Although we used a *F. tularensis* LVS model strain that is attenuated in comparison to the virulent strain, the resistance of this strain is identical to that of the virulent strains. *F. tularensis* is a Gram-negative, intracellular bacterium which is an important medical challenge. *F. tularensis* is included in category A on the Centers for Disease Control and Prevention (CDC) bioterrorism agent/disease list for the following reasons [45]: (a) it can be easily disseminated or transmitted from person to person; (b) it results in high mortality rates and has the potential for major public health impact; (c) it might cause public panic and social disruption; and (d) it requires special action for public health preparedness. In view of the above, any substance that can successfully kill *F. tularensis* is highly desirable. The time of exposure (5 min) and reference compounds (ethanol 70% and BAC 0.1%) were used to simulate more practical conditions. The obtained results showed high efficacy especially of **5b,** at least comparable to all reference drugs (Figure 6). Notably, substance **5b** at concentration 0.1% has an even better effect compared to ethanol, which is used as standard for disinfection and decontamination against pathogenic bacteria. Moreover, the effect of alkyl chain length on susceptibility to G- bacteria, represented by decreasing activity from **5b** to **5d**, corresponded to results obtained by microdilution assay. In addition, it is clear that the decontamination effect is proportionally dependent on the concentration (**5c** at concentration of 0.1%, 0.05% and 0.01% causes the elimination of 80.47 $\pm$ 4.61%, 58.16 $\pm$ 7.23% and 29.04 $\pm$ 8.80% of bacteria, respectively) (Figure 5).

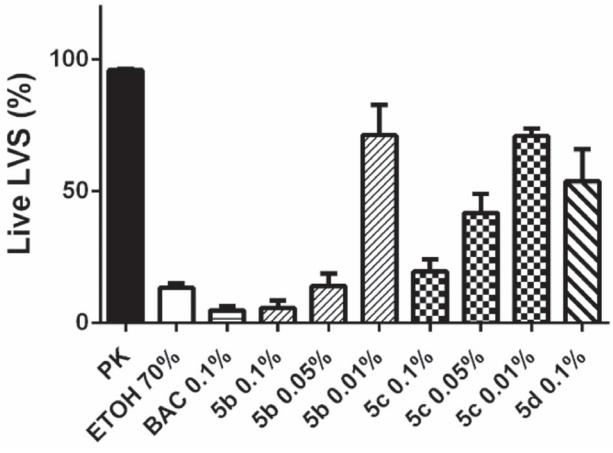

Figure 5. Susceptibility testing against *Francisella tularensis* LVS. The remaining ratio of living LVS after 5 min exposure is expressed as mean ± SEM (n = 3).

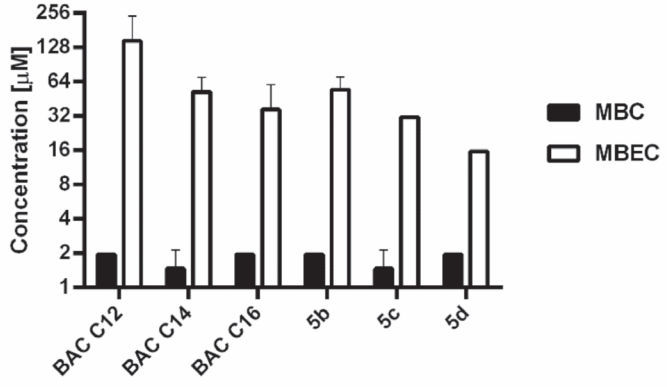

Figure 6. MBEC values and MBC values established for *S. aureus.* MBC and MBEC values were determined after 24 h of incubation for BAC and **5b-d** series by broth microdilution method and MBEC assay respectively. Results are expressed as the mean ± SD (n = 3).

3.5. Antibiofilm Activity and Comparison in Effectiveness against S. aureus in Planktonic and Biofilm Form

To evaluate the efficacy of the novel series against the biofilm form, which is much more resistant than the planktonic form and can often cause a relapse of the infection, a S. aureus biofilm formed on a polystyrene surface for 24 h was exposed for 24 h to the 5b, 5c, 5d and BAC derivatives with C12, C14 and C16 alkyl chains. The minimal biofilm eradication concentration (MBEC) showed comparable activity between both tested series, and notably the MBECs values of 5b-d derivatives were slightly lower than the values for the corresponding BAC derivatives. Comparison of established MBEC and MBC values have shown that S. aureus in biofilm form was 4–64 times less susceptible to the tested compounds than in planktonic form. All results are depicted in Figure 6.

3.6. Virucidal Activity against Enveloped Viruses

To evaluate the width of the spectrum against different microorganisms, the virucidal activity of **5b-d** on murine cytomegalovirus (MCMV) and SARS-CoV-2 virus was determined using a quantitative suspension assay. Virus titer was evaluated using the

Spearman-Karber method and expressed as logTCID50/mL [32]. In accordance with EN 14476 for disinfection with full virucidal activity, the substance should demonstrate a reduction in virus titer of at least 4 orders of magnitude, corresponding to 99.99% inactivation [33]. The morphological changes of one layer of cells were monitored to distinguish between the virus-induced cytopathic changes and the toxic effect caused by the test substance. The highest efficiency was shown by substance **5b**, where the virus titer decreased by more than 5 orders of magnitude at a concentration of 0.01% (Table 4). The decrease could not be determined exactly for the compounds at a concentration of 0.1% (marked>), as the tested substances at this concentration already affected the cell culture which was used for growing the virus. Evaluation against SARS-CoV-2 showed that **5b** and **5c** showed only a modest effect at a concentration of 0.01%. Unfortunately, at higher concentration (0.1%), growth of the cells for culturing the virus was affected and the effect reaching the required value of a decrease of 4 logarithms cannot be confirmed.

Table 4. Determination of virucidal activity against MCMV and SARS-CoV-2 (5 min exposure).

Compounds	Conc. (mM)	ΔlogTCID50 (MCMV)	ΔlogTCID50 (SARS-CoV-2)
5b	0.1% (2.690)	>3.34 [a]	>3.5 1[a]
	0.01% (0.269)	5.33	0.47
5c	0.1% (2.340)	>2.34 [a]	>3.51 [a]
	0.01% (0.234)	3.34	0.64
5d	0.1% (2.190)	>3.34 [a]	1.00
	0.01% (0.219)	−0.50	0.84

[a] The symbol > indicates that the concentration of the tested substances already affected the cell culture used for virus cultivation and it is not possible to determine the exact value.

3.7. Cell Viability Evaluation and Selectivity Index

To define the cytotoxic selectivity, i.e., safety, towards eukaryotic cells, in vitro cytotoxicity studies were performed using the mammalian Chinese hamster ovary (CHO)-K1 cell line. The values of IC_{50} (half maximal inhibitory concentration) confirmed the predicted trend of the correlation described earlier for the homolog group, i.e., elongation of the alkyl chain length increases the cytotoxic potential of the drugs (Table 5) [29,31]. This effect is related to the increasing lipophilicity expressed as the Clog *P* (Table 5), and most likely correlates with the easier ability to penetrate cells. Notably, considering the identical BAC homologs (BAC 12-16), we can conclude that the introduction of the hydroxyethyl groups into the structure increases the IC_{50} value and therefore reduces the toxicity of the substances. Furthermore, the selectivity indexes were calculated as the ration of IC_{50}/MIC (24 h) for all bacterial strains (Table 6).

Table 5. The effect of the tested compounds on CHO-K1 cell viability. Values are expressed as the IC_{50} (series **5a-e**): Mean ± SEM (n = 3).

Compound	IC_{50} ± SEM (μM)	Clog *P*
5a	128.40 ± 12.7	−1.91
5b	36.09 ± 0.5	−1.02
5c	27.34 ± 1.1	−0.13
5d	19.58 ± 0.5	0.76
5e	19.14 ± 1.3	1.64
BAC 12 [a]	19.54 ± 1.2	2.63
BAC 14 [a]	15.04 ± 0.1	3.52
BAC 16 [a]	12.85 ± 1.4	4.41

[a] The preparation of **BAC_{12-16}** has been described elsewhere [46].

Table 6. The selectivity indexes of benzoxonium-like salts calculated as ration IC_{50}/MIC (24h).

	SI (IC_{50}/MIC)							
Compounds	**STAU**	**MRSA**	**STEP**	**VRE**	**ESCO**	**KLPN-**	**KLPN+**	**PSAE MR**
5a	21.986	10.956	2.739	1.027	0.514	0.342	0.257	<0.257
5b	18.508	2.309	3.079	2.309	4.621	1.155	1.155	0.289
5c	55.796	5.602	9.331	3.501	1.166	0.875	0.875	<0.437
5d	19.980	4.012	6.683	1.671	<0.313	<0.313	<0.313	<0.313
5e	8.700	1.225	1.959	1.225	0.817	<0.612	<0.612	<0.612
BAC 12	3.750	0.625	0.625	0.375	0.313	0.156	0.094	0.039
BAC 14	13.193	5.127	3.847	2.310	0.722	0.577	0.241	0.030
BAC 16	19.668	0.987	4.936	3.946	1.234	0.822	0.822	<0.051

Abbreviations: STAU = *S. aureus*, MRSA = methicillin-resistant *S. aureus*, STEP = *S. epidermidis*, VRE = vancomycin-resistant *Enterococcus*, ESCO = *E. coli*, KLPN- = *K. pneumoniae*, KLPN+ = extended-spectrum β-lactamase-producing *K. pneumoniae*, PSAE MR = multidrug-resistant *P. aeruginosa*, SI—selectivity index, MIC—minimum inhibitory concentration (24 h).

4. Conclusions

The series of benzoxonium-like salts with alkyl chain length C_{10}, C_{12}, C_{14}, C_{16} and C_{18} was identified as promising active ingredients for chemical-biological decontamination. Critical micellar concentration as a standard characteristic of surfactants has shown a suitable concentration for chemical decontamination and the efficacy in fenitrothion degradation surpassed that of all the reference compounds. Biocidal activity against various strains of bacteria including *F. tularensis* and *S. aureus* in biofilm form was also determined to discover biological decontamination potential. The homolog with a chain length of C_{12} (**5b**) shows the highest biocidal activity. However, the best effect for chemical decontamination is observed for derivatives with a longer alkyl chain (i.e., compounds **5d**, **5e**). In addition, the compounds seem to be safe on mammalian cell lines as a basic safety parameter for potential use in practice. Finally, BOC-type compounds have been found to have a significant dual effect against both chemical and biological agents. It is thus possible to envisage their use, individually or in a mixture, as active components of multi-purpose decontamination products.

Supplementary Materials: The following are available online at https://www.mdpi.com/article/10.3390/toxics9090222/s1, Figure S1: Figure S1: ^{1}H NMR (500 MHz, Chloroform-*d*) – 5a, Figure S2: 13C NMR (126 MHz, Chloroform-d) – 5a, Figure S3: 1H NMR (500 MHz, Chloroform-d) – 5b, Figure S4: 13C NMR (126 MHz, Chloroform-d) – 5b, Figure S5: ^{1}H NMR (500 MHz, Methanol-d_4) – 5c, Figure S6: ^{13}C NMR (126 MHz, Methanol-d_4) – 5c, Figure S7: ^{1}H NMR (500 MHz, Chloroform-*d*) – 5d, Figure S8: ^{13}C NMR (126 MHz, Chloroform-*d*) – 5d, Figure S9: ^{1}H NMR (500 MHz, Chloroform-*d*) – 5e, Figure S10: ^{13}C NMR (126 MHz, Chloroform-d) – 5e, Figure S11: MS spectrum of 5a in Rt 3.15 min, Figure S12: MS spectrum of 5b in R_t 3.28 min, Figure S13: MS spectrum of 5c in Rt 3.46 min, Figure S14: MS spectrum of 5d in Rt 3.64 min, Figure S15: MS spectrum of 5e in Rt 3.84 min.

Author Contributions: A.M. was responsible for the preparation of benzoxonium salts and characterization of their structure and writing the manuscript; M.H. was responsible for the evaluation of antibacterial and antibiofilm properties; A.M. and M.M. assessed the critical micellar concentration of prepared QAS and micellar catalysis measurement; L.P. (Lukas Prchal) performed HPLC analysis including calculation of lipophilicity; R.S. assessed the antiviral activity; M.B. and L.P. (Lenka Pulkrabkova) were responsible for the evaluation of cytotoxicity assessment; Z.K. was responsible for the evaluation of susceptibility of *Francisella tularensis*; O.S., D.J. and J.M. participated in the QAS design, management of the study and final correction of the manuscript and correspondence. All authors have read and agreed to the published version of the manuscript.

Funding: This research was funded by the Czech Health Research Council (no. NV19-09-00198 and NV18-09-00181), by Ministry of Education, Youth and Sports of the Czech Republic (project SV/FVZ201808), and by a grant of Ministry of Defence "Long Term Development Plan" Medical

Aspects of Weapons of Mass Destruction of the Faculty of Military Health Sciences, University of Defence.

Institutional Review Board Statement: Not applicable.

Informed Consent Statement: Not applicable.

Data Availability Statement: Not applicable.

Acknowledgments: The authors are grateful to Ian McColl for assistance with the manuscript.

Conflicts of Interest: Authors declare no conflict of interest.

References

1. EP3061864A1—Textiles Having Antimicrobial Properties—Google Patents. Available online: https://patents.google.com/patent/EP3061864A1/en (accessed on 18 September 2020).
2. Weibel, M.A.; Cortat, M.; Lebek, G.; LeCotonnec, J.Y.; Kitler, M.E.; Barcherini, G. An Approach of the in Vivo Antibacterial Activity of Benzoxonium Chloride and Comparison with Other Buccopharyngeal Disinfectants. *Arzneimittelforschung* **1987**, *37*, 467–471. [PubMed]
3. Benzoxonium Chloride. Available online: https://www.drugs.com/international/benzoxonium-chloride.html (accessed on 18 September 2020).
4. Ponzielli, G.; Taidelli-Palmizi, G. Dodecyl-di-beta-oxyethyl-benzylammonium chloride in the topical therapy of burns. *Clin. Ter.* **1979**, *90*, 251–259. [PubMed]
5. Firestone, A.R.; Schmid, R.; Mühlemann, H.R. Topical Effects of a Quaternary Ammonium Compound on Caries Incidence and Bacterial Agglomerate Formation in the Rat. *Caries Res.* **1981**, *15*, 338–340. [CrossRef] [PubMed]
6. Daie Parizi, M.H.; Karvar, M.; Sharifi, I.; Bahrampour, A.; Heshmat Khah, A.; Rahnama, Z.; Baziar, Z.; Amiri, R. The Topical Treatment of Anthroponotic Cutaneous Leishmaniasis with the Tincture of Thioxolone plus Benzoxonium Chloride (Thio-Ben) along with Cryotherapy: A Single-Blind Randomized Clinical Trial. *Dermatol. Ther.* **2015**, *28*, 140–146. [CrossRef]
7. Hakimi Parizi, M.; Pardakhty, A.; sharifi, I.; Farajzadeh, S.; Daie Parizi, M.H.; Sharifi, H.; Keyhani, A.R.; Mostafavi, M.; Bamorovat, M.; Ghaffari, D. Antileishmanial Activity and Immune Modulatory Effects of Benzoxonium Chloride and Its Entrapped Forms in Niosome on Leishmania Tropica. *J. Parasit. Dis.* **2019**, *43*, 406–415. [CrossRef] [PubMed]
8. Kis, G.L. Antimicrobial Compositions. CA2025728C, 26 February 2002. Available online: https://worldwide.espacenet.com/patent/search/family/004256126/publication/CA2025728C?q=CA2025728C (accessed on 18 September 2020).
9. Szekacs, A. Mechanism-Related Teratogenic, Hormone Modulant and Other Toxicological Effects of Veterinary and Agricultural Surfactants. *Insights Vet. Sci.* **2017**, *1*, 24–31. [CrossRef]
10. Labranche, L.-P.; Dumont, S.N.; Levesque, S.; Carrier, A. Rapid Determination of Total Benzalkonium Chloride Content in Ophthalmic Formulation. *J. Pharm. Biomed. Anal.* **2007**, *43*, 989–993. [CrossRef] [PubMed]
11. Horn, G. Method and Composition Which Reduces Stimulation of Muscles Which Dilate the Eye. U.S. Patent 20060211753A1, 21 September 2006.
12. Ioannou, C.J.; Hanlon, G.W.; Denyer, S.P. Action of Disinfectant Quaternary Ammonium Compounds against Staphylococcus Aureus. *Antimicrob. Agents Chemother.* **2007**, *51*, 296–306. [CrossRef]
13. Minbiole, K.P.C.; Jennings, M.C.; Ator, L.E.; Black, J.W.; Grenier, M.C.; LaDow, J.E.; Caran, K.L.; Seifert, K.; Wuest, W.M. From Antimicrobial Activity to Mechanism of Resistance: The Multifaceted Role of Simple Quaternary Ammonium Compounds in Bacterial Eradication. *Tetrahedron* **2016**, *72*, 3559–3566. [CrossRef]
14. Dolezal, R.; Soukup, O.; Malinak, D.; Savedra, R.M.L.; Marek, J.; Dolezalova, M.; Pasdiorova, M.; Salajkova, S.; Korabecny, J.; Honegr, J.; et al. Towards Understanding the Mechanism of Action of Antibacterial N-Alkyl-3-Hydroxypyridinium Salts: Biological Activities, Molecular Modeling and QSAR Studies. *Eur. J. Med. Chem.* **2016**, *121*, 699–711. [CrossRef]
15. Jennings, M.C.; Minbiole, K.P.C.; Wuest, W.M. Quaternary Ammonium Compounds: An Antimicrobial Mainstay and Platform for Innovation to Address Bacterial Resistance. *ACS Infect. Dis.* **2015**, *1*, 288–303. [CrossRef]
16. Tiwari, S.; Ghosh, K.; Marek, J.; Kuca, K. Cationic Micellar-Catalyzed Hydrolysis of Pesticide Fenitrothion Using α-Nucleophiles. *Lett. Drug Des. Discov.* **2010**, *7*, 194–199. [CrossRef]
17. Sharma, R.; Gupta, B.; Yadav, T.; Sinha, S.; Sahu, A.K.; Karpichev, Y.; Gathergood, N.; Marek, J.; Kuca, K.; Ghosh, K.K. Degradation of Organophosphate Pesticides Using Pyridinium Based Functional Surfactants. *ACS Sustain. Chem. Eng.* **2016**, *4*, 6962–6973. [CrossRef]
18. Singh, N.; Karpichev, Y.; Gupta, B.; Satnami, M.L.; Marek, J.; Kuca, K.; Ghosh, K.K. Physicochemical Properties and Supernucleophilicity of Oxime-Functionalized Surfactants: Hydrolytic Catalysts toward Dephosphorylation of Di- and Triphosphate Esters. *J. Phys. Chem. B* **2013**, *117*, 3806–3817. [CrossRef] [PubMed]

19. Singh, N.; Ghosh, K.K.; Marek, J.; Kuca, K. Hydrolysis of Carboxylate and Phosphate Esters Using Monopyridinium Oximes in Cationic Micellar Media. *Int. J. Chem. Kinet.* **2011**, *43*, 569–578. [CrossRef]
20. Banjare, M.K.; Kurrey, R.; Yadav, T.; Sinha, S.; Satnami, M.L.; Ghosh, K.K. A Comparative Study on the Effect of Imidazolium-Based Ionic Liquid on Self-Aggregation of Cationic, Anionic and Nonionic Surfactants Studied by Surface Tension, Conductivity, Fluorescence and FTIR Spectroscopy. *J. Mol. Liq.* **2017**, *241*, 622–632. [CrossRef]
21. Domagk, G. A Method for Disinfection and Preservation. DE680599C, 1 September 1939.
22. Ceri, H.; Olson, M.E.; Stremick, C.; Read, R.R.; Morck, D.; Buret, A. The Calgary Biofilm Device: New Technology for Rapid Determination of Antibiotic Susceptibilities of Bacterial Biofilms. *J. Clin. Microbiol.* **2020**, *37*. Available online: https://jcm.asm.org/content/37/6/1771/figures-only (accessed on 8 April 2021).
23. Singh, S.; Singh, S.K.; Chowdhury, I.; Singh, R. Understanding the Mechanism of Bacterial Biofilms Resistance to Antimicrobial Agents. *Open Microbiol. J.* **2017**, *11*, 53–62. [CrossRef]
24. Azeredo, J.; Azevedo, N.F.; Briandet, R.; Cerca, N.; Coenye, T.; Costa, A.R.; Desvaux, M.; Di Bonaventura, G.; Hébraud, M.; Jaglic, Z.; et al. Critical Review on Biofilm Methods. *Crit. Rev. Microbiol.* **2017**, *43*, 313–351. [CrossRef] [PubMed]
25. Guggenheim, E.A. XLVI. On the Determination of the Velocity Constant of a Unimolecular Reaction. *Lond. Edinb. Dublin Philos. Mag. J. Sci.* **1926**, *2*, 538–543. [CrossRef]
26. Zajicek, M.; Radl, Z. Katalyticky Vliv Kationaktivniho Tenzidu Na Hydrolyzu Fosfonatu. In *Sbornik Vyzkumneho Ustavu 070*; Ministry of Defense: Brno, Czech Republic, 1979; pp. 115–129. (In Czech)
27. Cabal, J.; Kuča, K.; Míčová, J. Kinetics of Decompositition of Organophosphate Fenitrothion by Decontaminating Foam-Making Blends. *J. Appl. Biomed.* **2007**, *5*, 167–170. [CrossRef]
28. Clinical and Laboratory Standards Institute (Ed.) *Methods for Dilution Antimicrobial Susceptibility Tests for Bacteria That Grow Aerobically: M07-A10; Approved Standard*, 10th ed.; Documents/Clinical and Laboratory Standards Institute; Committee for Clinical Laboratory Standards: Wayne, PA, USA, 2015.
29. Marek, J.; Malinak, D.; Dolezal, R.; Soukup, O.; Pasdiorova, M.; Dolezal, M.; Kuca, K. Synthesis and Disinfection Effect of the Pyridine-4-Aldoxime Based Salts. *Molecules* **2015**, *20*, 3681–3696. [CrossRef] [PubMed]
30. Malinak, D.; Dolezal, R.; Marek, J.; Salajkova, S.; Soukup, O.; Vejsova, M.; Korabecny, J.; Honegr, J.; Penhaker, M.; Musilek, K.; et al. 6-Hydroxyquinolinium Salts Differing in the Length of Alkyl Side-Chain: Synthesis and Antimicrobial Activity. *Bioorg. Med. Chem. Lett.* **2014**, *24*, 5238–5241. [CrossRef]
31. Soukup, O.; Benkova, M.; Dolezal, R.; Sleha, R.; Malinak, D.; Salajkova, S.; Markova, A.; Hympanova, M.; Prchal, L.; Ryskova, L.; et al. The Wide-Spectrum Antimicrobial Effect of Novel N-Alkyl Monoquaternary Ammonium Salts and Their Mixtures; the QSAR Study against Bacteria. *Eur. J. Med. Chem.* **2020**, *206*, 112584. [CrossRef]
32. Spearman, C. The Method of 'Right and Wrong Cases' ('Constant Stimuli') Without Gauss's Formulae. *Br. J. Psychol.* **1908**, *2*, 227–242. [CrossRef]
33. BS EN 14476:2013+A2:2019—Chemical Disinfectants and Antiseptics. Quantitative Suspension Test for the Evaluation of Virucidal Activity in the Medical Area. Test Method and Requirements (Phase 2/Step 1). 31 August 2019. Available online: https://shop.bsigroup.com/ProductDetail?pid=000000000030401479 (accessed on 8 April 2021).
34. van Meerloo, J.; Kaspers, G.J.L.; Cloos, J. Cell Sensitivity Assays: The MTT Assay. In *Cancer Cell Culture: Methods and Protocols*; Cree, I.A., Ed.; Methods in Molecular Biology; Humana Press: Totowa, NJ, USA, 2011; pp. 237–245. [CrossRef]
35. Limanov, V.E.; Épshtein, A.E.; Skvortsova, E.K.; Aref'eva, L.I.; Gleiberman, S.E.; Volkova, A.P. Synthesis and Antibacterial Action of Surface-Active Quaternary Ammonium Salts Containing Hydroxyethyl Radicals. *Pharm. Chem. J.* **1976**, *10*, 55–58. [CrossRef]
36. Chernyavskaya, M.A.; Stefanovich, V.V.; Sergeeva, I.A.; Belova, A.S. Antimicrobial and Surface-Active Properties of Cationic Surfactants Based on Chloroalkanes and Alkylbenzenes. *Pharm. Chem. J.* **1984**, *18*, 784–787. [CrossRef]
37. Stefanović, G.; Ćirić, J. Synthese und bacterizide Wirkung einiger quaternärer, höherer Alkyl- und Alkenyl-bis-(2-oxyäthyl)-Ammoniumsalze. *Recl. Trav. Chim. Pays-Bas* **1954**, *73*, 401–409. [CrossRef]
38. Benkova, M.; Soukup, O.; Prchal, L.; Sleha, R.; Eleršek, T.; Novak, M.; Sepčić, K.; Gunde-Cimerman, N.; Dolezal, R.; Bostik, V.; et al. Synthesis, Antimicrobial Effect and Lipophilicity-Activity Dependence of Three Series of Dichained *N* -Alkylammonium Salts. *ChemistrySelect* **2019**, *4*, 12076–12084. [CrossRef]
39. Traube, I. Über Die Kapillaritätskonstanten Organischer Stoffe in Wässriger Lösung. *Annu. Chem.* **1891**, *265*, 27–55. [CrossRef]
40. Han, X.; Balakrishnan, V.K.; VanLoon, G.W.; Buncel, E. Degradation of the Pesticide Fenitrothion as Mediated by Cationic Surfactants and Alpha-Nucleophilic Reagents. *Langmuir ACS J. Surf. Colloids* **2006**, *22*, 9009–9017. [CrossRef]
41. Balakrishnan, V.K.; Han, X.; VanLoon, G.W.; Dust, J.M.; Toullec, J.; Buncel, E. Acceleration of Nucleophilic Attack on an Organophosphorothioate Neurotoxin, Fenitrothion, by Reactive Counterion Cationic Micelles. Regioselectivity as a Probe of Substrate Orientation within the Micelle. *Langmuir* **2004**, *20*, 6586–6593. [CrossRef]
42. Bunton, C.A. Micellar Catalysis and Inhibition. *Prog. Solid State Chem.* **1973**, *8*, 239–281. [CrossRef]
43. Tischer, M.; Pradel, G.; Ohlsen, K.; Holzgrabe, U. Quaternary Ammonium Salts and Their Antimicrobial Potential: Targets or Nonspecific Interactions? *ChemMedChem* **2012**, *7*, 22–31. [CrossRef] [PubMed]
44. Shtyrlin, N.V.; Sapozhnikov, S.V.; Galiullina, A.S.; Kayumov, A.R.; Bondar, O.V.; Mirchink, E.P.; Isakova, E.B.; Firsov, A.A.; Balakin, K.V.; Shtyrlin, Y.G. Synthesis and Antibacterial Activity of Quaternary Ammonium 4-Deoxypyridoxine Derivatives. *BioMed Res. Int.* **2016**, *2016*, 3864193. [CrossRef] [PubMed]

45. CDC/Bioterrorism Agents/Diseases (by category)/Emergency Preparedness & Response. Available online: https://emergency.cdc.gov/agent/agentlist-category.asp (accessed on 9 April 2021).
46. Kuca, K.; Marek, J.; Stodulka, P.; Musilek, K.; Hanusova, P.; Hrabinova, M.; Jun, D. Preparation of Benzalkonium Salts Differing in the Length of a Side Alkyl Chain. *Mol. J. Synth. Chem. Nat. Prod. Chem.* **2007**, *12*, 2341–2347. [CrossRef]

toxics

MDPI

Article

Reactive Organic Suspensions Comprising ZnO, TiO_2, and Zeolite Nanosized Adsorbents: Evaluation of Decontamination Efficiency on Soman and Sulfur Mustard

Raluca Elena Ginghina [1,†], Adriana Elena Bratu [1,†], Gabriela Toader [2,*], Andreea Elena Moldovan [2,*], Tudor Viorel Tiganescu [2], Ramona Elena Oncioiu [1], Panaghia Deliu [1], Razvan Petre [1], Gabriel Epure [1] and Munizer Purica [3]

[1] Research and Innovation Center for CBRN Defense and Ecology, 225 Oltenitei Ave., 041327 Bucharest, Romania; ginghinaraluca@gmail.com (R.E.G.); adriana.bratu@nbce.ro (A.E.B.); ramona.oncioiu@nbce.ro (R.E.O.); panaghia.deliu@nbce.ro (P.D.); razvan.petre@nbce.ro (R.P.); gabriel.epure@nbce.ro (G.E.)
[2] Faculty of Weapon Systems Engineering and Mechatronics, Military Technical Academy "Ferdinand I", 39-49 George Cosbuc Boulevard, 050141 Bucharest, Romania; tiganescu.viorel.t@gmail.com
[3] National Institute for R&D in Microtechnologies, 126A Erou Iancu Nicolae Street, 077190 Voluntari, Romania; munizer.purica@imt.ro
* Correspondence: nitagabriela.t@gmail.com (G.T.); andreea.voicu89@gmail.com (A.E.M.)
† Co-first authors, equally contributed to this work.

Citation: Ginghina, R.E.; Bratu, A.E.; Toader, G.; Moldovan, A.E.; Tiganescu, T.V.; Oncioiu, R.E.; Deliu, P.; Petre, R.; Epure, G.; Purica, M. Reactive Organic Suspensions Comprising ZnO, TiO_2, and Zeolite Nanosized Adsorbents: Evaluation of Decontamination Efficiency on Soman and Sulfur Mustard. *Toxics* **2021**, *9*, 334. https://doi.org/10.3390/toxics9120334

Academic Editors: Ondrej Soukup and Jan Korabecny

Received: 11 November 2021
Accepted: 29 November 2021
Published: 3 December 2021

Abstract: This paper comprises an extensive study on the evaluation of decontamination efficiency of three types of reactive organic suspensions (based on nanosized adsorbents) on two real chemical warfare agents: soman (GD) and sulfur mustard (HD). Three types of nanoparticles (ZnO, TiO_2, and zeolite) were employed in the decontamination formulations, for enhancing the degradation of the toxic agents. The efficacy of each decontamination solution was investigated by means of GC-MS analysis, considering the initial concentration of toxic agent and the residual toxic concentration, measured at different time intervals, until the completion of the decontamination process. The conversion of the two chemical warfare agents (HD and GD) into their decontamination products was also monitored for 24 h.

Keywords: chemical warfare agents; decontamination solution; nanoparticles; GC-MS; degradation; conversion rate; soman; sulfur mustard

1. Introduction

Chemical warfare agents (CWAs) represent, undoubtedly, some of the cruelest weapons of mass destruction (WMDs) created by mankind. The modern use of chemical weapons began with The First World War [1]. On 29 April 1997, the Chemical Weapons Convention [2] entered into force and officially banned the use of chemical agents. Nevertheless, large stockpiles of chemical weapons still exist. Moreover, chemical terrorism still represents an imminent threat because chemical agents are inexpensive and are relatively easy to obtain [3], even by small terrorist groups, and can cause mass casualties with small amounts of toxic. The main current CWA threats involve easily produced agents potentially manufacturable on large scales: blister agents (e.g., sulfur mustard) and nerve agents (e.g., soman, sarin, tabun or Vx). Blister agents alkylate molecules such as nucleic acids, proteins, and cellular membrane components [2]. This results in a surge of medical problems: the eyes are firstly impacted, exhibiting redness and irritation which can progress to corneal damage with photophobia, blepharospasm, and temporary blindness [2]. When in contact with skin, these highly electrophilic compounds cause the formation of large and extremely painful blisters [4]. Figure 1 illustrates a comparative representation of the toxicity of six of the most notorious CWAs, and the values plotted were selected from ref. [5].

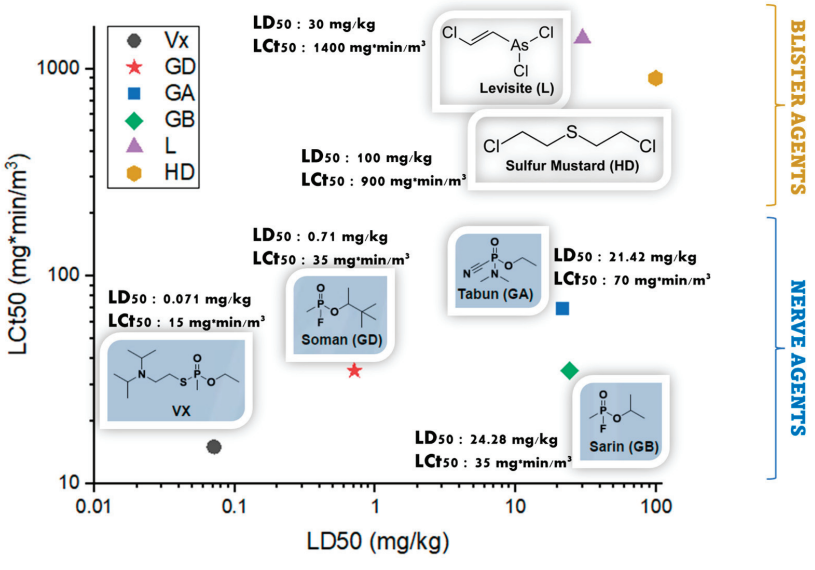

Figure 1. Relative toxicity of chemical warfare agents; LCt_{50} refers to lethal concentration, in mg·min/m^3 and LD_{50} stands for median lethal dose, in mg/kg (skin exposure).

Nerve agents are much more toxic than blister agents, because they are lethal in very small amounts: V-agents are considered the most toxic, with LD_{50} = 0.071 mg/kg (VX), followed by G-agents, LD_{50} = 0.71 mg/kg (soman) or LD_{50} = 24.28 mg/kg (sarin) [2,6]. Their mechanism of action consists of the irreversible inhibition of the acetylcholinesterase enzyme (AChE), with fatal cardiac and respiratory effects [4].

Over time, considerable efforts have been made to create efficient tools suitable for the neutralization of CWAs. The impacts of CWAs can be diminished through the neutralization of their toxic effects by employing adequate media with essential physico-chemical properties, specially designed for this purpose. The process used for the neutralization and removal of CWAs is known as 'decontamination'. Chemical decontamination converts the toxic CW agents into less toxic and non-toxic products, which can be handled safely. The chemical reactions that are generally employed in chemical decontamination methods are either nucleophilic reactions or oxidations [7–10]. To restrict the spread of the contaminants, the decontamination must be carried out rapidly and efficiently because a CWA event represents an emergency which can result in injury, illness, or loss of life. Therefore, emergency intervention departments/offices need to have the appropriate facilities, equipment, and capabilities to respond to chemical agents' exposure, in order to save lives and to mitigate injuries. In this context, the decontamination of warfare agents has become a major challenge for researchers as well as for soldiers. The efficiency of decontamination is conditioned by a set of variables: contamination time, nature of the agent and nature of decontaminants, type of surface contaminated, contamination density, and decontamination formulation, pH, and temperature [3]. An ideal decontamination formulation should be highly compatible with the chemical agents to be able to perform a rapid and efficient decontamination while being non-corrosive and stable in storage. Even though several decontamination formulations have been developed so far, there are intrinsic limitations of their application: low solubility of the CW agents, low neutralization efficiency, toxicity, and corrosivity [11]. Bleaching powder, calcium hypochlorite, and sodium hypochlorite were the first decontaminants that were employed for CWA neutralization. Many commercially available decontamination formulations have been developed over time. Solutions based on ethanol, phenol, sodium hydroxide, ammonia,

calcium hypochlorite, tetrachloroethylene, surfactants, and water were developed and were introduced in the endowment of the armies, but they presented drawbacks related to their poor performances at certain pH levels and also to the potential damages produced to the decontaminated substrate (metal [12], glass [13], plastics [14], rubber [15], wood flooring [16], concrete [17], painted surfaces [18], or the surface of sensitive equipment [19], etc.). Solid adsorbents, such as Fuller's earth [20], have been used as an alternative because they do not affect the surface subjected to decontamination, but the major inconvenience in this case is that they only physically remove the contaminants, not neutralize them [11]. Active sorbents, also called destructive sorbents, represent a prospective development in this field. These solid materials absorb CWAs on their surface, followed by chemical decomposition. Unfortunately, practical CWAs decontamination studies have shown that not all solid decontamination sorbents react with CWAs to the required degree of decomposition [21].

In contrast, nanosized particles (NPs) have been reported as promising prospective reactive sorbent materials [7,11,22] which have the ability to potentiate the neutralization of CWAs [23,24]. In comparison with the conventional materials, nanostructures have attracted great interest due to their enhanced reactivity towards CWAs, owing to large specific surface and reactive edges, corner defects and unusual lattice planes [22]. Prasad et al. reported the decontamination of sulfur mustard (HD) and its surrogate, 2-chloroethyl ethyl sulfide (CEES) by manganese oxide nanosheets and nanotubes and also by titania nanotubes [11,22,25]. CWAs underwent degradation on the surface of these nanostructures through hydrolysis reactions [4,11,22]. Crystalline porous oxides known as zeolites [26] can also adsorb and potentially detoxify simulants and CWAs [27]. When employed in the appropriate decontamination formulations, the nanoparticles can improve the efficiency of CWA decontamination.

Regarding the formulations employed for chemical decontamination, they can be either aqueous or organic, or even biphasic. Certain studies have demonstrated that aqueous systems may delay the oxidation process of CEES simulants while an organic solvent would bring a benefic contribution to the oxidation reaction [28]. Moreover, mustard agents and their analogous simulants are highly soluble in organic solvents. In some cases, for the inactivation of nerve agents, such as soman, a 10% NaOH aqueous solution may prove to be efficient, but with a consumption norm of about 0.5–1 L/m^2, specific for aqueous decontamination solutions, making this decontamination process a producer of high amounts of liquid wastes, whereas an organic decontamination solution has a consumption norm of 0.5 to 0.1 L/m^2. These aqueous decontamination solutions also have the inconvenience of being highly corrosive [16].

In other cases, an organic decontamination solution can be more practical because it includes some advantages, in comparison with aqueous systems: the consumption norm of decontamination solution per square meter can be considerably lower; the preferential solubility of CWAs in specific organic solvents recommend the utilization of organic solutions for the improvement of the decontamination capacity; the compatibility between the organic solvents and CWAs leads to shorter reaction times; organic formulations have better resistance to low temperatures than aqueous systems; organic system are more stable in storage and, in general, they do not require additional preparation at the contaminated site, thus improving the response time of the decontamination actions; and using lower amounts of solvents, the organic systems do not require additional operations prior to analysis (such as extraction and concentration in case of an aqueous solution).

Taking into consideration the need for extensive studies on real warfare agents and for a better understanding of the systems that streamline the decontamination process, we herein report an original survey on novel highly reactive organic suspensions comprising ZnO, TiO_2, and zeolite nanosized adsorbents together with the evaluation of their decontamination efficiency on soman and sulfur mustard. As far as we are concerned, there are scant data in the literature about the influence of these types of nanostructures on the decontamination efficiency of real CWAs in organic media.

The novelty of this study consists of the development of new organic decontamination formulations, with enhanced decontamination efficiency brought by the nanosized particles selected for this type of application, and also in revealing, by thorough investigations, how they influence the degradation of two real warfare agents: a blister agent—sulfur mustard (HD), and a nerve agent—soman (GD).

Thus, in this article, we describe the preparation of three different types of NP-based decontamination formulations and an extensive evaluation of their decontamination efficiency for HD and GD warfare agents by means of a GC-MS technique. We also identified and quantified the main degradation products of GD and HD produced during the decontamination process.

2. Materials and Methods

2.1. Materials

The materials employed for the preparation of the decontamination formulations—2-ethoxyethanol (≥99.8%, ethylene glycol monoethyl ether, Sigma Aldrich, St. Louis, MO, USA), monoethanolamine (≥98%, Sigma Aldrich, St. Louis, MO, USA), sodium hydroxide (≥98%, Sigma Aldrich, St. Louis, MO, USA), isopropyl alcohol (≥99.7%, Sigma Aldrich, St. Louis, MO, USA), and sodium lauryl sulfate (SDS, Sigma Aldrich, St. Louis, MO, USA)—were used as received. Nanosized adsorbents ZnO, TiO_2, and zeolite were provided by the National Institute for Research and Development in Microtechnologies (IMT, Bucharest, Romania), they were obtained according to ref. [29] (ZnO), ref. [30] (TiO_2), ref. [31] (zeolite-NPs) and were used as received, for the decontamination solutions.

For decontamination tests, real chemical warfare agents were utilized: bis(2-chloroethyl) sulfide (HD, sulfur mustard, purity: 95%, CAS: 505-60-2, Schedule 1A(4) in the Chemical Weapons Convention (CWC), own synthesis) and soman (GD, Pinacolyl methylfluorophosphonate, purity 90%, CAS: 96-64-0, Schedule 1A(1) in the CWC, own synthesis). The sample preparations for the GC-MS analyses involved dichloromethane (≥99.8%, DCM, Merck Millipore, Burlington, MA, USA) extractions, anhydrous sodium sulphate (Sigma Aldrich, St. Louis, MO, USA) drying and derivatization with N,O-Bis(trimethylsilyl)trifluoroacetamide (≥99%, BSTFA, Sigma Aldrich, St. Louis, MO, USA) silylation reagent. All the tests involving the CWA utilized in this study were performed at the Research and Innovation Center for CBRN Defense and Ecology, in the 'Chemical Analysis Laboratory', the OPCW Designated Laboratory from Romania.

2.2. Methods

2.2.1. Synthesis of Decontamination Solutions

The organic decontamination solution (SD) was prepared in a three-neck flask equipped with dropping funnel with pressure compensation, ascending refrigerant, and mechanic stirrer. The components of the decontamination formulations were added progressively, maintaining a temperature of 30 °C with the aid of a cooling bath. Ethylene glycol monoethyl ether (50–60 wt.%) was the first reagent introduced in the three-neck flask, followed by the dropwise addition of monoethanolamine (20–30 wt.%). Meanwhile, a solution of sodium hydroxide 48 wt.% was prepared. After completing monoethanolamine addition, NaOH solution (2–5 wt.%) was introduced dropwise in the decontamination solution. In the meantime, sodium lauryl sulfate (1–3 wt.%) was dissolved in isopropyl alcohol (10–20 wt.%). Afterwards, this solution was slowly added to the decontamination formulation. The last step consisted of the dispersion of the nanosized adsorbents with the aid of a probe sonicator (750-Watt Ultrasonic Processor, 30 min at 40% amplitude). Table 1 summarizes the decontamination formulations obtained.

Table 1. Nanosized components of the decontamination formulations.

NPs / Sample	Blank (SD) *	S1	S2	S3	S4
ZnO (wt.%)	0	0.1	0.5	1	2
TiO_2 (wt.%)	0	0.1	0.5	1	2
Zeolite (wt.%)	0	0.1	0.5	1	2

* SD: 2-ethoxyethanol, monoethanolamine, sodium hydroxide, isopropyl alcohol, SDS. S1, S2, S3 and S4, contain, in addition to SD, the corresponding amounts of NPs mentioned above.

Therefore, the last stage of the synthesis of the reported decontamination solutions consisted of preparing four suspensions with different concentrations of NPs (0.1, 0.5, 1 and 2 wt.% NPs in SD) for each type of nanosized adsorbent (ZnO, TiO_2, and zeolite), as detailed in Table 1.

2.2.2. Preliminary Evaluation of the Neat Organic Decontamination Solution

The density of the organic decontamination solution was calculated with the aid of a pycnometer. The alkalinity of the neat organic decontamination solution was determined by titration with HCl (1N). All measurements were effectuated in triplicates and the mean values were reported.

The SD was especially designed not to damage the decontaminated surfaces and not to affect the operational capability of military equipment. In this way, the solution has been tested in accordance with AEP-7 (nuclear, biological, and chemical (NBC) defense factors in the design, testing, and acceptance of military equipment), by immersing painted metallic samples in SD for 30 min, rinsing with water, drying, and evaluating the samples immediately and after 24 h, in accordance with ISO 4628-2:2016, for cracking, exfoliation, discoloration or other visible defects. The solution was exposed to cycles of extreme temperature and humidity conditions characteristic for the Romanian region and neighborhoods (−33 °C to +49 °C), i.e., two cycles (24 h each), one for low temperatures (extreme temperature −33 °C) and one for high temperatures (extreme temperature +49 °C), provided by NATO AECTP 230 standard (climatic conditions) [32], and afterwards, it was investigated whether it preserved its decontamination efficiency.

2.2.3. Decontamination Procedure

The evaluation of the decontamination efficiency of the novel organic formulations on real CWA, HD, and GD was performed in two main stages: controlled contamination with CWA followed by sample preparation of the decontaminated samples for GC-MS analyses.

Five milliliters from each of the twelve synthesized suspensions were contaminated with 5.25 µL HD, with 5.55 µL GD, meaning 1000 ppm of pure toxic in the suspension. The decontamination process was performed under magnetic stirring (300 rpm) at room temperature (20 °C). Two control samples (SD) were also contaminated with 1000 ppm toxic. After specific decontamination times (2 min, 10 min, 30 min, 60 min, 3 h, 5 h, and 24 h), 200 µL of each suspension were extracted with 3.8 mL dichloromethane (DCM), dried for water traces over sodium sulphate, filtered on 45 µm Sartorius filter, and analyzed by GC-MS/EI. In order to identify and quantify the degradation products produced after the decontamination process, 1 mL sample was derivatized with 20 µL BSTFA (N,O-Bis(trimethylsilyl)trifluoroacetamide) at 60 °C for 30 min and analyzed by GC-MS. BSTFA is a derivatizing agent widely used in the derivatization of low or no volatility compounds, thereby resulting in the formation of trimethylsilyl (TMS) derivative.

For the evaluation of the decontamination efficiency, the decontamination factor (*DF*) was calculated taking into account the initial concentration of the toxic chemical and the residual toxic after decontamination, resulted from the GC-MS investigations. The formula for the calculation of the decontamination factor is: $DF = 100 * \left(C_0 - C_f\right)/C_0$, where DF is the decontamination factor, C_0 is the initial toxic concentration, and C_f is the final concentration, indicating the residual contamination. Controlled contamination and the

decontamination procedure, followed by GC-MS analyses, were repeated in triplicates and the average values obtained were reported.

2.3. Characterization

The morphology and dimensions of ZnO, TiO_2, and zeolite NPs were examined by an ultra-high-resolution field emission scanning electron microscope (FE-SEM)—FEI Company Nova NanoSEM 630. The characterization was performed at magnifications of 120 kx and 100 kx, and acceleration voltages of 10 kV and 15 kV, through the lens SE detector (TLD). The FT-IR spectra of the decontamination solutions were obtained at 4 cm^{-1} resolution, from 550 to 4000 cm^{-1}, with the aid of a Pekrin Elmer Spectrum Two instrument, ATR mode. Gas chromatography mass spectrometry analyses were performed on a GC Thermo Scientific Trace 1310–TSQ 9000 triple quadrupole MS. GC analysis method: carrier gas—helium, 1.5 mL constant flow, 270 °C injector temperature, splitless injection mode, TR5MS gold column, 5% phenyl 95% dimethylpolysiloxane phase, 30 m × 0.25 mm × 0.25 µm, temperature program—40 °C to 300 °C with a heating rate of 10 °C/min. MS analysis method: solvent delay—2.5 min and 8.5 min (derivatization method), electron impact (EI) ionization mode, 40 eV electron energy, 40–650 m/z scan range. Qualitative analyses and the identification of the toxic compounds and their degradation products were performed by comparing the mass spectra of the chemicals with NIST (National Institute of Standards and Technology) and OCAD (OPCW Central Analytical Database) spectra libraries. Quantitative analyses were performed with the addition of an internal standard.

3. Results and Discussion

The first step in our study consisted of the development of the organic decontamination solution, which subsequently served as the dispersion media for the investigated nanoparticles. The synthesis of the organic decontamination solutions, with and without the nano adsorbents, is described in the Methods section. Before adding the NPs, the neat organic decontamination solution (SD), considered as a blank sample for these decontamination experiments, was subjected to a series of specific analyses in order to obtain some preliminary information. Therefore, following the above-described procedures, we obtained decontamination solutions with 0.91 ± 0.02 g/cm^3 density and total alkalinity of 2.4678 ± 0.5 cm^3 HCl 1 N/1 g analyzed solution. The neat organic solution did not degrade the tested painted metallic surfaces; therefore, we can affirm that these solutions do not affect the operational capability of military techniques when employed for decontamination. In addition, this solution proved that it maintained its decontamination efficiency even after being exposed to multiple cycles of extreme temperature and humidity conditions.

The second step of this research involved the addition of three types of nano adsorbents, ZnO, TiO_2, and zeolite, to the organic decontamination solution, in order to investigate their ability of enhancing the decontamination efficiency for HD and GD. The morphology of the nanosized adsorbents employed in the decontamination solutions was investigated through SEM analysis.

In Figure 2, it can be observed that the morphology of the ZnO (Figure 2A) and TiO_2 (Figure 2B) nano adsorbents was very similar. Their dimensions can also be measured on comparable scales, the sizes of the particles varying between 60 and 100 nm in both cases. The zeolite adsorbent has a different morphology due to its porous structure (Figure 2C). The size of the particles measured falls within 100–500 nm, being larger than ZnO and nanoparticle-sized TiO_2. The nanosized adsorbents presented in Figure 2 were used as received for the decontamination suspensions, by simply being added and sonicated (details in the Methods section) in the organic solution, prior to the decontamination stage.

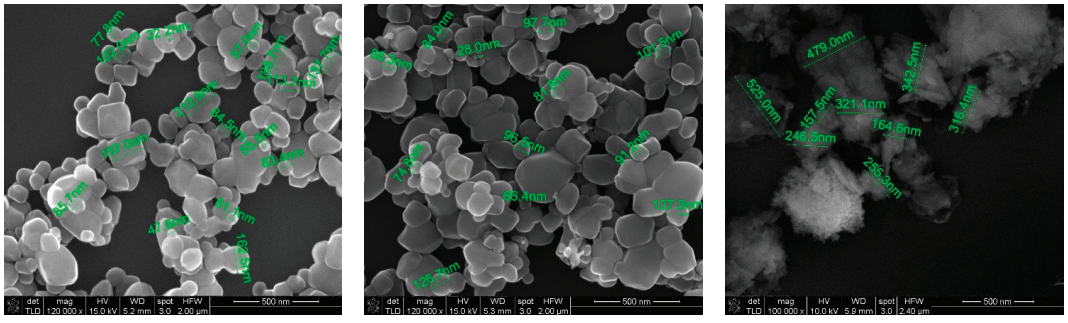

(**A**) (**B**) (**C**)

Figure 2. SEM images of the NPs employed in the decontamination solutions: (**A**) ZnO NPs; (**B**) TiO_2 NPs; (**C**) zeolite NPs.

The chemical composition of the decontamination solution and the interactions between its components and the CWAs directly influences the decontamination performance. Comparative FT-IR plots for neat SD and for the decontamination solutions enriched with different concentrations of nanosized adsorbents are illustrated in Figure 3.

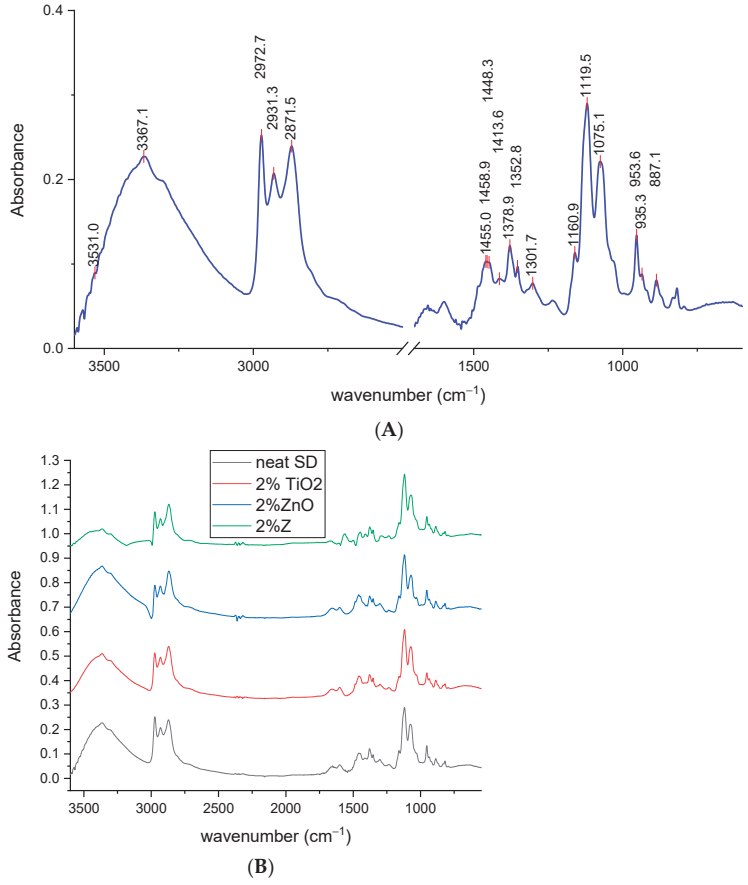

Figure 3. FT-IR spectra: (**A**) neat SD and (**B**) decontamination solutions with NPs.

The broad peak specific for O-H stretching vibrations partially overlapped with the peak specific for N-H stretching vibrations in the 3500–3300 cm^{-1} region, due to the presence of monoethanolamine in the decontamination solution (Figure 3A). A characteristic absorption band of the C–H stretching bond could be observed around 2973 cm^{-1}. The high intensity of this peak can be attributed to the overlap of the absorptions of a large number of C–H bonds [33] from $–CH_2–$ groups present in the DS, particularly those found in the structure of the surfactant. The peaks found at 2973 cm^{-1} and 2871 cm^{-1} can be associated with C–H stretching from CH_3 groups. Peaks situated at around 1450 cm^{-1} and 1378 cm^{-1} can also be assigned to methyl groups. The intense sharp peak found at 1119 cm^{-1} can be attributed to C–O stretching. Primary alcohols from SD composition exhibited a strong C–C–O asymmetric stretch at around 1075 cm^{-1}. The decontamination solutions are complex blends; therefore, some of the adsorption bands, specific for a certain component, may possibly overlap with those of the other components, and thus some of them may have been omitted because they were not clearly visible on the spectra. Even so, the FT-IR analysis offers valuable information about the main groups present in the structure of the components from the decontamination solutions.

The decontamination tests on real warfare agents offered the possibility of evaluating the decontamination performances of the solutions developed in this study. A comprehensive assessment of the decontamination capacity of the organic solutions enriched with ZnO, TiO_2, and zeolite nanoparticles for GD and HD was effectuated as described in Methods section, and it is detailed below.

The main degradation products of CWA obtained in this study are summarized in the schematic illustration found in Figure 4.

The interaction of each type of decontamination solution with HD and GD was thoroughly investigated and the results are explained below.

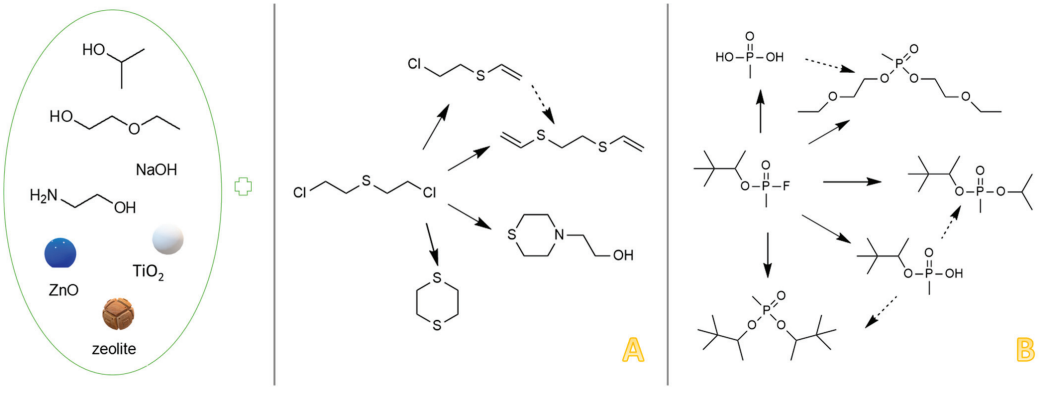

Figure 4. Schematic illustration of the main degradation products of HD (**A**) and GD (**B**) obtained through the decontamination process with SD-NP suspensions.

HD employed in this study has been identified by m/z (109, 111, 63, 158) and by comparing the spectra with NIST and OCAD analytical libraries. HD decontamination tests performed on the neat organic solution showed a very fast decontamination reaction, leading to a decontamination degree (Figures 5A, 6A and 7A) of 76.42% after 2 min. The decontamination reaction progressed another 6.5% in the next 58 min and continued advancing by 3.5%/h in the next 4 h. The residual HD (Figures 5B, 6B and 7B) indicated concentrations decreasing from 236 ppm (after 2 min) towards 37 ppm (after 5 h), from an initial contamination of 1000 ppm. After 24 h, the decontamination process could be considered complete with a 99.99% decontamination efficiency. The next step consisted of evaluating the influence of the nanosized adsorbents on the decontamination efficacy of HD. Therefore, SD—1% ZnO NP suspensions—revealed decontamination efficiencies (Figure 5A) between 66.96% (immediately after initial contact meaning 2 min) and 97.42% (5 h), with an increase in decontamination efficiency of 19.83%/h in the first hour and slowing down to approximately 2.65%/h in the next 4 h. The residual HD after decontamination with S3—1% ZnO suspension—indicated values (Figure 5B) starting from 330 ppm (after 2 min) and reaching 26 ppm (after 5 h). The decontamination efficiency was 1.15% higher compared with one of neat SDs after 5 h. Evaluating the four concentrations of ZnO NP suspensions, we observed a higher decontamination efficiency with the increase in the concentration from 0.1% to 1%. The suspension with 2% ZnO NPs exhibited lower decontamination efficacy, probably due to the agglomeration of the NPs, which may have slowed down the reaction rate and reduced the overall active surface available for the adsorption of toxic. SD—0.1% TiO_2 NP suspensions reacted instantly and through an almost complete decontamination reaction with HD, showing a decontamination efficiency (Figure 6A) of 94.95% (after 2 min), 97.01% (after 1 h) and 99.90% (after 5 h). After an almost instantaneous behavior of the decontamination reactions, the conversion rates continued to increase by another 2.06% in the first hour; afterwards, it started to slow down to 0.72%/h in the next 4 h. The residual HD after decontamination with S1—0.1% TiO_2 NPs, showed values (Figure 6B) between 51 ppm (2 min) and 1 ppm (5 h). The decontamination efficiency of S1—0.1% TiO_2 NPs after 5 h was higher with 3.63% in comparison with SD. When comparing the immediate decontamination efficiency (after 2 min) we can affirm that the decontamination efficiency of SD-TiO_2 NPs (0.1 wt.%) was 18.53% higher than that of neat SD, decisive fact in operational field. SD-zeolite NP suspensions shower slightly superior results than SD-TiO_2 NP suspensions. The initial decontamination reaction showed a higher conversion rate of about 95.64% (after 2 min), and even a slightly higher decontamination efficiency of 99.92%, after 5 h (Figure 7A). In the first hour, the conversion rate continued to increase by another 1.56%, and approximately 0.68%/h in the next 4 h. The residual HD (Figure 7B) firstly indicated 44 ppm (after 2 min) and 1 ppm later (after 5 h). The decontamination efficiency was 3.65% higher in comparison with that of neat SD after 5 h, and 19.22% higher after only 2 min. SD-zeolite NPs (0.1 wt.%) showed the best decontamination efficiency of HD. After 24 h, all decontamination solutions showed a decontamination efficiency of about 99.99% or 100%. Analyzing Figures 5–7, we can affirm that for all TiO_2 NPs and zeolite NP suspensions, we observed that decontamination efficiency slightly decreased with the increase in NP concentration, whereas for ZnO NP suspensions, the optimal concentration for decontamination seemed to be 1 wt.%, because these solutions exhibited the best results.

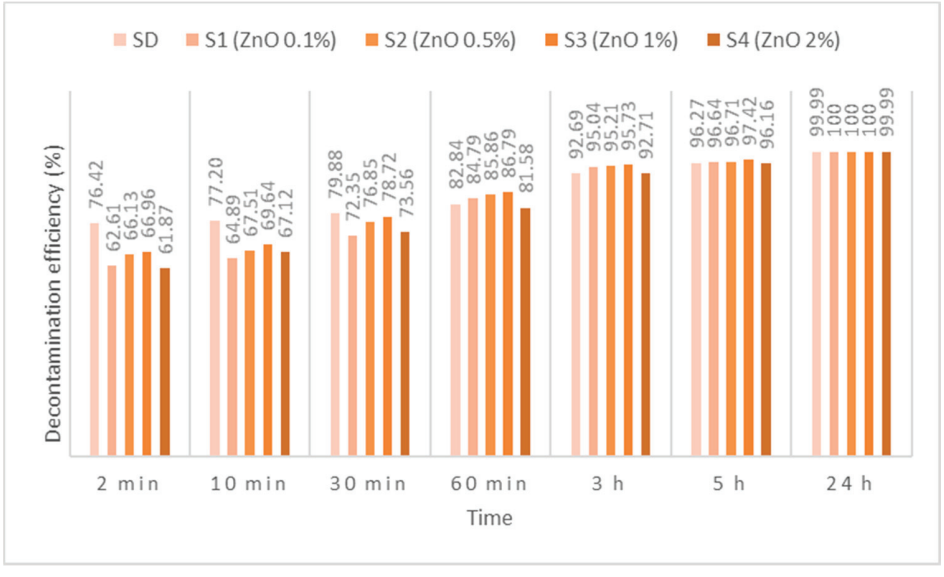

(**A**)

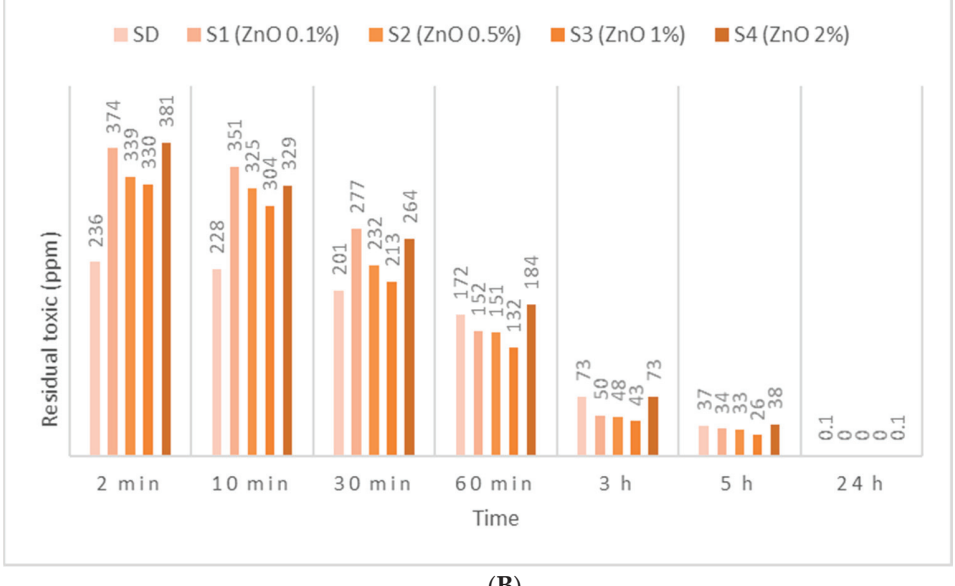

(**B**)

Figure 5. (**A**) HD decontamination efficiency with organic decontamination suspensions of ZnO NPs with concentrations of 0.1%, 0.5%, 1%, 2%, and (**B**) HD residual concentrations after the decontamination process.

(**A**)

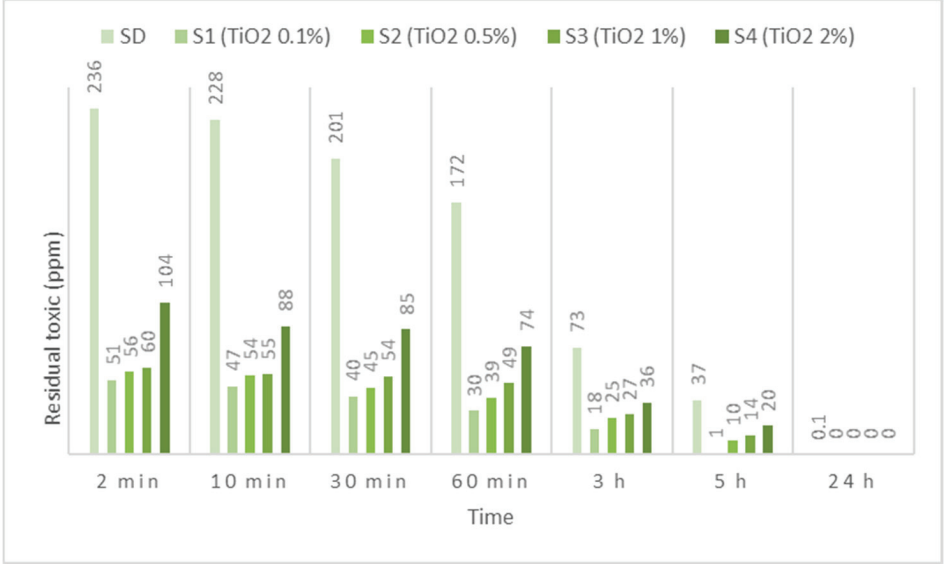

(**B**)

Figure 6. (**A**) HD decontamination efficiency with organic decontamination suspensions of TiO_2 NPs with concentrations of 0.1%, 0.5%, 1%, 2%, and (**B**) HD residual concentrations after the decontamination process.

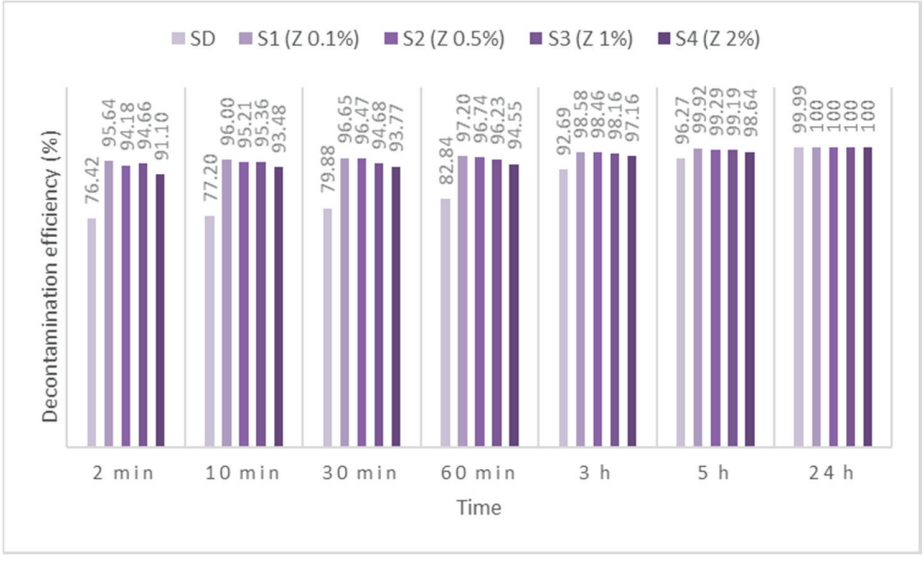

(**A**)

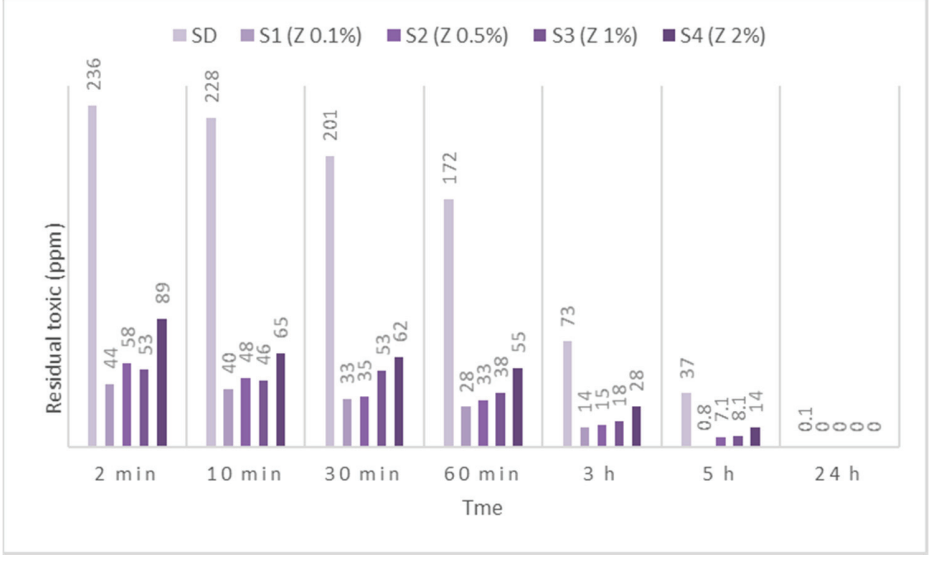

(**B**)

Figure 7. (**A**) HD decontamination efficiency with organic decontamination suspensions of zeolite NPs with concentrations of 0.1%, 0.5%, 1%, 2%, and (**B**) HD residual concentrations after the decontamination process.

The second warfare agent investigated in this study, GD, was identified by m/z (99, 126, 82, 69) and by comparing the spectra with NIST and OCAD analytical libraries. GD decontamination tests showed a very fast decontamination reaction, leading to a decontamination degree of 99.83% after 2 min. The decontamination progressed by another 0.98% in the next 58 min, leading to a decontamination efficiency of 99.91% and an equivalent of 0.9 ppm (after 1 h) from an initial contamination of 1000 ppm. SD-ZnO NP suspensions showed an instant and almost complete decontamination reaction, exhibiting a decontamination efficiency (Figure 8A) of 99.91% after 2 min and 99.97% after 10 min (for SD—1% ZnO), with equivalents of 0.9 ppm and 0.3 ppm GD remnants, respectively, after the decontamination process (Figure 8B). The decontamination efficiency was 0.98% higher compared with SD after 2 min. Comparing the four concentrations of ZnO NP suspensions, we observed a higher decontamination efficiency when increasing the concentration of ZnO from 0.1% to 1%. The suspension with 2% ZnO NPs showed poorer results, probably due to the agglomeration of the NPs, thus decreasing the adsorption surface and lowering the efficiency of decontamination. SD—0.1% TiO_2 NP suspensions showed an instant decontamination efficiency of 99.95% and a complete reaction after 10 min (Figure 9A), equivalent of 0.5 ppm and 0.1 ppm GD remanent after decontamination (Figure 9B). SD—0.1% zeolite NP suspensions showed an instant decontamination efficiency of 99.96% and a complete reaction after 10 min (Figure 10A), equivalent of 0.4 ppm and 0.1 ppm GD remanent after decontamination (Figure 10B). In both cases, the decontamination efficiency was approximately 1% higher than neat SD after 2 min. Comparing the four concentrations for both TiO_2 NPs and zeolite NP suspensions, we observed that decontamination efficiency decrease was directly proportional with the increasing concentration of the NPs, and that some differences appeared between 1% and 2% concentrations. SD-zeolite NPs (0.1 wt.%) showed the best decontamination efficiency of HD. The decontamination reactions involving NP suspensions were all completed after 30 min, and in the case of SD, the decontamination was finished after more than 1 h. In the case of TiO_2, and the zeolite NP (0.1 wt.%) suspension, the reaction was completed after 10 min.

The solutions that exhibited the highest decontamination efficiency from each class of NP suspensions (S3-ZnO, S1-TiO_2, S1-Zeolite), together with the neat organic solution (SD), were presented comparatively, considering their residual contamination for HD and for GD, as can be observed in Figure 11. It was observed that the organic suspensions containing 0.1 wt.% of TiO_2 or zeolite reduced the decontamination time from 1 h to 10 min for GD. In the case of HD, the decontamination efficiency of these suspensions after 2 to 10 min was equivalent to the decontamination efficiency of the neat organic solution after 5 h, circumstances which may have had a crucial role in the operational field. Thus, by analyzing all the results illustrated above, we can affirm that the hypothesis about the possibility of enhancing the decontamination efficiency of our organic solution through the addition of small amounts (0.1–1 wt.%) of NPs (ZnO, TiO_2, or zeolite) was confirmed and demonstrated through reproducible results.

The final step of this work consisted of identifying the decontamination products produced in this process, quantifying their abundance proportionally with time, evaluating the conversion rate of the CWA into its main decontamination products. Four main degradation products resulting from the decontamination of HD, and five main degradation products resulting from the decontamination of GD were identified and are illustrated in Figure 4.

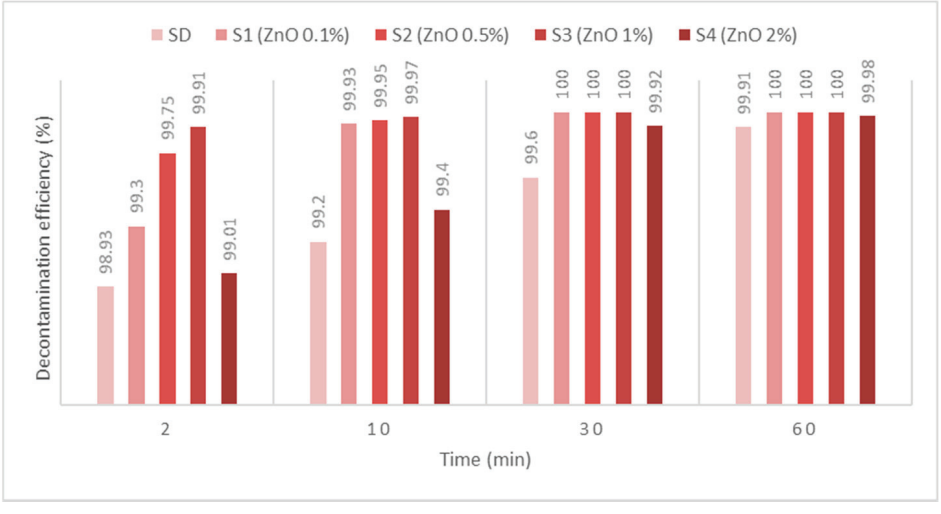

(**A**)

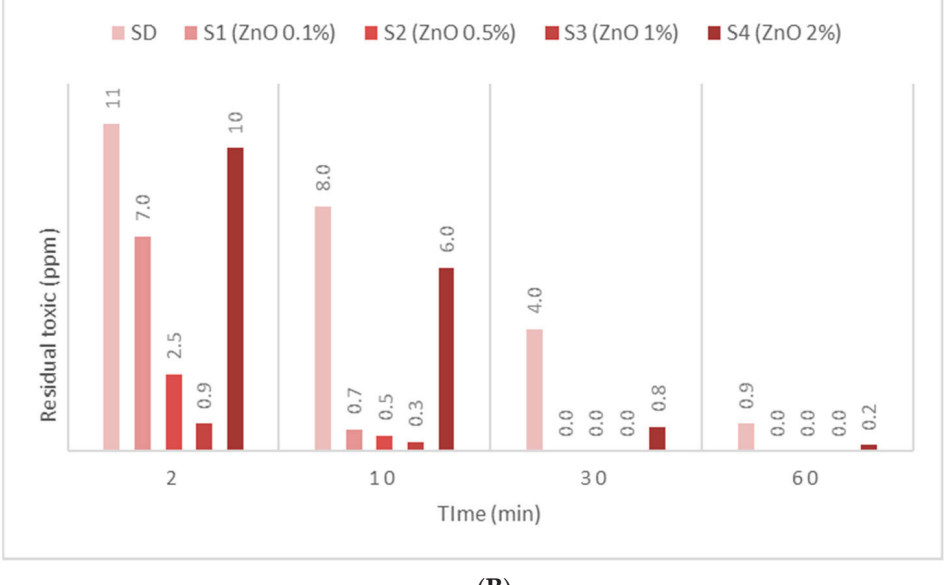

(**B**)

Figure 8. (**A**) GD decontamination efficiency with organic decontamination suspensions of ZnO NPs with concentrations of 0.1%, 0.5%, 1%, 2%, and (**B**) GD residual concentrations after the decontamination process.

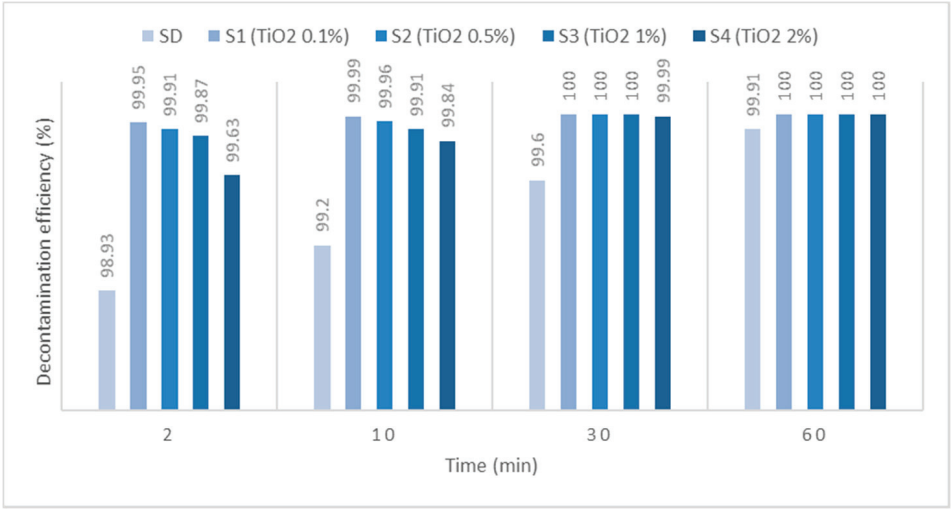

(**A**)

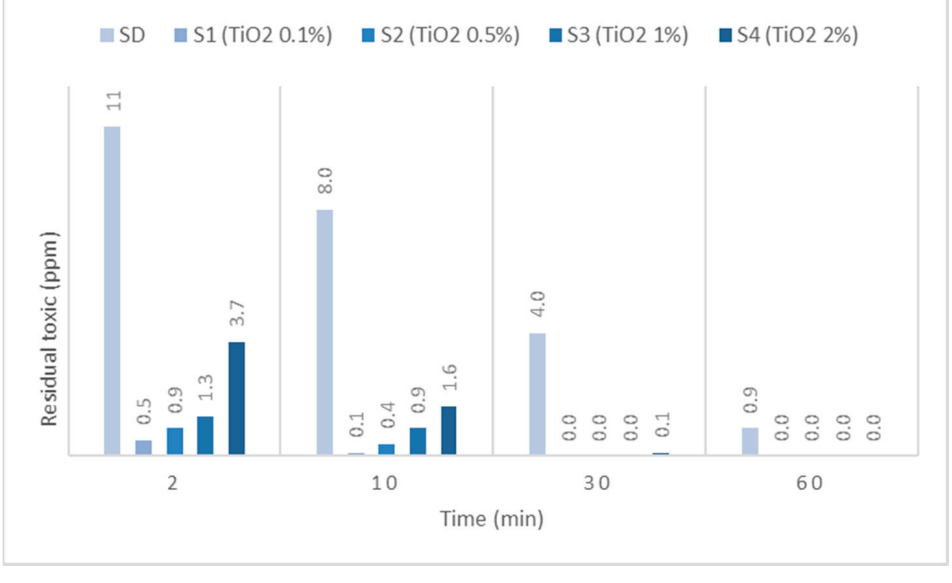

(**B**)

Figure 9. (**A**) GD decontamination efficiency with organic decontamination suspensions of TiO_2 NPs with concentrations of 0.1%, 0.5%, 1%, 2%, and (**B**) GD residual concentrations after the decontamination process.

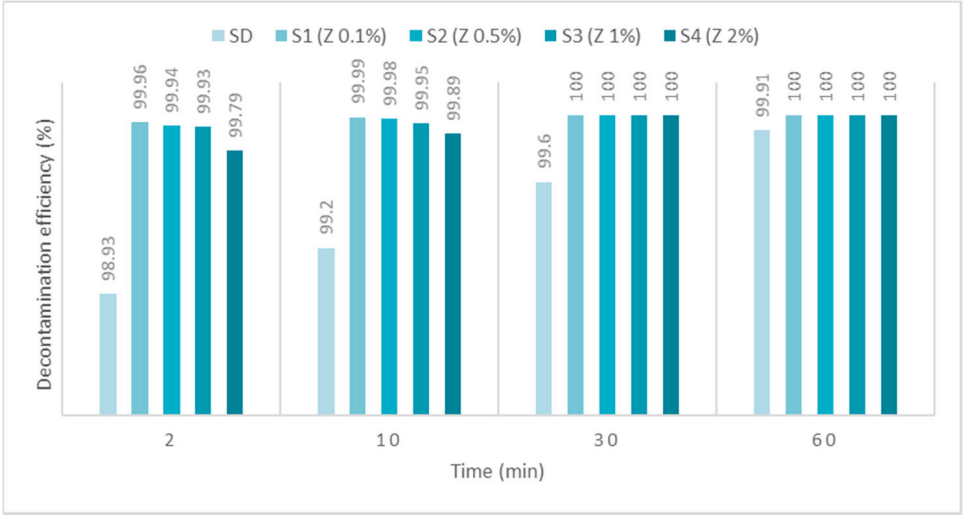

(**A**)

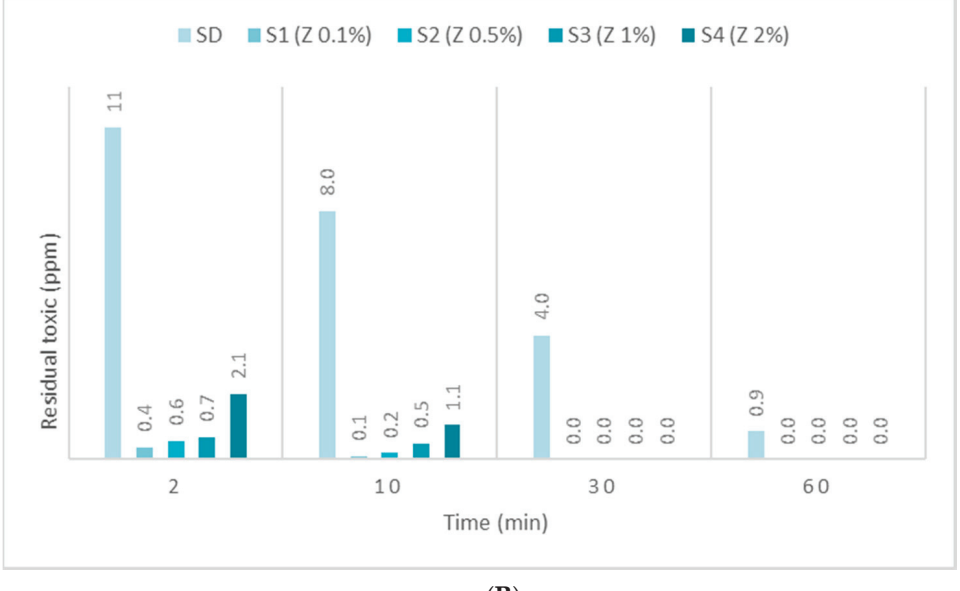

(**B**)

Figure 10. (**A**) GD decontamination efficiency with organic decontamination suspensions of zeolite NPs with concentrations of 0.1%, 0.5%, 1%, 2%, and (**B**) GD residual concentrations after the decontamination process.

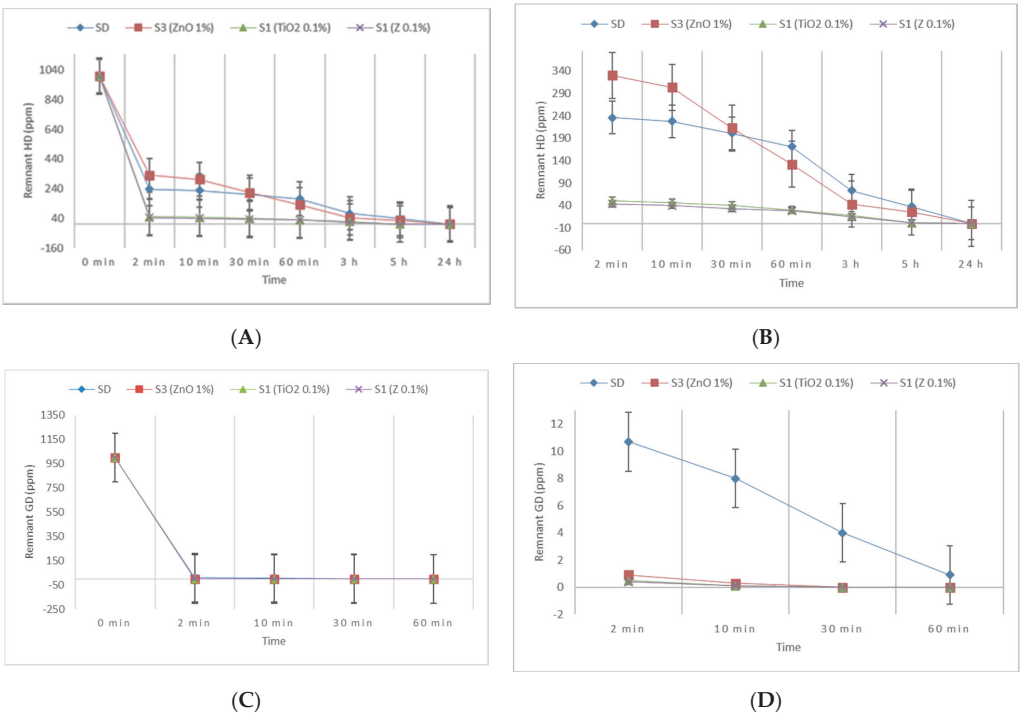

Figure 11. Remnant contamination with HD (**A**) and GD (**C**) after decontamination with S3-ZnO, S1-TiO_2, S1-Z, and neat SD; (**B**) detail extracted from (**A**) for smaller ppm ranges of HD; (**D**) detail extracted from (**C**) for smaller ppm ranges of GD.

The four main degradation products resulting from the decontamination of HD were identified and quantified by the GC-MS technique. The first degradation product, 2-chloroethyl vinyl sulfide (CAS 81142-02-1, Non-Schedule—N.S.) was identified by m/z (73, 122, 60, 45) at a retention time (RT) of 6.45 min. This product was slightly visible at the beginning of the decontamination process (after 2 min) in small concentrations, and its concentration increased to a maximum value after 3 h. After this point, the concentration dropped, showing that this compound had started to transform into a subsequent decontamination product. Its concentration after 24 h was equivalent to the concentration measured after 2 min (Figure 12). A linear concentration increment of 2-chloroethyl vinyl sulfide was observed as the concentration of nanoparticles in the suspension increased in all the three cases. The second degradation product of HD found by GC-MS investigation was 1,4-dithiane (CAS 505-29-3, N.S.), which was identified by m/z (120, 46, 61, 45) at RT for 9.11 min. The abundance of this compound in the decontamination solution was almost constant at any point of the decontamination process, which sustains the hypothesis that the compound existed at time zero of the decontamination process, and the neat decontamination solution had a neglectable effect in this case. Even so, the concentration of this compound increased in the NP suspensions, directly proportional with the NP concentrations, which demonstrates the enhanced formation of degradation products in the suspensions containing nanoparticles (Figure 13). In the specific case of SD—2 wt.% TiO_2, the abundance of 1,4-dithiane was double than that in the case of neat SD. The third degradation product formed was 1,2-bis(vinylthio)ethane (CAS 4413-12-1, N.S.), identified by m/z (45, 59, 87, 58) at RT for 10.60 min. This degradation product showed a linear increase with time, up to 5 h from the start of the decontamination process. In the time interval between 5 h and 24 h, an exponential increase in its concentration was observed

(Figure 14). A slight increment of its abundance with the increase in NP concentration has also been observed. The last main degradation product of HD identified in this study was 2-thiomorpholinoethanol (CAS 6007-64-3, N.S.). This chemical compound was identified as TMS-derivative, in the silylated samples with BSTFA, N-(2-trimethylsilyloxyethyl) thiomorpholine (CAS 959040-20-1) by m/z (116, 88, 73, 204) at RT for 14.34 min. Its formation started at the beginning of the decontamination process and increased to a maximum after 30 min; afterwards, it slowly decreased. In a particular case, SD—2 wt.% ZnO, this maximum was reached after 1 h (Figure 15). The decrease in concentration after a specific moment leads to the idea that this compound was transforming into a different decontamination product.

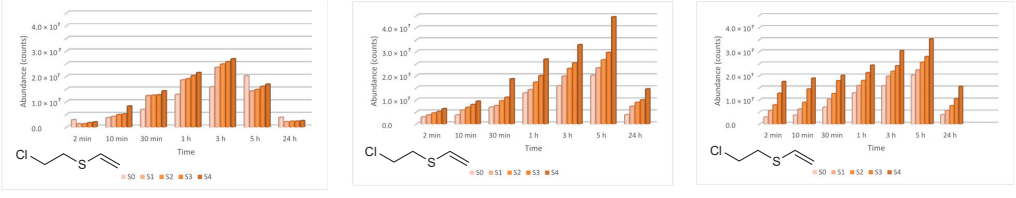

(**A**) (**B**) (**C**)

Figure 12. 2-Chloroethyl vinyl sulfide abundance in time in the HD decontamination process with (**A**) ZnO, (**B**) TiO_2, and (**C**) zeolite suspensions.

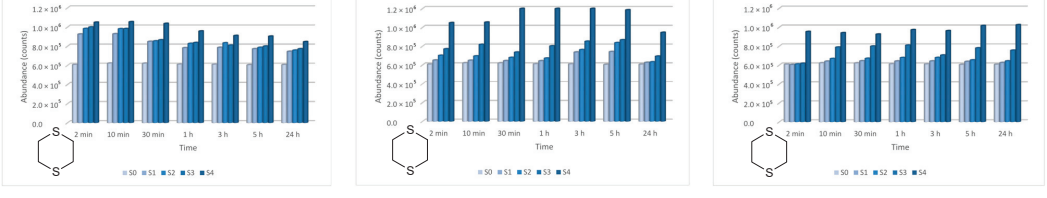

(**A**) (**B**) (**C**)

Figure 13. 1,4-Dithiane abundance in time in the HD decontamination process with (**A**) ZnO, (**B**) TiO_2, and (**C**) zeolite suspensions.

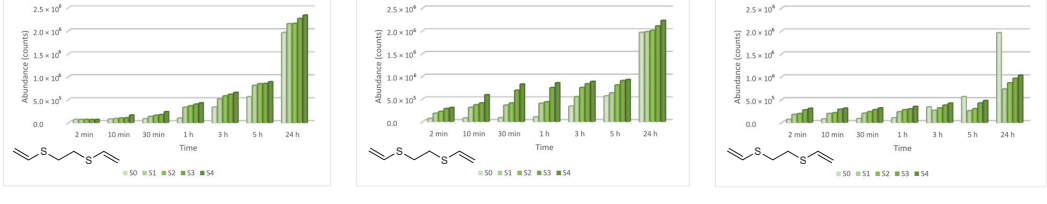

(**A**) (**B**) (**C**)

Figure 14. 1,2-Bis(vinylthio)ethane abundance in time in the HD decontamination process with (**A**) ZnO, (**B**) TiO_2, and (**C**) zeolite suspensions.

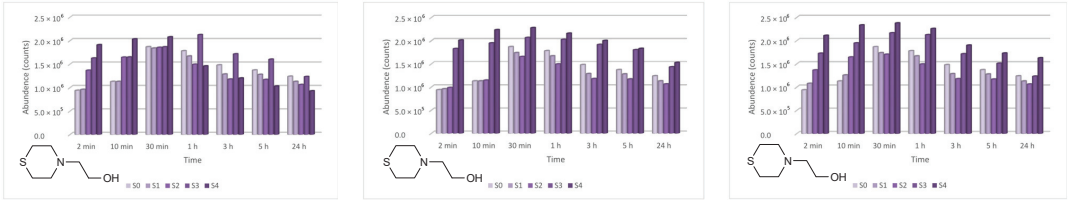

(**A**) (**B**) (**C**)

Figure 15. Thiomorpholinoethanol abundance in time in the HD decontamination process with (**A**) ZnO, (**B**) TiO_2, and (**C**) zeolite suspensions.

The proposed mechanism of reaction for the degradation of HD is schematically illustrated in Figure 16.

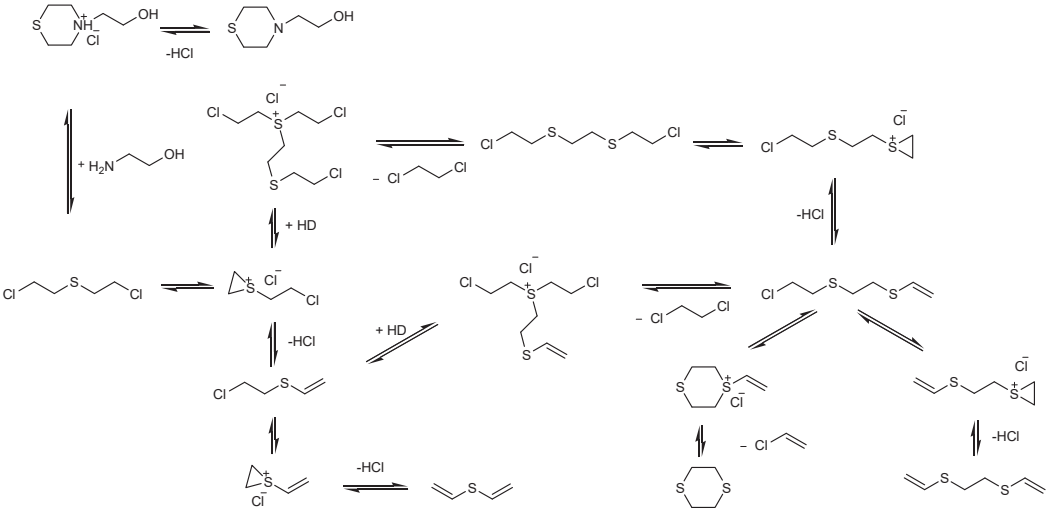

Figure 16. Hypothetical degradation mechanism for HD.

In the case of GD, five major degradation products resulted from its decontamination. These compounds were identified and quantified by GC-MS technique as well. The first degradation product of GD, methylphosphonic acid (CAS 993-13-5, Schedule 2B(4)), was identified as di-TMS-derivative in the silylated samples with BSTFA, bis(trimethylsilyl) methylphosphonate (CAS 18279-83-9) by m/z (225, 73, 226, 147) at RT of 10.44 min. This compound appeared after 2 min, but after this moment its abundance dropped down to zero. In case of ZnO suspensions, the highest concentration of methylphosphonic acid, after 2 min, was observed in the case of S3 (1 wt.% ZnO) (Figure 17). The other suspensions which presented a lower concentration of this GD degradation product showed a delay in the process of conversion, indicated by the fact that the product has also been observed after 10 min in small concentrations. In both cases, TiO_2 and zeolite, the highest concentration of this degradation product, after 2 min, was observed in the case of S1 (0.1 wt.% NPs). Delayed conversion was also observed (Figure 17), in comparison with ZnO suspensions. The second GD degradation product found was isopropyl pinacolyl methylphosphonate (CAS 92411-67-1, Schedule 2B(4)), which has been identified by m/z (123, 97, 124, 125) at RT of 12.24 min. Its formation started at the beginning of the decontamination process and continued with a slightly increasing trend (Figure 18). The decontamination product showed a higher abundance in neat SD, in comparison with NP suspensions. The third

GD degradation product identified was pinacolyl methylphosphonic acid (CAS 616-52-4, Schedule 2B(4)). This chemical compound was identified as TMS-derivative in the silylated samples with BSTFA, pinacolyl trimethylsilyl methylphosphonate (CAS 199116-10-4) by m/z (153, 169, 195, 151) at RT of 12.78 min (Figure 19). Pinacolyl methylphosphonic acid was the second most abundant decontamination product of GD in this decontamination process. Its concentration reached a maximum at 3 h from the beginning of the decontamination process, which suggests the idea that it further transformed into another degradation product. The fourth degradation product of GD, dipinacolyl methylphosphonate (CAS 7040-58-6, Schedule 2B(4)) was identified by m/z (123, 97, 124, 85) at RT for 15.22–15.25 min. This compound was formed from the beginning of the decontamination process (2 min) and its abundance exhibited a slightly increasing trend (Figure 20). A more visible increment was observed in zeolite suspensions (Figure 20C). The last main degradation product of GD was methylphosphonic acid di(2-ethoxyethyl) ester (CAS 6069-07-4, Schedule 2B(4)), identified by m/z (72, 45, 123, 97) at RT for 15.35–15.50 min. It was the most abundant decontamination product, formed in high amounts from the beginning of the process and continued with a slightly decreasing trend (Figure 21). It is highlighted that the 0.1 wt.% NP suspensions showed a better conversion of GD into this chemical, compared with the other NPs solutions. As NP concentrations increased, GD showed a decreasing tendency of converting into methylphosphonic acid di(2-ethoxyethyl) ester.

The proposed mechanism of reaction for the degradation of GD is schematically illustrated in Figure 22.

The conversion rates of the chemical warfare agents into degradation products were evaluated and presented in Figure 23A,B. In the decontamination process of HD, the major decontamination product was 2-chloroethyl vinyl sulfide. This compound was formed from the beginning of the reaction and its concentration continued to increase until 3 h had elapsed. After this moment, its concentration dropped down, which leads to the assumption that 2-chloroethyl vinyl sulfide was probably transformed into 1,2-bis(vinylthio)ethane. After 5 h, the concentration of 1,2-bis(vinylthio)ethane increased exponentially. On the other hand, 1,4-dithiane was found in small concentrations, as impurity in the HD was tested. However, in the decontamination process utilizing NP suspensions, an increase in its concentration of about 40% to 50% was observed, compared with the neat organic solution. Another specific degradation product for these organic compositions was 2-thiomorpholinoethanol, which resulted from the reaction between HD and monoethanolamine (present in the organic solution, 20–30 wt.%). In the decontamination process of GD, the most abundant and specific degradation product was methylphosphonic acid, di(2-ethoxyethyl) ester. This compound resulted from the reaction between GD and 2-ethoxyethanol (present in over 50% in the organic decontamination formulation). The reaction took place almost instantly, with a high conversion rate. Pinacolyl methylphosphonic acid is the second most abundant degradation product observed. The concentration of this chemical compound exhibited an increasing trend in the first 3 h. After this moment, the concentration started to decrease, probably because pinacolyl methylphosphonic acid tends to transform into dipinacolyl methylphosphonate and isopropyl pinacolyl methylphosphonate, both compounds displaying higher concentrations after this point. Isopropyl pinacolyl methylphosphonate resulted from the reaction between GD and isopropyl alcohol (present in 10–20 wt.% in the organic decontamination solution).

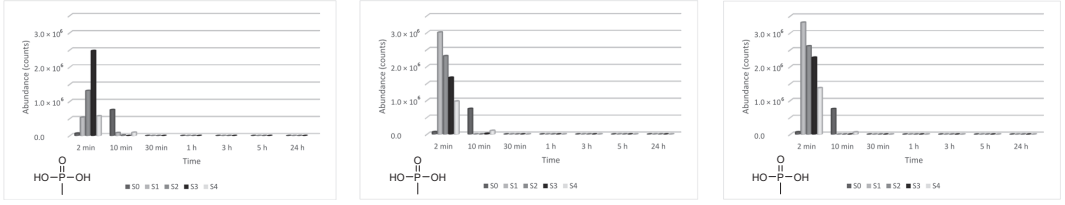

(**A**) (**B**) (**C**)

Figure 17. Methylphosphonic acid abundance as a function of time in the process of GD decontamination with (**A**) ZnO, (**B**) TiO_2, and (**C**) zeolite suspensions.

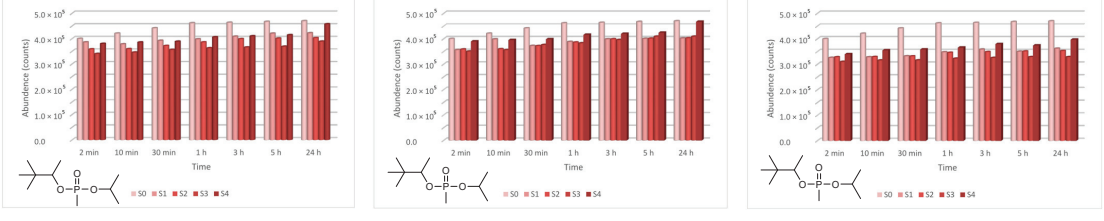

(**A**) (**B**) (**C**)

Figure 18. Isopropyl pinacolyl methylphosphonate abundance as a function of time in the process of GD decontamination with (**A**) ZnO, (**B**) TiO_2, and (**C**) zeolite suspensions.

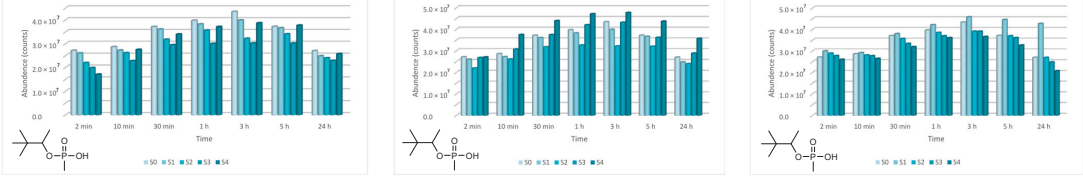

(**A**) (**B**) (**C**)

Figure 19. Pinacolyl methylphosphonic acid abundance as a function of time in the process of GD decontamination with (**A**) ZnO, (**B**) TiO_2, and (**C**) zeolite suspensions.

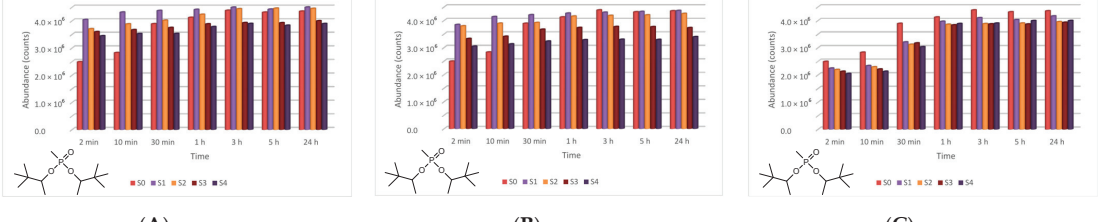

(**A**) (**B**) (**C**)

Figure 20. Dipinacolyl methylphosphonate abundance as a function of time in the process of GD decontamination with (**A**) ZnO, (**B**) TiO_2, and (**C**) zeolite suspensions.

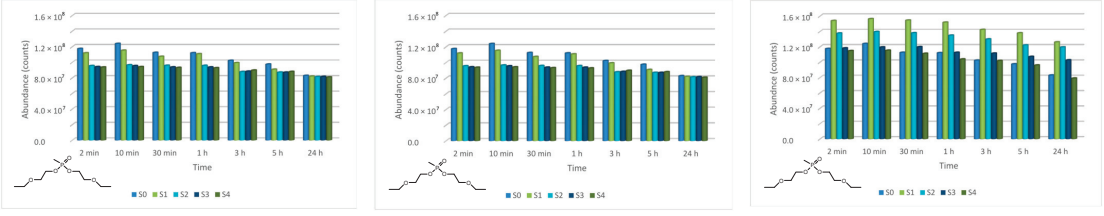

(**A**) (**B**) (**C**)

Figure 21. Methylphosphonic acid, di(2-ethoxyethyl) ester abundance as a function of time in the process of GD decontamination with (**A**) ZnO, (**B**) TiO_2, and (**C**) zeolite suspensions.

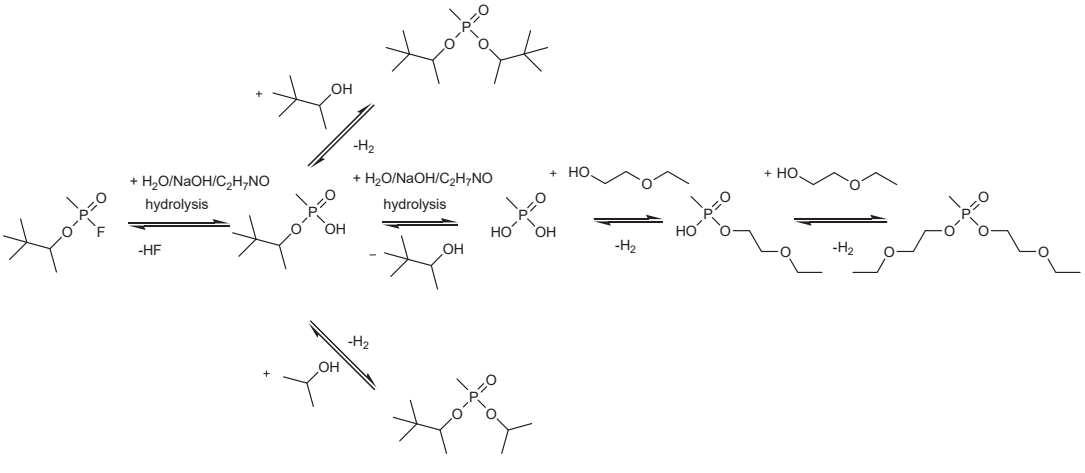

Figure 22. Hypothetical degradation mechanism for GD.

The relative acute toxicity of the obtained degradation products is included in category 3 and 4, meaning slightly toxic and irritating, non-toxic and non-irritating, respectively. The LD50 for these two categories ranges between 500 and 5000 mg/kg, respectively; over 5000 mg/kg for oral toxicity and between 2000 and 5000 mg/kg, respectively; and over 5000 mg/kg for dermal toxicity, as stated by the Environmental Protection Agency (EPA). For the degradation products methylphosphonic acid, di(2-ethoxyethyl) ester, dipinacolyl methylphosphonate, thiomorpholinoethanol, 1,2-bis(vinylthio)ethane, no toxicological data are currently available. In fact, the purpose of a decontamination process does not seek to eliminate toxicity altogether, but to transform highly toxic substances into substances that are not harmful to humans.

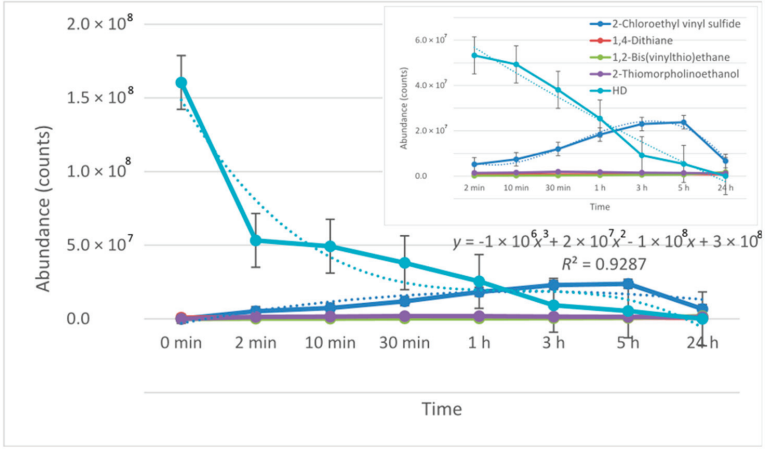

(**A**)

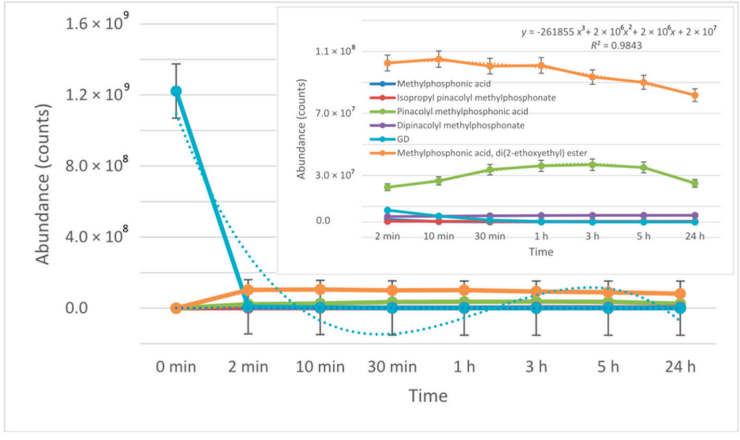

(**B**)

Figure 23. The conversion rate of the toxic chemicals (**A**) HD and (**B**) GD into their degradation products during 24 h decontamination process.

4. Conclusions

An organic decontamination solution, which subsequently served as dispersion media for three different types of nanoparticles, especially designed for the decontamination of chemical warfare agents, was synthesized and characterized. Density, pH, and total alkalinity of this organic solution were assessed, and the specific preliminary tests demonstrated that it preserved its decontamination performances after being exposed to multiple cycles of extreme temperature and humidity conditions, in accordance with NATO standard AEP 58 requirements for chemical warfare decontamination solutions [33]. The next step consisted of obtaining three types of reactive organic suspensions (based on ZnO, TiO_2, and zeolite nanosized adsorbents), briefly characterized by means of FT-IR and SEM analyses.

In this study, the main focus was on the comprehensive examination of the decontamination performances of these solutions for two real chemical warfare agents: GD and HD. For this purpose, the initial concentration of toxic agent and the residual toxic concentrations were determined and compared with the aid of a GC-MS technique. Measuring the concentration of residual toxic agent at different time intervals offered evidence on the progression

of the decontamination process. It was observed that the decontamination efficiency for HD slightly decreased with the increase in NP concentration, whereas for ZnO NP suspensions, the optimal concentration for decontamination seemed to be 1 wt.%. The positive influence of NPs on the enhancement of the decontamination performance was more noticeable in the case of soman decontamination. The decontamination organic suspensions showed higher decontamination factors for GD than the neat organic solutions. In comparison with HD, which required between 5 and 24 h for complete decontamination, the complete degradation of GD was fulfilled in a maximum of 60 min, due to the different chemical properties of these two chemical warfare agents. When comparing the improvements brought by the nanosized adsorbents, we observed that in the case of HD, TiO_2 and zeolite led to higher decontamination factors more rapidly than ZnO, whereas for GD, they behaved in a similar manner.

The conversion of the two chemical warfare agents into their decontamination products was also monitored up to 24 h. Four main degradation products resulting from the decontamination of sulfur mustard, and five main degradation products resulting from the decontamination of GD were identified and quantified by the GC-MS technique as well.

We can conclude that these organic suspensions comprising ZnO, TiO_2, and zeolite nanoparticles proved their decontamination efficiency on soman and sulfur mustard, whereas extensive study on their conversion into harmless degradation products offers a comprehensive image on the decontamination process.

Author Contributions: Conceptualization, R.E.G. and R.P.; Data curation, A.E.B. and R.E.O.; Formal analysis, R.E.G., G.T., A.E.M., R.E.O., R.P. and G.E.; Funding acquisition, R.E.G. and M.P.; Investigation, R.E.G., A.E.B., A.E.M., R.E.O., P.D. and M.P.; Methodology, R.E.G., P.D., R.P. and G.E.; Project administration, A.E.M., T.V.T. and M.P.; Resources, P.D.; Supervision, G.T., T.V.T., R.P. and G.E.; Validation, A.E.B., G.T., T.V.T. and G.E.; Visualization, A.E.M.; Writing—original draft, R.E.G. and G.T. All authors have read and agreed to the published version of the manuscript.

Funding: This work was supported by a grant of the Ministry of Research, Innovation and Digitization, CNCS/CCCDI—UEFISCDI, PN-III-P2-2.1-PED-2019-4222 ctr. no 427PED/2020.

Institutional Review Board Statement: Not applicable.

Informed Consent Statement: Not applicable.

Data Availability Statement: The data presented in this study are available on request from the corresponding author.

Acknowledgments: The authors would like to give thanks for the financial support provided by the Executive Agency for Higher Education, Research, Development, and Innovation Funding (UEFISCDI) trough PN-III-P2-2.1-PTE-2019-0400 ctr. no 49PTE/2020.

Conflicts of Interest: The authors declare no conflict of interest.

References

1. Vilches, D.; Alburquerque, G.; Ramirez-Tagle, R. One hundred and one years after a milestone: Modern chemical weapons and World War I. *Educ. Química* **2016**, *27*, 233–236. Available online: http://www.scielo.org.mx/scielo.php?script=sci_arttext&pid=S0187-893X2016000300233&nrm=iso (accessed on 1 November 2021). [CrossRef]
2. The Convention on the Prohibition of the Development, Production, Stockpiling and Use of Chemical Weapons and on Their Destruction (the Chemical Weapons Convention or CWC). 29 April 1997. Available online: https://www.opcw.org/chemical-weapons-convention (accessed on 1 November 2021).
3. Ganesan, K.; Raza, S.K.; Vijayaraghavan, R. Chemical warfare agents. *J. Pharm. Bioallied Sci.* **2010**, *2*, 166–178. [CrossRef]
4. Picard, B.; Chataigner, I.; Maddaluno, J.; Legros, J. Introduction to chemical warfare agents, relevant simulants and modern neutralisation methods. *Org. Biomol. Chem. R. Soc. Chem.* **2019**, *17*, 27. [CrossRef] [PubMed]
5. OPCW. Visual Guide to Science & Technology Relevant to the Chemical Weapons Convention. Office of Strategy & Policy Organisation for the Prohibition of Chemical Weapons, 2018. Available online: https://www.opcw.org/sites/default/files/documents/2018/08/2018_Visual_Guide-web.pdf (accessed on 1 November 2021).
6. Misik, J.; Pavlikova, R.; Cabal, J.; Kuca, K. Acute toxicity of some nerve agents and pesticides in rats. *Drug Chem. Toxicol.* **2014**, *38*, 32–36. [CrossRef]
7. Wagner, G.W.; Koper, O.B.; Lucas, E.; Decker, A.S.; Klabunde, K.J. Reactions of VX, GD, and HD with Nanosize CaO: Autocatalytic Dehydrohalogenation of HD. *J. Phys. Chem. B* **2000**, *104*, 5118–5123. [CrossRef]

8. Wagner, G.W.; Procell, L.R.; Klabunde, K.J. Decontamination of Chemical Warfare Agents with Nanosize Metal Oxides. *ACS Symp. Ser.* **2005**, *891*, 139–152. [CrossRef]
9. Wagner, G.W.; Yang, Y.-C. Rapid Nucleophilic/Oxidative Decontamination of Chemical Warfare Agents. *Ind. Eng. Chem. Res.* **2002**, *41*, 1925–1928. [CrossRef]
10. Wang, H.; Wagner, G.W.; Lu, A.X.; Nguyen, D.L.; Buchanan, J.H.; McNutt, P.; Karwacki, C.J. Photocatalytic Oxidation of Sulfur Mustard and Its Simulant on BODIPY-Incorporated Polymer Coatings and Fabrics. *ACS Appl. Mater. Interfaces* **2018**, *10*, 18771–18777. [CrossRef]
11. Prasad, G.K.; Mahato, T.H.; Singh, B.; Ganesan, K.; Srivastava, A.R.; Kaushik, M.P.; Vijayraghavan, R. Decontamination of sulfur mustard and sarin on titania nanotubes. *AIChE J.* **2008**, *54*, 2957–2963. [CrossRef]
12. Oudejans, L. *Decontamination of Sulfur Mustard and Thickened Sulfur Mustard Using Chlorine Dioxide Fumigation*; U.S. Environmental Protection Agency: Raleigh, NC, USA, 2011.
13. Stone, H.; See, D.; Smiley, A.; Ellingson, A.; Schimmoeller, J.; Oudejans, L. Surface decontamination for blister agents Lewisite, sulfur mustard and agent yellow, a Lewisite and sulfur mustard mixture. *J. Hazard. Mater.* **2016**, *314*, 59–66. [CrossRef] [PubMed]
14. Razavi, S.M.; Karbakhsh, M.; Salamati, P. Preventive measures against the mustard gas: A review. *Med. J. Islam. Repub. Iran* **2013**, *27*, 83–90.
15. Otřísal, P.; Melichařík, Z.; Svorc, L.; Oancea, R.; Barsan, V. The Most Significant Influences of Decontamination Mixtures Containing Chlorinating and Oxidizing Agents on Barrier Materials Formed by Isobutylene-Isoprene Rubber. *Mater. Plast.* **2018**, *55*, 325–331. [CrossRef]
16. Oudejans, L. *Decontamination of Lewisite using Liquid Solutions: Neutralization and Arsenic Removal*; U.S. Environmental Protection Agency: Raleigh, NC, USA, 2014.
17. Capoun, T.; Krykorkova, J. Comparison of Selected Methods for Individual Decontamination of Chemical Warfare Agents. *Toxics* **2014**, *2*, 307–326. [CrossRef]
18. Štengl, V.; Grygar, T.M.; Opluštil, F.; Olšanská, M. Decontamination of Sulfur Mustard from Printed Circuit Board Using Zr-Doped Titania Suspension. *Ind. Eng. Chem. Res.* **2013**, *52*, 3436–3440. [CrossRef]
19. Hallam, A.; Sellwood, B.W. Origin of Fuller's Earth in the Mesozoic of Southern England. *Nat. Cell Biol.* **1968**, *220*, 1193–1195. [CrossRef]
20. Capoun, T.; Krykorkova, J. Study of Decomposition of Chemical Warfare Agents using Solid Decontamination Substances. *Toxics* **2019**, *7*, 63. [CrossRef]
21. Prasad, G.K.; Mahato, T.H.; Singh, B.; Pandey, P.; Rao, A.N.; Ganesan, K.; Vijayraghavan, R. Decontamination of sulfur mustard on manganese oxide nanostructures. *AIChE J.* **2007**, *53*, 1562–1567. [CrossRef]
22. Petrea, N.; Petre, R.; Pretorian, A.; Toader, C.; Şomoghi, V.; Neaţu, F.; Florea, M.; Neaţu, Ş. The Cu- and Zn-complex-catalyzed methanolysis of the chemical warfare nerve agents soman, sarin, and VX. *C. R. Chim.* **2018**, *21*, 339–345. [CrossRef]
23. Cojocaru, B.; Neatu, S.; Pârvulescu, V.I.; Şomoghi, V.; Petrea, N.; Epure, G.; Alvaro, M.; Garcia, H. Synergism of Activated Carbon and Undoped and Nitrogen-doped TiO2in the Photocatalytic Degradation of the Chemical Warfare Agents Soman, VX, and Yperite. *ChemSusChem* **2009**, *2*, 427–436. [CrossRef] [PubMed]
24. Prasad, G.; Mahato, T.; Pandey, P.; Singh, B.; Suryanarayana, M.; Saxena, A.; Shekhar, K. Reactive sorbent based on manganese oxide nanotubes and nanosheets for the decontamination of 2-chloro-ethyl ethyl sulphide. *Microporous Mesoporous Mater.* **2007**, *106*, 256–261. [CrossRef]
25. Novak, T.G.; DeSario, P.A.; Long, J.W.; Rolison, D.R. Designing Oxide Aerogels with Enhanced Sorptive and Degradative Activity for Acute Chemical Threats. *Front. Mater.* **2021**, *8*, 164. [CrossRef]
26. Yekta, S.; Sadeghi, M.; Mirzaei, D.; Zabardasti, A.; Farhadi, S. Removal of nerve agent sarin simulant from aqueous solution using the ZSM-5/CoFe2O4 NPs adsorbent. *J. Iran. Chem. Soc.* **2018**, *16*, 269–282. [CrossRef]
27. Hiscock, J.R.; Bustone, G.P.; Clark, E.R. Decontamination and Remediation of the Sulfur Mustard Simulant CEES with "Off-the-Shelf" Reagents in Solution and Gel States: A Proof-of-Concept Study. *ChemistryOpen* **2017**, *6*, 497–500. [CrossRef] [PubMed]
28. Wojnarowicz, J.; Chudoba, T.; Koltsov, I.; Gierlotka, S.; Dworakowska, S.; Lojkowski, W. Size control mechanism of ZnO nanoparticles obtained in microwave solvothermal synthesis. *Nanotechnology* **2017**, *29*, 065601. [CrossRef] [PubMed]
29. Viana, M.; Soares, V.; Mohallem, N. Synthesis and characterization of TiO_2 nanoparticles. *Ceram. Int.* **2010**, *36*, 2047–2053. [CrossRef]
30. Neag, E.; Török, A.I.; Tanaselia, C.; Aschilean, I.; Senila, M. Kinetics and Equilibrium Studies for the Removal of Mn and Fe from Binary Metal Solution Systems Using a Romanian Thermally Activated Natural Zeolite. *Water* **2020**, *12*, 1614. [CrossRef]
31. NATO. AECTP-230 Climatic Conditions. 2009. Available online: https://nso.nato.int/nso/nsdd/main/standards/ap-details/1225 (accessed on 1 November 2021).
32. De Carvalho, G.C.; Moura, M.D.F.V.D.; De Castro, H.G.C.; Júnior, J.H.D.S.; Da Silva, H.E.B.; Dos Santos, K.M.; Rocha, Z.M.S. Influence of the atmosphere on the decomposition of vegetable oils: Study of the profiles of FTIR spectra and evolution of gaseous products. *J. Therm. Anal. Calorim.* **2020**, *140*, 2247–2258. [CrossRef]
33. NATO. AEP 58-Combined Operational Characteristics, Technical Specifications, Test Procedures and Evaluation Criteria for Chemical, Biological, Radiological and Nuclear Decontamination Equipment. 2014. Available online: https://nso.nato.int/nso/nsdd/main/list-promulg (accessed on 1 November 2021).

toxics

MDPI

Review

Scientific Evidence about the Risks of Micro and Nanoplastics (MNPLs) to Human Health and Their Exposure Routes through the Environment

Ana Clara Bastos Rodrigues [1], Gabriel Pereira de Jesus [1], Dunia Waked [1], Gabriel Leandro Gomes [1], Thamires Moraes Silva [1], Victor Yuji Yariwake [1], Mariane Paula da Silva [1], Antônio José Magaldi [2] and Mariana Matera Veras [1,*]

[1] Laboratory of Experimental and Environmental Pathology–LIM05, Department of Pathology, Faculty of Medicine, University of Sao Paulo, Sao Paulo 01246-000, Brazil; anaclarabr@usp.br (A.C.B.R.); gabrielamaral5555@gmail.com (G.P.d.J.); duniawaked@usp.br (D.W.); gomesglbio@gmail.com (G.L.G.); moraesthami44@gmail.com (T.M.S.); victoryuji.13@gmail.com (V.Y.Y.); marianepaula@ymail.com (M.P.d.S.)

[2] Kidney Research Laboratory–LIM12, Department of Nephrology, Faculty of Medicine, University of Sao Paulo, Sao Paulo 01246-000, Brazil; biomag@usp.br

* Correspondence: verasine@usp.br

Abstract: Nowadays, a large amount and variety of plastic is being produced and consumed by human beings on an enormous scale. Microplastics and nanoplastics (MNPLs) have become ubiquitous since they can be found in many ecosystem components. Plastic particles can be found in soil, water, and air. The routes of human exposure are numerous, mainly involving ingestion and inhalation. Once ingested, these particles interact with the gastrointestinal tract and digestive fluids. They can adsorb substances such as additives, heavy metals, proteins, or even microorganisms on their surface, which can cause toxicity. During inhalation, they can be inhaled according to their respective sizes. Studies have reported that exposure to MNPLs can cause damage to the respiratory tract, creating problems such as bronchitis, asthma, fibrosis, and pneumothorax. The reports of boards and committees indicate that there is little data published and available on the toxicity of MNPLs as well as the exposure levels in humans. Despite the well-established concept of MNPLs, their characteristics, and presence in the environment, little is known about their real effects on human health and the environment.

Keywords: microplastics; ecosystem; human health; toxicity

Citation: Rodrigues, A.C.B.; de Jesus, G.P.; Waked, D.; Gomes, G.L.; Silva, T.M.; Yariwake, V.Y.; da Silva, M.P.; Magaldi, A.J.; Veras, M.M. Scientific Evidence about the Risks of Micro and Nanoplastics (MNPLs) to Human Health and Their Exposure Routes through the Environment. *Toxics* **2022**, *10*, 308. https://doi.org/10.3390/toxics10060308

Academic Editors: Ondrej Soukup, Jan Korabecny and Susanne M. Brander

Received: 30 March 2022
Accepted: 20 May 2022
Published: 8 June 2022

1. Introduction

Nowadays, a wide variety and large quantity of plastic is being produced and consumed on a large scale by human beings. Plastics are synthetic polymers mainly derived from the petrochemical industry. Although some sources of biodegradable plastics are produced by natural sources (cellulose, cornstarch, soybeans, etc.), those coming from the oil industry are the most commonly manufactured and can cause a greater impact on nature since they remain longer in the environment [1].

Since it is mostly a synthetic polymerized product, plastic has desirable characteristics when considering durability, resistance, inertia, and its low cost. These properties, while beneficial to industry, have created a significant problem for the environment and human health. The pollution of the environment and the oceans with large amounts of plastic, in all its varieties, has become a global issue in environmental pollution [2].

As previously mentioned, synthetic plastic has incredible characteristics for use in industry, but these same characteristics make these products virtually indestructible due to their composition and material hardness. When in contact with air, soil, and fresh or saltwater, plastic deteriorates into smaller particles called micro and nanoplastics (MNPLs).

Consequently, long and short fragments are released from the chains of polymerized organic molecules which can remain in the environment for hundreds of years [3].

Microplastics (MPs) are plastic particles that range from 1 μm to less than 5 mm, while nanoplastics (NPs) are plastic particles smaller than 1 μm [4]. MNPLs are mainly classified in two ways—primary or secondary—taking into account their origin [5]. Primary MNPLs are plastic particles intentionally manufactured to have a small size (1 μm to less than 5 mm), e.g., pellet beads, which are used as raw material for the production of cosmetics, such as toothpastes, exfoliating treatments, body wash, and other personal care products.

Secondary MNPLs are products derived from the degradation and fragmentation of larger plastics, such as bottles, tire and road wear particles (TRWPs), or caps which generate plastic microparticles. This fragmentation occurs due to mechanical actions, UV radiation, temperature, humidity, etc., producing both micro and nanoplastics [6]. In addition to these two types of MNPLs, synthetic microfibers used in the manufacture of clothing and fabrics are also found in the environment [7]. These filaments are released during processes such as washing, reaching urban sewers, and consequently, the environment, and affecting human health [8].

Despite the well-established concept of microplastics and nanoplastics (MNPLs) and their characteristics and presence in the environment, little is known about their real effects on human health. This review considers the scientific evidence of their harmful effects on the environment and human health.

2. Routes of Exposure

Micro and nanoplastics (MNPLs) have become ubiquitous since they can be found in many ecosystem components. Plastic particles can be found in soil, water, and air. There are many routes of human exposure to microplastics. These can include oral exposure through contaminated water and food (mainly of marine origin); via the dermal route through the use of soaps, scrubs, or via contact with soil; and via inhalation through the precipitation of particles in the air [9], which was found in pulmonary tissue samples from the first study to identify MNPLs in lung tissues [10]. Figure 1 shows a summary of the main exposure routes to humans and animals, showing that humans can experience more exposure to to MNPLs from these different sources.

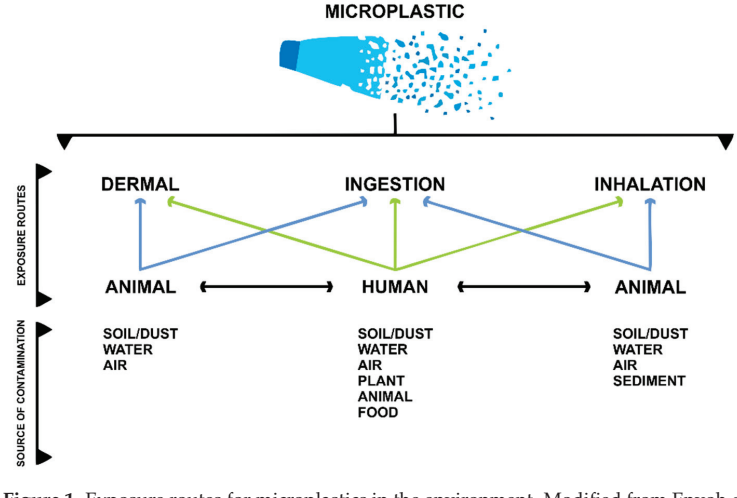

Figure 1. Exposure routes for microplastics in the environment. Modified from Enyoh et al., 2020 [9].

2.1. Respiratory Exposure to Micro and Nanoplastics

MNPL particles, derived from the degradation of plastic in the environment, have been observed in atmospheric precipitations. Depending on the sizes of these particles,

they can be inhaled. We must clarify that particles capable of entering through the nose and mouth and being deposited in the upper respiratory tract are classified as inhalables, and particles that are deposited in the lungs are classified as breathable [11]. These particles may be subject to non-specific host defense mechanisms that remove mucus through the mucociliary process. Alveolar macrophages may capture these particles and transport them to the intestine to be removed [12].

Studies have reported that exposure to MNPLs can cause damage to human health, creating problems such as bronchitis, asthma, fibrosis, and pneumothorax. In an experimental study with rats, in which the toxicological potential of MNPLs inhaled for 14 days was investigated, it was observed that levels of transforming growth factor beta (TGF-beta), factors related to fibrosis, and tumor necrosis factor alpha (TNF-alpha) were altered [13].

Studies with polystyrene nanoplastics using alveolar basal epithelial cells (A549) have shown that they are able to disturb gene expression, resulting in inflammatory responses and the launch of apoptosis pathways, particularly when smaller PS-NPs are used. The results of one study suggest that nanoplastics can cause definite damage and functional disturbance to human and mammalian respiratory systems [14].

Regarding the involvement of MNPLs in the respiratory tract of humans, for the first time, a recent study identified plastic particles ranging in size from 1.60 to 5.58 µm in the bronchoalveolar region in more than 50% of analyzed lung samples, confirming that the respiratory system is an important route of exposure and that the lungs act as a site of accumulation of MNPLs in human beings [10]. Environmental exposure to MNPLs through the air occurs through several sources, such as synthetic textiles, tire erosion, synthetic rubber, and urban dust [15]. Other sources of airborne MNPLs include plastics from clothes and household furniture. Of note are synthetic textiles, which may be responsible for human exposure in both internal and external environments [16].

The persistence of these particles in the atmosphere is determined by atmospheric precipitation, which is influenced by rain, wind, local conditions, and particle size. Particles with lower densities can be easily carried by the wind, which causes the contamination of terrestrial and aquatic environments [17,18].

Plastic nanoparticles have diameters smaller than 1 µm. These nanoparticles can generate distinct toxicities due to their smaller dimensions [19,20]. The inhalation of MPs and NPs is related to some pathologies and a higher incidence of cancer. Studies carried out using animal models indicate that exposure can induce granulomatous lesions [21–23]. MNPLs can have the same toxicity as other atmospheric nanoparticles, which makes it difficult to compare them. Therefore, it is necessary to carry out studies regarding the toxicity of different sizes of polymers and their surface properties [24].

With the arrival of the new coronavirus, the use of masks has become essential for the population, with N95 surgical masks being the most effective at reducing the risk of virus transmission. However, due to the scarcity of masks, people have chosen to use masks made of other materials, such as cotton, nylon, clothing cloth, and textile mixed with polypropylene. During the process of disinfecting masks, the fabric may suffer wear and tear [25,26], causing distress in the material, leading to the risk of inhalation through respiration [27,28].

Li and colleagues [29] carried out a study using seven types of masks—N95, cotton, sky surgery, ply surgery, fashion, activated carbon, and non-woven—for the detection of MNPLs using Raman spectroscopy and infrared spectrometry. The N95 mask performed well and reduced particle inhalation even after disinfection. In addition, fashionable cotton masks and those made of non-woven fabrics and activated carbon were shown to reduce the risk of MNPL inhalation. When compared to not wearing a mask, it was concluded that using the above-mentioned masks for at least two hours could reduce the inhalation of plastic particles [29].

2.2. Oral Exposure to Micro and Nanoplastics

The presence of MNPLs in food and beverages has evidently increased. Recent studies have reported the detection of plastic particles in common food products, such as salt, milk, honey, fruits, vegetables, mineral water, and marine foods. Thus, human exposure through ingestion is quite likely and needs to be studied while taking into account the entire food production chain, from cultivation to consumption [30–32].

Despite being a subject of interest, there are still many obstacles in relation to the methodologies used to detect MNPLs in foods and beverages and characterization parameters, such as exposure dose. A first issue is the diversity of these particles, which can have different chemical compositions, in addition to different densities, sizes, and formats, which makes it difficult to standardize techniques. In addition, there is an absence of reference values and precise definitions [32]. Such obstacles make research on oral exposure to MNPLs challenging. However, advances have been reported. Recent studies estimate that each person ingests an amount of MNPLs ranging from 39,000 to 52,000 particles annually [31]. Such findings highlight the importance of and the need for further investigation on this subject [33,34].

Some of the most studied foods are those of aquatic origin [35]. Generally, fish accumulate MNPLs in their gills, liver, and intestine, parts that are generally not eaten by humans [36]. However, in some filtering animals, such as shrimps, a relatively large amount of MNPLs was observed. It is estimated that consumers of these animals ingest about 11,000 particles annually [37]. In addition to food of aquatic origin, commercial mineral water showed traces of plastic particles, even in bottled water in glass containers [38], while polypropylene particles have been identified in various brands of table salt [39]. Plastic particles have also been found in fruits, such as apples and pears, and vegetables, such as potatoes, broccoli, carrots, and lettuce [40]. The presence of microplastics in fecal samples from humans reinforces the idea that particles are ingested by humans [41]. However, the effects of this kind of oral exposure are still unclear.

Once ingested, particles can interact with the gastrointestinal tract and digestive fluids. Despite being considered chemically inert particles, plastics can adsorb substances, such as additives, heavy metals, proteins, or even microorganisms, on their surface, which can cause greater toxicity. In this situation, MNPLs work like a Trojan horse, bringing a series of environmental contaminants with them. When ingested, the particles can interact with the mucus that lines the gastrointestinal tract, with the epithelial cells themselves, and even with intestinal microbiota, causing cellular responses and diverse physiological changes (Figure 2) [42–45].

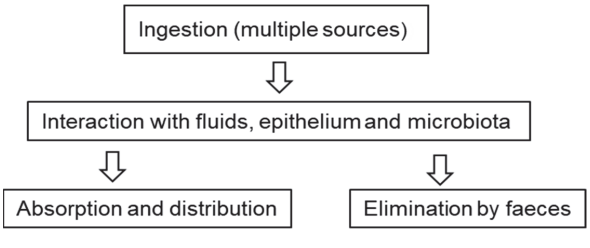

Figure 2. Oral exposure to microplastics. Possible routes and interactions that are currently under study.

Recent research suggests that, depending on the size, particles can be internalized by intestinal epithelial cells (endocytosis) or they can pass between intestinal cells (paracellular transport) [46]. Animal studies have shown the distribution and deposition of MNPLs in organs such as the kidneys, liver, and lymph nodes [47–49]. However, this systemic distribution remains controversial, and further studies are needed to corroborate this hypothesis.

2.3. Dermal Exposure to Micro and Nanoplastics

Although oral exposure is the most notable type of exposure, there are also other types of exposure—one of these is dermal exposure. Even though it is a less efficient route, studies show that micro and nanoplastics can cross the dermal barrier [50]. These nanoparticles are applied, for example, in cosmetics and in the continuous reduction of textile microfibers. In addition, microplastic microspheres (less than 1 mm in diameter) are widely used in dermal exfoliation products, such as toothpastes and denture restorations [51].

Another area in which dermal exposure is discussed is in medicine. In suturing, for example, plastics are known to induce low inflammatory reactions and a foreign body reaction with fibrous encapsulation. In a study of mice, the effects of polyethylene and polyvinyl chloride (PVC) were evaluated, showing that polyethylene was associated with lower inflammation compared to PVC. However, micro and nanoplastics can also induce inflammation and foreign body reactions, with differences in surface properties leading to different results. Human epithelial cells undergo oxidative stress from exposure to micro and nanoplastics, confirming the need for studies that evaluate the effects of exposure to MNPLs [50].

3. Epidemiological Studies

Epidemiological studies have already indicated that adverse respiratory and cardiovascular effects are closely linked to air pollution via environmental atmospheric particles [52]. Some studies also demonstrate possible significant correlations between BPA levels (adsorbed in both air and food) in urine and cardiovascular disease and type 2 diabetes [53]. Moreover, recent data have shown the presence of airborne MNPLs in human lung tissue [10] and the bloodstream [54]. Atmospheric research on MNPLs highlights that they can impact remote and under-developed areas that do not have any local sources of plastic [55]. In addition, the dynamics of ocean circulation and marine currents represent important space–time scales in terms of the destination, transport, and effects of micro and nanoplastics on the environment, affecting fauna, and consequently, human life [56].

In addition to the respiratory tract, MNPLs can be ingested by several organisms, mainly by species widely consumed by humans [57–59]. However, it is still not fully understood how the interaction between human organic systems and these particles work [60]. This is mainly due to the absence of extensive and significant epidemiological studies to detect their impacts at the population level and the lack of technology available to detect and track these particles in vivo. Research is fundamental for understanding how atmospheric air and the main foods established by nutritional health standards are contributing to the transport of microplastics by the human body, as well as the risks to health [35].

Reports of boards and committees, such as the Scientific Council of the European Commission, Science Advice for Policy by European Academies (SAPEA), and the World Health Organization (WHO), show that there is little data published and available on the toxicity of MNPLs, as well as the exposure levels in humans [60,61]. These reports also highlight some of the main challenges when trying to gather concrete information about the relationships between MNPLs and human health [62].

4. Experimental Studies

4.1. In Vivo

Since human exposure to MPs and NPs occurs mainly via ingestion, in vivo studies have been prioritized in animal models for a better understanding of the biological effects of these particles on humans. Research indicates that MNPLs, after being adsorbed by the organism, are systemically distributed to organs and tissues, both through the blood and lymphatic currents [63].

According to Stock and colleagues [64], in a study using a murine model and oral exposure via gavage, the histological absence of detectable lesions and inflammatory responses was observed, suggesting that the particles taken in through oral exposure under experimental conditions did not represent relevant acute risks to the health of mammals.

In contrast, in another study, a negative load of polystyrene nanoparticles (PS-NPs) in the lungs, testis, spleen, kidney and heart of an animal model after oral administration was observed [49]. These divergent results may be due to the properties of the particles, such as the size, concentration, and dosage.

Questionable findings may also arise, such as the study carried out by Deng and colleagues [65], which identified a high number of 5 μm and 20 μm polystyrene microplastic (PS-MPs) particles crossing the intestinal barrier and distributing to organs, while most studies in mammals have suggested the low oral bioavailability of microplastic particles.

Recent publications have elucidated mechanisms of plastic absorption in female rats and the effect of plastic absorption on the reproductive system, indicating that these polystyrene particles cause fibrosis through the Wnt/B-Catenin signaling pathway and the apoptosis of granular cells in the ovary, resulting in decreased ovarian reserve capacity [66]. In addition, MNPLs also function as adsorbents for heavy metals, causing toxicity in combination with other pollutants in the environment. With respect to testicular toxicity, Hou and colleagues [67] demonstrated a reduction in viable sperm from the epididymis after exposure to 5 μm polystyrene particles in mice, showing atrophy, shedding, and the apoptosis of sperm cells at all levels of the testis after exposure.

With respect to in vivo tracing in aquatic organisms, a study was developed to improve the tracking, transport, and localization of MNPLs in shrimp, medaka, zebrafish, and water fleas, which involved real-time observation for the whole in vivo process of ingestion and egestion in a zebrafish model using manufactured fluorescent fibers. In shrimp, medaka and water fleas, the fibers were observed directly using a fluorescent microscope without dissection [68].

4.2. In Vitro

In vitro studies have highlighted important characteristics of MNPLs, such as their hydrophobicity. According to Wright and Kelly [69], the hydrophobicity of these particles is correlated to their more effective transport in intestinal mucus, influencing the adsorption of proteins to the surface of the particle, suggesting that internalization via "M" cells and persorption were the most likely mechanisms responsible for MNPL uptake. In contrast, in vitro studies have also demonstrated that the intestinal epithelium is an important and robust barrier against these types of materials [70].

The size of particles is also an influential factor; for example, 100 nm PS-MNPLs showed greater intestinal toxicity than 5 mm PS-MNPLs. Such studies suggest that direct cytotoxicity assays for PS-MNPLs may erroneously assess their intestinal effects, offering new insights into assessing the toxicity of PS-MNPLs via oral exposure [70].

Another important point relates to in vitro studies using cells from the digestive tract, which is an important target organ with respect to the absorption and distribution of MNPLs [71]. To investigate their effects in relation to the toxicological evaluation of plastic components, some research has been undertaken using differentiated Caco-2 cells, an important experimental model in the study of the intestinal epithelial barrier, especially when combined with HT29 or Raji-B cells [72]. Research has suggested [70] that the digestive process does not alter the chemical constitution of PS-MNPLs, which may be an explanation for the reduced toxicity of MNPLs. In another study, an absence of toxicity was observed in an intestinal cellular model; despite this, it was found that MNPLs could be absorbed by Caco-2 cells [64]. Due to this absorption by the cells, suggesting damage to the plasma membrane, we can infer that MNPLs may induce indirect harmful effects to the gastrointestinal tract, increasing the pro-inflammatory effects of these components.

With respect to acute toxicity in vitro, Hesler et al. [73] evaluated the placental and intestinal barrier using advanced in vitro co-culture models, showing that PS-MNPLs did not have important embryotoxic and genotoxic effects. In recent publications, an increased level of pro-inflammatory cytokines has been demonstrated when plastics are present in high concentrations, consequently causing inflammatory and oxidative lesions. According to previous studies, MNPLs can induce cell death, inflammation, and oxidative stress in

various types of cells, decrease cell viability, induce cell apoptosis, alter mitochondrial membrane potential, and deregulate mitochondrial function in lymphocytes, impairing immune function.

As can be seen, size is an important matter—micro and nanoplastics can be ingested by organisms and appear to have some impact on biological functions due to their small size and biological penetration, but nanoplastics seem to have more serious effects. A study on MNPLs (polystyrene) ranging in size from 50 nm, 500 nm, and 5 μm (PS50, PS500, and PS5000), which aimed to analyze the interaction and distribution of these particles with cell membranes, showed that PS particles could enter cells through endocytosis and passive membrane penetration, especially PS50 and PS500, which were both able to cross the cell membrane via energy-independent membrane penetration, though through different pathways. PS50 was endocytosed by RBL-2H3 cells through clathrin-mediated, caveolin-mediated pathways and macropinocytosis, while PS500 was endocytosed via macropinocytosis [74]. PS5000 had no obvious adsorption on the cell because its large particle size made it difficult for it to diffuse to the membrane surface.

5. Gaps in Knowledge

Currently, much is being said about MNPLs and their presence in the environment as a pollutant. Despite promising studies, after many years of investigation, little is known about the real toxic and adverse effect of these particles for humans. Furthermore, most of the experimental studies undertaken so far have used nanopolystyrene (MNPLs) as a model for all microplastics. Thus, caution is needed, because we are not sure whether other types of microplastics have similar characteristics and whether they elicit the same responses. Studies have already reported changes in murine models relating to reproductive disorders and inflammatory, respiratory, and intestinal toxicity changes, and have suggested that these particles act in a toxic manner in the body.

In the past 10 years, research has shown that human beings are indeed consuming more and interacting more with plastic microparticles, both through contact, as well as through inhalation and the consumption of food and water. There is great difficulty in biomonitoring MNPLs in the human body, as the existing techniques lack precision [75], making the data obtained unreliable due to their lack of accuracy. Therefore, improvements in the techniques and research methods on animal models are important because the effects of MNPLs on human health are increasingly concerning. To fill the knowledge gaps, it is necessary to ensure more reliable and accurate analysis, standardizing the quantification of MNPLs in the environment and promoting better laboratory standards for research into these particles.

Current exposure scenarios are still speculative and imprecise; however, we suggest that, according to recent studies using animal models, MNPLs may have toxic potential, since they can be absorbed by organs and distributed in human beings.

Author Contributions: Conceptualization, A.C.B.R., G.P.d.J. and M.M.V.; methodology, M.M.V.; formal analysis, A.J.M. and M.M.V.; investigation, A.J.M. and M.M.V.; data curation, A.C.B.R.; writing—original draft preparation, A.C.B.R., G.P.d.J., D.W., T.M.S., G.L.G., M.P.d.S. and V.Y.Y.; writing—review and editing, A.C.B.R., G.P.d.J., D.W., T.M.S., G.L.G., M.P.d.S., V.Y.Y.; illustrations, G.L.G.; supervision, A.J.M. and M.M.V.; project administration, M.M.V. All authors have read and agreed to the published version of the manuscript.

Funding: This research received no external funding.

Data Availability Statement: Data were obtained through research in virtual libraries, such as Pubmed, Web of Science, and Google Scholar. The review was carried out in a narrative way, without systematic criteria for the search.

Acknowledgments: This study was financed in part by the Coordenação de Aperfeiçoamento de Pessoal de Nível Superior-Brasil (CAPES)-Finance Code 001.

Conflicts of Interest: The authors declare no conflict of interest.

References

1. Sharma, S.; Chatterjee, S. Microplastic pollution, a threat to marine ecosystem and human health: A short review. *Environ. Sci. Pollut. Res.* **2017**, *24*, 21530–21547. [CrossRef] [PubMed]
2. Crawford, C.B.; Quinn, B. *Microplastic Pollutants*, 1st ed.; Elsevier: Amsterdam, The Netherlands, 2016; Volume 1, pp. 2–5.
3. Dehaut, A.; Cassone, A.L.; Frère, L.; Hermabessiere, L.; Himber, C.; Rinnert, E.; Rivière, G.; Lambert, C.; Soudant, P.; Huvet, A.; et al. Microplastic in sea food: Benchmark protocol for their characterization. *Environ. Poll.* **2016**, *215*, 223–233. [CrossRef] [PubMed]
4. Alimi, O.; Budarz, J.; Hernandez, L.; Tufenkji, N. Microplastics and nanoplastics in aquatic environments: Aggregation, deposition, and enhanced contaminant transport. *Environ. Sci. Technol.* **2018**, *52*, 1704–1724. [CrossRef]
5. Penalver, R.; Manzanares, N.A.; García, I.L.; Córdoba, M.H. An overview of microplastics characterization by thermal analysis. *Chemosphere* **2020**, *242*, 125170. [CrossRef] [PubMed]
6. Qi, R.; Jones, D.; Li, Z.; Liu, Q.; Yan, C. Behavior of microplastics and plastic film residues in the soil environment: A critical review. *Sci. Total Environ.* **2020**, *703*, 134722. [CrossRef]
7. Machado, A.; Horton, A.; Davis, T.; Maaß, S. Microplastics and their effects on soil function as a life-supporting system. *Microplast. Terr. Environ. Chem.* **2020**, *96*, 199–222.
8. Olivatto, G.; Martins, M.; Montagner, C.; Henry, T.; Carreira, R. Microplastic contamination in surface waters in Guanabara Bay, Rio de Janeiro, Brazil. *Mar. Pollut. Bull.* **2019**, *139*, 157–162. [CrossRef]
9. Enyoh, C.; Verla, A.; Verla, E.; Ibe, F.; Amaobi, C. Airborne microplastics: A review study on method for analysis, occurrence, movement and risks. *Environ. Monit. Assess.* **2019**, *191*. [CrossRef]
10. Amato-Lourenço, L.; Carvalho-Oliveira, R.; Junior, G.; Galvão, L.; Ando, R.; Mauad, T. Presence of airborne microplastics in human lung tissue. *J. Hazard. Mater.* **2021**, *416*, 126124. [CrossRef]
11. Donaldson, K.; Tran, C. Inflammation caused by particles and fibers. *Inhal. Toxicol.* **2002**, *14*, 5–27. [CrossRef]
12. Gasperi, J.; Wright, S.; Dris, R.; Collard, F.; Mandin, C.; Guerrouache, M.; Langlois, V.; Kelly, F.; Tassin, B. Microplastics in air: Are we breathing it in? *Curr. Opin. Environ. Sci. Health* **2018**, *1*, 1–5. [CrossRef]
13. Lim, D.; Jeong, J.; Song, K.; Sung, J.; Oh, S.; Choi, J. Inhalation toxicity of polystyrene micro (nano) plastics using modified OECD TG 412. *Chemosphere* **2021**, *262*, 128330. [CrossRef] [PubMed]
14. Xu, M.; Halimu, G.; Zhang, Q.; Song, Y.; Fu, X.; Li, Y.; Li, Y.; Zhang, H. Internalization and toxicity: A preliminary study of effects of nanoplastic particles on human lung epithelial. *Sci. Total Environ.* **2019**, *694*, 107199. [CrossRef] [PubMed]
15. Boucher, J.; Friot, D. *Primary Microplastics in the Oceans: A Global Evaluation of Sources*; Iucn: Gland, Switzerland, 2017.
16. Dris, R.; Gasperi, J.; Saad, M.; Mirande, C.; Tassin, B. Synthetic fibers in atmospheric fallout: A source of microplastics in the environment? *Mar. Pollut. Bull.* **2016**, *104*, 290–293. [CrossRef] [PubMed]
17. Horton, A.; Walton, A.; Spurgeon, D.; Lahive, E.; Svendsen, C. Microplastics in freshwater and terrestrial environments: Evaluating the current understanding to identify the knowledge gaps and future research priorities. *Sci. Total Environ.* **2017**, *586*, 127–141. [CrossRef]
18. Nizzetto, L.; Bussi, G.; Futter, M.; Butterfield, D.; Whitehead, P. A theoretical assessment of microplastic transport in river catchments and their retention by soils and river sediments. *Environ. Sci. Process. Impacts* **2016**, *18*, 1050–1059. [CrossRef]
19. Elsaesser, A.; Howard, C. Toxicology of nanoparticles. *Adv. Drug Deliv. Rev.* **2012**, *64*, 129–137. [CrossRef]
20. Yildirimer, L.; Thanh, N.; Loizidou, M.; Seifalian, A. Toxicological considerations of clinically applicable nanoparticles. *Nano Today* **2011**, *6*, 585–607. [CrossRef]
21. Mastrangelo, G.; Fedeli, U.; Fadda, E.; Milan, G.; Lange, J. Epidemiologic evidence of cancer risk in textile industry workers: A review and update. *Toxicol. Ind. Health* **2002**, *18*, 171–181. [CrossRef]
22. Agarwal, D.; Kaw, J.; Srivastava, S.; Seth, P. Some biochemical and histopathological changes induced by polyvinyl chloride dust in rat lung. *Environ. Res.* **1978**, *16*, 333–341. [CrossRef]
23. Hext, P.; Tomenson, J.; Thompson, P. Titanium dioxide: Inhalation toxicology and epidemiology. *Ann. Occup. Hyg.* **2005**, *49*, 461–472. [PubMed]
24. Prata, J. Airborne microplastics: Consequences to human health? *Environ. Pollut.* **2018**, *234*, 115–126. [CrossRef] [PubMed]
25. Greenhalgh, T.; Howard, J. Masks for all? The science says yes. *Fast. Ai.* 2020. Available online: https://www.fast.ai/2020/04/13/masks-summary/ (accessed on 15 February 2022).
26. Santos, M.; Torres, D.; Cardoso, P.; Pandis, N.; Flores-Mir, C.; Medeiros, R.; Normal, A. Are cloth masks a substitute to medical masks in reducing transmission and contamination? A systematic review. *Braz. Oral Res.* **2020**, *34*. [CrossRef]
27. Aragaw, T. Surgical face masks as a potential source for microplastic pollution in the COVID-19 scenario. *Mar. Pollut. Bull.* **2020**, *159*, 11517. [CrossRef]
28. Fadare, O.; Okoffo, E. COVID-19 face masks: A potential source of microplastic fibers in the environment. *Sci. Total Environ.* **2020**, *737*, 140279. [CrossRef]
29. Li, L.; Zhao, X.; Li, Z.; Song, K. COVID-19: Performance study of microplastic inhalation risk posed by wearing masks. *J. Hazard. Mater.* **2021**, *411*, 124955. [CrossRef]
30. EFSA Panel on Contaminants in the Food Chain (CONTAM). Presence of microplastics and nanoplastics in food, with particular focus on seafood. *EFSA J.* **2016**, *14*, e04501.

31. Cox, K.; Covernton, G.; Davies, H.; Dower, J.; Juanes, F.; Dudas, S. Human consumption of microplastics. *Environ. Sci. Technol.* **2019**, *53*, 7068–7074. [CrossRef]
32. Paul, M.; Stock, V.; Cara-Carmona, J.; Lisicki, E.; Shopova, S.; Fessard, V.; Braeuning, A.; Sieg, H.; Bohmert, L. Micro-and nanoplastics—Current state of knowledge with the focus on oral uptake and toxicity. *Nanoscale Adv.* **2020**, *2*, 4350–4367. [CrossRef]
33. Shim, W.; Hong, S.; Eo, S. Identification methods in microplastic analysis: A review. *Anal. Methods* **2017**, *9*, 1384–1391. [CrossRef]
34. Silva, A.; Bastos, A.; Justino, C.; da Costa, J.; Duarte, A.; Rocha-Santos, T. Microplastics in the environment: Challenges in analytical chemistry-A review. *Anal. Chim. Acta* **2018**, *1017*, 1–9. [CrossRef] [PubMed]
35. Smith, M.; Love, D.; Rochman, C.; Neff, R. Microplastics in seafood and the implications for human health. *Curr. Environ. Health Rep.* **2018**, *5*, 375–386. [CrossRef] [PubMed]
36. Waring, R.; Harris, R.; Mitchell, S. Plastic contamination of the food chain: A threat to human health? *Maturitas* **2018**, *115*, 64–68. [CrossRef] [PubMed]
37. Cauwenberghe, L.; Janssen, C. Microplastics in bivalves cultured for human consumption. *Environ. Pollut.* **2014**, *193*, 65–70. [CrossRef] [PubMed]
38. Schymanski, D.; Goldbeck, C.; Humpf, H.; Fürst, P. Analysis of microplastics in water by micro-Raman spectroscopy: Release of plastic particles from different packaging into mineral water. *Water Res.* **2018**, *129*, 154–162. [CrossRef]
39. Karami, A.; Golieskardi, A.; Ho, Y.; Larat, V.; Salamatinia, B. Microplastics in eviscerated flesh and excised organs of dried fish. *Sci. Rep.* **2017**, *7*, 5473. [CrossRef] [PubMed]
40. Conti, G.O.; Ferrante, M.; Banni, M.; Favara, C.; Nicolosi, I.; Cristaldi, A.; Fiore, M.; Zuccarello, P. Micro-and nano-plastics in edible fruit and vegetables. The first diet risks assessment for the general population. *Environ. Res.* **2020**, *187*, 109677. [CrossRef]
41. Schwabl, P.; Köppel, S.; Königshofer, P.; Bucsics, T.; Trauner, M.; Reiberger, T.; Liebmann, B. Detection of various microplastics in human stool: A prospective case series. *Ann. Intern. Med.* **2019**, *171*, 453–457. [CrossRef]
42. Lundqvist, M.; Stigler, J.; Elia, G.; Lynch, I.; Cedervall, T.; Dawson, K. Nanoparticle size and surface properties determine the protein corona with possible implications for biological impacts. *Proc. Natl. Acad. Sci. USA* **2008**, *105*, 14265–14270. [CrossRef]
43. Sinnecker, H.; Ramaker, K.; Frey, A. Coating with luminal gut-constituents alters adherence of nanoparticles to intestinal epithelial cells. *Beilstein J. Nanotechnol.* **2014**, *5*, 2308–2315. [CrossRef] [PubMed]
44. Galloway, T.; Cole, M.; Lewis, C. Interactions of microplastic debris throughout the marine ecosystem. *Nat. Ecol. Evol.* **2017**, *1*, 116. [CrossRef] [PubMed]
45. Jin, Y.; Lu, L.; Tu, W.; Luo, T.; Fu, Z. Impacts of polystyrene microplastic on the gut barrier, microbiota and metabolism of mice. *Sci. Total Environ.* **2019**, *649*, 308–317. [CrossRef]
46. Stock, V.; Fahrenson, C.; Thuenemann, A.; Dönmez, M.H.; Voss, L.; Böhmert, L.; Braeuning, A.; Lampen, A.; Sieg, H. Impact of artificial digestion on the sizes and shapes of microplastic particles. *Food Chem. Toxicol.* **2020**, *135*, 111010. [CrossRef] [PubMed]
47. Jani, P.; Halbert, G.; Langridge, J.; Florence, A. Nanoparticle uptake by the rat gastrointestinal mucosa: Quantitation and particle size dependency. *J. Pharm. Pharmacol.* **1990**, *42*, 821–826. [CrossRef] [PubMed]
48. Tomazic-Jezic, V.; Merritt, K.; Umbreit, T. Significance of the type and the size of biomaterial particles on phagocytosis and tissue distribution. *J. Biomed. Mater.* **2001**, *55*, 523–529. [CrossRef]
49. Walczak, A.; Hendriksen, P.; Woutersen, R.; Van der Zande, M.; Undas, A.; Helsdingen, R.; Berg, H.; Rietjens, I.; Bouwmeester, H. Bioavailability and biodistribution of differently charged polystyrene nanoparticles upon oral exposure in rats. *J. Nanopart. Res.* **2015**, *17*, 231. [CrossRef]
50. Revel, M.; Châtel, A.; Mouneyrac, C. Micro(nano)plastics: A threat to human health? *Curr. Opin. Environ. Sci. Health* **2018**, *1*, 17–23. [CrossRef]
51. Ageel, H.; Harrad, S.; Abdallah, M. Occurrence, human exposure, and risk of microplastics in the indoor environment. *Environ. Sci. Proc. Impact* **2022**, *24*, 17–31. [CrossRef]
52. Churg, A.; Brauer, M. Ambient atmospheric particles in the airways of human lungs. *Ultrastruct. Pathol.* **2000**, *24*, 353–361.
53. Melzer, D.; Rice, N.; Lewis, C.; Henley, W.; Galloway, T. Association of urinary bisphenol a concentration with heart disease: Evidence from NHANES 2003/06. *PLoS ONE* **2010**, *5*, e8673. [CrossRef] [PubMed]
54. Leslie, H.; Velzen, M.; Brandsma, S.; Vethaak, D.; Garcia-Vallejo, J.; Lamoree, M. Discovery and quantification of plastic particle pollution in human blood. *Environ. Int.* **2022**, *163*, 107199. [CrossRef] [PubMed]
55. Allen, S.; Allen, D.; Phoenix, V.R.; Le Roux, G.; Durántez Jiménez, P.; Simonneau, A.; Binet, S.; Galop, D. Atmospheric transport and deposition of microplastics in a remote mountain catchment. *Nat. Geosci.* **2019**, *12*, 339–344. [CrossRef]
56. Bank, M.; Hansson, S. The plastic cycle: A novel and holistic paradigm for the anthropocene. *Environ. Sci. Technol.* **2019**, *13*, 7177–7179. [CrossRef]
57. Li, J.; Green, C.; Reynolds, A.; Shi, H.; Rotchell, J. Microplastics in mussels sampled from coastal waters and supermarkets in the United Kingdom. *Environ. Pollut.* **2018**, *24*, 35–44. [CrossRef]
58. Prata, J. Microplastics in wastewater: State of the knowledge on sources, fate and solutions. *Mar. Pollut. Bull.* **2018**, *129*, 262–265. [CrossRef]
59. Rochman, C.M.; Kross, S.M.; Armstrong, J.B.; Bogan, M.T.; Darling, E.S.; Green, S.J.; Smyth, A.R.; Veríssimo, D. Scientific evidence supports a ban on microbeads. *Environ. Sci. Technol.* **2015**, *49*, 10759–10761. [CrossRef]

60. Science Advice for Policy by European Academies (SAPEA). *A Scientific Perspective on Microplastics in Nature and Society*; SAPEA: Berlin, Germany, 2019. [CrossRef]
61. World Health Organization. Microplastics in Drinking-Water. Geneva. License: CCBY-NC-SA 3.0 IGO. 2019. Available online: https://www.who.int/publications/i/item/9789241516198 (accessed on 27 February 2022).
62. Leslie, H.A.; Depledge, M.H. Where is the evidence that human exposure to microplastics is safe? *Environ. Int.* **2020**, *142*, 105807. [CrossRef]
63. Volkheimer, G. Persorption of microparticles. *Path* **1993**, *14*, 52–247.
64. Stock, V.; Böhmert, L.; Lisicki, E.; Block, R.; Cara-Carmona, J.; Pack, L.K.; Selb, R.; Lichtenstein, D.; Voss, L.; Henderson, C.J.; et al. Uptake and efects of orally ingested polystyrene microplastic particles in vitro and in vivo. *Arch. Toxicol.* **2019**, *93*, 1817–1833. [CrossRef]
65. Deng, Y.; Zhang, Y.; Lemos, B.; Ren, H. Tissue accumulation of microplastics in mice and biomarker responses suggest widespread health risks of exposure. *Sci. Rep.* **2017**, *7*, 46687. [CrossRef] [PubMed]
66. An, R.; Wang, X.; Yang, L.; Zhang, J.; Wang, N.; Xu, F.; Hou, Y.; Zhang, H.; Zhang, L. Polystyrene microplastics cause granulosa cells apoptosis and fibrosis in ovary through oxidative stress in rats. *Toxicology* **2021**, *449*, 152665. [CrossRef] [PubMed]
67. Hou, B.; Wang, F.; Liu, T.; Wang, Z. Reproductive toxicity of polystyrene microplastics: In vivo experimental study on testicular toxicity in mice. *J. Hazar. Mater.* **2021**, *405*, 124028. [CrossRef] [PubMed]
68. Ma, C.; Li, L.; Chen, Q.; Lee, J.; Gong, J.; Shi, H. Application of Internal persistent flourescent fibers in tracking microplastics in vivo processes in aquatic organisms. *J. Hazar. Mater.* **2021**, *401*, 123336. [CrossRef]
69. Wright, S.; Kelly, F. Plastic and human health: A micro issue? *Environ. Sci. Technol.* **2017**, *51*, 6634–6647. [CrossRef]
70. Rubio, L.; Marcos, R.; Hernández, A. Potential adverse health effects of ingested micro- and nanoplastics on humans. Lessons learned from in vivo and in vitro mammalian models. *J. Toxicol. Environ. Health* **2019**, *23*, 51–68. [CrossRef]
71. Su, L.; Xiaomei, W.; Weiqing, G.; Jing, Y.; Bing, W. Influence of the digestive process on intestinal toxicity of polystyrene microplastics as determined by in vitro Caco-2 models. *Chemosphere* **2020**, *256*, 127204.
72. Valente, J.; Barros, R.; Cristovão, A.; Pastorinho, M.; Sousa, A. Avaliação do potencial citotóxico de microplásticos em linhas celulares intestinais, hepáticas e neuronais. *Rev. Captar Ciência Ambiente Todos* **2021**, *10*, 4.
73. Hesler, M.; Aengenheister, L.; Ellinger, B.; Drexel, R.; Straskraba, S.; Jost, C.; Wagner, S.; Meier, F.; von Briesen, H.; Büchel, C.; et al. Multi-endpoint toxicological assessment of polystyrene nano- and microparticles in different biological models in vitro. *Toxicol. In Vitro* **2019**, *61*, 104610. [CrossRef]
74. Liu, L.; Xu, K.; Zhang, B.; Ye, Y.; Zhang, Q.; Jiang, W. Cellular internalization and release of polystyrene microplastics and nanoplastics. *Sci. Total Environ.* **2021**, *779*, 146523. [CrossRef]
75. Mariano, S.; Tacconi, S.; Fidaleo, M.; Rossi, M.; Dini, L. Micro and nanoplastics identification: Classic methods and innovative detection techniques. *Front. Toxicol.* **2021**, *3*, 146523. [CrossRef] [PubMed]

toxics

MDPI

Article

Diacetyl Vapor Inhalation Induces Mixed, Granulocytic Lung Inflammation with Increased $CD4^+CD25^+$ T Cells in the Rat

Emma L. House [1,2], So-Young Kim [2,3], Carl J. Johnston [3,4,5], Angela M. Groves [2,4], Eric Hernady [3,4], Ravi S. Misra [5] and Matthew D. McGraw [2,3,*]

1 Department of Pathology, University of Rochester Medical Center, Rochester, NY 14642, USA; emma_house@urmc.rochester.edu
2 Division of Pediatric Pulmonology, Department of Pediatrics, School of Medicine & Dentistry, University of Rochester Medical Center, Rochester, NY 14642, USA; soyoung_kim@urmc.rochester.edu (S.-Y.K.); angela_groves@urmc.rochester.edu (A.M.G.)
3 Department of Environmental Medicine, School of Medicine & Dentistry, University of Rochester Medical Center, Rochester, NY 14642, USA; carl_johnston@urmc.rochester.edu (C.J.J.); eric_hernady@urmc.rochester.edu (E.H.)
4 Department of Radiation Oncology, University of Rochester Medical Center, Rochester, NY 14642, USA
5 Division of Neonatology, Department of Pediatrics, University of Rochester Medical Center, Rochester, NY 14642, USA; ravi_misra@urmc.rochester.edu
* Correspondence: matthew_mcgraw@urmc.rochester.edu

Abstract: Diacetyl (DA) is a highly reactive alpha diketone associated with flavoring-related lung disease. In rodents, acute DA vapor exposure can initiate an airway-centric, inflammatory response. However, this immune response has yet to be fully characterized in the context of flavoring-related lung disease progression. The following studies were designed to characterize the different T cell populations within the lung following repetitive DA vapor exposures. Sprague-Dawley rats were exposed to 200 parts-per-million DA vapor for 5 consecutive days × 6 h/day. Lung tissue and bronchoalveolar lavage fluid (BALF) were analyzed for changes in histology by H&E and Trichrome stain, T cell markers by flow cytometry, total BALF cell counts and differentials, BALF IL17a and total protein immediately, 1 and 2 weeks post-exposure. Lung histology and BALF cell composition demonstrated mixed, granulocytic lung inflammation with bronchial lymphoid aggregates at all time points in DA-exposed lungs compared to air controls. While no significant change was seen in percent lung $CD3^+$, $CD4^+$, or $CD8^+$ T cells, a significant increase in lung $CD4^+CD25^+$ T cells developed at 1 week that persisted at 2 weeks post-exposure. Further characterization of this $CD4^+CD25^+$ T cell population identified $Foxp3^+$ T cells at 1 week that failed to persist at 2 weeks. Conversely, BALF IL-17a increased significantly at 2 weeks in DA-exposed rats compared to air controls. Lung $CD4^+CD25^+$ T cells and BALF IL17a correlated directly with BALF total protein and inversely with rat oxygen saturations. Repetitive DA vapor exposure at occupationally relevant concentrations induced mixed, granulocytic lung inflammation with increased $CD4^+CD25^+$ T cells in the rat lung.

Keywords: $CD4^+CD25^+$ T cells; lung; airways; diacetyl; 2,3-butanedione; flavorings-related lung disease; hazard potential; intoxication; occupational hazard; bronchiolitis obliterans

Citation: House, E.L.; Kim, S.-Y.; Johnston, C.J.; Groves, A.M.; Hernady, E.; Misra, R.S.; McGraw, M.D. Diacetyl Vapor Inhalation Induces Mixed, Granulocytic Lung Inflammation with Increased $CD4^+CD25^+$ T Cells in the Rat. *Toxics* **2021**, *9*, 359. https://doi.org/10.3390/toxics9120359

Academic Editor: Jan Korabecny

Received: 11 November 2021
Accepted: 13 December 2021
Published: 20 December 2021

1. Introduction

Diacetyl, (2,3-butanedione; DA) is a highly reactive alpha diketone used in commercial food manufacturing as an additive for its buttery flavor and aroma. DA also occurs naturally through coffee roasting and alcohol fermentation [1–3]. Due to its low boiling point (88 °C), DA frequently enters the vapor phase during the production process. DA is highly reactive due to its inherent chemical properties. It has two strong electrophilic carbonyl moieties that can easily and non-enzymatically modify nearby nucleophilic residues in adjacent cellular proteins [4]. These two chemical properties make DA a significant respiratory hazard. Over the past two decades, DA vapor exposures has been

well associated with the fibrotic lung disease known as bronchiolitis obliterans (BO), now labeled as "flavoring-related lung disease" [5]. BO is defined by histopathology with significant small airways, or bronchiolar, remodeling consisting of sub-epithelial collagen deposition and subsequent airway lumen occlusion due to circumferential narrowing [6]. Despite multiple reports of severe lung disease following DA exposure, DA remains a significant and relevant respiratory toxicity considering its more recent identification in other foods such as coffee roasting and e-cigarettes aerosols [1,7,8].

Preclinical studies of flavoring-related lung disease reveal primary injury to the airway epithelium as the sentinel event to disease pathogenesis [9–11]. Severe injury of the airway results in ulceration and necrosis of the epithelium, injury to the adjacent basement membrane, and subsequent initiation of an inflammatory and fibro-proliferative response. With sufficient injury, abnormal repair of the airway epithelium often occurs with epithelial hyperplasia and concentric overgrowth of sub-epithelial fibrous tissue [9,10]. This injury and abnormal epithelial repair initiates a potent inflammatory response seen in both mice and rats exposed repetitively to DA vapors [11,12]. Neutrophils are most frequently observed within the bronchoalveolar lavage fluid (BALF) as well as adjacent lamina propria of the airways. Other infiltrative cell types include lymphocytes and rare eosinophils [12,13]. BALF neutrophilia can persist for weeks after DA exposure despite exposure cessation [9,14]. This persistent BALF neutrophilia is consistent with those workers exposed to high concentrations of DA at popcorn factories as well as other individuals identified to have BO pathology [5]. Thus, this mixed granulocytic inflammation with BALF neutrophilia is an important characteristic of flavoring-related lung disease.

One associated but less characterized attribute of flavoring-related lung disease pathology is the adaptive immune response. Increased peribronchial lymphocytic aggregates have been noted in both mice and rats exposed to DA [11,12]. Additionally, mice exposed to 2,3-pentanedione, a chemically similar and highly reactive ketone, showed frequent nodular and linear lymphoid aggregates adjacent to exposed bronchioles and bronchi, supportive of a localized T cell response [15]. Most of the lymphoid growth seen after inhalation exposure is adjacent to injured airways with less growth of peripheral lymphoid aggregates. In one rare abstract, the T cell response was evaluated in athymic nude rats exposed to DA intratracheally [16]. Thymus-deficient rats exposed to DA developed worse airways pathology compared to DA-exposed rats alone [16], indicating a potentially protective effect of the adaptive immune response in DA-exposed animals with previous thymic resection.

The primary goal of the following studies was to further characterize the T cell phenotypes within the lung and their association with flavoring-induced lung disease progression. For studying the immune response, our lab previously developed an in vivo vapor exposure system using DA with a 14-day follow-up period for modeling the adaptive immune response in flavoring-induced lung disease [14]. We used this model for analyzing the proportions of $CD3^+$, $CD4^+$, $CD8^+$, $CD4^+CD25^+$ and $CD4^+CD25^+Foxp3^+$ (regulatory T cells; T_{regs}) immediately following DA exposure (Day 5), 1 week (Day 12) and 2 weeks (Day 19) post-exposure. We also analyzed bronchoalveolar fluid at these specified time points for changes in expression of the $CD4^+CD25^+$ T cell-related cytokine IL17a. We hypothesized that the balance of different $CD4^+CD25^+$ T cell populations within the lung contribute to the progression of flavoring-related lung disease.

2. Materials and Methods

2.1. Animals

All studies were approved by the Institutional Animal Care and Use Committee of the University of Rochester Medical Center (URMC). Investigators adhered to the National Institute of Health (NIH) Animal Welfare guidelines. Male outbred six to eight-week-old Sprague–Dawley rats (Charles River Laboratory, Wilmington, WA, USA) weighing between 200–250 g were maintained in an AALAC-accredited facility.

2.2. Diacetyl Vapor Exposures

Whole body exposures to diacetyl (DA, 2,3-butanedione; >98% pure; Sigma-Aldrich, St. Louis, MO, USA) were performed at the URMC inhalation exposure Facility (IEF), as described in the previous publication [14]. Briefly, animals were exposed to 200 parts-per-million (ppm) DA vapor in a whole-body exposure chamber for 5 consecutive days, 6 h/day. Weight and oxygen saturation (Starr Life Science Technologies, Oakmont, PA, USA) were monitored throughout the duration of the exposure and during a 14-day period following exposure. Animals were euthanized at Day 5 (immediately after last DA exposure), Day 12 (1 week post-exposure), and Day 19 (2 weeks post-exposure) for tissue harvest. Three (3×) separate DA exposures were performed for exposure replicates with representative datasets included for publication.

2.3. Bronchoalveolar Lavage Fluid (BALF), Tissue Harvest, and Histopathology

Animals were euthanized with an intraperitoneal injection of Euthasol (pentobarbital sodium and phenytoin sodium, Virbac, France). The descending aorta was transected for as a form of secondary euthanasia. The right ventricle was then injected with 10 mL 0.9% normal saline solution for lung perfusion. The trachea was cannulated with an 18 G cannula. The left mainstem bronchus was tied off, and the right lungs were lavaged with 5.0 mL 0.9% normal saline solution (bronchoalveolar lavage fluid, BALF). BALF samples were centrifuged at 200× *g* for 10 min at 4 °C, and supernatants frozen (−80 °C) for future analyses of 1 mL aliquots.

The right lung lobes were isolated and suture tied in order for the left lung lobes to be fixed in 10% neutral buffered formalin and later transferred to 70% ethanol. Lung tissue was embedded in paraffin, sectioned (5 µm) and stained with hematoxylin and eosin (H&E) or Masson's Trichrome. Lung tissue was also stained for the T cell marker CD3 (1:200, C7930, MilliporeSigma, St. Louis, MO, USA) or rabbit IgG (1:200, Agilent, Santa Clara, CA, USA; negative control). Staining in rat spleen was used as a CD3 positive control. In brief, sections were deparaffinized and rehydrated through ethanol. Heat-mediated antigen retrieval was performed in citrated retrieval solution for 30 min (Agilent). Slides were blocked for 1 hour with Rodent Block R (Biocare Medical, Pacheco, CA, USA) and then primary antibody Cambridge, UK) was applied for 1 h, and developed using DAB Chromagen (Biocare Medical, Pacheco, CA, USA). Slides were then counterstained with hematoxylin, dehydrated, and finished with cover slip.

Representative images of affected airways were taken from each left lung at sequential post-exposure time points. Lung scoring for airway lymphoid hyperplasia and subepithelial matrix deposition was performed on embedded lung tissue to semi-quantitate the changes in airway architecture observed on light microscopy [17]. Briefly, intrapulmonary bronchi were identified within each rat lung section, defined by a luminal diameter greater than 250 µm and not connecting directly to the alveolar space [10,15]. Five bronchi were graded for each rat at 4× (bar: 250 µm) (5 rats/time point × 5 bronchi/rat). For airway remodeling, the presence or absence of increased sub-epithelial, extracellular matrix was noted by Masson's Trichrome. For lymphoid hyperplasia, each aggregate adjacent to the bronchi was graded with: 0 for absence of an aggregate, 1+ for 1/3, 2+ for <2/3, and 3+ for >2/3 of the field obstructed by the aggregate. The cumulative average and standard deviation was then calculated for each time point.

2.4. Flow Cytometry for T Cells in Whole Lung Homogenates

The right medial lung was excised and placed in digestion buffer of 5% FBS and 7.5 µg/mL collagenase A (Roche, Basel, Switzerland) in PBS on ice for 30 min. Tissue was further dissociated using a GentleMacs (Miltenyi Biotec, Auburn, CA, USA) Tissue dissociator followed by needle aspiration through an 18 G needle and syringe. Afterwards, three aspiration homogenates were expelled onto 70 µM filter and disrupted with syringe plunger. To ensure maximal cell retrieval filters were washed with ice cold FACS buffer containing 5% FBS in PBS. After spinning for 5 min at 300× *g*, supernatants were discarded

and pellets re-suspended ammonium-chloride-potassium (ACK) buffer (Thermo Scientific, Waltham, MA, USA; Cat # A1049201) for red blood cell lysis prior to a final wash. Cell suspensions were adjusted to a concentration of approximately 1×10^7 cells/mL in FACS buffer for flow cytometric staining.

Single cell suspensions of whole lung homogenates were first stained for surface markers: CD3, CD8, CD4, and CD25 (see Supplemental Table S1). Next intracellular staining for Foxp3 was completed using Foxp3 fixation/permeabilization kit (eBioscience, San Diego, CA, USA; Cat. #2506527), per manufacturer's instructions. Complete information about clone and dilutions of antibodies used are also available in Table S1. LSR II flow cytometer (BD Biosciences, Franklin Lakes, NJ, USA) was used at the URMC Flow Cytometry Core (URMC FCR) to acquire data. FCS express (De Novo Software, Pasadena, CA, USA, version 7) was used to analyze data captured. Gates were set based on side scatter area (SSC-A) versus forward scatter area (FSC-A) to exclude debris and then sub-gated for forward and side scatter height to isolate single cells. $CD3^+$ T cells were then isolated from this single cell population. Sub-gates were applied to resolve the $CD4^+$ and $CD8^+$ T cell populations from this parent gate. Downstream $CD4^+CD25^+$ and $CD4^+CD25^+FoxP3^+$ T cell populations were also defined from this parent population.

2.5. Bronchoalveolar Fluid (BALF) Total Protein and Interleukin-17A (IL-17a)

Bronchoalveolar lavage fluid (BALF) was collected from all animals for total protein quantification. Total protein was determined using the Pierce bicinchoninic acid (BCA protein) assay kit (Thermo Scientific; Cat # PI23225). BALF IL-17a was determined using a Duoset ELISA immunoassay (R&D Systems, Minneapolis, MN, USA; Cat # DY8410-05). Standards and assays were prepared and performed according to manufacturer's instructions. Briefly, BALF was centrifuged at ($300\times$ *g*, 5 min) to remove debris. Supernatant was decanted and aliquots were applied to prepare for quantification.

2.6. Statistical Analysis

Linear regression modeling was performed (SAS v9.4, Cary, NC, USA) to estimate the sample size with the primary end-point being percent change in $CD4CD25^+$ T cells at Day 12 ('inflammatory period') when accounting for differences in survival. We assumed the average percent $CD4CD25^+$ T cells in the lung to be 8% with a standard deviation of 3% and a 50% increase (4% total change) with DA exposure [18]. With an alpha of 0.05 and power of 80%, the number of animals per group was 9 (total number: 36). Thus, we performed 3 exposure replicates (5 animals/group), accounting for animal loss. Prism v8.0 (GraphPad Software, San Diego, CA, USA) was used for post-exposure statistical analysis with ANOVA followed by correction for multiple comparisons assuming normal sample distribution while Kruskal–Wallis tests with Dunn's correction was performed for skewed samples.

3. Results

3.1. Mixed, Granulocytic Airways Inflammation with Adjacent Lymphoid Aggregates Following DA Vapor Exposures

Rat lungs were evaluated by histology for airways inflammation immediately after exposure (Day 5), 1 week post-exposure (Day 12) and 2 weeks post-exposure (Day 19); Figure 1. In all DA-exposed rats, intrapulmonary bronchi appeared with circumferential airways inflammation as early as Day 5 post-DA exposure that persisted until Day 19 in DA-exposed airways (n = 20 rats/group with >5 airways assessed/animal). Circumferential airways inflammation was most prominent 1 week post-exposure (Day 12, Figure 1c, asterisks). By Day 19, thickening of the bronchial walls with deposition of sub-epithelial, extracellular matrix was seen on H&E (Day 19, Figure 1d, arrows) and Masson's Trichrome (Figure S1). The number of bronchi affected by thickened sub-epithelial, extracellular matrix and lymphoid hyperplasia was semi-quantitated at each time point after DA exposure

(n = 5 rats × 5 bronchi/time point, Table 1). Both histologic parameters increased with respect to time after DA exposure.

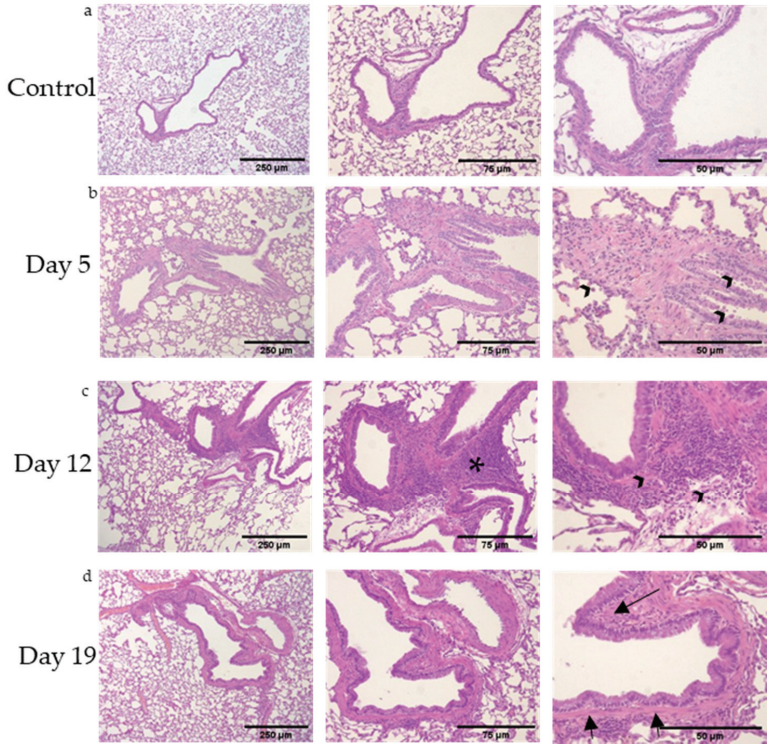

Figure 1. Representative rat lung tissue stained for hematoxylin and eosin (H&E) (bar: 250 µm (left column), 75 µm (middle column), and 50 µm (right column)). (**a**) Room air (control)-exposed rat airways, (**b**) Day 5 (immediately post-exposure) rat airways, (**c**) Day 12 (1 week following DA exposures) rat airways, and (**d**) Day 19 (2 weeks post-exposure) rat airways. Lymphoid aggregates are seen adjacent to affected airways with perivascular and bronchiolar edema (asterisk). Bronchial walls thickening identified at Day 12 and 19 (arrowheads and arrows, respectively).

Table 1. Bronchi affected by extracellular matrix deposition and adjacent lymphoid hyperplasia after DA exposure.

Group (n = 5 Rats/ Time Point)	Extracellular Matrix Deposition /Rat Lung Section	Bronchial Lymphoid Aggregates /Rat Lung Section
Air Control	0.0 +/− 0.0	0.0 +/− 0.0
DA D5	0.8 +/− 0.5	1.6 +/− 0.5
DA D12	2.0 +/− 1.0	2.6 +/− 0.5
DA D19	2.6 +/− 1.5	3.0 +/− 0.0

In line with previous in vivo DA exposures [9,10], airways inflammation consisted of mixed, granulocytic lung inflammation with a predominance of neutrophils, lymphocytes, macrophages and rare eosinophils (higher magnification image, Figure S2). Immunohistochemical staining for CD3, a common T cell marker, also identified that these airway-centric,

lymphoid aggregates stained positive (Figure S3). Collectively, these histopathologic findings support DA inducing mixed, granulocytic lung inflammation with airway remodeling and lymphoid hyperplasia adjacent to affected airways.

3.2. Bronchoalveolar Lavage Fluid (BALF) Cell Counts and Differentials after DA Exposures

To provide additional support of the inflammatory changes seen by histology, the total number of cells, percent cell differentials, and individual cell numbers by cell type were performed on BALF from room air, DA D5, D12, and D19 rat lungs (Figure 2). The total number of BALF cells increased significantly in DA-exposed animals 1 week after DA exposure (DA D12) compared to room air controls but did not differ significantly at DA D5 or DA D19 (Figure 2a). The percentage of BALF macrophages decreased significantly in DA-exposed animals at D19 compared to controls while the percent BALF neutrophils increased significantly in DA-exposed animals at D19 compared to air controls (Figure 2b). The percent BALF lymphocytes, eosinophils and basophils did not differ significantly between groups, however, the total number of BALF macrophages, neutrophils and lymphocytes increased significantly at D12 in DA-exposed animals compared to controls (Figure 2c). Hence, changes in BALF cell number and composition further support a mixed, granulocytic infiltrate within the rat lung after DA exposure composed predominantly of neutrophils and lymphocytes and peaking 1 week after DA exposure cessation (DA D12).

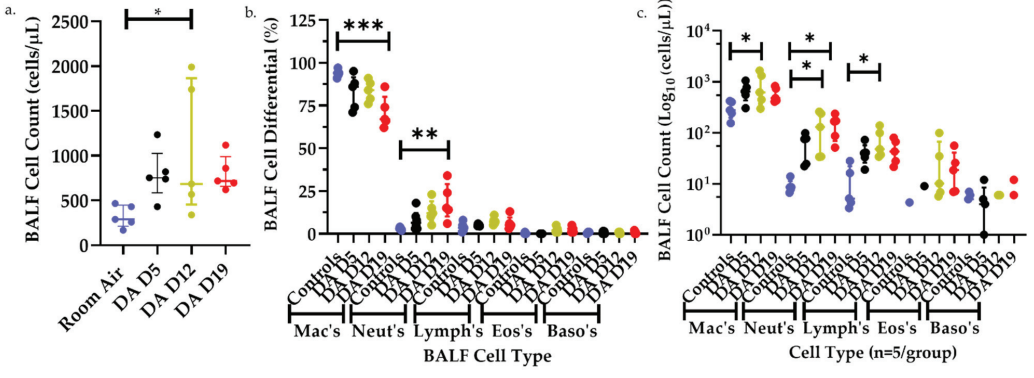

Figure 2. BALF total cell counts (**a**), percent cell differentials (**b**), and individual cell counts (**c**) from room air (blue), DA-exposed Day 5 (black), Day 12 (yellow), and Day 19 (red). (**a**) BALF total cell counts increased significantly in DA D12 compared to room air controls (Kruskal–Wallis, * $p < 0.05$). (**b**) BALF percent macrophages decreased significantly in DA D19 compared to room air controls (ANOVA, *** $p < 0.001$) while percent BALF neutrophils increased significantly in DA D19 rats compared to controls (ANOVA, ** $p < 0.01$). (**c**) Total BALF macrophages, neutrophils and lymphocytes increased significantly in DA D12 rats compared to controls (ANOVA, * $p < 0.05$), and BALF neutrophils increased significantly in DA D19 compared to controls (ANOVA, * $p < 0.05$).

3.3. T Cell Populations within the Rat Lung after DA Exposure

In light of the lymphoid hyperplasia seen on histology, flow cytometry was performed on whole lung homogenates to evaluate changes in T cell populations after DA exposures. Lung homogenates were stained for the common T cell surface markers CD3, CD4, CD8 and CD25 as well as the intracellular stain Foxp3. A schematic representation of flow gating is presented in Figure 3. Briefly, cells were gated first for size and granularity (SSC-A/FSC-A; FSC-H/FSC-A) to remove debris and "doublets", respectively. The $CD3^+$ population was then sub-gated directly from the singlet population. Next, $CD4^+$ and $CD8^+$ cell populations were discriminated by sub-gating of the $CD3^+$ parent population. Finally, gates were applied to discriminate the $CD4^+CD25^+$ and $CD4^+CD25^+Foxp3^+$ populations.

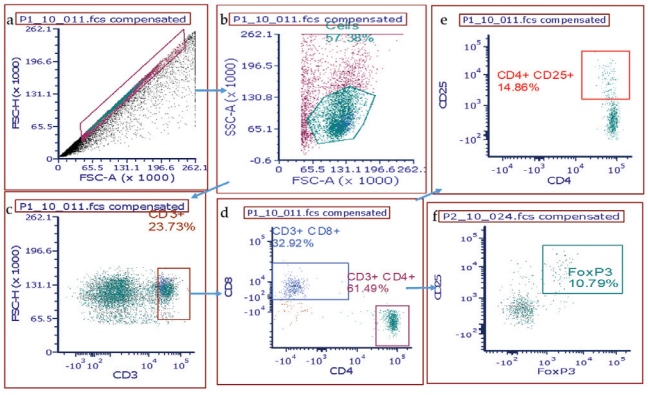

Figure 3. Gating scheme for T cell isolation and identification from whole rat lung homogenates. (**a**) Total isolated cells were first gated for singlets on FSC−A versus (vs.) FSC−H, then (**b**) SSC−A vs. FSC−A to exclude debris and followed by (**c**) $CD3^+$ cells vs. FSC−H. (**d**) Sub-gating for CD8+ or CD4+ sub-populations was then applied, and then further gated for CD25+ (**e**) and FoxP3+ T cell populations (**f**).

No significant difference in percent lung $CD3^+$, $CD4^+$, and $CD8^+$ T cell populations was seen between DA- and air-exposed rats at any of the time points assessed after DA exposure (one-way ANOVA; $p > 0.05$, Figure 4a–c respectively). However, the percent of $CD4^+CD25^+$ T cells increased significantly at Day 12 and remained increased at Day 19 in DA-exposed compared to air controls (ANOVA with Dunnett's, **** $p < 0.0001$; * $p < 0.05$, Figure 4d). Conversely, staining for $Foxp3^+$ T cell expression revealed a significant increase at Day 12 in DA-exposed compared to air-exposed controls that did not persist until Day 19 (ANOVA with Dunnett's, ** $p < 0.01$, Figure 4e).

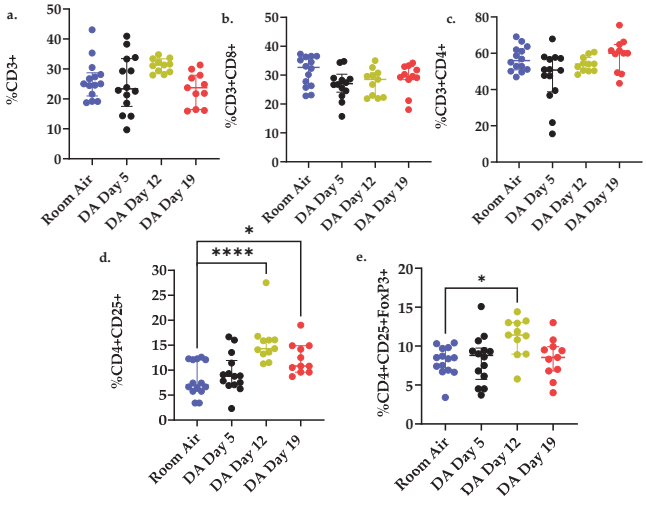

Figure 4. Percent (%) T cell populations from rat lung homogenates exposed to room air (blue) versus DA-exposed Day 5 (black), Day 12 (yellow), and Day 19 (red). (**a**) $CD3^+$%, (**b**) $CD3^+CD8$+%, (**c**) CD3+CD4+%, (**d**) CD4+CD25+%, and (**e**) $CD4^+CD25^+Foxp3^+$% lung T cells. * $p < 0.05$, ** $p < 0.01$, **** $p < 0.0001$. Cumulative results from 3 separate exposures (n = 11–14/group); differences in group size are due to animal death at later time points (D12, D19).

3.4. Increased IL-17a Expression and Total Albumin in Bronchoalveolar Lavage Fluid (BALF) after DA Exposure

Next, we evaluated for the presence of IL-17a protein expression and total albumin in BALF fluid at Day 12 and 19 after DA exposure (Figure 5). IL-17a is a pro inflammatory cytokine released by effector $CD4^+CD25^+$ cells under certain inflammatory diseases and associated with other forms of bronchiolitis obliterans [19,20]. A significant increase in BALF IL-17a expression was seen at Day 19 in DA-exposed rats compared to room air controls (* $p < 0.05$, Figure 5a). BALF albumin, a surrogate of lung permeability, also increased at Days 12 and 19 in DA-exposed animals compared to room air controls (* $p < 0.05$, Figure 5b). The increase in BALF IL-17a expression coincided temporally with the persistence of lung $CD4^+CD25^+$ T cells (Figure 4d), decrease in lung $CD4^+CD25^+Foxp3^+$ T cells (Figure 4e) and increase in BALF albumin after DA exposure (Figure 5b).

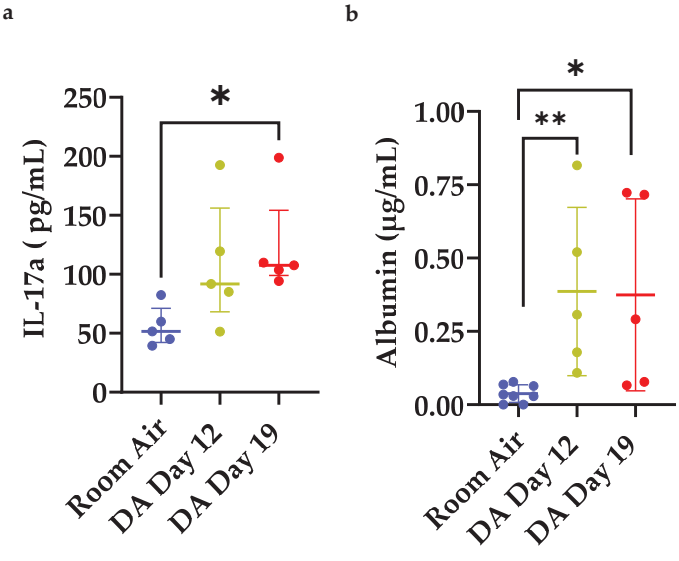

Figure 5. Bronchoalveolar lavage fluid (BALF) expression of (**a**) IL-17a and (**b**) albumin in room air (blue) and DA-exposed rats at Day 12 (yellow) and Day 19 (red). (**a**) BALF IL-17a expression increased significantly in DA D19 rats compared to room air controls (Kruskal–Wallis, * $p < 0.05$). (**b**) BALF albumin increased significantly in both DA D12 and D19 compared to room air controls (Kruskal-Wallis, ** $p < 0.01$ and * $p < 0.05$).

3.5. Percent $CD4^+CD25^+$ Lung T Cells Correlates with Reduced Oxygen Saturations and Increased Lung Permeability

To further characterize the physiologic consequences of increased $CD4^+CD25^+$ T cells within the lung after DA exposure, correlations were performed comparing percent lung $CD4^+CD25^+$ T cells, BALF albumin, BALF IL17a expression and percent oxygen saturations (% SpO_2) in DA-exposed animals (Figure 6). In our model of repetitive DA vapor exposures, oxygen saturations fell precipitously in DA-exposed rats at DA Day 12 and remained abnormal (below 90%) until study's end (Day 19) [14]. An inverse correlation was seen between percent lung $CD4^+CD25^+$ T cells and oxygen saturations at Day 12 (Figure 6a; $r = -0.6755$; $p < 0.001$). A positive correlation was observed at both Days 12 and 19 between percent lung $CD4^+CD25^+$ T cells to BALF albumin (Figure 6b; $r = 0.4490$; $p < 0.01$). While a direct correlation was seen between the percent $CD4^+CD25^+$ and $Foxp3^+$ T cells (Figure 6c), no significant correlation was found between the percent lung $CD4^+CD25^+Foxp3^+$ T cells and oxygen saturations. Conversely, an inverse correlation was seen between BALF IL-17a and oxygen saturations at D12 and D19 (Figure 6d; $r = 0.5315$, $p < 0.01$). Finally, a

positive correlation between percent lung $CD4^+CD25^+$ T cells and BALF IL-17a was also seen (Figure 6e; $r = 0.6828$, $p = 0.0001$). Collectively, these correlations suggest that this $CD4^+CD25^+$ T cell population found within the rat lung following DA exposure may contribute to worsening oxygen saturations and increasing lung permeability following repetitive DA vapor exposures.

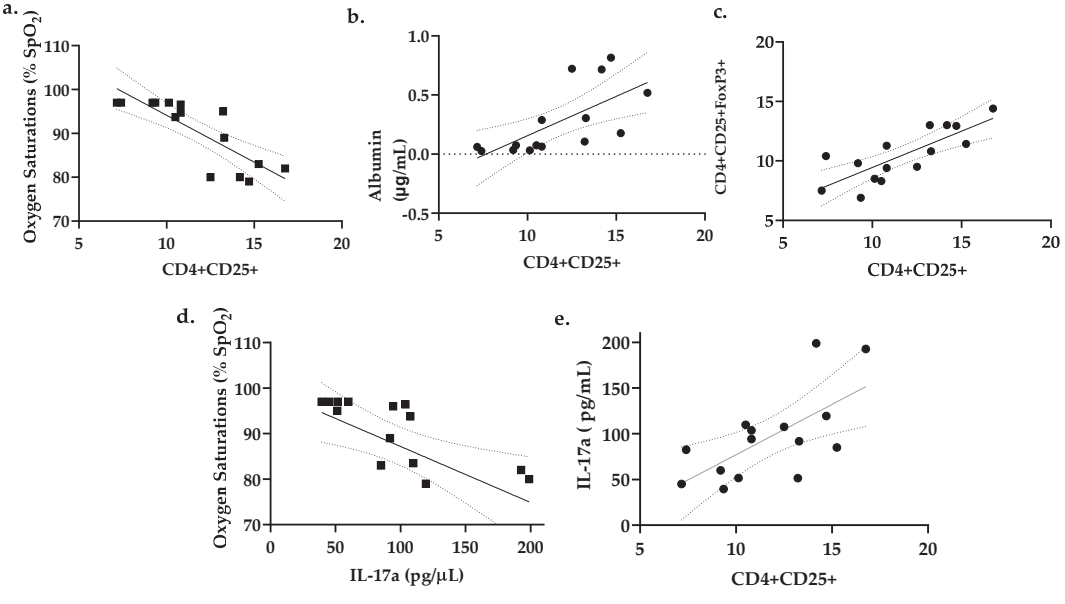

Figure 6. Pearson correlations between oxygen saturations, bronchoalveolar lavage fluid (BALF) albumin, BALF IL17a expression, and percent (%) total lung $CD4^+CD25^+$ T cells after diacetyl inhalation exposures. (**a**) Oxygen saturations correlated inversely with % lung $CD4^+CD25^+$ T cells ($r = -0.7320$, $p < 0.001$). (**b**) BALF albumin correlated directly with percent lung $CD4^+CD25^+$ T cells. ($r = 0.8942$, $p < 0.01$). (**c**) Foxp3 positive T cells correlated directly with $CD4^+CD25^+$ T cells. ($r = 0.796$, $p = 0.0005$) (**d**) Day 19 oxygen saturations correlated inversely with BALF IL-17a concentration. ($r = 0.5315$; $p < 0.01$). (**e**) BALF IL-17a correlated directly with percent lung $CD4^+CD25^+$ T cells ($r = 0.6828$; $p = 0.0001$).

4. Discussion

In the current study, we characterize the lung's T cell response in flavoring-related lung disease progression. While the overall percent of CD3, CD4, and CD8 T cells did not change, the percent of lung $CD4^+CD25^+$ T cells increased significantly after repetitive DA exposures with the development of persistent hypoxemia, increased lung permeability, and sub-epithelial fibrin deposition circumferential to affected airways. More specifically, two populations of $CD4^+CD25^+$ T cells increased within the lung after exposure: $Foxp3^+$ and IL17a-secreting T cells. Increases in expression of these two $CD4^+CD25^+$ T cell populations were inverse of one another with $Foxp3^+$ cells increasing 1 week post-exposure and BALF IL17a expression increasing at 2 weeks post-exposure.

A limited number of previous studies support our current findings that airway-centric, mixed granulocytic inflammation precedes bronchial fibrosis in DA inhalation exposures [11,12,14]. One such study demonstrated increased both B and T cell aggregates in mice exposed repetitively to DA vapors [11]. However, these DA-exposed mice did not develop the pathologic bronchial fibrosis seen in DA-exposed rats. One potential explanation for this difference in rodent response is the morphologic differences of rats and mice airways. In rats, keratin 5 positive airway epithelial cells extend into the intrapulmonary airways of rat that are not seen frequently in mouse intrapulmonary airways [21]. A second study using the structurally similar, volatile flavoring chemical 2,3–pentanedione found

increased circumferential and airway-centric lymphocytes in DA-exposed Sprague–Dawley rats [15]. Immunohistochemistry of DA-exposed rat lungs revealed a predominance of $CD3^+$ T cells within these lymphoid aggregates, consistent with the current study of further characterization of the different T cell subpopulations within the lung after DA exposures.

In comparison to flavoring-related lung disease, histopathology seen transplant-associated BO remains more commonly studied. In transplant-associated BO, disease pathogenesis is often described in three phases: (1) initial airway injury, (2) inflammatory induction, and subsequent (3) fibroproliferation [22]. Prior studies in transplant-associated BO strongly support dysregulation of the inflammatory phase that impairs epithelial repair and promotes BO development [20]. More recently, the appropriate balance of Th17 and regulatory ($Th17/T_{reg}$) T cells has been identified as critical in damage resolution. Additionally, skewing of this $Th17/T_{reg}$ axis toward a Th17-preferred phenotype has been reported in patients suffering from post-transplant BO [20,23]. Hence, targeting of this axis has been used to successfully modulate experimental BO in mice post-allograft lung transplant [24]. Furthermore, IL-17a blockade partially attenuates BO pathology in allograft lung transplant [24]. Similarly, Fan et al. reported partial attenuation of BO pathology after IL-17a neutralization in mice [25]. Similarly, Shi and colleagues reported adoptive transfer of $Foxp3^+$ T cells in a rat orthotropic tracheal transplant model reduced central airway obliteration and sub-epithelial fibrin deposition compared to control animals not receiving adoptive transfer [26]. While this $Th17/T_{reg}$ axis is now well characterized in transplant-associated BO, the beneficial effect of regulatory T cells and/or detrimental effects of Th17 cells has yet to be established in the development of flavoring-induced airways disease.

Imbalance of the $Th17/T_{reg}$ axis has also been implicated in the development of 'mustard lung disease' [27], another fibroproliferative, airways-centric lung disease following toxic chemical inhalation. In subjects previously exposed to sulfur mustard (SM), circulation levels of Foxp3 mRNA were lower than those levels found in healthy controls whereas mRNA levels of the Th17 transcription factor ROR-yt were increased in comparison to healthy control levels [28]. Additionally, Foxp3 mRNA levels correlated directly with the percent forced expiratory volume in 1 s (% FEV1), a common surrogate marker of lung function, while the inverse correlation was true for ROR-yt mRNA levels and %FEV1 in mustard lung subjects. Other Th17-related cytokines, including IL-17a, IL-1β, IL-23, and IL-6, were also elevated in the blood of sulfur mustard-exposed subjects with an inverse correlation with %FEV1 [27,28] Hence, dysregulation of the $Th17/T_{reg}$ axis is a potential pathway common to both flavoring-related lung disease and mustard lung disease.

Imbalance of $Th17/T_{reg}$ axis is similarly implicated in the immunopathogenesis of other inhalation-induced lung diseases, such as smoke-inhalation lung injury [29,30]. One such study found rats exposed to gun powder smoke, composed primarily of particulate matter 2.5 (PM2.5), experienced increased number of circulating and lung-specific Th17 cells with decreased $Foxp3^+$ T cells compared to T cells in air-exposed control rats [30]. Similarly, this group found the ratio of $Th17/T_{reg}$ was significantly increased in smoke-exposed animals compared to air-exposed controls [30]. Hence, this $Th17/T_{reg}$ axis is of increasing importance and may be common to many inhalation-induced lung diseases.

The lung microenvironment and its associated cytokine milieu is imperative in the differentiation and proliferation of certain inflammatory T cell phenotypes. There is evidence that pro-inflammatory signals within and surrounding the airways following epithelial injury impairs repair and promotes airway fibrosis. IL-17a acts directly on the airway epithelium as well as adjacent fibroblasts to induce pro-fibrotic cytokines [31]. Skewing of this local cytokine network has been implicated in the phenotypic plasticity of $CD4^+CD25^+$ T cells [32,33]. Particularly, cytokines in the IL-1 family are implicated in the differentiation of lung T cells toward a Th17 phenotype [34]. Future studies are underway by our lab to investigate the role of the lung microenvironment and its secreted cytokines in shifting this $Th17/T_{reg}$ axis and how changing this proportion contributes to flavoring-

related lung disease progression. More specifically, blocking either IL-1β or IL-36γ after DA inhalation exposure is of particular interest in attenuating lung disease progression.

Our study is not without a few limitations. First, significant differences exist in the anatomic structure of mice and rats. Specifically, the mouse lung lacks similar morphologic complexity and structure in comparison to rats for modeling human inhalation toxicology. Hence, the rat was used for modeling of flavoring-related lung disease but limited the number of reagents and antibodies available for T cell characterization. We failed to isolate Th17 cells directly, and thus used BALF IL-17a expression as an indirect assessment of Th17 cells within the lung. Second, a single concentration of diacetyl (200 ppm) was used in these studies. Extensive prior work has evaluated the dose response within the lung following DA inhalation exposure [9,11–13,35]. In our model, 200 ppm was previously determined to recapitulate human BO pathology in the Sprague-Dawley rats similar to prior rat DA exposure models [10,14]. Previous dosimetry modeling found this concentration (200 ppm DA) to be comparable to approximately 12 ppm exposure in humans [36], which is similar in range found in an occupational setting [37–39]. When lower concentrations are used in small rodents, significant scrubbing occurs within the nasal passages due to their high surface area, which ultimately prevents the majority of the DA to reach the intrapulmonary airways [13,36,40]. Third, the specific downstream effects and local cytokines that suppress the persistence of T_{reg} in the lungs were not identified but are currently under further investigation. Finally, there are risks associated with targeting this $CD4^+CD25^+$ T cell population as a potential therapy. Th17 cells are responsible for mitigating fungal infections and promoting barrier integrity within the lung, Hence, inhibiting Th17 cells may increase the risk of fungal infection or loss of mucosal integrity. Second, $CD4^+CD25^+$ T cells are known to express TGF-β. Overexpression of TGF-β may increase lung fibrosis through sustained or unbalanced proportions of $Foxp3^+$ T cells in the lung.

In conclusion, repetitive exposure to DA vapors at occupationally relevant concentrations results in temporal skewing of the IL-17a/Foxp3 axis in the rat lung. Increased percent lung $CD4^+CD25^+$ T cells were present in DA-exposed rat lungs at 1 and 2 weeks post-exposure compared to air controls. Percent lung $Foxp3^+$ T cells increased at 1 week post-exposure but did not persistent while BALF IL17a increased at 2 weeks, not seen at week 1. Increased $CD4^+CD25^+$ T cells and BALF IL-17a correlated with lower oxygen saturations and increased lung permeability, indicative of a potentially pathologic role of certain $CD4^+CD25^+$ T cells in the progression of flavorings-related lung disease.

Supplementary Materials: The following are available online at https://www.mdpi.com/article/10.3390/toxics9120359/s1, Figure S1: Representative rat lung sections stained for Masson's Trichrome demonstrating collagen I deposition (*blue*). (a) Room air (Control)-exposed rat airways, (b) DA Day 5 (immediately post-exposure) rat airways (c) DA Day 12 (1 week following DA exposures) rat airways, and (d) Day 19 (2 weeks post-exposure) rat airways. Organization of collagen I is noted in DA-exposed rats as early as Day 5 and persists to Day 19. Figure S2: Higher magnification image of hematoxylin & eosin (H&E) stained rat lung section at Day 12 post-diacetyl exposure. Mixed inflammatory infiltrate adjacent to DA affected airway with neutrophils (white arrow), eosinophils (black arrow), and clustered lymphocytes (arrow head) (bar: 25 μm). Figure S3: Rat lung sections stained for CD3, a T cell marker, and counterstained for hematoxylin in room air controls (a), DA-exposed Day 12 (b), and DA-exposed Day 19 (c) (bar: 250 μm). Inserts highlight the airway-centric, lymphoid aggregates with prominent $CD3^+$ T cell staining within lymphoid aggregates (bar: 25 μm). Table S1: Flow Cytometry Antibody Panel.

Author Contributions: Conceptualization, E.L.H. and M.D.M.; methodology, E.L.H., S.-Y.K., A.M.G., R.S.M., C.J.J., E.H. and M.D.M.; software, E.L.H.; validation, E.L.H., S.-Y.K. and M.D.M.; formal analysis, E.L.H. and M.D.M.; resources, M.D.M.; data curation, E.L.H. and M.D.M.; writing—original draft preparation, E.L.H. and M.D.M.; writing—review and editing, E.L.H., S.-Y.K., A.M.G., R.S.M., C.J.J., E.H. and M.D.M.; funding acquisition, M.D.M. All authors have read and agreed to the published version of the manuscript.

Funding: This research was funded by NIH NCATS grant number 5KL2 TR001999 (PI: R. Holloway; Sub-award PI: M.D.M.), NIH NIEHS grant number L40ES030909 (M.D.M.), NIH NHLBI grant

number 5T32HL06698-20 (MPI: SN Georas, MA O'Reilly; salary support E.L.H.), and NIH NIEHS grant number P30ES001247 (PI: P. Lawrence; Inhalation Exposure Facility).

Institutional Review Board Statement: The study was conducted according to the guidelines of the Declaration of Helsinki and approved by the University committee on Animal Resources at the University of Rochester Medical Center, Rochester, NY, USA (protocol code 102124; approval date: 8 December 2021–8 December 2024).

Informed Consent Statement: Not applicable.

Data Availability Statement: Not applicable.

Acknowledgments: Thank you to the University of Rochester Medical Center (URMC) Inhalation Exposure Facility (IEF), in particular, facility director Alison Elder, and David Chalupa. We also thank the URMC Flow Cytometry Shared Resource and Flow Core director Matt Cochran, for his direct assistance with flow panel development.

Conflicts of Interest: The authors declare no conflict of interest.

References

1. Kreiss, K. Flavoring-related bronchiolitis obliterans. *Curr. Opin. Allergy Clin. Immunol.* **2007**, *7*, 162–167. [CrossRef]
2. Hubbs, A.F.; Kreiss, K.; Cummings, K.J.; Fluharty, K.L.; O'Connell, R.; Cole, A.; Dodd, T.M.; Clingerman, S.M.; Flesher, J.R.; Lee, R.; et al. Flavorings-Related Lung Disease: A Brief Review and New Mechanistic Data. *Toxicol. Pathol.* **2019**, *47*, 1012–1026. [CrossRef]
3. LeBouf, R.F.; Blackley, B.H.; Fortner, A.R.; Stanton, M.; Martin, S.B.; Groth, C.P.; McClelland, T.L.; Duling, M.G.; Burns, D.A.; Ranpara, A.; et al. Exposures and Emissions in Coffee Roasting Facilities and Cafes: Diacetyl, 2,3-Pentanedione, and Other Volatile Organic Compounds. *Front. Public Health* **2020**, *8*, 561740. [CrossRef]
4. Mathews, J.M.; Watson, S.L.; Snyder, R.W.; Burgess, J.P.; Morgan, D.L. Reaction of the butter flavorant diacetyl (2,3-butanedione) with N-alpha-acetylarginine: A model for epitope formation with pulmonary proteins in the etiology of obliterative bronchiolitis. *J. Agric. Food Chem.* **2010**, *58*, 12761–12768. [CrossRef]
5. Kreiss, K.; Gomaa, A.; Kullman, G.; Fedan, K.; Simoes, E.J.; Enright, P.L. Clinical bronchiolitis obliterans in workers at a microwave-popcorn plant. *N. Engl. J. Med.* **2002**, *347*, 330–338. [CrossRef]
6. Kanwal, R.; Kullman, G.; Piacitelli, C.; Boylstein, R.; Sahakian, N.; Martin, S.; Fedan, K.; Kreiss, K. Evaluation of flavorings-related lung disease risk at six microwave popcorn plants. *J. Occup. Environ. Med.* **2006**, *48*, 149–157. [CrossRef] [PubMed]
7. Clark, S.; Winter, C.K. Diacetyl in Foods: A Review of Safety and Sensory Characteristics. *Compr. Rev. Food Sci. Food Saf.* **2015**, *14*, 634–643. [CrossRef]
8. Allen, J.G.; Flanigan, S.S.; LeBlanc, M.; Vallarino, J.; MacNaughton, P.; Stewart, J.H.; Christiani, D.C. Flavoring Chemicals in E-Cigarettes: Diacetyl, 2,3-Pentanedione, and Acetoin in a Sample of 51 Products, Including Fruit-, Candy-, and Cocktail-Flavored E-Cigarettes. *Environ. Health Perspect.* **2016**, *124*, 733–739. [CrossRef]
9. Palmer, S.M.; Flake, G.P.; Kelly, F.L.; Zhang, H.L.; Nugent, J.L.; Kirby, P.J.; Foley, J.F.; Gwinn, W.M.; Morgan, D.L. Severe airway epithelial injury, aberrant repair and bronchiolitis obliterans develops after diacetyl instillation in rats. *PLoS ONE* **2011**, *6*, e17644. [CrossRef]
10. Morgan, D.L.; Jokinen, M.P.; Johnson, C.L.; Price, H.C.; Gwinn, W.M.; Bousquet, R.W.; Flake, G.P. Chemical Reactivity and Respiratory Toxicity of the alpha-Diketone Flavoring Agents: 2,3-Butanedione, 2,3-Pentanedione, and 2,3-Hexanedione. *Toxicol. Pathol.* **2016**, *44*, 763–783. [CrossRef] [PubMed]
11. Morgan, D.L.; Flake, G.P.; Kirby, P.J.; Palmer, S.M. Respiratory toxicity of diacetyl in C57BL/6 mice. *Toxicol. Sci.* **2008**, *103*, 169–180. [CrossRef]
12. Flake, G.P.; Morgan, D.L. Pathology of diacetyl and 2,3-pentanedione airway lesions in a rat model of obliterative bronchiolitis. *Toxicology* **2017**, *388*, 40–47. [CrossRef]
13. Hubbs, A.F.; Goldsmith, W.T.; Kashon, M.L.; Frazer, D.; Mercer, R.R.; Battelli, L.A.; Kullman, G.J.; Schwegler-Berry, D.; Friend, S.; Castranova, V. Respiratory toxicologic pathology of inhaled diacetyl in sprague-dawley rats. *Toxicol. Pathol.* **2008**, *36*, 330–344. [CrossRef] [PubMed]
14. Wang, J.; Kim, S.Y.; House, E.; Olson, H.M.; Johnston, C.J.; Chalupa, D.; Hernady, E.; Mariani, T.J.; Clair, G.; Ansong, C.; et al. Repetitive diacetyl vapor exposure promotes ubiquitin proteasome stress and precedes bronchiolitis obliterans pathology. *Arch. Toxicol.* **2021**, *95*, 2469–2483. [CrossRef]
15. Morgan, D.L.; Jokinen, M.P.; Price, H.C.; Gwinn, W.M.; Palmer, S.M.; Flake, G.P. Bronchial and bronchiolar fibrosis in rats exposed to 2,3-pentanedione vapors: Implications for bronchiolitis obliterans in humans. *Toxicol. Pathol.* **2012**, *40*, 448–465. [CrossRef]
16. Martinu, T.; Kelly, F.L.; Sun, J.; Zhang, H.L.; Beasley, R.F.; Potts-Kant, E.N.; Flake, G.P.; Morgan, D.L.; Foster, W.M. T Cell-Deficiency Exacerbates Diacetyl-Induced Obliterative Bronchiolitis. *J. Heart Lung Transpl.* **2013**, 32. [CrossRef]

17. Banfi, A.; Tiszlavicz, L.; Szekely, E.; Petak, F.; Toth-Szuki, V.; Barati, L.; Bari, F.; Novak, Z. Development of bronchus-associated lymphoid tissue hyperplasia following lipopolysaccharide-induced lung inflammation in rats. *Exp. Lung Res.* **2009**, *35*, 186–197. [CrossRef] [PubMed]
18. Mock, J.R.; Garibaldi, B.T.; Aggarwal, N.R.; Jenkins, J.; Limjunyawong, N.; Singer, B.D.; Chau, E.; Rabold, R.; Files, D.C.; Sidhaye, V.; et al. Foxp3+ regulatory T cells promote lung epithelial proliferation. *Mucosal. Immunol.* **2014**, *7*, 1440–1451. [CrossRef]
19. Aaron, S.D.; Vandemheen, K.L.; Ramsay, T.; Zhang, C.; Avnur, Z.; Nikolcheva, T.; Quinn, A. Multi analyte profiling and variability of inflammatory markers in blood and induced sputum in patients with stable COPD. *Respir. Res.* **2010**, *11*, 41. [CrossRef]
20. Hanidziar, D.; Koulmanda, M. Inflammation and the balance of Treg and Th17 cells in transplant rejection and tolerance. *Curr. Opin. Organ. Transpl.* **2010**, *15*, 411–415. [CrossRef]
21. Mercer, R.R.; Russell, M.L.; Roggli, V.L.; Crapo, J.D. Cell number and distribution in human and rat airways. *Am. J. Respir. Cell Mol. Biol.* **1994**, *10*, 613–624. [CrossRef]
22. Glanville, A.R.; Verleden, G.M.; Todd, J.L.; Benden, C.; Calabrese, F.; Gottlieb, J.; Hachem, R.R.; Levine, D.; Meloni, F.; Palmer, S.M.; et al. Chronic lung allograft dysfunction: Definition and update of restrictive allograft syndrome-A consensus report from the Pulmonary Council of the ISHLT. *J. Heart Lung Transpl.* **2019**, *38*, 483–492. [CrossRef]
23. Shilling, R.A.; Wilkes, D.S. Role of Th17 cells and IL-17 in lung transplant rejection. *Semin. Immunopathol.* **2011**, *33*, 129–134. [CrossRef] [PubMed]
24. Gupta, P.K.; Wagner, S.R.; Wu, Q.; Shilling, R.A. IL-17A Blockade Attenuates Obliterative Bronchiolitis and IFN-γ Cellular Immune Response in Lung Allografts. *Am. J. Respir. Cell Mol. Biol.* **2017**, *56*, 708–715. [CrossRef] [PubMed]
25. Fan, L.; Benson, H.L.; Vittal, R.; Mickler, E.A.; Presson, R.; Fisher, A.J.; Cummings, O.W.; Heidler, K.M.; Keller, M.R.; Burlingham, W.J.; et al. Neutralizing IL-17 prevents obliterative bronchiolitis in murine orthotopic lung transplantation. *Am. J. Transpl.* **2011**, *11*, 911–922. [CrossRef]
26. Shi, Q.; Cao, H.; Liu, J.; Zhou, X.; Lan, Q.; Zheng, S.; Liu, Z.; Li, Q.; Fan, H. CD4+ Foxp3+ regulatory T cells induced by TGF-β, IL-2 and all-trans retinoic acid attenuate obliterative bronchiolitis in rat trachea transplantation. *Int. Immunopharmacol.* **2011**, *11*, 1887–1894. [CrossRef] [PubMed]
27. Imani, S.; Salimian, J.; Bozorgmehr, M.; Vahedi, E.; Ghazvini, A.; Ghanei, M.; Panahi, Y. Assessment of Treg/Th17 axis role in immunopathogenesis of chronic injuries of mustard lung disease. *J. Recept. Signal. Transduct. Res.* **2016**, *36*, 531–541. [CrossRef]
28. Iman, M.; Rezaei, R.; Azimzadeh Jamalkandi, S.; Shariati, P.; Kheradmand, F.; Salimian, J. Th17/Treg immunoregulation and implications in treatment of sulfur mustard gas-induced lung diseases. *Expert Rev. Clin. Immunol.* **2017**, *13*, 1173–1188. [CrossRef]
29. Baraniuk, J.N.; Casado, B.; Pannell, L.K.; McGarvey, P.B.; Boschetto, P.; Luisetti, M.; Iadarola, P. Protein networks in induced sputum from smokers and COPD patients. *Int. J. Chron. Obs. Pulmon. Dis.* **2015**, *10*, 1957–1975. [CrossRef]
30. Zhang, F.; Li, M.-y.; Lan, Y.-t.; Wang, C.-b. Imbalance of Th17/Tregs in rats with smoke inhalation-induced acute lung injury. *Sci. Rep.* **2016**, *6*, 21348. [CrossRef] [PubMed]
31. Gurczynski, S.J.; Moore, B.B. IL-17 in the lung: The good, the bad, and the ugly. *Am. J. Physiol. Lung Cell Mol. Physiol.* **2018**, *314*, L6–L16. [CrossRef]
32. Diller, M.L.; Kudchadkar, R.R.; Delman, K.A.; Lawson, D.H.; Ford, M.L. Balancing Inflammation: The Link between Th17 and Regulatory T Cells. *Mediat. Inflamm.* **2016**, *2016*, 6309219. [CrossRef]
33. Li, L.; Kim, J.; Boussiotis, V.A. IL-1beta-mediated signals preferentially drive conversion of regulatory T cells but not conventional T cells into IL-17-producing cells. *J. Immunol.* **2010**, *185*, 4148–4153. [CrossRef]
34. Li, H.; Hua, F.; Zhao, C.; Liu, G.; Zhou, Q. Diagnotic value of the combined determination of telomerase activity in induced sputum, pleural effusion and fiberobronchoscopic biopsy samples in lung cancer. *Zhongguo Fei Ai Za Zhi* **2010**, *13*, 128–131. [CrossRef]
35. Hubbs, A.F.; Fluharty, K.L.; Edwards, R.J.; Barnabei, J.L.; Grantham, J.T.; Palmer, S.M.; Kelly, F.; Sargent, L.M.; Reynolds, S.H.; Mercer, R.R.; et al. Accumulation of Ubiquitin and Sequestosome-1 Implicate Protein Damage in Diacetyl-Induced Cytotoxicity. *Am. J. Pathol.* **2016**, *186*, 2887–2908. [CrossRef]
36. Morris, J.B.; Hubbs, A.F. Inhalation dosimetry of diacetyl and butyric acid, two components of butter flavoring vapors. *Toxicol. Sci.* **2009**, *108*, 173–183. [CrossRef]
37. Pengelly, I.; O'Shea, H.; Smith, G.; Coggins, M.A. Measurement of Diacetyl and 2,3-Pentanedione in the Coffee Industry Using Thermal Desorption Tubes and Gas Chromatography-Mass Spectrometry. *Ann. Work Expo. Health* **2019**, *63*, 415–425. [CrossRef]
38. Beckett, E.M.; Cyrs, W.D.; Abelmann, A.; Monnot, A.D.; Gaffney, S.H.; Finley, B.L. Derivation of an occupational exposure limit for diacetyl using dose-response data from a chronic animal inhalation exposure study. *J. Appl. Toxicol.* **2019**, *39*, 688–701. [CrossRef]
39. LeBouf, R.F.; Hawley, B.; Cummings, K.J. Potential Hazards Not Communicated in Safety Data Sheets of Flavoring Formulations, Including Diacetyl and 2,3-Pentanedione. *Ann. Work Expo. Health* **2019**, *63*, 124–130. [CrossRef]
40. Hubbs, A.F.; Battelli, L.A.; Goldsmith, W.T.; Porter, D.W.; Frazer, D.; Friend, S.; Schwegler-Berry, D.; Mercer, R.R.; Reynolds, J.S.; Grote, A.; et al. Necrosis of nasal and airway epithelium in rats inhaling vapors of artificial butter flavoring. *Toxicol. Appl. Pharm.* **2002**, *185*, 128–135. [CrossRef]

toxics

MDPI

Article

Risk of Abdominal Obesity Associated with Phthalate Exposure of Nurses

Branislav Kolena [1,*], Henrieta Hlisníková [1], Ľubica Kečkéšová [1], Miroslava Šidlovská [1], Tomáš Trnovec [2] and Ida Petrovičová [1]

[1] Department of Zoology and Anthropology, Constantine the Philosopher University in Nitra, 94974 Nitra, Slovakia; hhlisnikova@ukf.sk (H.H.); lubica.keckesova@student.ukf.sk (Ľ.K.); msidlovska@ukf.sk (M.Š.); ipetrovicova@ukf.sk (I.P.)

[2] Department of Environmental Medicine, Slovak Medical University, 83303 Bratislava, Slovakia; tomas.trnovec@szu.sk

* Correspondence: bkolena@ukf.sk; Tel.: +421-37-6408-715

Abstract: Background: Occupational health hazards associated with phthalate exposure among nurses are still not well understood. Methods: We used high-performance liquid chromatography and tandem mass spectrometry to analyze phthalates. Anthropometric measurements and questionnaires were conducted. Results: We observed associations between mono-benzyl phthalate (MBzP) and body mass index (BMI), hip circumference (HC), waist circumference (WC), waist to height ratio (WHtR), and fat mass index (FMI), visceral fat content, BMI risk and hip index risk (HIrisk), adjusted to consumer behavior and consumer practices (r = 0.36–0.61; $p \leq 0.046$). In the same model, we detected an association between mono-n-butyl phthalate (MnBP) and waist to hip ratio (WHR; r = 0.36; $p = 0.046$), mono-carboxy-isononyl phthalate (cx-MiNP) and BMI (r = 0.37; $p = 0.043$), HC (r = 0.4; $p = 0.026$) and WHtR (r = 0.38; $p = 0.037$), between mono-oxo-isononyl phthalate oxo (MiNP) and HC (r = 0.36; $p = 0.045$), mono-2-ethylhexyl phthalate (MEHP), mono(2-ethyl-5-oxohexyl) phthalate (oxo-MEHP) and HIrisk (r = 0.38–0.41; $p \leq 0.036$), between oxo-MEHP and Anthropometric Risk Index (ARI risk; r = 0.4; $p = 0.028$). We detected a relationship between BMI and MBzP ($\beta = 0.655$; $p < 0.001$) and mono-2-ethylhexyl phthalate (MEHP; $\beta = -0.365$; $p = 0.003$), between hip circumference and MBzP ($\beta = 0.486$; $p < 0.001$), MEHP ($\beta = -0.402$; $p = 0.001$), and sum of secondary metabolites of diisononyl phthalate ($\sum$DiNP; $\beta = 0.307$; $p = 0.016$). We observed a relationship between fat content and MBzP ($\beta = 0.302$; $p = 0.033$), OH-MnBP ($\beta = -0.736$; $p = 0.006$) and MiBP ($\beta = 0.547$; $p = 0.046$), visceral fat content and MBzP ($\beta = 0.307$; $p = 0.030$), HI-risk and MBzP ($\beta = 0.444$; $p = 0.001$), ARI-risk and sum of di-n-butyl phthalate metabolites ($\sum$DnBP; $\beta = 0.337$; $p = 0.018$). We observed an association between the use of protective equipment with cx-MiNP. Conclusions: Occupational exposure to phthalates may induce abdominal obesity and result in obesity-related metabolic disorders.

Keywords: nurses; occupational exposure; phthalates; obesogenic effect; health risk

Citation: Kolena, B.; Hlisníková, H.; Kečkéšová, Ľ.; Šidlovská, M.; Trnovec, T.; Petrovičová, I. Risk of Abdominal Obesity Associated with Phthalate Exposure of Nurses. *Toxics* **2022**, *10*, 143. https://doi.org/10.3390/toxics10030143

Academic Editors: Ondrej Soukup and Jan Korabecny

Received: 7 March 2022
Accepted: 15 March 2022
Published: 18 March 2022

1. Introduction

The actual COVID era points to a long-overlooked status among front-line healthcare workers, especially nurses, in the context of the elimination of health-related risks. Nurses are an indispensable part of the health system in all countries committed to caring for patients. However, at the same time, nurses seem to be at increased occupational risk in several significant indicators such as for obesity, higher levels of stress, and lack of sleep.

The increasing prevalence of obesity is a major health concern [1–3] which does not pass over nurses [4,5]. Eating behavior, sleep deprivation, psychological, genetic, but also environmental, and behavioral stimuli play a part in obesity cofactors [6,7].

Anthropometrics is crucial in defining and assessing of abdominal obesity, and new anthropometric indices such as ABSI, HI, or ARI bring new insight into diagnosis and treatment options [8]. Body roundness index (BRI) allows for determining the human figure

shape as an ellipse, generated from the height and waist circumference. BRI values range from 1 to 16, and individuals with a more rounded figure are characterized by greater BRI values. BRI is a predictor of the percentage of adipose tissue and visceral tissue and can be a useful tool in the assessment of health status [9]. The Clinica Universidad de Navarra-Body Adiposity Estimator (CUN-BAE) index was suggested to evaluate the percentage of fat content in the body and is calculated using BMI, sex, and age. Fat percentage calculated using CUN-BAE showed a strong correlation with the real content of adipose tissue [10].

Evidence suggests that interactions between environmental and genetic factors can lead to acquired obesity [11,12]. Phthalates belong to endocrine disrupting chemicals (EDCs) [13] and, as toxic environmental factors, have been known to follow non-monotonic dose-response curves [14,15]. Phthalates and bisphenol A (BPA), such as potential obesogens, are substances of particular concern commonly found in medical devices [16,17]. Sources of phthalates are medical utilities produced from polyvinylchloride (PVC), e.g., infusion and transfusion sets, sets for hemodialysis, parenteral nutrition, and oxygen masks [18].

The purpose of this study was to identify the potential links between occupational phthalate exposure and overweight/obesity among nurses who worked in psychiatric and mental health wards in hospital.

2. Materials and Methods

The study consisted of native Slovak adult subjects-nurses who worked in psychiatric and mental health wards in hospital (females, n = 50) recruited in September 2020 as a pooled cohort, consisting of volunteers from departments of the Philippe Pinel Psychiatric Hospital in Pezinok (Slovakia).

The study was approved by the Institutional Review Board of the Philippe Pinel Psychiatric Hospital in Pezinok, Slovakia. Physical examination, questionnaires, and post-shift urine samples were collected. Participants signed informed consent before the study, and it was possible to withdraw participation anytime during the study. Subjects diagnosed with an illness or metabolic disorders (medications might be a source of high exposure to some phthalates), and with an incomplete questionnaire were excluded.

2.1. Anthropometry

All anthropometric measures were performed by a trained researcher using a standardized protocol. During the anthropometric measurements, participants were light clothing and barefoot. Height (the vertical distance from the plane where the subject stands barefooted to the vertex on the head with their back), weight, waist circumference (measured in the horizontal plane at the mid-point between the anterior iliac crest and the inferior margin of the rib, using a tape measure), and hip circumference (measured at the level of the widest circumference over the great trochanters) were measured to the nearest 0.1 cm, 0.1 kg, and 0.5 cm, respectively. BMI was calculated as weight (kg)/height (m)^2. Body composition (weight, body fat percentage, muscle mass percentage, and visceral fat level) was estimated by The Omron BF510 (Kyoto, Japan). Visceral fat level was estimated by Omron and describe intra-abdominal fat present around abdominal viscera in mesentery and omentum. Fat content means conversion of body fat percentage to kilograms.

WHtR was calculated as the waist circumference (cm) divided by the height (cm), waist to hip ratio (WHR) was calculated as dividing waist circumference (cm) by hip circumference (cm), FMI, and FFMI were calculated by standard anthropological procedure [19,20].

FMI was calculated as FM in kilograms divided by stature in square meters (kg/m^2) and FFMI was fat free mass in kilograms divided by stature in square meters (kg/m^2).

ABSI was estimated by formula: ABSI = WC/(BMI (2/3) $\times$ height (1/2)) [8]. HI and ARI were calculated according to Krakauer & Krakauer [21]. ABSI calculator is free available at https://nirkrakauer.net/sw/absi-calculator.html (accessed on 16/11/2021), and ARI calculator at https://nirkrakauer.net/sw/ari-calculator.html (accessed on 10/01/2021).

In BMI, ARI, ABSI and HI, the "z score" is define as: (value-mean)/standard deviation, where the mean and standard deviation are age and sex specific.

In BMI, ARi, ABSi and HI, "risk" define the death rate associated with given indices, normalized (risk of 1 = average death rate; risk of 2 = double the average death rate, etc.). A relative risk greater than 1 indicates greater than average death rate while numbers below 1 indicate a lower-than-average rate. For example, 1.2 indicates a 20 percent greater risk than average while 0.8 indicates a 20 percent lower risk.

2.2. Analyses of Phthalate

Nurses provided spot urine samples (2 × 2 mL) at the end of the work shift, (work duration at least 8 h per shift), and the day after the previous shift, which gives information about individual exposures during the last 24 h. We used high-performance liquid chromatography (HPLC) and tandem mass spectrometry (MS/MS) (Infinity 1260 and 6410 triplequad, Agilent, Santa Clara, CA, USA) to quantified urinary concentration of compounds: mono-methyl phthalate (MMP), mono-ethyl phthalate (MEP), mono-isobutyl phthalate (MiBP), mono-n-butyl phthalate (MnBP), mono(hydroxy-iso-butyl) phthalate (OH-MiBP), mono(hydroxy-n-butyl) phthalate (OH-MnBP), mono-benzyl phthalate (MBzP), mono-cyclohexyl phthalate (MCHP), mono-pentyl phthalate (MnPeP), mono-2-ethylhexyl phthalate (MEHP), mono(2-ethyl-5-hydroxyhexyl) phthalate (5OH-MEHP), mono(2-ethyl-5-oxohexyl) phthalate (5oxo-MEHP), mono(2-ethyl-5-carboxypentyl) phthalate (5cx-MEPP), mono-octyl phthalate (MnOP), mono-isononyl phthalate (MiNP), mono(oxo-methyl-octyl) phthalate (oxo-MiNP), mono(carboxy-methyl-heptyl) phthalate (cx-MiNP) by the method built on the basis of previously published off-line SPE and on-line HPLC-MS/MS methods [22,23]. The analysis was performed in Physiological Analytical Laboratory, Constantine the Philosopher University in Nitra, which has participated in the HBM4EU QA/QC programme, and its successful performance has resulted in its qualification as HBM4EU laboratory for the analysis of MEP, MBzP, MiBP, MnBP, MEHP, 5OH-MEHP, 5oxo-MEHP, 5cx-MEPP and cx-MiNP in human urine. Within this testing, we obtained very satisfactory Z-scores for previously meant compounds ranging from −1.1 to 0.7. The interlaboratory tests conditions for a successful passing were the Z scores $\leq |2|$. Detailed description of these tests is summarized in a paper written by Esteban López et al. [24]. Internal quality control was performed by analyses of 2 control materials (mixture of urine samples) with known concentrations (lower and higher concentration). The limits of quantification (LOQ) were estimated between 1 and 2.5 ng/mL.

2.3. Statistics

For the description of levels of urinary phthalate metabolites, the means with standard deviations (SDs), medians, and the 5th and 95th percentiles of concentrations were computed. Associations between anthropometric parameters (BMI—Body Mass Index, WHR-Waist to Hip Ratio, WHtR-Waist to Height Ratio, FMI-Fat Mass Index, FFMI—Fat-Free Mass Index, ABSI—a Body Shape Index, HI—Hip Index, z BMI, z ABSI, z HI, BMI risk, ABSI risk, HI risk, ARI risk) and concentrations of phthalate metabolites were examined by Pearson correlation analysis. Pearson partial correlation was used to explain the association between phthalate metabolites and anthropometric parameters adjusted to consumer behavior (physical activity; consuming meals heated in plastic containers in the microwave, consuming meals from the plastic container, drinking beverages from plastic cups or bottles, using personal protective equipment, presence of polyvinyl chloride flooring material)and consumer practices (using: hand cream, antiperspirant, perfume, body lotion, nail polish; consuming: margarine, cheese, and salaams packaged in plastic material, meat products, baguette, salads, biscuits, and chocolate) during last 24 h before sampling. Multivariate regression analysis was used to estimate the association between anthropometric parameters and occupational exposure to phthalates, monitored by urinary phthalate concentrations log-transformed to base 10. All statistical analyses were performed

using the SPSS for Windows statistical package (version 14.0; SPSS Inc., Chicago, IL, USA). A difference was considered statistically significant when $p \leq 0.05$.

3. Results

The study population consisted of females (n = 50; 100%) with a mean age of 48.12 ± 10.74 years. Descriptive statistic of the study population is shown in Table 1.

Table 1. Descriptive characteristic of the cohort.

Anthropometric Parameter					Percentile		
	Mean	**Median**	**MIN**	**MAX**	**5**	**95**	**SD**
Body height (cm)	164.79	163.43	155.06	197.93	157.33	172.33	6.99
Body weight (kg)	71.45	68.15	55.10	122.50	57.20	107.60	14.61
BMI (kg/m^2)	26.32	25.14	20.64	48.44	20.86	37.16	5.26
Hip circumference (cm)	103.63	102.50	90.00	148.33	92.00	128.33	10.55
Waist circumference (cm)	93.32	91.66	58.00	133.00	77.00	120.66	13.52
WHR	0.89	0.90	0.54	1.16	0.81	0.98	0.08
WHtR	0.56	0.55	0.35	0.84	0.46	0.72	0.08
FMI	9.06	7.82	1.14	26.35	2.62	17.54	4.52
Lean mass	46.76	46.30	38.08	60.15	38.17	59.50	6.37
FFMI	17.26	16.55	11.29	22.09	14.59	21.66	2.41
Visceral fat (%)	6.46	6.00	1.00	16.00	1.00	12.00	3.39
ABSI	0.08	0.08	0.05	0.10	0.08	0.09	0.01
HI	104.95	105.05	91.46	114.05	97.90	112.68	4.25
z BMI	−0.18	−0.36	−1.05	3.05	−1.01	1.38	0.79
z ABSI	0.63	0.65	−5.54	3.36	−0.78	2.25	1.29
z HI	0.07	0.13	−3.11	2.01	−1.56	1.71	0.96
BMI risk	0.94	0.89	0.84	1.85	0.84	1.17	0.16
ABSI risk	1.14	1.08	0.86	1.65	0.87	1.65	0.23
HI risk	1.00	0.96	0.95	1.36	0.95	1.14	0.08
ARI risk	1.07	0.97	0.73	2.18	0.80	1.62	0.30

Note: BMI, body mass index; WHR, waist to hip ratio; WHtR, waist to height ratio; FMI, fat mass index; FFMI, fat-free mass index; ABSI, A body shape index; HI, hip index; z BMI, BMI adjusted for age and sex; z ABSI, ABSI adjusted for age and sex; z HI, HI adjusted for age and sex; BMI risk, the risk of premature mortality based on the body mass index; ABSI risk, the risk of premature mortality based on the A body shape index; HI risk, the risk of premature mortality based on the hip index; ARI risk, the risk of premature mortality based on the anthropometric risk index.

Analysis of urine samples detected the presence of phthalate metabolites above LOQ of MEP in each urine sample. The presence of metabolites above LOQ in urine samples exceed the 90% limit in the case of MnBP, cx-MEPP (96%), of MiBP, of OH-MEHP (94%), of OH MnBP (92%), and oxo-MEHP a cx-MINP (90%), followed by the presence of phthalate metabolites OH-MiBP in 70% of samples, of MEHP and MBzP in 40% of samples, of oxo-MiNP in 38% of samples; of MnOP in 6% of samples and MCHP and MiNP in 2% of samples. The concentration of MnPeP was below the limit of quantification in all samples (100%) from the examined cohort. Descriptive statistics of urinary phthalate metabolites are shown in Table 2.

We observed associations between mono-benzyl phthalate (MBzP) and BMI risk (r = 0.49, $p \leq 0.001$),MBzP, mono-isobutyl phthalate (MiBP), mono-hydroxy-iso-buthyl phthalate (OH-MiBP), mono-n-butyl phthalate (MnBP), mono-hydroxy-n-buthyl phthalate (OH-MnBP), mono-2-ethylhexyl phthalate (MEHP) and Hip index risk (HI risk; r = 0.3–0.44; $p \leq 0.04$ respectively). Phthalate metabolites (MBzP, MiBP, MnBP, OH-MnBP), was associated with Anthropometric Risk Index (ARI risk; r = 0.32–0.33; $p \leq 0.03$). MBzP was also associated with BMI, HC, WC, WHtR, Fat mas index (FMI), FFMI and visceral fat content (r = 0.31–0.55; $p \leq 0.033$). Association was detected between mono-carboxy-isononyl phthalate (cx-MiNP) and Body mass index, hip circumference (HC), waist circumference (WC), Waist to height ratio (WHtR), and Fat free mass index (FFMI) (r = 0.31–0.4; $p \leq 0.03$).

Table 2. Descriptive statistics of urinary phthalate metabolites (ng/mL).

Phthalate Metabolite						Percentile	
	Mean	**Median**	**SD**	**MIN**	**MAX**	**5**	**95**
MMP	27.54	0.50	183.21	0.50	1297.04	0.50	8.95
MEP	102.00	33.77	177.44	1.81	823.21	2.91	487.29
MBzP	1.16	0.50	1.55	0.50	10.60	0.50	3.16
MiBP	23.35	15.82	24.97	1.77	122.90	1.77	86.67
OH-MiBP	4.77	2.00	9.39	0.50	60.33	0.50	11.76
MnBP	39.62	25.54	46.68	1.77	272.11	5.40	112.78
OH-MnBP	9.25	5.91	10.46	0.70	48.61	0.70	36.34
MEHP	1.99	1.00	1.55	1.00	7.19	1.00	5.17
OH MEHP	14.62	6.70	40.85	0.70	291.93	0.70	33.37
oxo MEHP	5.66	4.13	5.72	0.70	34.88	0.70	14.49
cx MEPP	10.66	9.17	9.73	0.70	66.66	2.56	19.97
MiNP	0.79	0.75	0.26	0.75	2.60	0.75	0.75
oxo MiNP	1.59	0.75	1.58	0.75	6.89	0.75	6.71
cx MiNP	3.89	2.97	3.38	0.70	19.75	0.70	9.69
MnPeP	1.25	1.25	0.00	1.25	1.25	1.25	1.25
MCHP	1.19	0.50	4.90	0.50	7.24	0.50	0.50
MnOP	0.83	0.75	0.33	0.75	2.42	0.75	1.74

Note: MMP, mono-methyl phthalate; MEP, mono-ethyl phthalate; MBzP, mono-benzyl phthalate, MiBP, mono-isobutyl phthalate; OH-MiBP, mono-hydroxy-iso-buthyl phthalate; MnBP, mono-n-butyl phthalate; OH-MnBP, mono-hydroxy-n-buthyl phthalate; MEHP, mono-2-ethylhexyl phthalate; OH MEHP, mono(2-ethyl-5-hydroxyhexyl) phthalate; oxo-MEHP, mono(2-ethyl-5-oxohexyl) phthalate; cx-MEPP, mono(2-ethyl-5-carboxypentyl) phthalate; MiNP, mono-isononyl phthalate; oxo MiNP, mono-oxo-isononyl phthalate; cx MiNP, mono-carboxy-isononyl phthalate; mnPeP, Mono-n-pentyl phthalate; MCHP, mono-cyclohexyl phthalate; MnOP, mono-n-octyl phthalate.

Using stepwise multiple linear regression analysis, we evaluated how the phthalate metabolites could affect the anthropometric parameters. Table 3 shows a significant relationship between BMI and levels of MBzP ($\beta = 0.655$; $p < 0.001$) and MEHP ($\beta = -0.365$; $p = 0.003$). We observed a similar pattern in the case of zBMI and BMI-risk. Furthermore, we found significant relationship between hip circumference and levels of MBzP ($\beta = 0.486$; $p < 0.001$), MEHP ($\beta = -0.402$; $p = 0.001$) and $\sum$DiNP secondary metabolites ($\beta = 0.307$; $p = 0.016$). We observed a similar pattern in the case of waist circumference, WHtR, FMI, and FFMI (Table 3). We found significant relationship between fat content and levels of MBzP ($\beta = 0.302$; $p = 0.033$), OH-MnBP ($\beta = -0.736$; $p = 0.006$) and MiBP ($\beta = 0.547$; $p = 0.046$); visceral fat content and levels of MBzP ($\beta = 0.307$; $p = 0.030$); HI-risk and levels of MBzP ($\beta = 0.444$; $p = 0.001$); ARI-risk and $\sum$DnBP ($\beta = 0.337$; $p = 0.018$).

We observed in addition to these results a statistically significant difference between phthalate concentrations in individuals who during the last 24 h consumed versus those who did not consume margarine (OH-MiBP 3.872 ng/mL vs. 1.479 ng/mL; r = 0.35, $p = 0.012$), sliced packaged cheeses (OH-MiBP 3.559 ng/mL vs. 1.433 ng/mL; r = 0.35, $p = 0.013$), packaged meat products (MEP 47.954 ng/mL vs. 22.140 ng/mL; r = 0.29, $p = 0.042$), and salami (MBzP 0.5 ng/mL vs. 0.78 ng/mL, r = 0.28, $p = 0.052$). Interestingly, we also observed a statistically significant higher concentration of cx-MiNP, depending on the use/non-use of protective equipment (vinyl medical gloves) (4.192 ng/mL vs. 2.319 ng/mL, r = −0.32, $p = 0.025$). On the other hand, we did not observe a statistically significant difference between concentration of phthalates and other aspects which monitored their consumer behavior (physical activity, heating and consuming meals from plastic container in microwave, drinking liquids from plastic caps or bottles, presence of polyvinyl chloride flooring material). In models adjusted to consumer behavior and consumer practices, we observed statistical significant associations between concentration of MBzP and BMI, HC, WC, WHtR, and FMI, visceral fat content, BMI risk and HI risk, adjusted to consumer behaviour and consumer practices ($p \leq 0.046$, Table S1),

Table 3. Stepwise multiple linear regression analysis of phthalate metabolites effect on the anthropometric parameters.

Anthropometric Parameter	Phthalate Metabolite	β (95% CI)	*p*
BMI	MBzP	0.655 (7.219; 15.064)	<0.001
	MEHP	−0.365 (−11.313; −2.558)	0.003
Hip circumference (cm)	MBzP	0.486 (8.123; 25.029)	<0.001
	MEHP	−0.402 (−24.170; −6.462)	0.001
	DiNP	0.307 (2.101; 19.085)	0.016
Waist circumference cm)	MBzP	0.497 (10.187; 33.283)	<0.001
	MEHP	−0.291 (−27.084; −1.310)	0.032
WHtR	MBzP	0.520 (0.068; 0.205)	<0.001
	MEHP	−0.312 (−0.168; −0.015)	0.019
Fat content (kg)	MBzP	0.302 (0.487; 20.047)	0.040
	OH-MnBP	−0.736 (−28.338; −5.101)	0.006
	MiBP	0.547 (0.279; 26.777)	0.046
FMI	MBzP	0.565 (4.592; 11.916)	0.000
	MEHP	−0.330 (−9.469; −1.295)	0.011
FFMI	MBzP	0.307 (0.321; 4.458)	0.025
	MMP	0.280 (0.055; 2.094)	0.039
Visceral fat content	MBzP	0.307 (0.338; 6.400)	0.030
zBMI	MBzP	0.600 (0.916; 2.138)	<0.001
	MEHP	−0.390 (−1.790; −0.426)	0.002
BMI-risk	MBzP	0.551 (0.150; 0.408)	<0.001
	MEHP	−0.309 (−0.318; −0.031)	0.019
HI-risk	MBzP	0.444 (0.047; 0.178)	0.001
ARI-risk	DnBP	0.337 (0.042; 0.429)	0.018

Note: BMI, body mass index; WHtR, waist to height ratio; FMI, fat mass index; FFMI, fat free mass index; z BMI, BMI adjusted for age and sex; BMI risk, the risk of premature mortality based on the body mass index; HI risk, the risk of premature mortality based on the hip index; ARI risk, the risk of premature mortality based on the anthropometric risk index; MMP, Mono-methyl phthalate; MiBP, mono-isobutyl phthalate; MBzP, Mono-benzyl phthalate; MEHP, Mono-2-ethylhexyl phthalate; OH-MnBP, Mono-hydroxy-n-butyl phthalate; DiNP, Sum of Mono-isononyl phthalate (MiNP), Mono-oxo-isononyl phthalate (oxo MiNP) and Mono-carboxy-isononyl phthalate (cx MiNP); DnBP, sum of Mono-n-butyl phthalate (MnBP), Mono-hydroxy-n-butyl phthalate (OH-MnBP).

In same model, an association between metabolite MnBP and WHR (r = 0.36; $p = 0.046$), metabolite cx-MiNP and BMI (r = 0.37; $p = 0.043$), HC (r = 0.4; $p = 0.026$), WC (r = 0.35; $p = 0.051$) and WHtR (r = 0.38; $p = 0.037$), between oxo -MiNP and HC (r = 0.36; $p = 0.045$), between MEHP and ABSI (r = 0.36; $p = 0.05$), HI risk (r = 0.41; $p = 0.022$), and between oxo-MEHP and HI risk and ARI risk (r = 0.38–0.4; $p \leq 0.04$) were detected.

4. Discussion

The main objective of our study was not only biomonitoring of occupational phthalate exposure of nurses but the assessment of obesity-related anthropometric indices of the participants based on actual measurements (not self-reported).

Results from biomonitoring of occupational phthalates exposure studies from Slovakia and worldwide [25] indicates lower exposure in current study. As expected, we observed temporal trends-declines in concentrations metabolites of phthalates that have been the focus of legislative activities in past. On the other hand, after comparison with our study from 2020 [26], nowadays we can observe an increase in the median MiNP, which is used as a DEHP substituent. These results correspond well with other findings that observed changes in phthalate exposure in the last decade in the general population. Although exposures to DnBP, BBzP, and DEHP have declined, exposures to replacement phthalates such as DiNP and DiBP have increased [27].

The main challenge when protecting high-risk groups in acute respiratory syndrome coronavirus 2 (SARS-CoV-2) situation is to increase the use of protective equipment. On the one hand, what appears positive can also have negative consequences, which applies to medical devices manufactured with the addition of plasticizers. Biocidal active substances, except others, pose as potential occupational health hazards. In a study analyzing hospital indoor air, PAEs (phthalate esters) pollution was ubiquitous. PAEs concentration in air varied widely between different hospital departments (hospitals' drugstores, transfusion rooms, nurses' workstations, wards, doctors' offices, and halls), and the pollution of hospitals was more severe than that of newly decorated homes [28]. A study from 2021 also mentioned the migration of plasticizers (DEHP, DEHT, and DINP) from vinyl gloves is worrying due to direct dermal contact and can contribute to greater concern with possible toxic effects in the human body [29]. There also exists evidence of the occurrence of phthalates and non-phthalate plasticizers in facemasks [30].

The cx-MINP is secondary metabolite of DiNP, which belongs to the plasticizer used as a substituent of DEHP [31] in the manufacturing of many vinyl (polyvinyl chloride/PVC) products, including general-purpose and medical examination gloves [32].

The concentration of this metabolite in our study was associated with the use of protective equipment (vinyl medical gloves).

Association of the metabolite cx-MiNP, with BMI reported in our work agree with a former study [33]. Associations between cx-MINP and other anthropometric parameters (z BMI, hip circumference, waist circumference, WHTR, and FFMI) observed in our study, therefore, suggest hypothetical linking with the metabolism of fat tissue (which deserves more attention in further studies). The information mentioned above is supported by the observation in which exposure to DiNP and DiDP (di-iso-decyl-phthalate) in mice resulted in increased lipid accumulation in 3T3-L1 adipocytes, an effect likely mediated through activation of PPARγ and interference at different levels with the transcriptional cascade driving adipogenesis [34]. Additionally, in the context of the potential adipogenic activity of phthalates, we observed an association between MBzP and BMI, HC, WC, WHtR, FMI, visceral fat content, BMI risk, HI risk, and ARI risk. An association between MBzP and BMI is consistent with Amin et al. [35]. In our study, ARI risk and HI risk was also associated with concentration of MiBP, MnBP, and OH-MnBP. Moreover, benzyl butyl phthalate (BBP) promoted the differentiation of 3T3-L1 through the activation of pathways in adipogenesis and metabolic disturbance [36].

Our findings differ from the results of the National Nutrition and Health Survey (NHANES) from 1992–2002, as well as from the study by Hatch et al. [37], presenting mainly the metabolite MEP in a negative association with BMI. In contrast to our previous study [38], showing a statistically significant correlation between FFMI and MiNP, in the current study, we observed a positive correlation with concentration of OH-MnBP ($r = 0.30$), MBzP ($r = 0.32$), MMP ($r = 0.3$) and cx-MiNP ($r = 0.32$). When comparing with our former results [39], noting statistically significant associations between the metabolite MEHP with WHtR, WHR, waist circumference, and hips, we did not show any statistically significant relationships in this work. On the other hand, in the current study, we observed an association between oxo MEHP and HI risk.

Discrepancies mentioned above may have been affected by the specificity of the cohort, which, in addition to specific job classification, has consisted exclusively of women, who have significant differences in body parameters and consumer habits compared to men.

The etiology of obesity is multifactorial and depends on gene-environment interactions. EDCs may interfere with hormonal receptors that regulate adipogenesis and metabolic pathways [40]. Phthalates are associated with metabolic syndrome [41,42], to be linked with insulin resistance and type 2 diabetes [43], and obesity [35,44–47]. Observed were direct associations between phthalates (MiBP and MBzP) and adiposity-related traits, BMI, and waist circumference [48]. Animal and human fat cell models point to activation of PPAR-γ by MEHP, which results in stimulating adipogenesis [49,50]. In vitro evidence of MEHP effects on lipolysis, glucose uptake/glycolysis, and mitochondrial respiration/biogenesis

has been published [51]. In conclusion, these findings support the theory that MEHP accumulation disturbs the energy metabolism of fat cells.

The results of stepwise multiple linear regression analysis might also point to the potential obesogenic effect of phthalates via their potential receptor-mediated activity. However, it is still unclear if they affect adipose tissue metabolism, and further study is needed to confirm or refute this hypothesis.

In evaluating the individual health risk, the case of BMI risk, HI risk, and ARI risk are important, namely where exposure to phthalates is associated with a risk of complications that affect quality and length of life (such as metabolic syndrome, diabetes mellitus, etc.). We hypothesize that not only exposure to specific phthalates and their concentration, but also the ratio between the concentration of specific phthalates would act in potential obesogenic effect as well as in other metabolic, reproductive, and neurobehavioral contexts.

We hypothesize that, although there were lower concentrations of phthalates in our study (in comparison to concentrations worldwide), which are commonly used in the manufacture of disinfectants, antimicrobials, cleaning products, biocides, personal care products, and biomedical materials (i.e., the daily occupational environment of nurses), long-term exposure scenarios could result in the obese-related findings observed in our study. This is only a hypothesis since the limitation of our study is also the absence of diester analyses from the air and medical devices. An aspect that we should take into account is also the higher age of the nurses in our study. Most were at an age when the perimenopausal transition occurs [52]. This suggests a hormonally sensitive period associated with changes in body weight. In a study from 2021, authors observed associations between MEHP, MEHHP, and MEOHP and one-year BMI change in women who transitioned from peri- to post-menopause from baseline to first follow-up [53]. In another study, phthalate metabolites were positively associated with hormones (estradiol, progesterone, and FSH) in premenopausal women [54]. The results of our study therefore hypothetically support the assumption that phthalates can act obesogenically (i.e., behave differently depending on their concentration and period of life when individuals are more hormonally sensitive).

Since some EDCs may interfere with hormonal receptors that regulate adipogenesis and metabolic pathways, we hypothesize that several phthalate esters act as agonists and/or antagonists via estrogen, androgen receptors, and PPARs [40,55,56]. The ratio between individual phthalates can be crucial for understanding different effects at the molecular level, and further studies are needed to elucidate this theory. Obviously, the synergic effect with other substances with endocrine-disrupting character and different routes of exposure has to be taken into account (lifestyle, consumer practices, etc.).

The other relevant aspect being discussed in the context of phthalates exposure is consumer behavior and consumer practices. One of these is practices related to meat packaging. In our study, individuals who consumed packaged meat products during the last 24 h compared to those who did not consume them had statistically higher concentrations of MEP (meat) and MBzP (salami, in which supports this hypothesis, in agreement to detection of high concentrations of phthalates in non-frozen packaged meat products [57].

In this study, we also observed increased concentrations of OH-MiBP in individuals who consumed sliced packaged cheeses during the last 24 h, and increased OH-MiBP in those who consumed margarine, compared to slightly higher concentrations of BBzP (8.4/g/mL) and DMP (11.7 µg/mL) compared to those consuming dairy products (eggs, milk, cheese) [58].

The results mentioned in the previous paragraphs deserve the attention of further studies in the context of associations between the concentration of MBzP and BMI, HC, WC, WHtR, and FMI, visceral fat content, BMI risk, and HI risk, an association between metabolite MnBP and WHR, cx-MiNP, and BMI, HC, WC, and WHtR, also between oxo -MiNP and HC, between MEHP and ABSI, HI risk, and between oxo-MEHP and HI risk and ARI risk, adjusted to the consumer behavior and consumer practices $p \leq 0.046$) observed in our study.

Further, the ability of DBP and MEHP to penetrate mineral waters was detected, showing that the intake of fluids packaged in plastic containers increases exposure to phthalates and endangers the health of the exposed person [59] in conformity to the presence of DBP, DMP, DEP, and BBP in mineral bottled waters stored at room temperature [60]. Similar results were achieved by monitoring the presence of migration of DBP, DMP, DEP, and DnOP from plastic bottles to bottled water [61]. This is in contrast to our findings, in which we did not observe associations between the concentration of phthalates and consumer behavior (e.g., physical activity, heating and consuming meals from the plastic container in the microwave, drinking liquids from plastic caps or bottles, presence of polyvinyl chloride flooring material).

We hypothesize the results of our study support the hypothesis that the prevalence of obesity, besides being well-known, may be supported by several many lesser-known environmental factors that act in parallel [62].

Our study has several limitations. The participants were recruited from one region of Slovakia. Hence, the results should be applied cautiously to other populations. On the other hand, in terms of cohort uniformity, it is an advantage. Limited understanding of confounding factors, making up lifestyle, and modifying the concentration-effect associations, has to be taken into account. There also exists evidence that exposure to artificial lighting can directly affect circadian rhythms, resulting in weight gain and obesity not only in animals [63] but in humans, as well [64–67]. Nighttime illumination and disruption of circadian rhythms due to night shifts may be one of the factors influencing the development of obesity in our cohort. Further studies are needed to determine whether the results are consistent under different criteria.

5. Conclusions

The results suggest a hypothetical non-monotonic dose-response obesogenic activity of phthalates, demonstrated by the increase of abdominal obesity among nurses and estimated through novel anthropometric indices (such as ABSI, HI, or ARI), pointing to a real increase of health risk in perimenopausal transition. The present findings also emphasize the need for monitoring chemicals in the workplace of nurses as synergic effects with other chemicals and stressors could result in obesity-related diseases. The small sample size was one of the limitations of our study to realize these results. For this reason, our results cannot be generalized to the broader community based on this study alone.

Risk reduction of phthalate occupational exposure may be attained by the use of non-toxic alternatives. In this context, healthcare facilities and professionals present an important step in substituting of hazardous chemicals due to an ethical responsibility to use less hazardous products for patients and less purchasing power.

As an alternative to this measure, the development and implementation of a health-related physical fitness intervention program can promote and improve health and promote the working efficiency of nurses. The prevention, based on wellness and physical exercise paid by an employer as compensation for occupational health risk, can be efficient.

Supplementary Materials: The following supporting information can be downloaded at: https://www.mdpi.com/article/10.3390/toxics10030143/s1, Table S1: Associations between phthalate metabolites on the anthropometric parameters adjusted to consumer behavior and consumer practices.

Author Contributions: Conceptualization, B.K.; methodology, B.K., I.P., T.T., M.Š., H.H. and Ľ.K.; software, B.K., M.Š. and H.H.; validation, B.K., I.P., T.T., M.Š., H.H. and Ľ.K.; formal analysis, B.K., I.P., T.T., M.Š., H.H. and Ľ.K.; investigation, B.K., Ľ.K. and M.Š.; resources, B.K., I.P., T.T., M.Š., H.H. and Ľ.K.; data curation, I.P.; writing—original draft preparation, B.K.; writing—review and editing, B.K.; visualization, B.K.; supervision, B.K., I.P. and T.T. All authors have read and agreed to the published version of the manuscript.

Funding: This research received no external funding.

Institutional Review Board Statement: The study was conducted in accordance with the Declaration of Helsinki, and approved by the Institutional Review Board of the Philippe Pinel Psychiatric Hospital

in Pezinok, Slovakia for studies involving humans. Approval Code: F/Z-P-10.SMK-03:03/2017; Approval Date: 05.06.2018.

Informed Consent Statement: Informed consent was obtained from all subjects involved in the study.

Data Availability Statement: Data available on request due to restrictions eg privacy or ethical.

Acknowledgments: We thank Michaela Földešiová for her excellent technical assistance. We thank all the volunteers for participating in this study.

Conflicts of Interest: The authors declare no conflict of interest.

References

1. Flegal, K.M.; Carroll, M.D.; Kit, B.K.; Ogden, C.L. Prevalence of obesity and trends in the distribution of body mass index among US adults, 1999–2010. *JAMA* **2012**, *307*, 491–497. [CrossRef] [PubMed]
2. Fryar, C.D.; Carroll, M.D.; Afful, J. Prevalence of Overweight, Obesity, and Severe Obesity among Adults Aged 20 and over: United States, 1960–1962 through 2017–2018. NCHS Health E-Stats. 2020. Available online: https://www.cdc.gov/nchs/data/hestat/obesity_adult_15_16/obesity_adult_15_16.html (accessed on 14 April 2021).
3. WHO Consultation on Obesity; World Health Organization. Obesity: Preventing and Managing the Global Epidemic: Report of a WHO Consultation. 2000. Available online: https://apps.who.int/iris/handle/10665/42330 (accessed on 6 June 2021).
4. Maroney, D.; Golub, S. Nurses' attitudes toward obese persons and certain ethnic groups. *Percept. Mot. Ski.* **2008**, *75*, 387–391. [CrossRef]
5. Niedhammer, I.; Lert, F.; Marne, M.J. Prevalence of overweight and weight gain in relation to night work in a nurses' cohort. *Int. J. Obes. Relat. Metab. Disord.* **1996**, *20*, 625–633. [PubMed]
6. Institute of Medicine (US) Committee on Assessing Interactions among Social. Behavioral, and Genetic Factors in Health. In *Genes, Behavior, and the Social Environment: Moving Beyond the Nature/Nurture Debate*; Hernandez, L.M., Blazer, D.G., Eds.; National Academies Press (US): Washington, DC, USA, 2006. [PubMed]
7. Office of the Surgeon General (US); Office of Disease Prevention and Health Promotion (US); Centers for Disease Control and Prevention (US); National Institutes of Health (US). *The Surgeon General's Call to Action to Prevent and Decrease Overweight and Obesity*; Office of the Surgeon General (US): Rockville, MD, USA, 2001. [PubMed]
8. Krakauer, N.Y.; Krakauer, J.C. The new anthropometrics and abdominal obesity: A body shape index, hip index, and anthropometric risk index. In *Nutrition in the Prevention and Treatment of Abdominal Obesity*, 2nd ed.; Watson, R.R., Ed.; Elsevier: New York, NY, USA, 2019; pp. 19–27.
9. Thomas, D.M.; Bredlau, C.; Bosy-Westphal, A.; Mueller, M.; Shen, W.; Gallagher, D.; Maeda, Y.; McDougall, A.; Peterson, C.M.; Ravussin, E.; et al. Relationships between body roundness with body fat and visceral adipose tissue emerging from a new geometrical model. *Obesity* **2013**, *21*, 2264–2271. [CrossRef] [PubMed]
10. Gomez-Ambrosi, J.; Silva, C.; Catalan, V.; Rodriguez, A.; Galofre, J.C.; Escalada, J.; Valentí, V.; Rotellar, F.; Romero, S.; Ramírez, B.; et al. Clinical usefulness of a new equation for estimating body fat. *Diabetes Care* **2012**, *35*, 383–388. [CrossRef] [PubMed]
11. Pigeyre, M.; Yazdi, F.T.; Kaur, Y.; Meyre, D. Recent progress in genetics, epigenetics and metagenomics unveils the pathophysiology of human obesity. *Clin. Sci.* **2016**, *130*, 943–986. [CrossRef] [PubMed]
12. Stel, J.; Legler, J. The Role of Epigenetics in the Latent Effects of Early Life Exposure to Obesogenic Endocrine Disrupting Chemicals. *Endocrinology* **2015**, *156*, 3466–3472. [CrossRef]
13. Dominguez, F. Phthalates and Other Endocrine-Disrupting Chemicals: The 21st Century's Plague for Reproductive Health. *Fertil. Steril.* **2019**, *115*, 885–886. [CrossRef]
14. Vandenberg, L.N.; Colborn, T.; Hayes, T.B.; Heindel, J.J.; Jacobs, D.R., Jr.; Lee, D.H.; Shioda, T.; Soto, A.M.; vom Saal, F.S.; Welshons, W.V.; et al. Hormones and endocrine-disrupting chemicals: Low-dose effects and non-monotonic dose responses. *Endocr. Rev.* **2012**, *33*, 378–455. [CrossRef]
15. Lagarde, F.; Beausoleil, C.; Belcher, S.M.; Belzunces, L.P.; Emond, C.; Guerbet, M.; Rousselle, C. Non-monotonic dose-response relationships and endocrine disruptors: A qualitative method of assessment. *Environ. Health* **2015**, *14*, 13. [CrossRef]
16. Vandentorren, S.; Zeman, F.; Morin, L.; Sarter, H.; Bidondo, M.L.; Oleko, A.; Leridon, H. Bisphenol-A and phthalates contamination of urine samples by catheters in the Elfe pilot study: Implications for large-scale biomonitoring studies. *Environ. Res.* **2011**, *111*, 761–764. [CrossRef] [PubMed]
17. Shang, J.; Corriveau, J.; Champoux-Jenane, A.; Gagnon, J.; Moss, E.; Dumas, P.; Gaudreau, E.; Chevrier, J.; Chalifour, L.E. Recovery from a Myocardial Infarction Is Impaired in Male C57bl/6 N Mice Acutely Exposed to the Bisphenols and Phthalates That Escape from Medical Devices Used in Cardiac Surgery. *Toxicol. Sci.* **2019**, *168*, 78–94. [CrossRef] [PubMed]
18. Šuta, M. Zdravotní rizika ftalátů v souvislosti se zdravotní péčí a možnosti jejich redukce. *Interní Med. Pro Praxi* **2007**, *9*, 288–291.
19. Kyle, U.G.; Schutz, Y.; Dupertuis, Y.M.; Pichard, C. Body composition interpretation. Contributions of the fat-free mass index and the body fat mass index. *Nutrition* **2003**, *19*, 597–604. [CrossRef]
20. He, H.; Pan, L.; Du, J.; Jin, Y.; Wang, L.; Jia, P.; Shan, G. Effect of fat mass index, fat free mass index and body mass index on childhood blood pressure: A cross-sectional study in south China. *Transl. Pediatrics* **2021**, *10*, 541–551. [CrossRef]

21. Krakauer, N.Y.; Krakauer, J.C. An Anthropometric Risk Index Based on Combining Height, Weight, Waist, and Hip Measurements. *J. Obes.* **2016**, *2016*, 8094275. [CrossRef]
22. Pilka, T.; Petrovicova, I.; Kolena, B.; Zatko, T.; Trnovec, T. Relationship between Variation of Seasonal Temperature and Extent of Occupational Exposure to Phthalates. *Environ. Sci. Pollut. Res. Int.* **2014**, *22*, 434–440. [CrossRef]
23. Koch, H.M.; Rüther, M.; Schütze, A.; Conrad, A.; Pälmke, C.; Apel, P.; Brüning, T.; Kolossa-Gehring, M. Phthalate metabolites in 24-h urine samples of the German Environmental Specimen Bank (ESB) from 1988 to 2015 and a comparison with US NHANES data from 1999 to 2012. *Int. J. Hyg. Environ. Health* **2017**, *220*, 130–141. [CrossRef]
24. Esteban López, M.; Göen, T.; Mol, H.; Nübler, S.; Haji-Abbas-Zarrabi, K.; Koch, H.M.; Kasper-Sonnenberg, M.; Dvorakova, D.; Hajslova, J.; Antignac, J.P.; et al. The European human biomonitoring platform—Design and implementation of a laboratory quality assurance/quality control (QA/QC) programme for selected priority chemicals. *Int. J. Hyg. Environ. Health* **2021**, *234*, 113740. [CrossRef]
25. Wang, Y.; Zhu, H.; Kannan, K. A Review of Biomonitoring of Phthalate Exposures. *Toxics* **2019**, *7*, 21. [CrossRef]
26. Kolena, B.; Petrovičová, I.; Šidlovská, M.; Hlisníková, H.; Bystričanová, L.; Wimmerová, S.; Trnovec, T. Occupational Hazards and Risks Associated with Phthalates among Slovakian Firefighters. *Int. J. Environ. Res. Public Health* **2020**, *17*, 2483. [CrossRef] [PubMed]
27. Zota, A.R.; Calafat, A.M.; Woodruff, T.J. Temporal trends in phthalate exposures: Findings from the National Health and Nutrition Examination Survey, 2001–2010. *Environ. Health Perspect.* **2014**, *122*, 235–241. [CrossRef] [PubMed]
28. Wang, X.; Song, M.; Guo, M.; Chi, C.; Mo, F.; Shen, X. Pollution levels and characteristics of phthalate esters in indoor air in hospitals. *J. Environ. Sci.* **2015**, *37*, 67–74. [CrossRef] [PubMed]
29. Poitou, K.; Rogez-Florent, T.; Lecoeur, M.; Danel, C.; Regnault, R.; Vérité, P.; Monteil, C.; Foulon, C. Analysis of Phthalates and Alternative Plasticizers in Gloves by Gas Chromatography-Mass Spectrometry and Liquid Chromatography-UV Detection: A Comparative Study. *Toxics* **2021**, *9*, 200. [CrossRef]
30. Vimalkumar, K.; Zhu, H.; Kannan, K. Widespread occurrence of phthalate and non-phthalate plasticizers in single-use facemasks collected in the United States. *Environ. Int.* **2022**, *158*, 106967. [CrossRef]
31. Chiang, H.C.; Kuo, Y.T.; Shen, C.C.; Lin, Y.H.; Wang, S.L.; Tsou, T.C. Mono(2-ethylhexyl)phthalate accumulation disturbs energy metabolism of fat cells. *Arch. Toxicol.* **2016**, *90*, 589–601. [CrossRef]
32. Hines, C.J.; Hopf, N.B.; Deddens, J.A.; Silva, M.J.; Calafat, A.M. Occupational exposure to diisononyl phthalate (DiNP) in polyvinyl chloride processing operations. *Int. Arch. Occup. Environ. Health* **2012**, *85*, 317–325. [CrossRef]
33. Vafeiadi, M.; Myridakis, A.; Roumeliotaki, T.; Margetaki, K.; Chalkiadaki, G.; Dermitzaki, E.; Venihaki, M.; Sarri, K.; Vassilaki, M.; Leventakou, V.; et al. Association of Early Life Exposure to Phthalates with Obesity and Cardiometabolic Traits in Childhood: Sex Specific Associations. *Front. Public Health* **2018**, *6*, 327. [CrossRef]
34. Pomatto, V.; Cottone, E.; Cocci, P.; Mozzicafreddo, M.; Mosconi, G.; Nelson, E.R.; Palermo, F.A.; Bovolin, P. Plasticizers used in food-contact materials affect adipogenesis in 3T3-L1 cells. *J. Steroid Biochem. Mol. Biol.* **2018**, *178*, 322–332. [CrossRef]
35. Amin, M.M.; Parastar, S.; Ebrahimpour, K.; Shoshtari-Yeganeh, B.; Hashemi, M.; Mansourian, M.; Kelishadi, R. Association of urinary phthalate metabolites concentrations with body mass index and waist circumference. *Environ. Sci. Pollut. Res. Int.* **2018**, *25*, 11143–11151. [CrossRef]
36. Yin, L.; Yu, K.S.; Lu, K.; Yu, X. Benzyl butyl phthalate promotes adipogenesis in 3T3-L1 preadipocytes: A High Content Cellomics and metabolomic analysis. *Toxicol. In Vitro* **2016**, *32*, 297–309. [CrossRef] [PubMed]
37. Hatch, E.E.; Nelson, J.W.; Qureshi, M.M.; Weinberg, J.; Moore, L.L.; Singer, M.; Webster, T.F. Association of urinary phthalate metabolite concentrations with body mass index and waist circumference: A cross-sectional study of NHANES data, 1999–2002. *Environ. Health* **2008**, *7*, 27. [CrossRef] [PubMed]
38. Kolena, B.; Petrovicova, I.; Pilka, T.; Pucherova, Z.; Munk, M.; Matula, B.; Vankova, V.; Petlus, P.; Jenisova, Z.; Rozova, Z.; et al. Phthalate exposure and health-related outcomes in specific types of work environment. *Int. J. Environ. Res. Public Health* **2017**, *11*, 5628. [CrossRef] [PubMed]
39. Petrovičová, I.; Kolena, B.; Šidlovská, M.; Pilka, T.; Wimmerová, S.; Trnovec, T. Occupational exposure to phthalates in relation to gender, consumer practices and body composition. *Environ. Sci. Pollut. Res. Int.* **2016**, *23*, 24125–24134. [CrossRef] [PubMed]
40. Biemann, R.; Blüher, M.; Isermann, B. Exposure to endocrine-disrupting compounds such as phthalates and bisphenol A is associated with an increased risk for obesity. *Best Pract. Res. Clin. Endocrinol. Metab.* **2021**, *35*, 101546. [CrossRef] [PubMed]
41. James-Todd, T.M.; Huang, T.; Seely, E.W.; Saxena, A.R. The association between phthalates and metabolic syndrome: The National Health and Nutrition Examination Survey 2001–2010. *Environ. Health.* **2016**, *15*, 52. [CrossRef]
42. Newbold, R.R.; Padilla-Banks, E.; Jefferson, W.N. Environmental estrogens and obesity. *Mol. Cell. Endocrinol.* **2009**, *304*, 84–89. [CrossRef]
43. Karabulut, G.; Barlas, N. The possible effects of mono butyl phthalate (MBP) and mono (2-ethylhexyl) phthalate (MEHP) on INS-1 pancreatic beta cells. *Toxicol. Res.* **2021**, *10*, 601–612. [CrossRef]
44. Stojanoska, M.M.; Milosevic, N.; Milic, N.; Abenavoli, L. The influence of phthalates and bisphenol A on the obesity development and glucose metabolism disorders. *Endocrine* **2016**, *55*, 666–681. [CrossRef]
45. Stahlhut, R.W.; van Wijngaarden, E.; Dye, T.D.; Cook, S.; Swan, S.H. Concentrations of urinary phthalate metabolites are associated with increased waist circumference and insulin resistance in adult U.S. males. *Environ. Health Perspect.* **2007**, *115*, 876–882. [CrossRef]

46. Song, Y.; Hauser, R.; Hu, F.B.; Franke, A.A.; Liu, S.; Sun, Q. Urinary concentrations of bisphenol A and phthalate metabolites and weight change: A prospective investigation in US women. *Int. J. Obes.* **2014**, *38*, 1532–1537. [CrossRef] [PubMed]
47. Lind, P.M.; Roos, V.; Rönn, M.; Johansson, L.; Ahlström, H.; Kullberg, J.; Lind, L. Serum concentrations of phthalate metabolites are related to abdominal fat distribution two years later in elderly women. *Environ. Health.* **2012**, *11*, 21. [CrossRef] [PubMed]
48. Van der Meer, T.P.; van Faassen, M.; van Beek, A.P.; Snieder, H.; Kema, I.P.; Wolffenbuttel, B.H.; van Vliet-Ostaptchouk, J.V. Exposure to Endocrine Disrupting Chemicals in the Dutch general population is associated with adiposity-related traits. *Sci. Rep.* **2020**, *10*, 9311. [CrossRef] [PubMed]
49. Campioli, E.; Batarseh, A.; Li, J.; Papadopoulos, V. The endocrine disruptor mono-(2-ethylhexyl) phthalate affects the differentiation of human liposarcoma cells (SW 872). *PLoS ONE* **2011**, *6*, e28750. [CrossRef]
50. Feige, J.N.; Gelman, L.; Rossi, D.; Zoete, V.; Métivier, R.; Tudor, C.; Anghel, S.I.; Grosdidier, A.; Lathion, C.; Engelborghs, Y.; et al. The endocrine disruptor monoethyl-hexyl-phthalate is a selective peroxisome proliferator-activated receptor gamma modulator that promotes adipogenesis. *J. Biol. Chem.* **2007**, *282*, 19152–19166. [CrossRef]
51. Chiang, C.; Flaws, J.A. Subchronic Exposure to Di(2-ethylhexyl) Phthalate and Diisononyl Phthalate During Adulthood Has Immediate and Long-Term Reproductive Consequences in Female Mice. *Toxicol. Sci.* **2019**, *168*, 620–631. [CrossRef]
52. Bacon, J.L. The Menopausal Transition. *Obstet. Gynecol. Clin.* **2017**, *44*, 285–296. [CrossRef]
53. Haggerty, D.K.; Flaws, J.A.; Li, Z.; Strakovsky, R.S. Phthalate exposures and one-year change in body mass index across the menopausal transition. *Environ. Res.* **2021**, *194*, 110598. [CrossRef]
54. Chiang, C.; Pacyga, D.C.; Strakovsky, R.S.; Smith, R.L.; James-Todd, T.; Williams, P.L.; Hauser, R.; Meling, D.D.; Li, Z.; Flaws, J.A. Urinary phthalate metabolite concentrations and serum hormone levels in pre- and perimenopausal women from the Midlife Women's Health Study. *Environ. Int.* **2021**, *156*, 106633. [CrossRef]
55. Takeuchi, S.; Iida, M.; Kobayashi, S.; Jin, K.; Matsuda, T.; Kojima, H. Differential effects of phthalate esters on transcriptional activities via human estrogen receptors alpha and beta, and androgen receptor. *Toxicology* **2005**, *210*, 223–233. [CrossRef]
56. Engel, A.; Buhrke, T.; Imber, F.; Jessel, S.; Seidel, A.; Völkel, W.; Lampen, A. Agonistic and antagonistic effects of phthalates and their urinary metabolites on the steroid hormone receptors ERα, ERβ, and AR. *Toxicol. Lett.* **2017**, *277*, 54–63. [CrossRef] [PubMed]
57. Page, B.D.; Lacroix, G.M. The occurrence of phthalate ester and di-2-ethylhexyl adipate plasticizers in Canadian packaging and food sampled in 1985–1989: A survey. *Food Addit. Contam.* **1995**, *12*, 129–151. [CrossRef] [PubMed]
58. Serrano, S.E.; Karr, C.J.; Seixas, N.S.; Nguyen, R.H.; Barrett, E.S.; Janssen, S.; Redmon, B.; Swan, S.H.; Sathyanarayana, S. Dietary phthalate exposure in pregnant women and the impact of consumer practices. *Int. J. Environ. Res. Public Health* **2014**, *11*, 6193–6215. [CrossRef] [PubMed]
59. Bošnir, J.; Puntari, D.; Gali, A.; Škes, I.; Dijanić, T.; Klarić, M.; Grgić, M.; Čurković, M.; Šmit, Z. Migration of Phthalates from Plastic Containers into Soft Drinks and Mineral Water. *Food Technol. Biotechnol.* **2007**, *45*, 91–95.
60. Al-Saleh, I.; Shinwari, N.; Alsabbaheen, A. Phthalates residues in plastic bottled waters. *J. Toxicol. Sci.* **2011**, *36*, 469–478. [CrossRef] [PubMed]
61. Zaki, G.; Shoeib, T. Concentrations of several phthalates contaminants in Egyptian bottled water: Effects of storage conditions and estimate of human exposure. *Sci. Total Environ.* **2018**, *618*, 142–150. [CrossRef]
62. Han, S.J.; Lee, S.H. Nontraditional Risk Factors for Obesity in Modern Society. *J. Obes. Metab. Syndr.* **2021**, *30*, 93–103. [CrossRef] [PubMed]
63. Fonken, L.K.; Aubrecht, T.G.; Meléndez-Fernández, O.H.; Weil, Z.M.; Nelson, R.J. Dim light at night disrupts molecular circadian rhythms and increases body weight. *J. Biol. Rhythm.* **2013**, *28*, 262–271. [CrossRef]
64. Rybnikova, N.A.; Haim, A.; Portnov, B.A. Does artificial light-at-night exposure contribute to the worldwide obesity pandemic? *Int. J. Obes.* **2016**, *40*, 815–823. [CrossRef]
65. Strohmaier, S.; Devore, E.E.; Zhang, Y.; Schernhammer, E.S. A Review of Data of Findings on Night Shift Work and the Development of DM and CVD Events: A Synthesis of the Proposed Molecular Mechanisms. *Curr. Diabetes Rep.* **2018**, *18*, 132. [CrossRef]
66. Park, Y.M.; White, A.J.; Jackson, C.L.; Weinberg, C.R.; Sandler, D.P. Association of Exposure to Artificial Light at Night While Sleeping with Risk of Obesity in Women. *JAMA Intern. Med.* **2019**, *179*, 1061–1071. [CrossRef] [PubMed]
67. Zhang, D.; Jones, R.R.; Powell-Wiley, T.M.; Jia, P.; James, P.; Xiao, Q. A large prospective investigation of outdoor light at night and obesity in the NIH-AARP Diet and Health Study. *Environ. Health.* **2020**, *19*, 74. [CrossRef] [PubMed]

MDPI
St. Alban-Anlage 66
4052 Basel
Switzerland
Tel. +41 61 683 77 34
Fax +41 61 302 89 18
www.mdpi.com

Toxics Editorial Office
E-mail: toxics@mdpi.com
www.mdpi.com/journal/toxics

MDPI
St. Alban-Anlage 66
4052 Basel
Switzerland

Tel: +41 61 683 77 34

www.mdpi.com

ISBN 978-3-0365-5038-1